Interactions of Antimicrobial Peptides (AMPs) with Model Membranes at Different pH Values

by

©Gagandeep K Sandhu

A thesis submitted to the
School of Graduate Studies
in partial fulfillment of the
requirements for the degree of
Doctor of Philosophy

Department of Physics and Physical Oceanography
Memorial University of Newfoundland
St. John's, NL, Canada

January 18, 2019

Abstract

Antimicrobial peptides (AMPs) are important components of the innate immune systems of many different organisms. Their amphipathic and cationic characteristics promote interactions with the cell membrane. Gad peptides are rich in histidine, and thus have the potential to exhibit pH-dependent activity. The major focus of this study was to understand how Gad peptides interact with model lipid membranes and how these interactions depend on the peptides' overall charge and the composition of the model membranes. ^{2}H NMR spectroscopy was used to study the effect of Gad peptides on lipid acyl chain order of model lipid bilayers at different pH values. ^{2}H NMR results revealed that membrane disruption by Gad peptides was not pH-dependent. Zeta potential measurements were used to study the binding of Gad peptides to model lipid membranes. The binding studies showed that for both Gad-1 and Gad-2 at low pH, less peptide binds to the membrane and the peptide interacts with a larger number of lipid molecules. Experiments performed with model membranes containing cardiolipin (CL) in the presence of Gad-1 showed that the presence of CL allows the membrane to accommodate more Gad-1. In the presence of CL the peptide binds more strongly with the membrane and interacts with a larger number of lipids. Taken together, these results suggest that Gad peptides might disrupt membrane integrity by clustering anionic lipids. Clustering of anionic lipids away from zwitterionic lipids by cationic AMPs might be a contributing mechanism, which does not exclude other mechanisms, including the carpet mechanism and pore formation. The chemical shift values of ^{15}N NMR spectroscopy can give an insight about the positioning of peptides in lipid bilayer surfaces. ^{15}N NMR observations showed that Gad-1 aligned parallel to the membrane surface. The study of AMP-membrane interactions will help to identify criteria to recognize the important features of natural

AMP sequences involved in the antimicrobial action and thus assist in the design of AMP-based antibiotics to help overcome the problem of antimicrobial resistance.

Acknowledgements

First and foremost, I would like to thank the Almighty GOD with a humble heart, for providing me with the strength to take up this project work and complete it with His grace.

I would like to express my sincere thanks and gratitude towards my honorable supervisors Dr. Michael Morrow and Dr. Valerie Booth for their guidance, excellent mentorship, and encouragement during the research and supervision of this thesis. I would like to thank them for providing me with financial support during the Ph.D. journey. I would like to thank Dr. Morrow for teaching me concepts of NMR and Dr. Valerie Booth for teaching me research ethics through a course "How to be a scientist". I could not have wished for better Ph.D. supervisors. I have learned a lot from them.

I would like to thank my advisory committee members Dr. Anand Yethiraj and Dr. Kris Poduska for their valuable suggestions and encouragement through the annual supervisory committee meetings. I am grateful to all of my course instructors, Dr. Guy Quirion, Dr. John Lewis, Dr. Kris Poduska, Dr. Valerie Booth. Dr. Kaushik Nag and Dr. H. Joseph Banoub for their interesting lectures.

I gratefully acknowledge the financial assistance provided by the National Sciences and Engineering Research Council, the Department of Physics and Physical Oceanography and the School of Graduate Studies. I also thank Memorial University for awarding me the Fellow of School of Graduate studies award and J. Bruce and Helen H. French Graduate Scholarship in Physics that acknowledged my achievement during my Ph.D. Program.

I especially thank Donna Jackman for her great help and support in assisting me how to prepare samples and working in the lab. I would also thank Dr. Celine

Schneider and Dave Davidson for teaching me how to work with and running NMR instrument for ^{15}N NMR experiments. I warmly thank Fred Perry for assisting me with computer support and assistance. I would like to thank Joy Simmons, Donna Coombs, and Maureen Wade for their administrative help during my Ph.D. program. I also wish to thank whole cryogenics facility for providing a continuous supply of cryogenic liquids.

I have great pleasure in acknowledging my gratitude to several current and former research group members: Nury Santisteban, Suhad Sbeih, Tadiwos Gatachew, Chris Miranda, Mohammad H. Khatami, Ashkan Rahmani, and Collin Knight for their valuable collaboration, assistance, and discussion. I would like to thank all my friends whose support made my stay in St. John's memorable and joyful.

My acknowledgment would be incomplete without thanking the biggest source of my strength, my family. I owe my most special thanks to my loving husband *Rupinder Dhaliwal* for his endless love, support, patience, and deep understanding throughout this entire journey of Ph.D. I thank him for being an active listener during my all presentation preparations. I would like to thank my loving brother and sister-in-law, *Ravinder and Aman*, for their continued support, encouragement, and hearing my concerns from thousands of miles away. I would like to thank my uncle, *Balbir Raiwal*, for his endless support during my educational years.

Last but by no means least, I must express my high regards and deep indebtedness to my respected parents whose blessing and inspiration have always encouraged me to move forward. I would like to thank them for trusting in me and encouraging me to follow my dreams. Without their loving upbringing and nurturing; I would not have been where I am today and what I am today.

I would like to dedicate this work to

Sham Singh Sandhu

Harpal Singh Raiwal

Avtar Singh Dhaliwal

Contents

Abstract ii

Acknowledgements iv

Dedication vi

List of Figures xii

List of Tables xvii

List of Abbreviations and symbols xix

1 Introduction 1
- 1.1 Biological and model membranes . . . 2
- 1.2 Antimicrobial peptides (AMPs) . . . 7
  - 1.2.1 AMPs background . . . 7
  - 1.2.2 Antibiotic-resistance and AMPs . . . 13
    - 1.2.2.1 Antibiotic-resistance: a growing concern . . . 13
    - 1.2.2.2 AMPs: a natural alternative to conventional antibiotics . . . 14
  - 1.2.3 Challenges in developing AMPs as therapeutics . . . 15
  - 1.2.4 Understanding the mechanism of action of AMPs . . . 16
    - 1.2.4.1 Molecular basis of the AMP selectivity . . . 17
    - 1.2.4.2 Pore forming mechanisms . . . 18
    - 1.2.4.3 Non-pore forming mechanisms . . . 21
    - 1.2.4.4 Describing membrane-peptide interactions with a phase diagram . . . 23
    - 1.2.4.5 Interfacial activity model . . . 25
  - 1.2.5 Antimicrobial to anticancer peptides: histidine-rich AMPs . 25
    - 1.2.5.1 Gad peptides . . . 27
  - 1.2.6 Model membrane studies . . . 29
- 1.3 Current AMP research questions and objective of present work . . . 31

2 Biophysical methods to study the interactions of AMPs with model membranes 33

2.1 Nuclear magnetic resonance (NMR) spectroscopy . . . 34
2.1.1 Introduction . . . 35
2.1.1.1 Equilibrium magnetization and Larmor precession . 35
2.1.1.2 Free induction decay (FID) signal and NMR spectrum . . . 38
2.1.1.3 Density operator formulation of spin $\frac{1}{2}$ system for $(\frac{\pi}{2})_x$ pulse . . . 40
2.1.2 NMR spectrometer . . . 40
2.1.3 ^{2}H NMR . . . 40
2.1.3.1 Quadrupole Hamiltonian . . . 40
2.1.3.2 Quadrupole splitting . . . 44
2.1.3.3 ^{2}H NMR powder pattern spectrum of lipid vesicles 46
2.1.3.4 Oriented spectrum and orientational order parameter (S_{CD}) . . . 49
2.1.3.5 Quadrupole echo . . . 52
2.1.3.5.1 Density operator treatment of spin 1 system 53
2.1.3.6 Quadrupole echo decay time T_2^{qe} . . . 53
2.1.4 ^{15}N NMR . . . 55
2.2 Zeta potential . . . 58
2.2.1 Electrical double layer . . . 58
2.2.2 Measurement of zeta potential by electrophoresis . . . 60
2.3 Circular dichroism (CD) spectroscopy . . . 62
2.3.1 CD spectrum of peptides . . . 63
2.3.2 Measurement of CD and percent helicity of α helical peptides 63

3 Interactions of Gad peptides with model membranes: insights from NMR and binding studies 66
3.1 Materials and methods . . . 67
3.1.1 Lipids . . . 67
3.1.2 ^{2}H NMR . . . 68
3.1.2.1 Sample preparation . . . 68
3.1.2.2 Experimental details . . . 69
3.1.3 Zeta potential (ζ-potential) measurements . . . 70
3.1.3.1 Sample preparation . . . 70
3.1.3.2 Experimental details . . . 71
3.1.4 Synthesis of Gad peptides . . . 71
3.2 Results . . . 73
3.2.1 ^{2}H NMR results . . . 73
3.2.1.1 Peptide-induced disorder in model lipid bilayers . 74
3.2.1.2 Effect of Gad peptides on slow motions of lipid bilayers as determined by quadrupole echo decay time (T_2^{qe}) . . . 80

3.2.2 Zeta potential (ζ-potential) results . . . 83
3.2.2.1 Binding isotherms . . . 84
3.2.2.2 A binding model to calculate the partition constant (K_P) . . . 88
3.2.2.3 Modeling peptide dependence of the zeta potential using a Langmuir isotherm approach . . . 102
3.3 Discussion . . . 115

4 Alignment of Gad peptides in mechanically oriented model lipid bilayers determined by ^{15}N NMR spectroscopy 129
4.1 Materials and methods . . . 130
4.1.1 Lipids . . . 130
4.1.2 Solid support (Mica) . . . 130
4.1.3 Mechanically Oriented Lipid Bilayers . . . 130
4.1.3.1 Appropriate lipid mixtures . . . 130
4.1.3.2 Circular Dichroism (CD) . . . 132
4.1.3.3 Protocol for making mechanically oriented lipid bilayers . . . 134
4.1.4 NMR experimental details . . . 136
4.1.4.1 ^{2}H NMR . . . 136
4.1.4.2 ^{15}N NMR . . . 137
4.1.5 Synthesis of ^{15}N-labelled Gad peptides . . . 138
4.1.6 Protein concentration assay . . . 139
4.2 Results . . . 140
4.2.1 Mechanically oriented samples of lipids only . . . 140
4.2.2 Mechanically oriented bilayer samples of POPC/POPG (5:1) lipid mixture with incorporated unlabelled Gad peptides . . . 143
4.2.3 Mechanically oriented bilayer samples of POPC/POPG (5:1) lipid mixture with incorporated ^{15}N-labelled Gad peptides . . . 145
4.2.4 Mechanically oriented lipid bilayers prepared using 24 mica plates . . . 148
4.2.5 Adjusting the pH of mechanically oriented lipid bilayers . . . 152
4.2.6 Alignment of Gad-1 in mechanically oriented lipid bilayers of POPC-d31/POPG (5:1) at pH 7.0 . . . 153
4.2.7 Alignment of Gad-2 in mechanically oriented lipid bilayers of POPC-d31/POPG (5:1) at pH 7.0 . . . 158
4.3 Discussion . . . 161

5 Investigating the role of cardiolipin in the AMP-membrane interactions 166
5.1 Introduction . . . 166
5.2 Cardiolipin in bacterial membranes . . . 167
5.3 Materials and Methods . . . 170
5.3.1 Lipids . . . 170

5.3.2 Gad-1 peptide . . . 170
5.3.3 ^{2}H NMR . . . 171
5.3.3.1 Sample preparation . . . 171
5.3.3.2 Experimental detail . . . 171
5.3.4 Zeta potential measurements . . . 171
5.3.4.1 Sample preparation and Experimental detail . . . 171
5.4 Results . . . 173
5.4.1 ^{2}H NMR . . . 174
5.4.1.1 ^{2}H NMR spectra of POPE/POPG-d_{31}/CL lipid bilayers at pH 7.0 and pH 5.0 . . . 174
5.4.1.2 Effect of CL on the slow motions of POPE/POPG-d_{31} lipid bilayers at pH 7.0 and pH 5.0 . . . 184
5.4.1.3 ^{2}H NMR spectra of POPE/POPG-d_{31}/CL lipid bilayers in the presence of Gad-1 at pH 7.0 and pH 5.0 . . . 187
5.4.1.4 Effects of Gad-1 on the slow motions of POPE/POPG-d_{31}/CL lipid bilayers at pH 7.0 and pH 5.0 . . . 193
5.4.2 Zeta potential . . . 196
5.4.2.1 Binding isotherm . . . 196
5.4.2.2 Characterizing the binding of Gad-1 to POPE/POPG/CL lipid bilayers using Freire et al. binding model . . . 199
5.4.2.3 Modeling peptide dependence of the zeta potential using the Langmuir isotherm approach . . . 204
5.5 Discussion . . . 208

6 Discussion **218**
6.0.1 Directions for future work . . . 223

Appendices **225**

A Density operator formulation of spin $\frac{1}{2}$ and spin 1 system **226**
A.1 Density operator . . . 226
A.2 Density operator formulation of spin $\frac{1}{2}$ system for $(\frac{\pi}{2})_x$ pulse . . . 228
A.3 Density operator treatment of spin 1 system . . . 233
A.3.1 $\frac{\pi}{2}$ pulse along x axis . . . 234
A.3.2 For time τ the spin system evolves under the Quadrupole Hamiltonian . . . 235
A.3.3 $\frac{\pi}{2}$ pulse along y axis . . . 236

B NMR spectrometer and the temperature controller **239**
B.1 NMR spectrometer . . . 239
B.1.1 The magnet . . . 239

B.1.2 The transmitter and the probe section 240
B.1.2.1 Matching and tuning 240
B.1.2.2 Quarter wavelength transmission line 241
B.1.3 Receiver section 243
B.2 Temperature controller 244

Bibliography **246**

List of Figures

1.1 A simplified view of membrane structure: lipid bilayer and protein embedded in it. . . . 2
1.2 The schematic representation of the different shapes of lipid molecules and corresponding membrane assemblies. . . . 5
1.3 Membrane selectivity by AMPs on the basis of lipid composition of the membrane. . . . 18
1.4 The antimicrobial activity of AMPs to kill bacteria lies in their ability to disrupt the membrane integrity which can be achieved in a number of ways. . . . 19
1.5 The phase diagrams of lipid-peptide mixtures as a function of membrane-bound peptide and membrane composition to depict the ability of a peptide to disrupt the lipid bilayer integrity. . . . 24
1.6 Minimal Inhibitory Concentration (MIC) results for Gad-1 and Gad-2 at pH 7.0 and pH 5.0. . . . 29

2.1 The depiction of the Zeeman splitting for spin $\frac{1}{2}$ system. . . . 37
2.2 In the absence of the external magnetic field, the magnetic moments of the individual spins are randomly oriented. . . . 37
2.3 The schematic representation of the precessional motion of the magnetization vector about the z axis. . . . 39
2.4 Energy level diagram for a spin 1 system in the presence of a magnetic field, showing Zeeman and quadrupole splitting. . . . 45
2.5 The angular orientation of the bilayer normal with respect to external magnetic field and carbon-deuteron bond. . . . 47
2.6 Powder pattern spectrum of a vesicle sample deuterated at single site. . . . 48
2.7 The oriented sample spectrum: different peaks correspond to different deuterons on the lipid acyl chain. . . . 51
2.8 The representation of the quadrupole echo pulse sequence. . . . 52
2.9 The components of chemical shift tensor positioned near to the peptide bond. . . . 56
2.10 The schematic representation of ^{15}N powder pattern spectrum for randomly distributed molecular orientations. . . . 57
2.11 The schematic representation of ^{15}N chemical shift values for different orientations of α helical peptides. . . . 58

2.12 The charge distribution around negatively charged particle represented by the black circle. 59
2.13 The schematic representation of (a) Hückel (b) Smoluchowski approximations. For the work reported in this thesis, the Smoluchowski approximation is used to determine the zeta potential. . . 61
2.14 CD spectrum of poly-peptides results from different absorption of R-CPL and L-CPL. 64
2.15 The representation of an ellipticity when L-CPL and R-CPL have different magnitude. 64

3.1 ^{2}H NMR spectra of multilamellar POPE/POPG-d_{31}(3:1) vesicles with and without Gad peptides at two pH values (a) at 25°C (b) 37°C. 76
3.2 The peptide-induced acyl chain disorder in POPE/POPG-d_{31}(3:1) lipid vesicles was quantitatively analysed by calculating orientational order parameter S_{CD}. 77
3.3 (a) The oriented spectra corresponding to the powder pattern spectra of POPE/POPG-d_{31}(3:1) lipid vesicles with and without Gad peptides at pH 5.0. 78
3.4 (a) The comparison of order parameter profiles for POPE/POPG-d_{31}(3:1) lipid bilayers interacting with Gad-1 at pH 7.0 and 5.0. . . 79
3.5 (a) The pH dependence of quadrupole echo decay time (T_2^{qe}) of POPE/POPG-d_{31} (3:1) lipid vesicles with and without the addition of Gad peptides at (a) 25°C (b) 37°C. 82
3.6 The binding isotherms of Gad-1 at (a) pH 7.0 (b) pH 5.0. 86
3.7 (a) The binding isotherms of Gad-2 at (a) pH 7.0 (b) pH 5.0. 87
3.8 (a) Zeta potential measurements for 40 μM POPE/POPG (3:1) in the presence of Gad-1 at pH 7.0. 95
3.9 (a) Zeta potential measurements for 40 μM POPE/POPG (3:1) in the presence of Gad-1 at pH 5.0. 96
3.10 (a) Zeta potential measurements for 40 μM POPE/POPG (3:1) in the presence of Gad-2 at pH 7.0. 97
3.11 (a) Zeta potential measurements for 40 μM POPE/POPG (3:1) in the presence of Gad-2 at pH 5.0. 98
3.12 Schematic representation of zeta potential parameters ζ_0, $\Delta\zeta$, and $\triangle\zeta_{max}$. ζ_0 is the value of zeta potential in the absence of peptide. . 106
3.13 a) $\frac{\Delta\zeta}{\Delta\zeta_{\max}}$ vs. $[P]_{\text{Total}}$ for Gad-1 at pH 7.0. 110
3.14 (a) $\frac{\Delta\zeta}{\Delta\zeta_{\max}}$ vs. $[P]_{\text{Total}}$ for Gad-1 at pH 5.0. 111
3.15 (a) $\frac{\Delta\zeta}{\Delta\zeta_{\max}}$ vs. $[P]_{\text{Total}}$ for Gad-2 at pH 7.0. 112
3.16 (a) $\frac{\Delta\zeta}{\Delta\zeta_{\max}}$ vs. $[P]_{\text{Total}}$ for Gad-2 at pH 5.0. 113

3.17 Schematic representation of the interaction of the peptide (in orange) with lipid molecules (in blue). . . . 116
3.18 The depiction of lipid-peptide interactions corresponding to the different points of the binding isotherm. . . . 119
3.19 An illustration of lipid-peptide interactions for (a) Gad-1 at pH 7.0 and pH 5.0. (b) Gad-2 at pH 7.0 and pH 5.0. . . . 123

4.1 Far-UV CD spectrum of Gad-1 in lipid mixture of POPC/POPG (5:1). . . . 133
4.2 The schematic representation of cross polarization (CP) pulse sequence. . . . 137
4.3 Gad peptides selectively labelled with ^{15}N isotopes at two sites indicated by red arrows. . . . 138
4.4 (a) ^{2}H NMR spectrum of mechanically oriented POPC/POPC-d_{31} (7:3) lipid bilayers. . . . 142
4.5 ^{2}H NMR spectra obtained at different intervals after sample preparation . . . 144
4.6 ^{2}H NMR spectra from a mechanically oriented sample prepared using 6 mg POPC-d_{31}/POPG (5:1) with the addition of 3 mole%, i.e. 0.6 mg, ^{15}N-labelled Gad-1 peptide. . . . 146
4.7 ^{15}N powder pattern spectrum obtained from 6 mg of Gad-1 dry powder at 25°C by averaging 12,000 transients. . . . 147
4.8 ^{2}H NMR spectrum of oriented bilayers prepared using 40 mg of POPC-d_{31}/POPG (5:1) lipids deposited on 24 mica plates. . . . 149
4.9 ^{2}H NMR spectra of 40 mg POPC-d_{31}/POPG (5:1) lipid mixture prepared using 24 mica plates. The mica plates were divided into four groups, each having six plates. . . . 150
4.10 ^{2}H NMR spectra of 40 mg POPC-d_{31}/POPG (5:1) containing 3.8 mg of Gad-1 peptide. . . . 151
4.11 ^{2}H NMR spectrum of oriented POPC-d_{31}/POPG (5:1) bilayers at pH 7.0 prepared using the protocol described in Section 4.3.5. . . . 153
4.12 ^{2}H NMR spectrum of POPC-d_{31}/POPG(5:1) at pH 7.0 containing ^{15}N-labelled Gad-1 peptide. . . . 154
4.13 (a) Proton-decoupled ^{15}N solid-state NMR spectrum of Gad-1 reconstituted into mechanically oriented lipid bilayers of POPC-d_{31}/POPG (5:1) at pH 7.0. . . . 156
4.14 Proton-decoupled ^{15}N solid-state NMR spectrum of Gad-1 reconstituted into mechanically oriented lipid bilayers of POPC-d_{31}/POPG (5:1) at pH 7.0. . . . 157
4.15 The comparison of two ^{15}N spectra of Gad-1 reconstituted into mechanically oriented lipid bilayers of POPC-d_{31}/POPG (5:1) at pH 7.0. . . . 158
4.16 ^{15}N powder pattern spectrum of Gad-2 acquired with 3.2 mg of ^{15}N-labelled Gad-2 dry powder. . . . 159

4.17 ^{2}H NMR spectra of mechanically oriented POPC-d_{31}/POPG (5:1) lipid bilayers at pH 7.0 containing ^{15}N-labelled Gad-2 peptide. . . 160
4.18 Proton-decoupled ^{15}N solid-state NMR spectrum of Gad-2 reconstituted into mechanically oriented lipid bilayers of POPC-d_{31}/POPG (5:1) at pH 7.0. 161

5.1 Chemical structure of cardiolipin (CL). 168
5.2 A series of ^{2}H NMR spectra of model membranes composed of POPE/POPG-d_{31}/CL (79/16/5 molar ratio) at pH 7.0. 175
5.3 A series of ^{2}H NMR spectra of model membrane composed of lipids POPE/POPG-d_{31}/CL (79/16/5 molar ratio) at pH 7.0. 176
5.4 The ^{2}H NMR spectra of POPE/POPG-d_{31} (3:1 molar ratio) and POPE/POPG-d_{31}/CL (79/16/5 molar ratio) at pH 7.0. 177
5.5 A series of ^{2}H NMR spectra of model membranes composed of lipids POPE/POPG-d_{31}/CL (75/15/10) at pH 7.0. 179
5.6 A series of ^{2}H NMR spectra of model membranes composed of lipids POPE/POPG-d_{31}/CL (83/6/11 molar ratio) at pH 7.0. 180
5.7 A series of ^{2}H NMR spectra of model membranes composed of lipids POPE/POPG-d_{31}/CL (79/16/5 molar ratio) at pH 5.0. 182
5.8 Comparison of ^{2}H NMR spectra of POPE/POPG-d_{31}/CL (79/16/5 molar ratio) at pH 7.0 and pH 5.0. 183
5.9 The quadrupole echo decay time of POPE/POPG-d_{31}/CL lipid mixture at pH 7.0 (a) at 25°C (b) 37°C. 185
5.10 The quadrupole echo decay time of POPE/POPG-d_{31} and POPE/POPG-d_{31}/CL lipid mixture at pH 5.0 (a) at 25°C (b) 37°C. 186
5.11 A series of ^{2}H NMR spectra of POPE/POPG-d_{31}/CL (79/16/5 molar ratio) + Gad-1 at pH 7.0. 188
5.12 ^{2}H NMR spectra of POPE/POPG-d_{31} acquired at 25°C with addition of CL and/or Gad-1 at pH 7.0. 189
5.13 A series of ^{2}H NMR spectra of model membrane composed of lipids POPE/POPG-d_{31}/CL(79/16/5) + Gad-1 at pH 5.0. 190
5.14 ^{2}H NMR spectra of POPE/POPG-d_{31} acquired at 25°C with addition of CL and/or Gad-1 at pH 5.0. 191
5.15 Comparison of the ^{2}H NMR spectra of POPE/POPG-d_{31}/CL with and without the addition of Gad-1 at pH 7.0 and pH 5.0. 192
5.16 The quadrupole echo decay time of POPE/POPG-d_{31} and POPE/POPG-d_{31}/CL lipid mixture with and without the addition of Gad-1 at pH 7.0 (a) at 25°C (b) 37°C. 194
5.17 The quadrupole echo decay time of POPE/POPG-d_{31} and POPE/POPG-d_{31}/CL lipid mixture with and without the addition of Gad-1 at pH 5.0 (a) at 25°C (b) 37°C 195
5.18 (a) The binding isotherms of Gad-1 at (a) pH 7.0 (b) pH 5.0. Each point represents the average of three independent measurements. . . 198

5.19 (a) Zeta potential measurements for 40 μM POPE/POPG/CL (79/16/5) in the presence of Gad-1 at pH 7.0. 201
5.20 (a) Zeta potential measurements for 40 μM POPE/POPG/CL (79/16/5 molar ratio) in the presence of Gad-1 at pH 5.0 202
5.21 (a) $\frac{\Delta\zeta}{\Delta\zeta_{max}}$ vs. $[P]_{Total}$ for Gad-1 at pH 7.0. 206
5.22 (a) $\frac{\Delta\zeta}{\Delta\zeta_{max}}$ vs. $[P]_{Total}$ for Gad-1 at pH 7.0. 207

A.1 When the external magnetic field is applied along the z axis, the equilibrium magnetization is formed in the direction of field. 232

B.1 (a) The schematic representation of the probe section of the NMR spectrometer with two crossed diode switches and $\frac{\lambda}{4}$ transmission line. 243
B.2 The output of a PID temperature controller is shown in the above figure. 245

List of Tables

1.1 The value of packing parameter determines the nature of intrinsic curvature adopted by a lipid molecule. . . . 3
1.2 The lipid composition of various Gram-positive and Gram-negative bacteria. . . . 6
1.3 AMPs from different sources with their known charge, secondary structure, and activity. . . . 13
1.4 Expected overall peptide charge of Gad-1 and Gad-2 at pH 7.0 and pH 5.0. . . . 28

2.1 The gyromagnetic ratio and corresponding Larmor frequency of various nuclei. . . . 38

3.1 The molecular weights and the hydrated bilayer gel to liquid crystal transition temperatures of different lipids used in this study. . . . 67
3.2 Calculated molar fractions of peptide bound to the membrane (X) and partition constants (K_P) from zeta potential measurements for Gad-1 at pH 7.0 and pH 5.0. . . . 99
3.3 Calculated molar fractions of peptide bound to the membrane (X) and partition constants (K_P) from zeta potential measurements for Gad-2 at pH 7.0 and pH 5.0. . . . 99
3.4 The global $L : P$ is calculated for the total peptide concentration 1 μM - 6 μM. . . . 100
3.5 The global $L : P$ is calculated for the total peptide concentration 5 μM- 15 μM. . . . 101
3.6 The values of X, $1/Q$, K_{eq} for Gad-1 at pH 7.0 and pH 5.0. . . . 114
3.7 The values of X, $1/Q$, K_{eq} for Gad-2 at pH 7.0 and pH 5.0. . . . 114
3.8 Comparison of values of X for Gad peptides calculated using Freier et al. approach and zeta potential model based on the Langmuir isotherm. . . . 120
3.9 The partition constant (K_P) and the equilibrium constant (K_P) for Gad-1 and Gad-2 at pH 7.0 and pH 5.0. . . . 121
3.10 Local lipid-to-peptide ratios determined using Freire et al. approach and zeta potential model based on the Langmuir isotherm. . . . 122

4.1 Percent helicity of Gad peptides in POPC and POPG lipid environment at different pH values. . . . 131

4.2 The list of acquisition parameters used in CP ^{15}N NMR experiments. 138
4.3 The apparent concentrations of Gad peptides determined using Bradford assay. 164
4.4 The mass of Gad peptides in powder and oriented lipid bilayer samples calculated using Bradford assay result. 164

5.1 The lipid composition of various Gram-positive and Gram-negative bacteria. 169
5.2 Calculated molar fractions of peptide bound to the membrane (X) and partition constants (K_{P}) from zeta potential measurements for Gad-1 at pH 7.0 and pH 5.0. 203
5.3 The global $L : P$ is calculated for the total peptide concentration 1 μM - 3 μM. 203
5.4 The values of X, $1/Q$, K_{eq} for Gad-1 at pH 7.0 and pH 5.0. 208
5.5 Comparison of values of X for Gad-1 peptide for POPE/POPG-d_{31} and POPE/POPG-d_{31}/CL bilayers at pH 7.0 and pH 5.0. 214
5.6 Comparison of values of K_{eq} for Gad-1 peptide for POPE/POPG-d_{31} and POPE/POPG-d_{31}/CL bilayers at pH 7.0 and pH 5.0. . . . 215
5.7 Comparison of values of $1/Q$ for Gad-1 peptide for POPE/POPG-d_{31} and POPE/POPG-d_{31}/CL bilayers at pH 7.0 and pH 5.0. . . . 216

List of Abbreviations and symbols

^{2}**H**	**Deuterium**
^{15}**N**	**Nitrogen**
^{31}**P**	**Phosphorus**
AMP	**Antimicrobial Peptide**
C-D	**Carbon-deuterium**
CD	**Circular Dichroism**
CL	**Cardiolipin**
EFG	**Electric Field Gradient**
FID	**Free Induction Decay**
Fmoc	**O-fluorenylmethyloxycarbonyl**
Gad	**Gaduscidin**
HPLC	**High Pressure Liquid Chromatography**
MIC	**Minimal Inhibitory Concentration**
NMR	**Nuclear Magnetic Resonance**
PAS	**Principal Axis System**
POPC	**1-palmitoyl-2-oleoyl-sn-glycero-3-phosphocholine**
POPE	**1-palmitoyl-2-oleoyl-sn-glycero-3-phosphoethanolamine**
POPG	**1-palmitoyl-2-oleoyl-sn-glycero-3-phospho-(1'-rac-glycerol)**
ppm	**Parts per million**
T_2^{qe}	**Quadrupole Echo Decay**

Chapter 1

Introduction

Antimicrobial peptides (AMPs) are an integral component of many organisms' innate immune systems. To help overcome the problem of antimicrobial resistance, AMPs are currently being considered as potential alternatives for conventional antibiotics. AMPs interact with cell membranes as a part of their mechanism [1, 2]. AMPs can perturb membrane organization in many different ways depending on the properties of a peptide as well as on the nature of the membrane [3]. The main focus of this study was to investigate the interactions of Gad peptides, which are histidine-rich AMPs, with model membranes at different pH values. This chapter starts with the introduction of biological and model membranes and goes on with the description of structure, properties, and modes of action of AMPs.

1.1 Biological and model membranes

Membranes are barriers which give cells their outer boundary (plasma membrane) and inner compartments (organelles). More than just a covering, biological membranes play a fundamental role in many cellular processes. Membranes are selectively permeabale and able to regulate what enters and exits the cell. Cell membranes mainly consist of three components: lipids, proteins, and carbohydrates. All membranes have a common general structure consisting of lipid bilayers with proteins embedded in them [4]. Lipid bilayers are the fundamental components of these membranes formed by a double layer of lipids, with the polar ends pointing outwards and the non-polar ends pointing inwards. A schematic representation of the general membrane structure is shown in Figure 1.1. Membrane lipids are am-

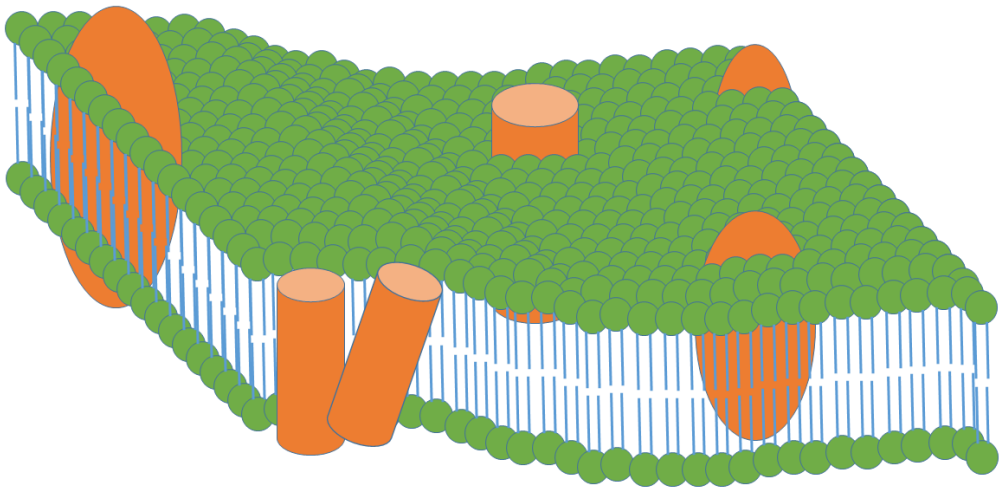

Figure 1.1: A simplified view of membrane structure: lipid bilayer and protein embedded in it. Membrane curvature is also illustrated here.

phiphilic, i.e, they are composed of hydrophilic (water loving/polar) head groups and hydrophobic (water avoiding/non-polar) tails. Depending on their molecular

shapes, lipid molecules form structures of different intrinsic curvature. Quantitatively, the nature of intrinsic curvature of a bilayer composed of single lipid species can be described by the packing parameter (P)

$$P = \frac{V}{L \times A} \tag{1.1}$$

where V is the volume of a lipid molecule, L is the length of a lipid molecule, and A is the cross-sectional area of the lipid head group [5]. The value of P and corresponding intrinsic curvature of lipid bilayers is given in Table 1.1.

Packing parameter	Intrinsic curvature	Lipid
$= 1$	zero	POPC(1-palmitoyl-2-oleoyl-sn-glycero-3-phosphocholine)
< 1	positive	lyso POPC(1-palmitoyl-2-oleoyl-sn-glycero-3-phosphocholine)
> 1	negative	POPE(1-palmitoyl-2-oleoyl-sn-glycero-3-phosphoethanolamine)

Table 1.1: The value of packing parameter determines the nature of intrinsic curvature adopted by a lipid structure. Three possible values of packing parameter and the corresponding intrinsic curvature of a lipid structures are listed.

When the cross-sectional areas of head group and acyl chain are the same, lipids can be represented as a cylinder. Cylindrical lipids pack well in bilayer structures which have zero intrinsic curvature. If a lipid's head group area is larger than its acyl chain area, it will fill a conical space. Conical lipids cluster together in the form micelles with their wider head groups curved around the smaller tails. These micelles have positive intrinsic curvature. On the other hand, if a lipid's head group area is smaller than its acyl chain area, it can be seen as an inverse cone [6]. The inverted conical lipids have a propensity to form inverted micelles with

negative intrinsic curvature. In this case, layers are curved with lipid head groups on the inside of the curve and tail regions on the outside of the curve. Different shapes of individual lipids and corresponding membrane curvature are shown in Figure 1.2.

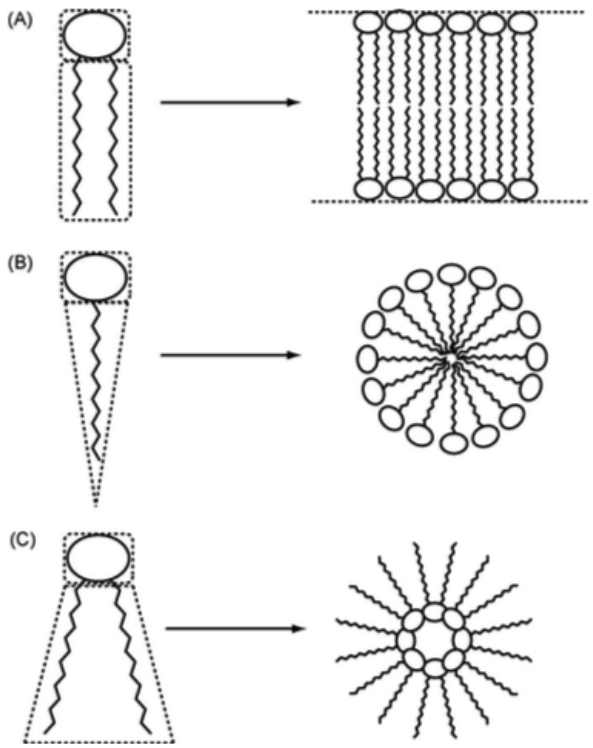

Figure 1.2: The schematic representation of the different shapes of lipid molecules and corresponding membrane assemblies with different intrinsic curvature. This figure is adapted from Haney et al. [6] and reprinted with permission from Elsevier.

Any single membrane can contain hundreds of distinct lipids and the lipid bilayer forms a stable structure in which proteins can work. The lipid compositions of eukaryotic (human, animals, plants, and fungi) and prokaryotic (bacterial) membranes are different from each other. Eukaryotic cell membranes are mainly composed of zwitterionic lipids (they are neutral in charge but contain positive and negative charge separation in the headgroup) while prokaryotic cell membranes have a high proportion of anionic (negatively charged) lipids. Eukaryotic membranes are rich in POPC (1-palmitoyl-2-oleoyl-sn-glycero-3-phosphocholine),

sphingomyelin, and cholesterol, whereas prokaryotic membranes contain POPE (1-palmitoyl-2-oleoyl-sn-glycero-3-phosphoethanolamine), POPG(1-palmitoyl-2-oleoyl-sn-glycero-3-phospho-rac-glycerol), and cardiolipin (1',3'-bis[1,2-dimyristoyl-sn-glycero-3-phospho]-sn-glycerol). The lipid compositions of various bacteria are given in Table 1.2.

Bacterial species	CL(% of total lipids by weight)	PG(% of total lipids by weight)	PE(% of total lipids by weight)
Gram-negative bacteria			
Escherichia coli	5	15	80
Escherichia cloacae	3	21	74
Yersinia kristensenii	20	20	60
Proteus mirabilis	5	10	80
Klebsiella pneumoniae	6	5	82
Pseudomonas aeruginosa	11	21	60
Gram-positive bacteria			
S*taphylococcus aureus*	42	58	0
Streptococcus pneumonia	50	50	0
Bacillus cereus	17	43	40
Bacillus polymyxa	8	3	60

Table 1.2: The lipid composition of various Gram-positive and Gram-negative bacteria. Table is adapted from Wang et. al [7] and reused with permission from Elsevier.

Biological membranes are very complex in nature but model membranes, which are composed of synthetic lipids, can be used to mimic the essential components of cell membranes. Such model membranes can be composed entirely of one type

of lipid or of a mixture of lipids, and poly-peptides can be added to them to study lipid-protein interactions and their effects on protein function [8, 9].

1.2 Antimicrobial peptides (AMPs)

1.2.1 AMPs background

AMPs are an integral component of the innate immune system and interact with the membrane as a part of their mechanism. They are naturally produced by various organisms, including humans, invertebrate animals, plants, and microbes. For example, frog skin is a source of more than 300 different AMPs [10–15]. These AMPs form the first line of defense against invading pathogens and can have a broad spectrum of activity against bacteria, viruses, fungi, parasites, and sometimes against cancer cells. Based on their target, AMPs can be categorized as antibacterial, antivirus, antifungal, antiparasite, and anticancer peptides. Generally, AMPs consist of ∼10-50 amino acid residues and are very diverse in sequence. This diversity reflects the adaptation of AMPs to act specifically against particular microbial membrane compositions. In spite of this diversity, most AMPs have certain features in common: positive charge and hydrophobicity. The overall positive charge derives from the presence of arginine, lysine, and histidine. A significant proportion of AMP amino acid residues, such as alanine, valine, and leucine, are hydrophobic/non-polar. These features make AMPs well suited to interact with membranes, via both the hydrophilic head groups and hydrophobic core [10, 13, 16–18]. A structural feature common to most AMPs is that they are unstructured in aqueous solution and adopt an amphipathic secondary structure (separate hydrophobic and hydrophilic patches) upon interaction with the membrane [13, 15, 16, 18]. Based on their secondary structure, AMPs can be

divided into different groups. The largest group corresponds to α-helical peptides. The second group consists of AMPs which make stable β-sheets upon interacting with membranes and may contain disulphide bonds. The third group represents extended AMPs which are predominately rich in specific amino acid such as proline, histidine, and arginine. These AMPs may not have any regular secondary structure elements. The fourth group corresponds to AMPs which adopt a loop formation with one disulfide bond [18–20]. Examples of different AMPs, along with their sources of origin, charge, secondary structure, and activity are given in Table 1.3. In addition to the direct killing of microbes, some AMPs also protect the host from pathogen attack by modulating the immune system [11, 13, 21]. Immunomodulatory AMPs do not target the pathogen directly, but rather selectively enhance and/or alter the host defense mechanisms. Some AMPs that combine antimicrobial properties and innate immune modularity function, are called host defense peptides [10, 13, 21].

Table 1.3

AMP	Charge at neutral pH	Origin	Structure	Activity	References
Cecropin-A	+6	Insect, Animal	α- helix	anti-bacterial, anti-fungal	[16, 18, 22, 23]
Magainin	+3	Frog	α- helix	anti-bacterial, anti-virus, anti-fungal, anti-cancer, wound healing	[16, 18, 20, 22–24]
Dermaseptin-B2	+4	Frog	α- helix	anti-bacterial, anti-fungal, anti-cancer	[16, 18, 22, 23]
Clavanin-A	+1	Invertebrate	α- helix	anti-bacterial	[16, 22]
Styelin-A	+5	Sea squirt	α- helix	anti-bacterial	[16, 22]
Pleurocidin	+4	Fish	α- helix	anti-bacterial	[16, 22]
Moronecidin	+3	Fish	α- helix	anti-bacterial	[16, 22]
LL-37	+6	Human	α- helix	anti-bacterial, anti-parasite, anti-biofilm	[16, 18, 20, 22]

Table 1.3 continued

AMP	Charge at neutral pH	Origin	Structure	Activity	References
Melittin	+6	Honey bee	α- helix	anti-bacterial, anti-virus, anti-fungal, anti-parasite, anti-HIV, anti-cancer	[16, 20, 22, 24]
MSI-78	+3	Analogue of Magainin	α- helix	anti-bacterial, anti-fungal, anti-parasite, wound healing, anti-malarian, immunomodulatory	[16, 20, 22]
Alamethicin	-1	Fungi	α- helix	anti-bacterial, anti-fungal	[16, 20, 22]
Indolicidin	+4	Bovine	β turn	anti-bacterial, anti-virus, anti-fungal, anti-HIV	[16, 18, 22, 23]
Protegrin-1	+7	Pig	β- sheet	anti-bacterial, anti-fungal, anti-HIV	[16, 18, 22]

Table 1.3 continued

AMP	Charge at neutral pH	Origin	Structure	Activity	References
Spepherin-I	0	Plants	random coil	anti-bacterial, anti-fungal	[16, 22]
Spepherin-II	0	Plants	random coil	anti-bacterial, anti-fungal, anti-virus, anti-HIV	[16, 22]
Hepcidin	+2	Fish, Animal	β- sheet	anti-bacterial	[16, 22]
Bactenecin	+4	Bovine	loop	anti-bacterial, wound healing	[16, 22, 23]
Lactoferricin	+10	Human	Loop	anti-bacterial, anti-cancer, anti-biofilm	[16, 22, 24]
α-defensins	+2	Human	β sheet	anti-virus, anti-fungal	[16, 18, 22]
β-defensins	0	Human	β sheet	anti-bacterial, anti-fungal	[16, 18, 22]
Piscidin-1	+3	Fish	α- helix	anti-bacterial, anti-virus, anti-fungal	[16, 22]

Table 1.3 continued

AMP	Charge at neutral pH	Origin	Structure	Activity	References
Omiganan	+4	Indolicidin derivative	β sheet	anti-bacterial, anti-biofilm, imuunomodula-tory	[16, 22]
Gad-1	+3	Fish	α-helix	anti-bacterial	[25, 26]
Gad-2	+1	Fish	α-helix	anti-bacterial	[25, 26]
Aurein 1.2	+1	Frog	α-helix	anti-bacterial, anti-viral, anti-fungal, anti-HIV, anti-cancer	[22]
Citropin 1.1	+2	Frog	α-helix	anti-bacterial, anti-fungal, anti-biofilm, anti-cancer	[22]
Maculatin	+1	Frog	α-helix	anti-bacterial, anti-fungal, anti-HIV, anti-cancer	[22]

Table 1.3 continued					
AMP	Charge at neutral pH	Origin	Structure	Activity	References
Caerin	+1	Frog	α-helix	anti-bacterial, anti-viral, anti-parasitic, anti-HIV, anti-cancer	[22]

Table 1.3: AMPs from different sources with their known charge, secondary structure, and activity.

1.2.2 Antibiotic-resistance and AMPs

AMPs have gained attention because they can be effective against pathogens which are resistant to conventional antibiotics. Their mechanism of action is different from conventional antibiotics, which makes them less likely to induce resistance.

1.2.2.1 Antibiotic-resistance: a growing concern

Conventional antibiotics are losing their ability to treat bacterial infections. This has resulted in the emergence of multi-drug resistant bacteria. Accordingly, there is a continuous search to overcome or control such problems. Due to their unique mode of action, AMPs are potential alternatives to traditional antibiotics for tackling the issue of bacterial multi-drug resistance.

Drug resistance is a capacity of bacteria to evade antibiotic attack. Resistance can be seen as a two-component mechanism: (i) an antibiotic which kills susceptible organisms and leaves resistant ones, and (ii) a resistant component in the organism. Antibiotic resistance occurs when these two components come together in a host. Although antibiotic resistance evolves with time, over-prescribing, insufficient doses, and insufficient duration of treatment all are contributing factors. The concerning factor about this resistance problem is that once it is acquired it can not be easily abolished [11, 27–29]. A report titled "Antibiotic Threats in the United States 2013" prepared by the Centers for Disease Control and Prevention gives an idea of the burden to public health posed by this drug resistance problem. According to this report, at least 2 million people become infected with bacteria that are resistant to antibiotics and at least 23,000 people die each year as a direct result of these infections in the United States alone. Many more people die from other conditions that were complicated by antibiotic-resistant infections because doctors have run out of drugs to treat these infections [30]. Several studies have examined the costs of antibiotic resistance. According to the U.S. Center for Disease Control and Prevention (CDC), the treatment of antibiotic-resistant infections costs $35 billion and 8 million hospital days per year in the United States [31]. Antibiotic resistant infections increase the duration of hospital stays and the mortality and morbidity rates as compared to drug-susceptible infections [32, 33].

1.2.2.2 AMPs: a natural alternative to conventional antibiotics

Given their broad spectrum of activity and lower propensity to induce resistance, AMPs provide an excellent starting point for the development of therapeutics with a novel mechanism of action. The cationic nature of AMPs makes them specific to negatively charged bacterial membranes. AMPs act by breaking the bacterial cell membrane integrity since it is not easy for bacteria to function with

a highly altered membrane composition and the risk of developing resistance is very low. On the other hand, conventional antibiotics have specific targets which allow bacteria to develop mechanisms to avoid antibiotic damage.

Moreover, cationic and amphipathic peptides seem to be perfect molecular structures to achieve a maximum number of interactions with the membrane [34, 35]. Drugs designed to mimic them can have extensive medical applications. AMPs can be used individually or in combination with other antibiotics to control multi-drug resistance problem [10, 36]. In addition to killing isolated bacteria, AMPs have the potential to work against biofilms. Biofilms are immobile bacterial populations attached to surfaces such as human tissues and medical implants. Currently, biofilms are a serious threat in hospitals and medical facilities. The United States National Institute of Health found that 80% of chronic infections are related to biofilm formation and more than $3 billion is spent to treat implant-associated biofilm infections in the United States alone [37]. Biofilms are highly resistant to conventional antibiotics due to multiple tolerance mechanisms. On the other hand, it has been found that AMPs can destroy these multilayered communities of bacteria. The AMP mechanism against biofilms may involve the degradation of the membrane potential of biofilm embedded cells, interruption of bacterial cell signaling systems, degradation of the polysaccharide and biofilm matrix, downregulation of genes responsible for biofilm formation and transportation of binding proteins [38]. Lactoferrin, LL-37, and human cathelicidin are examples of AMPs which are effective against biofilms [23, 37, 39].

1.2.3 Challenges in developing AMPs as therapeutics

Using the chemical structure of naturally occurring AMPs as the basis for synthetic drugs provides a promising strategy to fight against antibiotic-resistant pathogens.

So far success has been achieved in the development of AMP therapeutics for topical use only. The use of AMP-based drugs for systemic use is reduced by the level of toxicity associated with them. In other words, even though AMPs are more specific towards bacterial membranes, the concentration at which they are able to kill bacteria is still very toxic to host cells. Another hurdle in the commercialization of AMPs is their high cost of manufacturing. This has limited the development and testing of AMPs as therapeutics.

The bottleneck of these disadvantages lies in our incomplete understanding of the selectivity of natural AMP sequences towards different microbes. To overcome these difficulties, it is critical to understand how AMPs interact with cells and disrupt them. Detailed knowledge of AMP mechanisms will help to decipher the structure-activity relationships and support the identification of essential components of AMP sequences with possible sites of substitution. Altogether, this will help researchers to design short, compositionally simple, and potent AMPs [36, 40, 41].

1.2.4 Understanding the mechanism of action of AMPs

The conventional understanding of AMP mechanisms centers around their ability to disrupt the bacterial membrane [19, 37, 42]. This results in the leakage of cell contents, or possibly transport of the peptide into the cell. After translocating, the peptide can have contact with intracellular components [43]. The methods by which AMPs traverse/permeabilize the membrane are not common to all peptides. They depend on the properties of the peptide (amino acid sequence, charge, and conformation) and on the target membrane composition. AMPs are thought to display specificity for bacterial cells over host cells due to the difference in the cell membrane compositions [26].

1.2.4.1 Molecular basis of the AMP selectivity

The cationic nature of AMPs contributes to cell selectivity. The main driving forces in the binding of AMPs to cell membranes are hydrophobic interactions (between the non-polar amino acids of AMPs and the hydrophobic core of the membrane) and electrostatic interactions (between cationic AMPs and the anionic lipids of the membrane). The bacterial membrane is composed of a phospholipid bilayer with a high proportion of anionic lipids which results in strong electrostatic interactions between AMPs and bacterial membranes. On the other hand, in eukaryotic cells, such as human cells, the membrane is abundant in zwitterionic lipids. There are hydrophobic and electrostatic forces (between cationic AMPs and head groups of zwitterionic lipids) between AMPs and host membranes but these are weaker in comparison to the forces between AMPs and bacterial membranes as shown in Figure 1.3. It is thus the higher anionic lipid content of bacterial membranes that make them more vulnerable to AMPs. Upon interacting with bacterial membrane, AMPs can achieve antimicrobial activity in many different ways as explained below.

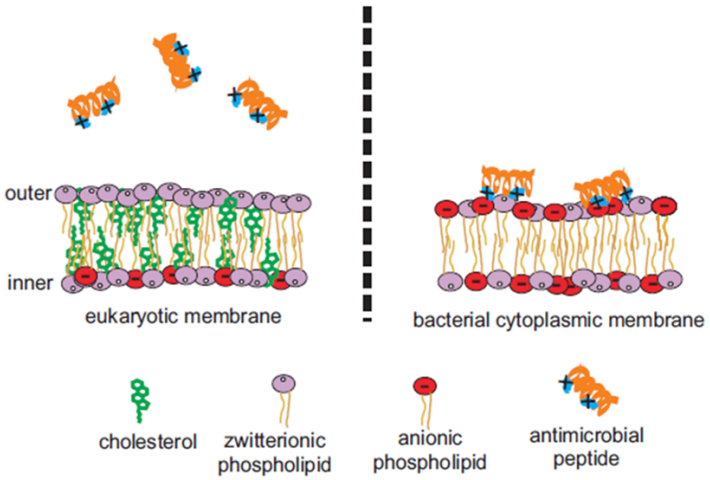

Figure 1.3: Membrane selectivity by AMPs on the basis of lipid composition of the membrane. This figure is reproduced with the permission of Dr. Michael Morrow.

1.2.4.2 Pore forming mechanisms

The precise details of AMP action are not fully understood yet but their interactions with bacterial membrane appear to be the first steps in their antimicrobial activity. There are several basic models which might explain the increase in membrane permeability as a result of peptide-induced pores in the lipid bilayer (Figure 1.4). In these models, the interaction starts with adsorption of the peptide to the membrane surface which results in the peptide assuming a specific conformation. The initial interaction of the peptide with the membrane surface, more specifically in the lipid head groups, leads to lateral expansion of the membrane. To reduce the tension imposed on the lipid bilayer by the peptide, the membrane can respond in several ways each of which results in transmembrane pores in the lipid bilayer [44].

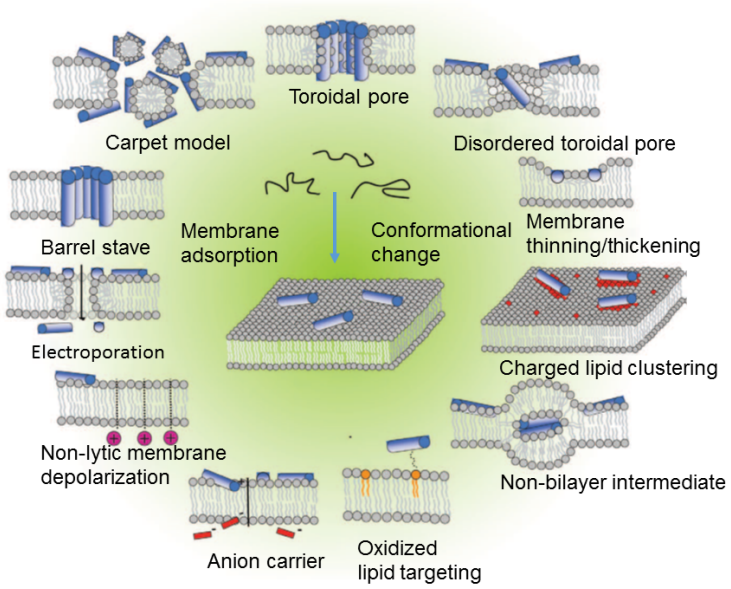

Figure 1.4: The antimicrobial activity of AMPs to kill bacteria lies in their ability to disrupt the membrane integrity which can be achieved in a number of ways. The initial membrane-peptide interaction can be followed by many different membrane disruptive events. A peptide can work via a single mechanism or it can have multiple mechanisms. This figure is from Nguyen et al. [16] and reprinted with permission from Elsevier.

(i) Barrel stave model

The barrel stave model was the first model proposed to describe the formation of transmembrane channels/pores by bundles of amphipathic α helical peptides [2, 35, 45, 46]. Firstly, the peptide adopts an amphipathic conformation upon interacting with the membrane and then the peptides interact laterally with one another to form a large structure. Next, the peptide bundle inserts into the membrane such that the peptide hydrophobic surfaces interact with the lipid core of the membrane and their hydrophilic surfaces point inward producing an aqueous pore. This allows for minimal exposure of the hydrophilic residues of AMP to the hydrophobic tails of the lipids. This model explains the formation of transmembrane pores by direct insertion of the peptide into the membrane core through peptide-peptide interactions. The addition of more peptide molecules may result

in the formation of extra pores or it may increase the size of the existing pore. This pore formation leads to the leakage of cell contents which ultimately results in cell death. Neutron diffraction and X-ray scattering have shown that Alamethicin works via the barrel stave model [16, 17, 19, 37, 43, 44, 47–49]. To date, it is the only AMP known to work via this mechanism.

(ii) Toroidal pore model

In this model, the peptides are initially attracted to the membrane and undergo similar secondary structural changes as for the barrel stave model [2, 35, 45, 46]. In contrast, to the barrel stave, peptide-peptide interactions are not present. Instead, the peptide changes the membrane curvature by bending the lipid monolayers to connect the inner and outer surfaces into a continuous channel. Neutron in-plane scattering and Molecular dynamics (MD) simulations have shown that the AMPs Magainin 2, Melittin, and Protegrin make pores by toroidal model [16, 17, 19, 37, 43, 44, 49–51].

(iii) Disordered toroidal pore model

The MD simulations have shown that the toroidal pores formed by AMPs involve a significant disorder [52]. In the disordered toroidal model, a toroidal shaped pore is formed by one or more α-helical or β-sheet peptide that inserts into the membrane due to the tension induced by the peptide in the membrane [45]. Above a threshold number of membrane-bound peptides, one peptide molecule becomes deeply embedded into the membrane and the membrane-water interface becomes unstable. This results in the interaction of solvent molecules with the hydrophilic part of the embedded peptide to make a continuous pore. In contrast to the classical toroidal pore model, in this model, only one peptide needs to be near the center of the pore and the remaining peptide molecules lie near the edge of the pore. The resulting pore is sufficient to allow the passage of peptides from one side of the membrane to another.

(iv) Carpet model

In this model, peptide molecules orient themselves parallel to the membrane surface and cover the membrane surface with their hydrophobic faces toward the interior of the membrane and hydrophilic faces toward the head groups [2, 35, 45, 46]. The accumulation of peptide on the membrane surface induces tension in two leaflets of the lipid bilayer. Above the threshold concentration, this strain results in the disintegration of the membrane. MD simulations, vesicle leakage, and atomic force microscopy (AFM) have shown that the peptides Dermaseptin, Citropin 1.1, Aurein, and Cecropin disrupt bacterial membrane in a manner consistent with the carpet model [53–55]. This model suggests that the peptide mechanism could be concentration dependent. For example, below a threshold concentration, the peptide might make transmembrane pores, while concentrations above the threshold might result in the complete fragmentation of the membrane. Also for the carpet model, specific peptide-peptide interactions are not essential [56]. A particular AMP might function by more than one mechanism, depending on parameters such as peptide to lipid ratio [16, 17, 19, 37, 43, 44, 49].

1.2.4.3 Non-pore forming mechanisms

In addition to the pore forming mechanisms described above, AMPs might disrupt the bacterial membrane in other ways which do not result in pore formation. It has been reported that AMPs can induce membrane thinning/thickening and non-lamellar lipid phases [6]. Depending on the membrane composition, AMPs can induce positive and negative curvature which leads to redistribution of lipids. In some cases, the presence of peptide leads to the formation of domains of charged lipid clusters surrounding the peptide [57]. The migration of charged lipids towards cationic AMPs might result in the weak attachment of surface proteins to the re-organized membrane, causing protein delocalization and loss of function

[58]. Also, adsorption of the peptide in the outer leaflet of the membrane might increase the membrane potential and restrict the permeability of the membrane to many molecules. The peptide might interact with anions across the lipid bilayer and result in their leakage from the membrane [16]. All these mechanisms are schematically shown in Figure 1.4.

Besides the ability to make changes to the cell membrane, the peptide might have intracellular targets as well. Regardless of which model is correct for peptide-induced disruption in the membrane, they all provide a means for AMPs to cross the membrane. After crossing the membrane, a peptide might target many cellular components to achieve antimicrobial activity. Examples of an intracellular activity include inhibition of protein synthesis, DNA synthesis, inhibition of enzymatic activity, and inhibition of cell wall synthesis [37, 43, 59]. It is noted that in both pore/non-pore forming mechanisms the interactions of the peptide with cell membrane are very important as in each case peptide needs to permeabilize the membrane. Furthermore, one peptide can act via multiple mechanisms which makes the peptide less likely to induce resistance against bacteria.

Different methods can be used to study the membrane-peptide interactions with each method giving a different level of information about the mechanism of AMPs. The ability of AMPs to permeabilize the lipid membranes can be studied by the release of internal fluorescent-labelled probes [60]. The orientation of a peptide in the membrane can be examined using solid-state NMR spectroscopy [60, 61]. Neutron scattering/diffraction and atomic force microscopy are useful techniques to study the pore formation by AMPs in the membrane [62]. X-ray scattering can be used to study the membrane thinning/thickening induced by a peptide in the membrane [63]. Thermodynamics of lipid phase transitions can be studied using differential scanning calorimetry (DSC). Peptide-induced phase transitions and peptide aggregation at the membrane surface can be studied by isothermal

titration calorimetry (ITC) [61]. Molecular dynamics simulations are also a useful technique to study peptide interactions with lipid membranes [64]. These methods can be used alone or in combination to study the peptide-membrane interactions.

1.2.4.4 Describing membrane-peptide interactions with a phase diagram

Membrane-peptide interactions are very complex and diverse in nature. Due to these interactions, membranes may experience many structural changes as described by the pore and non-pore mechanisms. Different peptides may utilize different interaction mechanisms or a combination of mechanisms. Furthermore, the mechanism of interaction might change depending upon peptide concentration and membrane composition. The complexity of membrane-peptide interactions can be explained with a phase diagram [65–67] as shown in Figure 1.5(a). The different models of membrane disruption by AMPs could be different regions in this phase diagram. The phase boundaries are illustrated as a function of membrane-bound peptide concentration and lipid composition from POPC to POPE. The vertical arrow in Figure 1.5 (b) indicates that the phase observed depends on lipid to peptide ratio. At lower lipid to peptide ratio, peptide might disrupt the membrane by making toroidal pores, while at a higher lipid to peptide ratio, membrane disruption can occur by the carpet model. The effect of replacing POPC lipid with POPE lipid to mimic the bacterial membrane composition is indicated by the horizontal arrow. The horizontal arrow indicates that the size of the lipid head group can have an effect on the lipid structures induced by the AMP. For a given lipid to peptide ratio, the more POPE that is in the bilayer the more likely, the membrane will take on the “wormhole” structure.

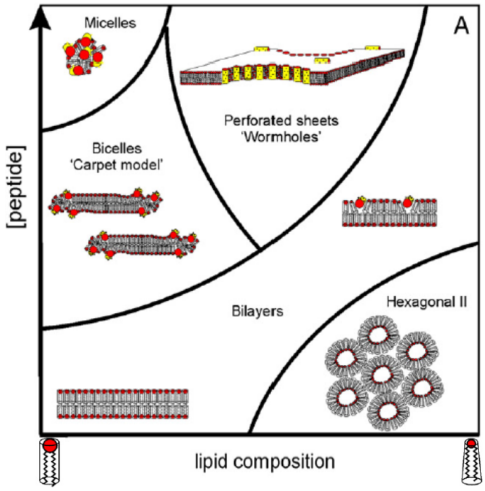

(a)

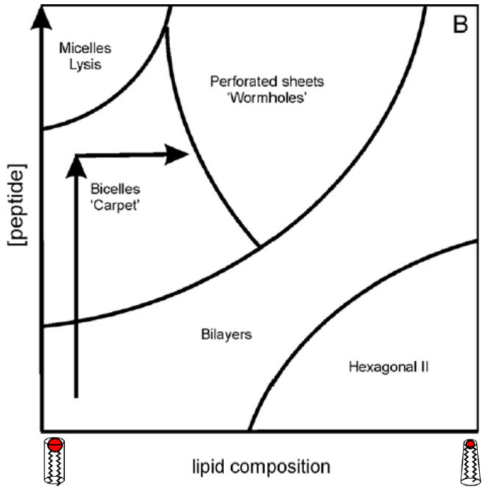

(b)

Figure 1.5: The phase diagrams of lipid-peptide mixtures as a function of membrane-bound peptide and membrane composition to depict the ability of a peptide to disrupt the lipid bilayer integrity. (a) Different models that have been suggested to explain the pore formation by the peptide in the membrane are shown. (b) The illustration that the observed phase depends on the lipid to peptide ratio as indicated by the vertical arrow. Furthermore, the horizontal arrow shows that the size of the lipid head group can have an effect on the lipid structures induced by the AMP. For a given lipid to peptide ratio, the more POPE that is in the bilayer the more likely the membrane will take on the "wormhole" structure. This figure is adapted from Burkhard Bechinger et al. [65] and reprinted with permission from Elsevier.

1.2.4.5 Interfacial activity model

The interfacial activity model describes the ability of a peptide to bind to a membrane and induce local rearrangements of lipids. In all the models explained in Section 1.2.4.2 and 1.2.4.3, AMPs permeabilize the membrane and perturb the bilayer integrity to achieve antimicrobial activity. According to interfacial activity model [35], the peptide-induced destabilization of the membrane does not depend on specific amino acid sequences or specific peptide secondary structure. It does depend on the amino acid composition and physical-chemical properties of the peptide. The cationic nature and amphipathicity of AMPs result in their broad spectrum of activity but perfect amphipathicity is not essential. Instead, imperfect amphipathicity is necessary for interfacial activity. Also, it is not the net charge alone that determines the membrane permeabilizing ability of a peptide but also its charge distribution [68]. The exact spatial arrangement of hydrophobic and polar residues in the AMP is not important. Instead, the physical-chemical balance between these two properties helps position the peptide inside the membrane. When a peptide with an appropriate distribution of polar and non-polar groups binds to the membrane, the hydrophobic groups partition deep into the interfacial (hydrophobic) zone while polar residues of peptide interact with lipid polar head groups and push them deep in the membrane. This might lead to the membrane translocation of peptide even at low peptide concentration, while high peptide concentration may result in the formation of pores [35].

1.2.5 Antimicrobial to anticancer peptides: histidine-rich AMPs

Cancer is caused by the abnormal cell growth in an uncontrolled manner. Chemotherapy and radiation are the usual methods to treat cancer. These methods have only

partial success rates, in large part due to their lack of specificity [69]. They target rapidly dividing cells with relatively small discrimination between the cancer cells and the normal proliferating cells. Moreover, cancer cells can develop resistance to anticancer agents and pump drug out from the cell. To control the mortality and morbidity rate due to cancer, it is necessary to develop more efficient and selective anti-cancer therapeutics that can be used in place of or in combination with conventional anti-cancer therapeutics.

Cationic AMPs are under consideration as alternative chemotherapeutic agents due to their selective toxicity towards cancer cells, ability to avoid resistance and additive effects in combination therapy [70, 71]. AMPs have been primarily studied to develop new therapeutics to fight various infections but it has been reported that certain AMPs like Cecropin A, Cecropin B, BMAP-27, BMAP-28, LL-37, Magainin, Melittin, Defensins, Lactoferricin, Tachyplesin, Buforin II, and Buforin IIb, have the ability to kill cancer cells. The cancer cell membranes are different from normal cells in many ways. Firstly, cancer cell membranes have an anionic character that is similar to bacterial membranes. For this reason, electrostatic interactions might be the core of the selectivity mechanism of AMPs towards cancer cells instead of normal cells. Another major difference between cancer and normal cells is their acidic environment. The pH level of the extracellular space surrounding solid tumors is significantly lower than the pH around normal cells. Therefore, many attempts have been made to develop new pH-dependent anti-cancer therapies which can be active in the lower pH space of solid tumors [72]. There are few AMPs (Histatin, Clavanin, and Chrysophsin, LAH4) which have histidine residues in their sequences. These histidine-rich AMPs are potentially pH sensitive and have an ability to become more active at acidic pH values, as histidine side chain has a pK_a value of 6. Thus at neutral pH its side chain is uncharged but at acidic pH values, it has charge of +1. So the presence of histidine

can make the overall charge of a peptide sensitive to pH which, in turn, can affect the peptide-membrane interaction [73]. Furthermore, cancer cell membranes are more fluid than healthy cells. This might help AMPs to cause destabilization of the cell membrane. In addition to this, cancer cells have a larger surface area than normal cells and this can result in AMP-mediated cytotoxicity due to larger numbers of AMP molecules interacting with the membrane [74].

Even though AMPs are expected to be selective towards cancer cells without reduced toxicity to normal body cells, the development of AMP-based anti-cancer drugs is very challenging because their selectivity is poorly understood and it is not possible to predict the anti-cancer activity based on AMP structure. A detailed knowledge of membrane-peptide interactions is needed in order to use AMPs as anticancer drugs [69].

1.2.5.1 Gad peptides

Gad peptides, Gad-1 and Gad-2, belong to the Piscidin family of AMP from fish. Piscidins fight against various pathogens in aquatic environments as part of the innate immune system [25]. Gad peptides are found in Atlantic cod (*Gadus morhua*) and are paralogs (coded by related genes). Gad-1 and Gad-2 are 21 and 19 residues long respectively and have tendencies to form α helical structure in a membrane environment [26]. The primary amino acid sequences of C-terminus amidated Gad peptides are:

Gad-1:FIHHIIGWISHGVRAIHRAIH-NH_2

Gad-2:FLHHIVGLIHHGLSLFGDR-NH_2

Gad peptides are natural histidine-rich peptides. Gad-1 has 5 histidines and Gad-2 has 4. The charge of Gad peptides at pH 7.0 and pH 5.0 is listed in Table 1.4.

peptide	pH 7.0	pH 5.0
Gad-1	+3	+8
Gad-2	+1	+5

Table 1.4: Expected overall peptide charge of Gad-1 and Gad-2 at pH 7.0 and pH 5.0.

There are other histidine-rich peptides such as LAH4 that are artificial, as opposed to the Gads which are sequences found in nature. Gad peptides provide a means to understand how nature tunes a peptide's pH-dependent activity. It has been shown that there is a relationship between the pH sensitivity of antimicrobial activity and the number of histidine residues present in the sequence of a peptide [75–77]. In order to test their pH sensitivity, MIC assay experiments with *E.coli* were done in the presence of Gad-1 and Gad-2 at pH 7.0 and pH 5.0 shown in Figure 1.6. MIC stands for Minimal Inhibitory Concentration and it represents the minimum concentration of peptide that is sufficient to stop bacterial growth. For Gad-1, MIC of 5.1 μM (12.5 μg/mL) was found in 4 out of 6 repeated experiments at pH 5, and in 5 out of 6 experiments at pH 7. For Gad-2, MIC of 11.5 μM (25 μg/mL) was found in 4 out of 6 experiments at pH 5, but the MIC found was greater than 23.0 μM (50 μg/mL) in 4 out of 6 experiments at neutral pH. This is interesting considering that Gad-1 has five histidine residues and Gad-2 only four. At both pHs, Gad-1 was more active than Gad-2 [26].

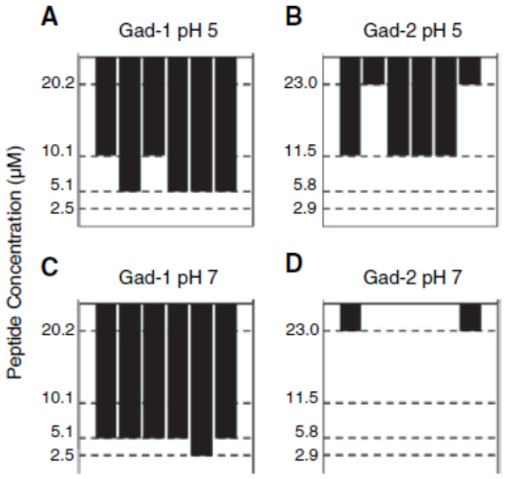

Figure 1.6: Minimal Inhibitory Concentration (MIC) results for Gad-1 and Gad-2 at pH 7.0 and pH 5.0. Each bar represents one of six replicate experiments and the length of the bars indicates the minimum peptide concentration required to inhibit bacterial growth. No bar indicates an MIC greater than 50 μg/mL (20.2 μM for Gad-1 and 23.0 μM for Gad-2). This figure is taken from McDonald et al. [26] and reprinted with permission from Elsevier.

1.2.6 Model membrane studies

To fully understand the mechanism of membrane destabilization by AMPs, it is important to elucidate how membrane properties are affected by the binding of AMPs. Biological membranes are complex and heterogeneous structures composed of hundreds of lipids and proteins. The direct analysis of peptide interactions with real cellular membranes is difficult. For that reason, simple model lipid membranes are commonly used to understand the role of membrane lipids in the membrane-peptide interactions.

AMP interactions with model membranes composed of zwitterionic and anionic

lipids had been investigated for different peptides. AMPs such as Magainin 1, Aurein 1.2, Citropin 1.1, Maculatin 1.1, Caerin 1.1, Dermaseptins, Cecropins, Cathelicidins, Protegrins, Defensins, Temporins and two hybrid peptides of Cecropin A and Melittin (CA(1−8)M(1−18) and CA(1−7)M(2−9)), had shown higher affinities for model membranes composed of DMPG lipids than with DMPC membranes [78–80]. These results suggest that electrostatic interactions might be responsible for the initial attraction of the peptide on the membrane surface. In addition to this, it was also found that membrane-peptide interactions do not depend only on the charge of lipid but also on the head group structure [78]. In model membranes, peptides were shown to disrupt the bilayer integrity by inducing non-lamellar lipid phases. MSI-78, Tritrpticin, Indolicidin, LL-37, and bovine Lactoferricin were shown to induce positive membrane curvature in the membranes composed of POPE lipids [6]. AMP-induced structures and dynamics of lipid assemblies were investigated in model membranes using solid-state NMR spectroscopy. ^{2}H and ^{31}P solid-state NMR spectra revealed that Magainin-2 and Aurein-3.3 peptides induce pores and bilayer thinning in oriented lipid bilayers of POPC and POPG [81]. Melittin and CEME (Cercropin and Melittin hybrid) peptides intercalate into model lipid membranes and induce expansion of the outer leaflet of the lipid bilayer [82]. PG-1 peptide makes toroidal pores in anionic model lipid membranes. The mutation of charged residues of PG-1 results in changes in the peptide-membrane binding underlining the importance of charged residues [41].

To gain further insight into the interactions of AMPs with membranes, the angle (transmembrane, parallel, or in between) of the peptide in model membranes has been studied by solid-state NMR spectroscopy. It has been shown that peptides in transmembrane orientation induce less disorder in the membrane than when the peptide is oriented parallel to membrane surface [83]. The ^{15}N chemical shift shows that Alamethicin adopts a transmembrane orientation in POPC/POPG

lipid bilayers [84], while Magainin 2, aligns parallel to membrane surface [85].

The pH-sensitive antimicrobial activity of the synthetic histidine-rich AMPs LAH4 has been studied in model membranes. At neutral pH, the membrane disruption is weak, but at acidic pH, the disruption of lipid acyl chains in the presence of peptide is more drastic [75].

1.3 Current AMP research questions and objective of present work

Although AMPs provide a promising alternative for conventional antibiotics to treat various infections, there are only a few success stories. The poor understanding of their selectivity is a major obstacle in the development of injectable AMPs. To improve AMP-drug design, it is essential to know which properties of natural AMP sequences make them selective to different microbe membrane compositions and how membrane properties are affected by the addition of AMPs.

One way to understand the selectivity of AMPs is to modify their overall charge and study the effect on peptide-membrane interactions. Gad peptides are histidine-rich peptides and provide a means to tune the peptide charge by changing the pH. This pH-dependent activity will help us to understand the role of electrostatic interactions in AMP selectivity which will further improve our knowledge about AMP-membrane interactions. The change in pH from 7.0 to 5.0 is not expected to alter the membrane charge as the pKa values of lipids used in this work, POPE, POPC, and POPG are between 2-3 [86]. In addition to understanding the pH-dependent membrane interaction of Gad peptides, we are also interested in studying differences between the activities of Gad-1 and Gad-2 in response to pH alterations. As Gad peptides are encoded by paralogous genes i.e. related

genes, their activity might be specific to different pathogens. This study will help us to understand how specificity is tuned to different pathogens in natural AMP sequences. This knowledge may help to improve AMPs' therapeutic ratios, a comparison of the amount of a therapeutic agent that causes the therapeutic effect to the amount that causes toxicity.

The main objective of this thesis is to study the interactions of Gad peptides with model membranes at different pH values. This thesis is organized in the following way: Chapter 1 provides the background of membranes and AMPs. Chapter 2 describes of the biophysical methods used in this work. It starts with the description of NMR theory with a focus on ^{2}H NMR and goes on with the explanation of zeta potential and circular dichroism spectroscopy. The first part of Chapter 3 describes the abilities of Gad peptides to perturb the bilayer integrity of vesicle model membranes at different pH values. In addition to this, the effect of Gad peptides on fast and slow motions of lipid bilayers are also discussed. The second part of this chapter is focused on the zeta potential measurements which provide a link between binding affinities and membrane disruption abilities of Gad peptides at different pH values. In order to better understand the interaction of Gad peptides with membranes and how differences in peptide-membrane interaction might be correlated with differences in function, the alignment of Gad peptides in mechanically oriented lipid bilayers is studied and presented in Chapter 4. An investigation of the effect of the lipid cardiolipin on Gad membrane disruption is given in Chapter 5. Finally, a discussion of results from different experiments is presented in Chapter 6.

Chapter 2

Biophysical methods to study the interactions of AMPs with model membranes

A wide range of biophysical techniques have been used to study the interactions of AMPs with membranes. Some of these techniques, nuclear magnetic resonance (NMR) spectroscopy, zeta potential, and circular dichroism (CD) spectroscopy are described in this chapter. NMR spectroscopy can be used to study peptide-induced disorder in the membrane lipid bilayer, the effect of the peptide on the slow and fast motion of lipid bilayer, and the alignment of the peptide in the membrane. Zeta potential measurements provide information about the binding affinities of peptides. CD spectroscopy can be employed to investigate the secondary structure of a peptide in the membrane environment.

2.1 Nuclear magnetic resonance (NMR) spectroscopy

NMR spectroscopy is based on the magnetic properties of a nucleus. A nucleus with non-zero spin angular momentum also possesses a nuclear magnetic dipole moment. In the absence of the magnetic field, the nuclear magnetic moments do not have any preferred orientation. On the other hand, when an external static magnetic field is applied, the interaction of the nuclear magnetic moment with the magnetic field results in the different orientations (spin states) of magnetic moments with respect to the magnetic field having different energies. The alignment of magnetic moments parallel to the applied magnetic field generates the net magnetization in the direction of field. If nuclear spins are then subjected to another oscillating magnetic field at a particular frequency, a spin can flip from one orientation (spin state) to another, with respect to the static magnetic field. This happens only when the frequency of the oscillating magnetic field matches the energy difference between the two spin states. This is termed as the resonance condition in NMR spectroscopy. Once perturbed from its equilibrium state, the magnetization vector rotates about the applied field and this motion gives rise to the NMR signal.

Solid-state NMR is an excellent tool to study molecular orientation and molecular motion because some nuclear spin interactions are anisotropic, i.e. they depend on the molecular orientation. Hence, the change in the orientation of a molecular segment containing a nuclear spin due to the motion of the molecule affects the resonance frequency of nuclei in a way that changes the shape of the NMR spectrum.

2.1.1 Introduction

2.1.1.1 Equilibrium magnetization and Larmor precession

Nuclear spin is represented by an operator $\hat{I}$ associated with the spin quantum number I. The value of I corresponds to a spin angular momentum which is given by $\hbar\hat{I}$. Nuclei with a certain value of spin angular momentum can be visualized as tiny bar magnets with a magnetic dipole moment [87–89]

$$\hat{\mu} = \gamma\hbar\hat{I} \tag{2.1}$$

where γ is the gyromagnetic ratio of a nucleus. The z component of the magnetic moment is given by

$$\hat{\mu_z} = \gamma\hbar\hat{I}_z. \tag{2.2}$$

In the absence of an external magnetic field, all magnetic moments in a sample are randomly oriented. This results in a net zero magnetic moment. When an external magnetic field is applied, the interaction between the magnetic field and the dipole moment is governed by the Hamiltonian [87–90]

$$\hat{H} = -\hat{\mu} \cdot \vec{B}. \tag{2.3}$$

When the applied magnetic field is in the z direction, this Hamiltonian is becomes

$$\hat{H}_z = -\gamma\hbar\hat{I}_Z B_0. \tag{2.4}$$

The energy eigenvalues corresponding to the above Hamiltonian can be found by using the Schrodinger equation [87–89]

$$H\left|\Psi\right\rangle = E\left|\Psi\right\rangle \tag{2.5}$$

$$\begin{aligned} H_z \left|\Psi\right\rangle &= -\gamma\hbar B_0 I_z \left|\Psi\right\rangle \\ &= -\gamma\hbar B_0 m \left|\Psi\right\rangle \end{aligned} \tag{2.6}$$

where m is the magnetic spin quantum number. Therefore, the energy of the magnetic interaction is given as

$$E_m = -\gamma\hbar m \tag{2.7}$$

and it depends on the spin state of the nucleus. For a spin $\frac{1}{2}$ system, m has two values $\pm\frac{1}{2}$. The energy corresponding to each value of m are

$$E_{m=1/2} = -\frac{1}{2}\hbar\gamma B_0. \tag{2.8}$$

$$E_{m=-1/2} = \frac{1}{2}\hbar\gamma B_0. \tag{2.9}$$

The $m = \frac{1}{2}$ state is lower in energy and corresponds to the parallel orientation of the dipole moment with respect to the external magnetic field. This energy state is represented by α. The $m = -\frac{1}{2}$ state is higher in energy and represents the anti-parallel orientation of the magnetic moment with the applied magnetic field. This energy state is represented by β. Hence, in the presence of an external magnetic field, the degenerate nuclear spin states split into different energy levels according to their alignment with the direction of field. This is called the Zeeman splitting [88–91] and is schematically shown in Figure 2.1 for a spin $\frac{1}{2}$ system. At thermal equilibrium, the relative populations of the states α and β are given by the Boltzmann distribution. According to this distribution, the α state is more populated than the β state [89, 92]. Therefore, in the presence of an external magnetic field, the alignment of magnetic moments in the direction of the field gives rise to the net magnetic moment. Averaged over an entire sample, this net magnetic moment is called the equilibrium magnetization. This is schematically

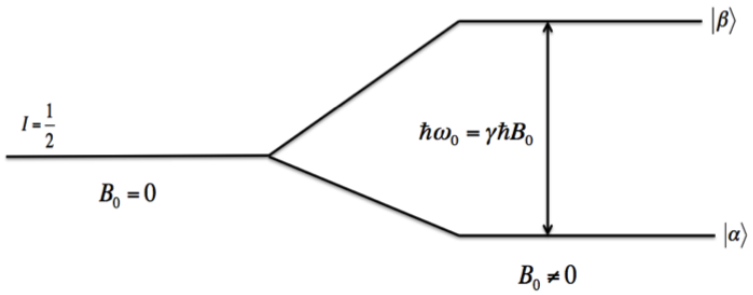

Figure 2.1: The depiction of the Zeeman splitting for spin $\frac{1}{2}$ system. In the presence of the external magnetic field, the degenerate energy states split into two non-degenerate states. The splitting between the two energy states depends on the strength of the external magnetic field.

shown in Figure 2.2. Once the equilibrium magnetization is established, it does

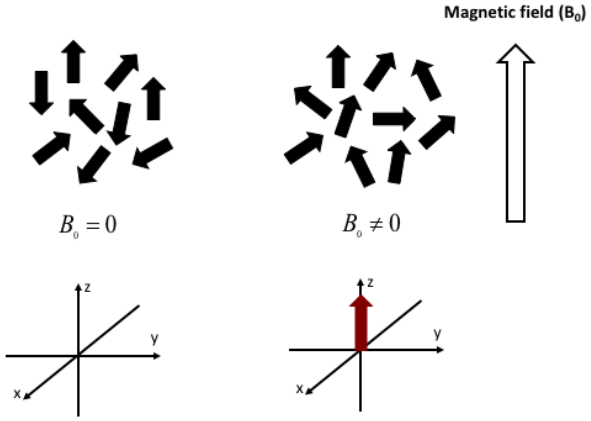

Figure 2.2: In the absence of the external magnetic field, the magnetic moments of the individual spins are randomly oriented. On the other hand, if a magnetic field is applied in the z direction, then there is a slight energy preference for magnetic moments in the direction of the field. This results in a net magnetization in the direction of the field.

not change with time unless perturbed by some torque. This external torque can be provided by an oscillating magnetic field produced by a radio frequency (RF) pulse. Once the magnetization vector moves away from the z axis, it rotates about the direction of the magnetic field. This is called Larmor precession and

the corresponding frequency is called the Larmor frequency [87–90, 92]

$$\omega_0 = -\gamma B_0 \tag{2.10}$$

where γ is the gyromagnetic ratio. The values of γ for common NMR-active nuclei are given in Table 2.1. The gyromagnetic ratio of a nucleus can be positive or negative and determines the direction of precession. For example, a ^{1}H has a positive value of γ and hence precesses clockwise in the presence of the external magnetic field, while ^{15}N has negative a gyromagnetic ratio that results in counterclockwise precession.

Nuclei	Spin	$\gamma(MHzT^{-1})$	$\omega_0(MHz)$
^{1}H	$\frac{1}{2}$	42.576	400.0
^{2}H	1	6.536	61.4
^{15}N	$\frac{1}{2}$	-4.316	40.5
^{31}P	$\frac{1}{2}$	17.235	162.0
^{13}C	$\frac{1}{2}$	10.705	94.7

Table 2.1: The gyromagnetic ratio and corresponding Larmor frequency of various nuclei. The Larmor frequency is calculated in a magnetic field strength of 9.4 T.

2.1.1.2 Free induction decay (FID) signal and NMR spectrum

In an NMR experiment, the magnetization is manipulated via RF pulses. For this purpose, a coil is mounted around the sample. The axis of the coil is aligned in the *xy* plane and the external magnetic field is along the *z* axis. The RF pulse generates an oscillating magnetic field in the coil which flips the equilibrium magnetization vector away from the *z* axis. This is illustrated in Figure 2.3 (a). The precessing magnetization vector produces an oscillating current in the coil that can be amplified and detected as a time-domain signal. This signal is termed

the Free Induction Decay (FID) signal. The NMR spectrum is acquired by Fourier transformation of the FID signal which gives the spectrum in the frequency domain [87, 90, 92]. An FID signal and the corresponding NMR spectrum are shown schematically in Figure 2.3 (b).

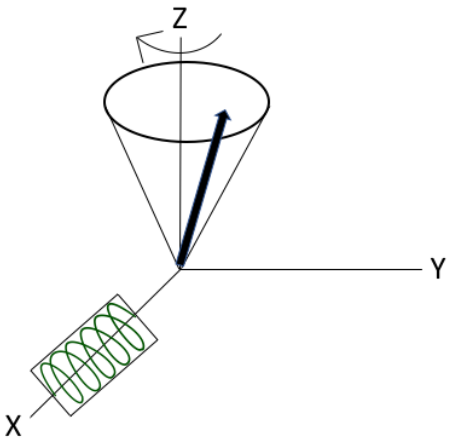

(a)

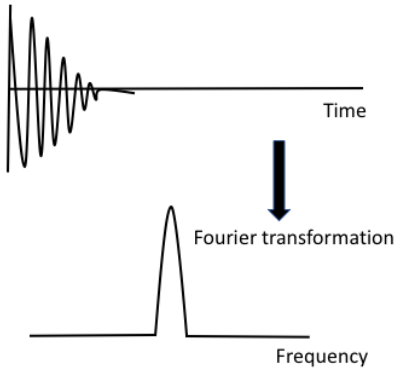

(b)

Figure 2.3: (a) The schematic representation of the precessional motion of the magnetization vector about the z axis. A coil positioned along the x axis is used to apply the RF pulse and to detect the FID signal.(b) The time domain FID signal and the corresponding Fourier transformed NMR spectrum. This figure is inspired from "Understanding NMR spectroscopy" by James Keeler [92].

2.1.1.3 Density operator formulation of spin $\frac{1}{2}$ system for $(\frac{\pi}{2})_x$ pulse

In order to understand how an oscillating magnetic field produced by a RF pulse perturbs the equilibrium magnetization away from the z axis, it is helpful to explain the behavior of a spin system in terms of the density operator [87, 89, 90, 93]. The density operator represents the quantum mechanical state of an entire spin system without referring to the individual spins. For more details on density operator and for an effect of an RF pulse on a spin $\frac{1}{2}$ nucleus in the density operating formulations refer to Appendix A.

2.1.2 NMR spectrometer

Different parts of the NMR spectrometer are described in Appendix B.

2.1.3 ^{2}H NMR

The deuteron is a spin 1 nucleus. Due to non-spherically-symmetric charge distribution, it has an electric quadrupole moment. This quadrupole moment interacts with the Electric Field Gradient (EFG) at the nucleus. These interactions are termed quadrupole interactions and can be treated as first order perturbations to the Zeeman interactions where Zeeman interactions are responsible for the splitting of degenerate spin states (in the absence of magnetic field) into non degenerate states (in the presence of magnetic field).

2.1.3.1 Quadrupole Hamiltonian

Consider a nucleus with a charge density $\rho(\vec{r})$. An electrostatic potential due to the external source is represented by $V(\vec{r})$. Therefore, the Hamiltonian is given

as [88, 94]

$$H = \int \rho(\vec{r})V(\vec{r})d\tau. \tag{2.11}$$

The potential $V(\vec{r})$ can be expanded about the nuclear center of mass to give

$$V(\vec{r}) = \{V_0 + \sum_i x_i \left(\frac{\partial V}{\partial x_i}\right)_{r=0} + \frac{1}{2}\sum_{j,k} x_j x_k \left(\frac{\partial^2 V}{\partial x_j \partial x_k}\right)_{r=0} + ...\}. \tag{2.12}$$

Equation 2.11 then becomes

$$H = \int d\tau \rho(\vec{r})\{V_0 + \sum_i x_i \left(\frac{\partial V}{\partial x_i}\right)_{r=0} + \frac{1}{2}\sum_{j,k} x_j x_k \left(\frac{\partial^2 V}{\partial x_j \partial x_k}\right)_{r=0} + ...\}. \tag{2.13}$$

It is convenient to define

$$\left(\frac{\partial V}{\partial x_i}\right)_{r=0} = V_i \tag{2.14}$$

$$\left(\frac{\partial^2 V}{\partial x_j \partial x_k}\right)_{r=0} = V_{jk}. \tag{2.15}$$

Using Equations 2.14 and 2.15, the quadrupole Hamiltonian becomes

$$\begin{aligned} H &= \int d\tau \rho(\vec{r})\{V_0 + \sum_i x_i V_i + \frac{1}{2}\sum_{j,k} x_j x_k V_{jk} + ...\} \\ &= V_0 \int d\tau \rho(\vec{r}) + \sum_i V_i \int d\tau \rho(\vec{r}) x_i + \frac{1}{2}\sum_{j,k} V_{jk} \int d\tau \rho(\vec{r}) x_j x_k + ... \end{aligned} \tag{2.16}$$

The first term in the above equation represents the electrostatic energy of a nucleus. It does not depend on the shape, size, or orientation of a nucleus and can be neglected here. The second term involves a dipole moment and vanishes as the center of mass and the center of charge coincide [94]. Therefore, the quadrupole Hamiltonian is given as

$$H_Q = \frac{1}{2}\sum_{j,k} V_{jk} \int d\tau \rho(\vec{r}) x_j x_k. \tag{2.17}$$

Using the definition of quadrupole moment [88, 94],

$$Q_{jk} = \int (3x_j x_k - \delta_{jk} r^2)\rho(\vec{r})d\tau, \tag{2.18}$$

we then have

$$\int x_j x_k \rho(\vec{r})d\tau = \frac{1}{3}\{Q_{jk} + \int \delta_{jk} r^2 \rho(\vec{r})d\tau\} \tag{2.19}$$

Using Equation 2.19, the Quadrupole Hamiltonian can be written as

$$\begin{aligned} H_Q &= \frac{1}{2}\sum_{j,k} V_{jk} \int d\tau \rho(\vec{r}) x_j x_k \\ &= \frac{1}{6}\sum_{j,k}\{V_{jk}Q_{jk} + V_{jk}\delta_{jk}\int r^2 \rho(\vec{r})d\tau\}. \end{aligned} \tag{2.20}$$

V_{jk} satisfies the Laplace equation. Therefore, the second term on the right hand side of the above equation vanishes. Hence, we have

$$H_Q = \frac{1}{6}\sum_{j,k}\{V_{jk}Q_{jk}\}. \tag{2.21}$$

Both Q_{jk} and V_{jk} are symmetric second rank tensors. Furthermore, V_{jk} can be written as [94]

$$V_{jk} = -\frac{\partial E_k}{\partial x_j} \tag{2.22}$$

where E_k is the electric field at the nuclear position. Therefore, quadrupole interactions represent the interaction between the quadrupole moment tensor Q_{jk} and the EFG, V_{jk}.

The quadrupole Hamiltonian can be written in terms of angular momentum operators by using the Wigner-Eckart theorem [93–95] to give

$$H_Q = \frac{eQ}{6I(2I-1)}\sum_{j,k} V_{jk}[\frac{3}{2}\{I_j I_k + I_k I_j\} - \delta_{jk} I^2]. \tag{2.23}$$

In the principal axis system (PAS) of EFG tensor, the above Hamiltonian becomes

$$H_Q = \frac{eQ}{6I(2I-1)}[V_{xx}(3I_x^2 - I^2) + V_{yy}(3I_y^2 - I^2) + V_{zz}(3I_z^2 - I^2)]. \tag{2.24}$$

Using the Laplace equation, H_Q can be written as

$$H_Q = \frac{eQ}{4I(2I-1)}[V_{zz}(3I_z^2 - I^2) + (V_{xx} - V_{yy})(I_x^2 - I_y^2)]. \tag{2.25}$$

It is convenient to define two parameters η and eq [94–96]

$$\begin{aligned} \eta &= \frac{V_{xx} - V_{yy}}{V_{zz}} \\ eq &= V_{zz}. \end{aligned} \tag{2.26}$$

In terms of these parameters the quadrupole Hamiltonian becomes

$$H_Q = \frac{e^2qQ}{4I(2I-1)}[(3I_z^2 - I^2) + \eta(I_x^2 - I_y^2)]. \tag{2.27}$$

The next step is to transfer this Hamiltonian from the EFG principal axis system to the laboratory frame of reference. The spherical coordinates can be used to make this transformation using Euler angles (θ, ϕ). The angles (θ, ϕ) describe the orientation of the lab frame z-axis in the PAS. In the lab frame, the quadrupole Hamiltonian takes the form [96]

$$H_Q = \frac{e^2qQ}{4I(I-1)}[\frac{1}{2}(3cos^2\theta - 1) + \frac{1}{2}\eta sin^2\theta cos2\phi][3I_z^2 - I^2]. \tag{2.28}$$

2.1.3.2 Quadrupole splitting

The total Hamiltonian for a spin 1 system is given as [96, 97]

$$H = H_Z + H_Q + H_{CS} + H_D \tag{2.29}$$

where H_Z and H_Q are the Zeeman and quadrupole Hamiltonians respectively. H_{CS} is a chemical shift Hamiltonian and H_D represents the dipolar coupling Hamiltonian. The chemical shift and dipolar splitting for a ^{2}H nucleus are of the order of 4 kHz and 1 kHz respectively. These interactions are very weak in comparison to quadrupole interactions which give rise to maximum splittings of 250 kHz [96]. Therefore, the chemical shift and dipolar interactions can be neglected. The total Hamiltonian becomes

$$H = H_Z + H_Q \tag{2.30}$$

$$H = \gamma\hbar\hat{I_Z}B_0 + \frac{e^2qQ}{4I(I-1)}[\frac{1}{2}(3cos^2\theta - 1) + \frac{1}{2}\eta sin^2\theta cos2\phi][3\hat{I_z^2} - \hat{I^2}] \tag{2.31}$$

For $I = 1$, the energy eigenvalues corresponding to the total Hamiltonian are given as

$$E_m = \gamma\hbar m B_0 + \frac{e^2qQ}{4}[3m^2 - 2)][\frac{1}{2}(3cos^2\theta - 1) + \frac{1}{2}\eta sin^2\theta cos2\phi] \tag{2.32}$$

For a carbon-deuterium bond, $\eta = .007$ and so the above expression is independent of ϕ and

$$E_m = \gamma\hbar m B_0 + \frac{e^2qQ}{4}[3m^2 - 2][\frac{1}{2}(3cos^2\theta - 1)]. \tag{2.33}$$

The second term in Equation 2.33 reflects the perturbation of the Zeeman splitting by the quadrupole interactions. Because of this perturbation, there will be two transitions allowed by the selection rule $\Delta m = \pm 1$, as shown in Figure 2.4.

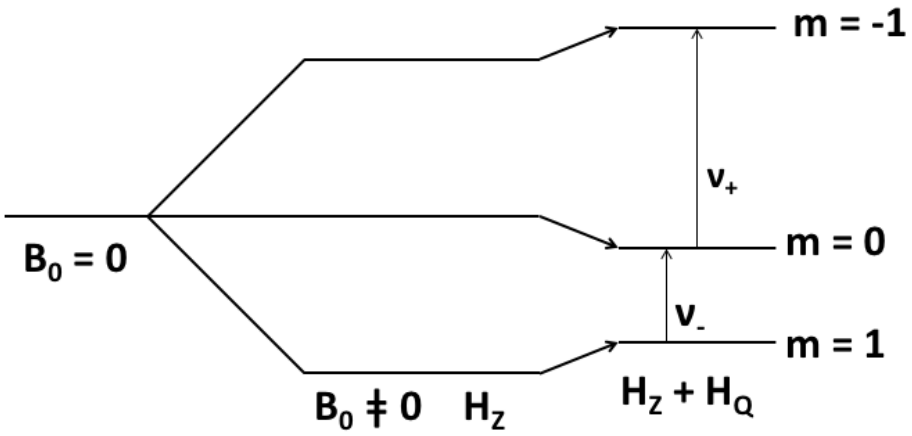

Figure 2.4: Energy level diagram for a spin 1 system in the presence of a magnetic field, showing Zeeman and quadrupole splitting.

The resonance energies corresponding to the two transitions are given as

$$\hbar\nu_{\pm} = \gamma\hbar B_0 \pm \frac{3}{4}e^2qQ\frac{(3cos^2\theta - 1)}{2}. \tag{2.34}$$

The resulting quadrupole splitting is defined as

$$\begin{aligned}\Delta\nu(\theta) &= \nu_+ - \nu_- \\ &= \frac{3}{2}\frac{e^2qQ}{\hbar}\left[\frac{3cos^2\theta - 1}{2}\right] \\ &= 2\nu_Q P_2(cos\theta)\end{aligned} \tag{2.35}$$

where

$$\nu_Q = \frac{3}{4}\frac{e^2qQ}{\hbar} \tag{2.36}$$

and $P_2(cos\theta)$ is the second Legendre polynomial [96].

2.1.3.3 ^{2}H NMR powder pattern spectrum of lipid vesicles

In order to use ^{2}H NMR for lipids, hydrogens on the lipid acyl chains need to be replaced with deuterons. If this replacement is done only at a single site, the sample is specifically deuterated. On the other hand if deuterons are placed all along the lipid acyl chain, then the resulting sample is a chain per-deuterated sample.

In a lipid bilayer, the bilayer normal is the symmetry axis for molecular reorientation. The EFG of a carbon-deuteron bond is attached to the molecule which reorients about a local symmetry axis (the bilayer normal) and may, in turn, be oriented along a direction other than that of the static magnetic field. For this reason, we need to change the frame of reference of the Hamiltonian from the lab frame to a frame in which we can express the orientation of the EFG with respect to the bilayer normal. This can be done by using Wigner rotation matrices. The resulting expression for orientation dependence of the quadrupole splitting for a particular deuteron is :

$$\Delta\nu(\theta,\beta) = \frac{3}{2}\frac{e^2qQ}{\hbar} < \frac{3cos^2\theta - 1}{2} > [\frac{3cos^2\beta - 1}{2}] \tag{2.37}$$

where θ is the angle between the principle axis of the EFG and the bilayer normal and β is an angle between the bilayer normal and the static magnetic field. The angled brackets represent the motional averaging of the quadrupole interaction by the C-^{2}H bond orientational fluctuations. The schematic representation of these angles with respect to the static magnetic field is shown in Figure 2.5.

In a vesicle sample, the bilayer normal is randomly oriented with respect to the external magnetic field. In this case β can have any value between 0° to 90° with weighting proportionally equal to the fraction of spherical surface represented

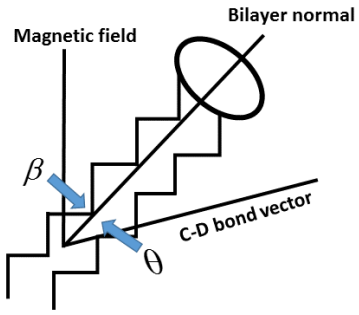

Figure 2.5: The angular orientation of the bilayer normal with respect to external magnetic field and carbon-deuteron bond.

by that orientation. So the intensity of the NMR spectrum varies with β, with higher intensity coming from $\beta = 90^{\circ}$ [96]. The resulting NMR spectrum has a characteristic line shape called a Pake doublet, as shown in Figure 2.6 (a). The averaged motion of the lipid acyl chain with respect to the bilayer normal determines the splitting of the Pake doublet spectrum. It is given by the average of the second Legendre polynomial $P_2(cos\theta)$ in Equation 2.37. For a chain per-deuterated vesicle sample, the NMR spectrum is a superposition of Pake doublets, corresponding to all deuterons on the lipid acyl chain, as shown in Figure 2.6 (b). The splitting of these doublets is given by the averaged motion of the lipid acyl chains. Close to the lipid head groups, lipid acyl chain motion is more constrained, resulting in larger splittings while, towards the end of the acyl chain, the large amplitude of motion gives rise to smaller splittings.

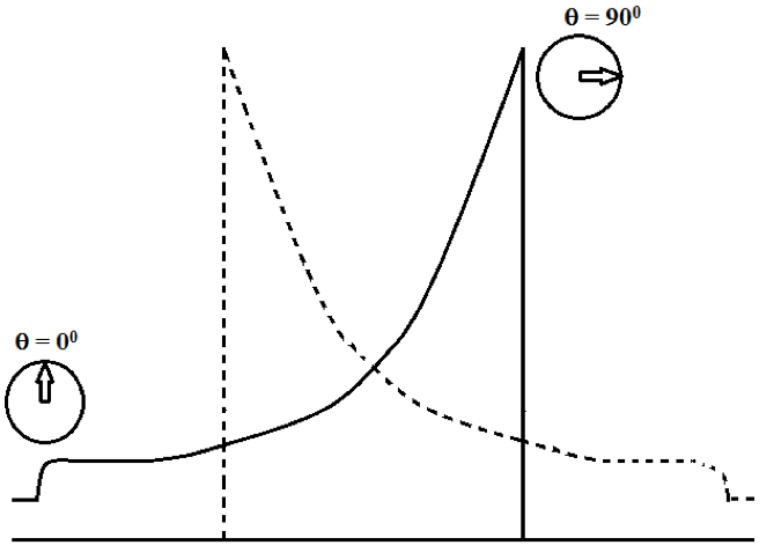

(a)

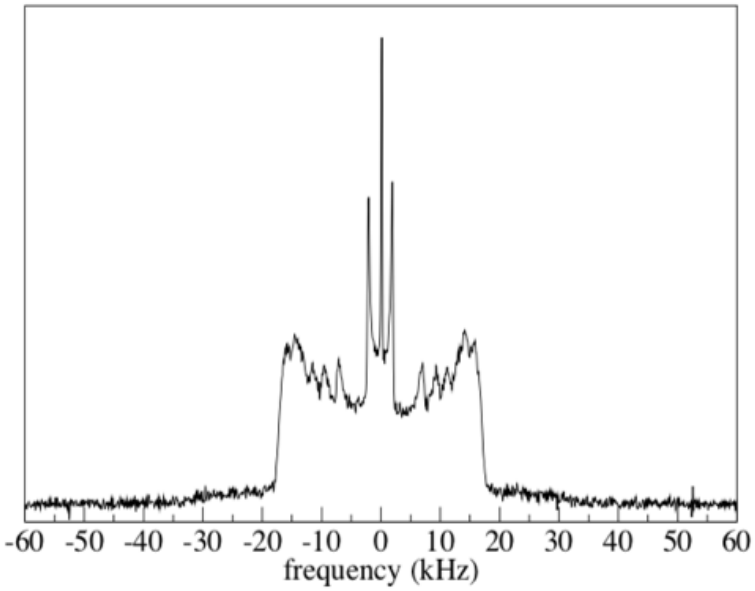

(b)

Figure 2.6: (a) Powder pattern spectrum of a vesicle sample deuterated at single site. Solid and dashed lines represent the two transitions for the deuteron and the intensity varies with β. (b) Powder pattern spectrum for a bilayer vesicle sample of chain per-deuterated lipids. This spectrum is the superposition of doublets corresponding to each deuteron on the lipid acyl chain.

2.1.3.4 Oriented spectrum and orientational order parameter (S_{CD})

When the bilayer normal has one particular direction with respect to the static magnetic field, β has only a single value and the resulting spectrum is an oriented-sample spectrum, as shown in Figure 2.7 (a). Now consider two frames: one lab frame (x, y, z) and a second frame attached to the molecule. The bilayer normal points in the direction of the z axis of the lab frame. The average fluctuations of the molecular frame around the bilayer normal are measured by the orientational order parameter S_{ii} [95, 96] which is given by:

$$S_{ii} = \frac{1}{2} < 3cos^2\theta_i - 1 > (i = x, y, z) \tag{2.38}$$

where $cos^2\theta_i$ is the time average of the angular fluctuations of the i^{th} coordinate axis with respect to bilayer normal. The property of direction cosines gives

$$\begin{aligned} \sum_{i=1}^{n} cos^2\theta_i &= 1. \\ \sum_{i=1}^{3} S_{ii} &= 0. \end{aligned} \tag{2.39}$$

For axially symmetric reorientation, we find $S_{11} = S_{22}$.

The quadrupole splitting (the splitting of 90° edges of the Pake doublet) is given as

$$\Delta\nu_Q = \frac{3}{2}\frac{e^2qQ}{\hbar}[S_{33} + \frac{1}{2}\eta(S_{11} - S_{22})]. \tag{2.40}$$

For $\eta = 0$, this gives

$$\Delta\nu_Q = \frac{3}{2}\frac{e^2qQ}{\hbar}[S_{33}]. \tag{2.41}$$

Using Equation 2.41, we can calculate the orientational order parameter if we know the quadrupole splitting, since the factor $\frac{e^2qQ}{\hbar}$ multiplying S_{33} is a constant known as the quadrupole coupling constant and has a value of 167 kHz

for carbon-deuterium bonds. In order to calculate the orientational order parameter from the powder pattern of chain perdeuterated lipids, we first need to convert the powder pattern into an oriented spectrum. This can be easily done by using a technique called "dePaking" [98–100] which transforms a powder pattern spectrum to the corresponding oriented-sample spectrum. From the dePaked spectrum, quadrupole splittings for all deuterons at different carbon positions can be calculated, which in turn gives the orientational order parameter. The plot of orientational order parameter vs. carbon position is called the smoothed order parameter profile. It assumes a monotonic decrease of the order along the acyl chain. For acyl chain segments close to the headgroup (the order parameter "plateau" region), orientational order may not change monotonically with position and the smoothed order parameter profile does not provide details of the orientational order parameter dependence on chain position for this part of the lipid acyl chain [101]. An example of order parameter profile is shown in Figure 2.7 (b).

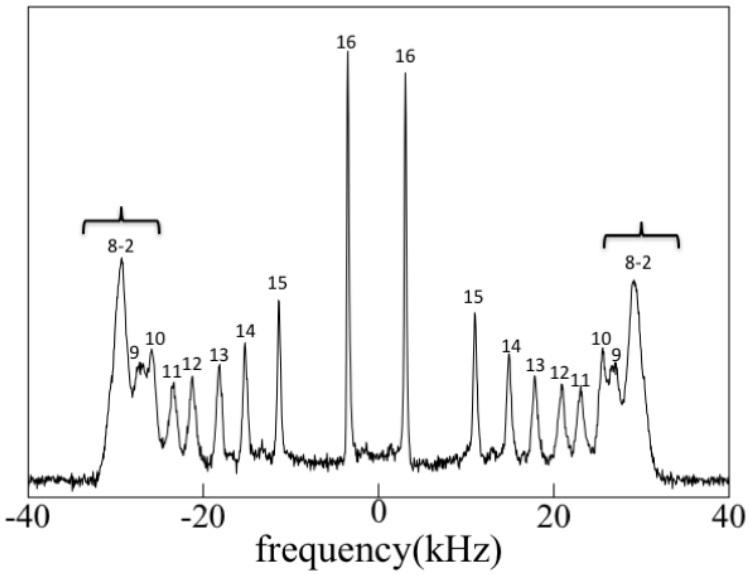

(a)

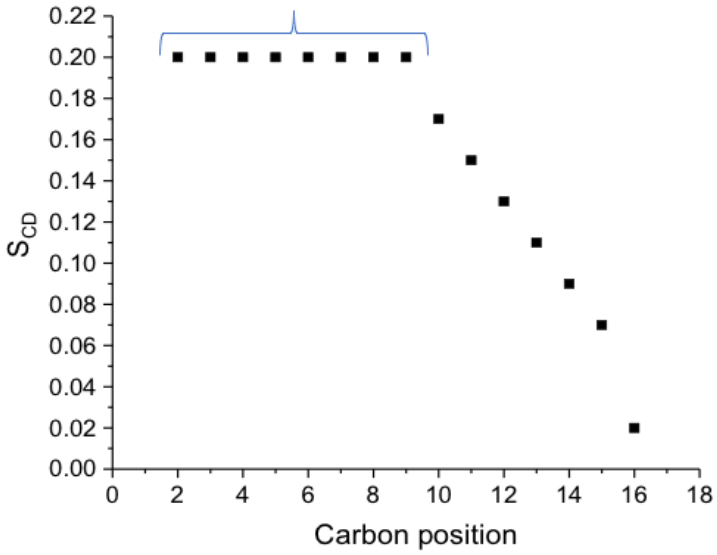

(b)

Figure 2.7: (a) The oriented sample spectrum: different peaks correspond to different deuterons on the lipid acyl chain. (b) The orientational order parameter extracted from an oriented sample spectrum: close to the lipid head groups, chain motion is more restricted and the smaller averaged motion results in higher quadrupole splittings and larger order parameter values. Close to the end of the lipid acyl chain, less constrained motion gives rise to small splittings and order parameter values decrease from carbon number 2 to 16.

2.1.3.5 Quadrupole echo

The concept of quadrupole echo was introduced by Davis et al. and co-workers [102]. In the NMR spectrometer used in this work, we use the same coil to excite the nuclei and to detect the FID signal. Due to the imperfect isolation of the high power transmitter from the low power receiver, the preamplifier is overloaded by the strong RF pulse and it is blinded for a short period ($\sim$ 20 μs) referred to as the receiver "dead time" or "recovery time" [103]. The NMR spectral width used for lipid bilayers typically is 250 kHz, so important information is contained in the very early part of the initial FID. This part of FID can not be detected in a single pulse experiment because the receiver is affected by the strong RF pulse in this interval. The practical solution to this recovery time issue is to translate the FID t=0 point to beyond the receiver's dead time. This time translation is done by applying the quadrupole echo pulse sequence shown in Figure 2.8.

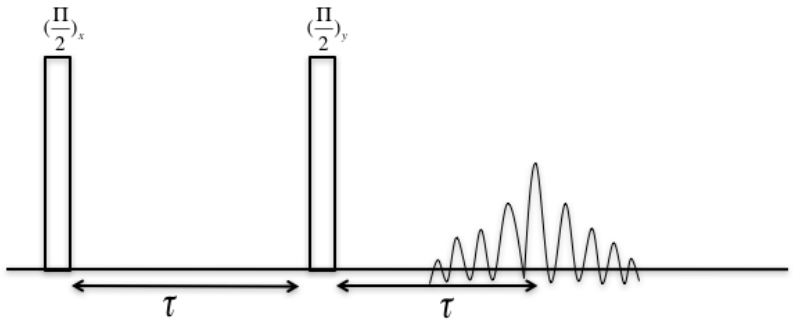

Figure 2.8: The representation of the quadrupole echo pulse sequence. A $\frac{\pi}{2}$ pulse along x axis brings the magnetization along y axis. For time τ, spin system evolves under the quadrupole Hamiltonian. At the end of τ a second $\frac{\pi}{2}$ pulse is applied along y axis. The echo occurs at the end of time period 2τ.

The quadrupole echo experiment consists of two $\frac{\pi}{2}$ pulses 90°out of phase with each other and separated by a time much longer than the receiver's dead time. The first pulse, $(\frac{\pi}{2})_x$, flips the magnetization from the z axis to the y axis. Then, for a

period τ, the system evolves under the influence of the quadrupole Hamiltonian. The quadrupole interactions vary from nucleus to nucleus as a result of differences in the EFG local orientations. This orientational dependence causes the spins to get out of phase with each other. At the end of period τ, the second pulse $(\frac{\pi}{2})_y$ is applied. This pulse refocuses the dephasing which occurred due to spread in $\nu(\theta, \beta)$ [96].

2.1.3.5.1 Density operator treatment of spin 1 system

The density operator treatment of spin 1 system is based on the description presented by Bloom [93]. The density operator formulation can be used to understand the refocusing of magnetization with the quadrupole pulse sequence. For details refer to Appendix A.

2.1.3.6 Quadrupole echo decay time T_2^{qe}

The quadrupole echo sequence consists of two $\frac{\pi}{2}$ pulses that are 90° out of phase with each other. The echo is formed at 2τ, where τ is the separation between the two $\frac{\pi}{2}$ pulses. By varying the interval between the pulses, it is possible to measure the characteristic echo decay time. This provides information about the motions that modulate the orientation-dependent quadrupole interactions during the interval 2τ. Quadrupole echo decay is characterized by an averaged decay time T_2^{qe}. The amplitude of the observed echo reflects the extent to which orientation-dependent quadrupole interactions are left unperturbed by molecular motions [104, 105]. For a given separation, τ, of the $\frac{\pi}{2}$ pulses in the quadrupole echo sequence, the echo amplitude A(2τ) can be written as [93, 106]

$$A(2\tau) = \sum_i A_i(0) e^{-R_i 2\tau} \tag{2.42}$$

where summation over i represents the contribution from all deuterons at all sites along the lipid acyl chain and over all orientations of the bilayer normal. R_i is the echo decay rate for a given deuteron i due to all motions that modulate the quadrupole interactions for that deuteron. For short τ, the amplitude of the echo can be written as

$$A(2\tau) = \sum_i A_i(0)(1 - R_i 2\tau) \tag{2.43}$$

$$= A(0) - A(0)2\tau \sum_i \frac{A_i(0)}{A(0)} R_i \tag{2.44}$$

$$= A(0)e^{-<R>2\tau}. \tag{2.45}$$

In the limit of short τ, the quadrupole echo decays exponentially with a characteristic time T_2^{qe}, which is given as

$$< R >= (T_2^{qe})^{-1}. \tag{2.46}$$

$< R >$ is an average over the entire population of deuterons. If we plot $\ln\left(\frac{A(\tau)}{A(0)}\right)$ vs. 2τ, the negative inverse of the slope will give T_2^{qe}.

All motions have associated correlation times τ_{ci}. The distinction between fast and slow motions is made by comparing τ_{ci} with $(\Delta M_{2i})^{-1/2}$, where ΔM_{2i} is the second moment of that portion of the quadrupole interaction modulated by motion i. It represents the range over which quadrupole splittings vary due to the molecular motion. In the fast motion regime, the echo decay rate, $(T_2^{qe})^{-1}$, is proportional to the correlation time [93, 107] so that

$$\frac{1}{T_2^{qe}} = \triangle M_{2j} \tau_{cj}. \tag{2.47}$$

In the slow motion regime, the echo decay rate, $(T_2^{qe})^{-1}$, is inversely proportional to the correlation time so that

$$T_2^{qe} = \tau_{cj}. \tag{2.48}$$

In particular, quadrupole echo decay can indicate a peptide-induced perturbation of slow motions, like bilayer undulation, that may be too slow to be directly detectable by changes in quadrupole splitting.

2.1.4 ^{15}N NMR

^{15}N is a spin $\frac{1}{2}$ nucleus. As explained earlier, the application of a static magnetic field results in precession at the Larmor frequency. The actual resonance frequencies observed in NMR experiments are slightly different from Larmor frequencies and this difference is termed chemical shift. In a semi-classical view, the mechanism by which this shift occurs can be thought of in two steps: 1) The external magnetic field induces currents in electron clouds; 2) These currents in turn induce a magnetic field, $B_j^{induced}$ [90]. Because of this effect, the resultant local magnetic field experienced by each nucleus is

$$B_j^{loc} = B_0 + B_j^{induced}. \tag{2.49}$$

In this expression, the local induced field can be expressed as

$$B_j^{induced} = \sigma_j \cdot B_0 \tag{2.50}$$

where σ_j, the second rank chemical shift tensor, characterizes how the shift depends on orientation for a specific chemical spin environment. In the principal axis system (PAS), the chemical shift tensor has three diagonal elements σ_{11}, σ_{22} and σ_{33}. These elements near a peptide bond are shown in Figure 2.9 (a). When

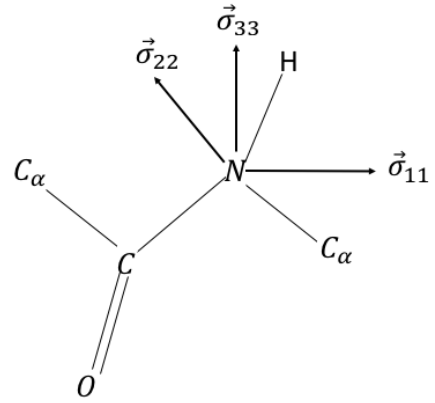

(a)

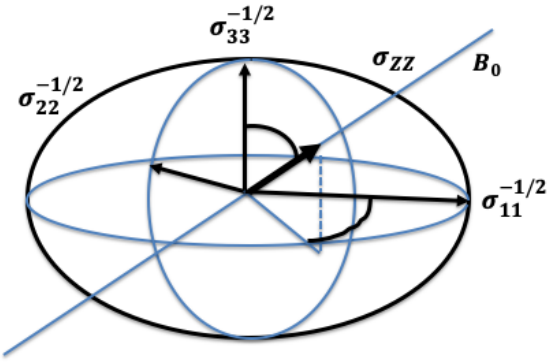

(b)

Figure 2.9: (a) The components of chemical shift tensor positioned near to the peptide bond. (b) The representation of chemical shift tensor in the principal axis system. This figure is inspired from Bechinger et al. [108].

transformed from the PAS to the lab frame using Euler angles Θ, Φ, and Ψ, the z component in the direction of the applied field corresponds to the measured value

of chemical shift

$$\sigma_{zz} = \sigma_{11} sin^2\Theta cos^2\Phi + \sigma_{22} sin^2\Theta sin^2\Phi + \sigma_{33} cos^2\Theta. \tag{2.51}$$

Graphically, the ^{15}N chemical shift tensor can be represented by an ellipsoid, as shown in Figure 2.9 (b) [108]. The axes of the ellipsoid are represented by $\frac{1}{\sqrt{\sigma_{ii}}}$ where σ_{11}, σ_{22}, σ_{33} are the main tensor elements. The intersection of the ellipsoid and magnetic field direction gives an observable chemical shift for a given orientation of the molecule.

For α helical peptides, the N-H vector and σ_{33} are within 18° of each other and both are oriented to within a few degrees of the helical axis [109, 110]. Therefore, the observed ^{15}N chemical shift gives the information about the alignment of α helical peptides within oriented lipid bilayers. For randomly distributed molecular orientations, a powder pattern spectrum is shown in Figure 2.10. It has

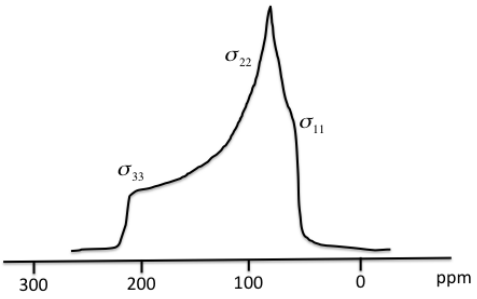

Figure 2.10: The schematic representation of ^{15}N powder pattern spectrum for randomly distributed molecular orientations. The tensor elements of the ^{15}N chemical shift tensor of the amide bond have approximate values of 61, 75, and 223 ppm (σ_{11}, σ_{22}, and σ_{33}).

been shown that in oriented lipid bilayers, with the bilayer normal parallel to the static magnetic field, transmembrane alignment of an AMP results in a chemical shift $>$ 180 ppm while chemical shifts $<$ 100 ppm are observed for in-plane peptide orientation of peptides [109]. The two alignments of peptide with respect to

membrane surface and corresponding value of ^{15}N chemical shift are schematically shown in Figure 2.11.

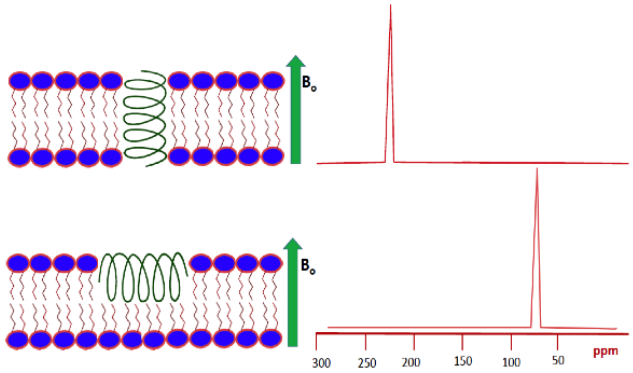

Figure 2.11: The schematic representation of ^{15}N chemical shift values for different orientations of α helical peptides. This figure is inspired from Bechinger et al. [109]

2.2 Zeta potential

In an electrical double layer, the slipping plane makes an envelope around a charged particle in which counter-ions make a rigid layer tightly bound to the charged particle. The electrical potential generated by the charge enclosed by the slipping plane is called the zeta potential [111].

2.2.1 Electrical double layer

The electrical double layer model explains the distribution of ions in the vicinity of a charged particle [112–114]. For a negatively charged particle dispersed in solution, positive counter-ions tend to accumulate around it. The distribution of ions around a negatively charged particle is assumed to exist in two parts: the inner (Stern) layer, where ions are strongly bound to the negatively charged surface and the outer (diffuse) region, where they are less firmly attached to the surface.

Within the diffuse layer, there is a boundary, when a particle moves, ions within the boundary move with it, but any ions beyond the boundary do not travel with the particle. This boundary is called the slipping plane or the surface of shear [115]. The configuration of the electrical double layer is schematically shown in Figure 2.12. The concentration of counter-ions is high near the negatively charged surface and it decreases gradually with distance. When an electric field is applied,

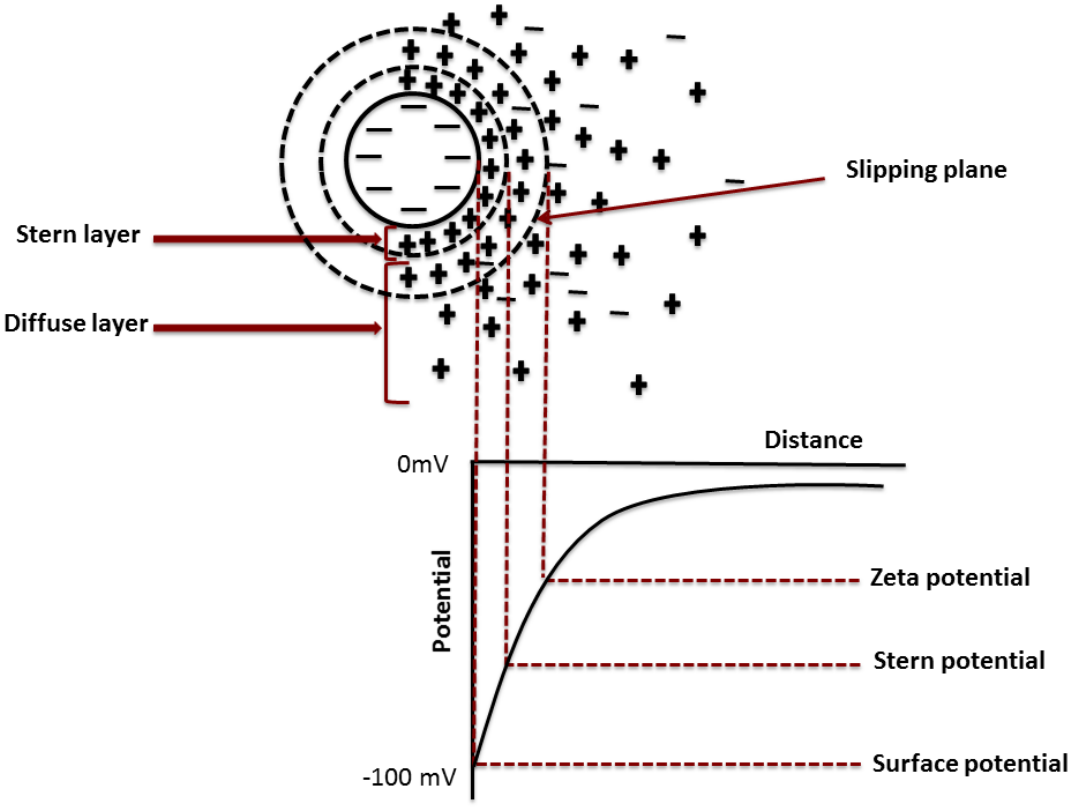

Figure 2.12: The charge distribution around negatively charged particle represented by the black circle. The inner dotted circle represents the Stern layer and the outer dotted circle shows the slipping plane. This figure is inspired from Freire et al. [116]

the ions in the Stern layer that are firmly attached to the negatively charged surface, move with the particle. The ions beyond the slipping plane stay with the bulk solution. Therefore, the slipping plane is a boundary where bound charge and solution move in different directions. The potential at the slipping plane is

called the zeta potential. Basically, it is the difference between the potential at the slipping plane and at a point at infinity in the bulk solution [115, 117].

2.2.2 Measurement of zeta potential by electrophoresis

The zeta potential is calculated from the experimentally determined electrophoretic mobility using Henry's equation [116]:

$$U_E = \frac{2\varepsilon\zeta f(\kappa a)}{3\eta} \tag{2.52}$$

where U_E is electrophoretic mobility, ζ is the zeta potential, ε is the dielectric constant, η is the viscosity. The function $f(\kappa a)$ is called the Henry's function where κ is the inverse Debye length and a is the particle size. For the low potential regime, the linearized version of Poisson-Boltzmann equation gives the the variation of electric potential in an electric double layer [113]

$$\nabla^2\Psi = -e^2\frac{\sum_i z_i^2 n_i}{\varepsilon_0\varepsilon kT}\Psi \tag{2.53}$$

$$= \kappa^2\Psi \tag{2.54}$$

where

$$\kappa = \sqrt{e^2\frac{\sum_i z_i^2 n_i}{\varepsilon_0\varepsilon kT}} \tag{2.55}$$

is the inverse Debye length, n_i represents the bulk concentration of each type of ion and z_i is the charge of the ion. Debye length $(1/\kappa)$ represents the thickness of the electrical double layer and has units of length.

The general form of the Henry's function is given by the numerical solution of O'Brien and White [118]. Henry's function distinguishes between Hückel and Smoluchowski approximations. These two approximations are two limiting cases

for very small and very large values of κa. The Hückel approximation is applicable when the size of a particle is smaller than the Debye length, while the Smoluchowski approximation is used when particle size is greater than the Debye length. This is schematically shown in Figure 2.13.

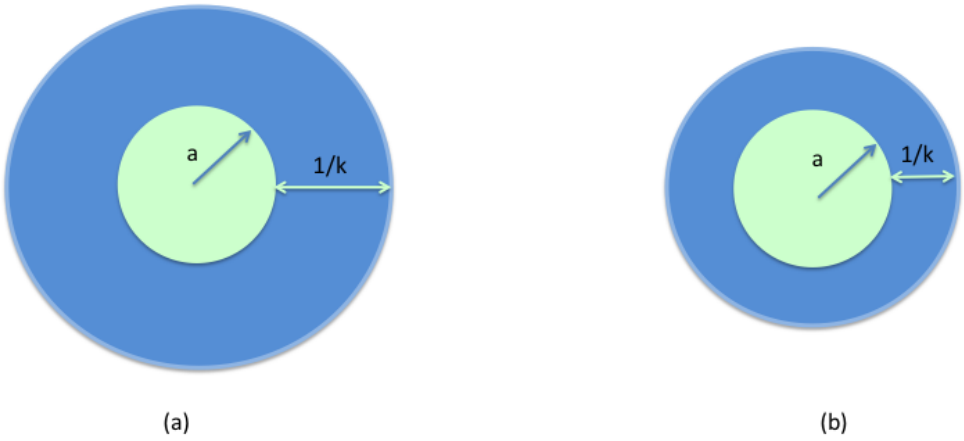

Figure 2.13: The schematic representation of (a) Hückel (b) Smoluchowski approximations. For the work reported in this thesis, the Smoluchowski approximation is used to determine the zeta potential.

The values of Henry's function for both approximations are given below

$$\begin{aligned} f(\kappa a) &= 1.5 \quad if \quad a >> \frac{1}{\kappa} \\ &= 1.0 \quad if \quad a << \frac{1}{\kappa}. \end{aligned} \tag{2.56}$$

The electrophoretic mobility of particles is measured experimentally by using the Phase Analysis Light Scattering (PALS) technique. As the name suggests, in this technique the phase shift in the light scattered by moving particles is measured. The laser beam is split into two parts by a beam splitter; one beam is called the reference beam and the other is called the scattering beam. The scattering beam passes through the sample cell that has a pair of electrodes. When a voltage is applied across the electrodes, the charged particles move towards the opposite

electrodes. The light scattered by moving particles is detected at an angle of 13°. The phase shift is measured by comparing the phase of scattered light with the phase of the reference beam [115, 117, 119, 120]. Knowledge of the phase shift in the scattered light provides information about electrophoretic mobility from which the zeta potential can be calculated.

2.3 Circular dichroism (CD) spectroscopy

Circular dichroism (CD) refers to the difference in a chiral molecule's absorption of left-handed circularly polarised light (L-CPL) and right-handed circularly polarised light (R-CPL)

$$CD = \Delta A(\lambda) = A(\lambda)_{L-CPL} - A(\lambda)_{R-CPL}. \tag{2.57}$$

The interaction of the electric field component of light with a chiral molecule results in the linear displacement of charge. This is termed an electric transition and it is associated with an electric transition moment. On the other hand, when the magnetic field component of light interacts with a molecule it results in the circular movement of charge. This is called a magnetic transition and it corresponds to some finite value of magnetic transition moment. Rotational strength is a property of a given electronic or magnetic transition $i \rightarrow f$ and given as

$$R_{if} = Im(\mu_{if} \cdot m_{if}) \tag{2.58}$$

where μ_{if} and m_{if} are the electric and magnetic dipole transition moments respectively for the transition $i \rightarrow f$ and Im represents the imaginary part of $(\mu_{if} \cdot m_{if})$. The rotational strength is non-zero if a transition from $i \rightarrow f$ state is associated with both the linear motion of charge in a particular direction and circular motion

about that direction. This linear and circular motion together corresponds to the helical motion of charge. The right and left-handed helical motions of charge determine whether R-CPL or L-CPL is absorbed more strongly by a molecule which in turn leads to CD [121, 122].

2.3.1 CD spectrum of peptides

The most common chromophore in the case of a peptide is the peptide bond which links different amino acid residues. The alpha carbon in a peptide bond is asymmetric in nature and gives a chiral character to the peptide backbone. The CD spectrum of a poly-peptide has a characteristic shape based on its secondary structure, as shown in Figure 2.14. For α-helical peptides, the CD spectrum consists of two negative minima near 222 nm and 208 nm and a stronger positive peak near 190 nm. In the case of β sheet, two negative peaks near 217 nm and 180 nm and one positive peak at 195 nm are observed. For random-coil peptides, the CD spectrum consists of a stronger negative peak near 200 nm [121, 123].

2.3.2 Measurement of CD and percent helicity of α helical peptides

The magnitude of CD is measured in terms of ellipticity (θ), an angle expressed in millidegrees. This angle is schematically shown in Figure 2.15 and is the tangent of the ratio of the minor to major elliptical axes. It is possible to calculate the percent helicity from the normalized CD spectrum of α-helical peptides. For this purpose the experimentally observed CD is converted into the Mean Residue Ellipticity (MRE)

$$[\theta]MRE = \frac{\theta}{c \times L \times N_R} \tag{2.59}$$

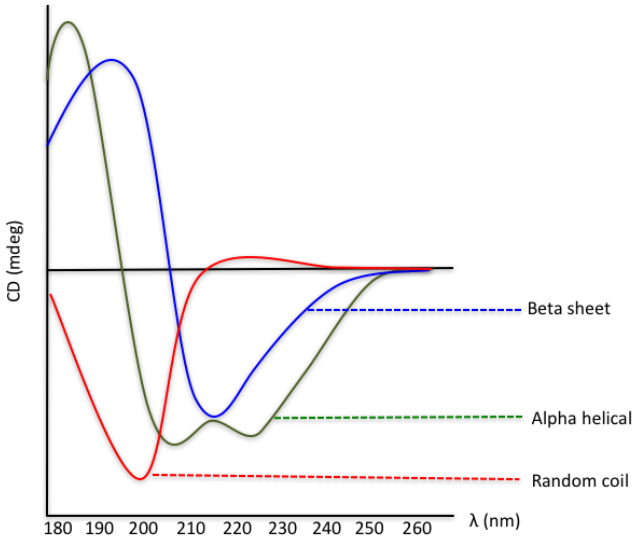

Figure 2.14: CD spectrum of poly-peptides results from different absorption of R-CPL and L-CPL. The curve has a different shape according to the secondary structure of the poly-peptide.

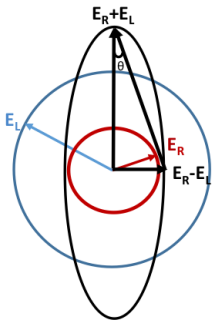

Figure 2.15: The representation of an ellipticity when L-CPL and R-CPL have different magnitude. The E_R and E_L represent the electric field component of R-CPL and L-CPL respectively.

where θ is recorded ellipticity, c is the peptide concentration in dmol/L, N_R is the number of residues in the peptide, and L is path length in cm. The fractional helicity of a peptide sequence is the difference between the mean residue ellipticity and the random coil ellipticity divided by the difference between the helix ellipticity and the coil ellipticity, all measured at 222 nm [124]. It can thus be expressed

as

$$f_H = \frac{\theta_{222} - \theta_C}{\theta_H - \theta_C} \tag{2.60}$$

where, θ_C and θ_H are the ellipticities for the random coil and complete helical structure. θ_C and θ_H both vary linearly as a fuction of temperature

$$\begin{aligned} \theta_C &= 2200 - 53T \\ \theta_H &= \frac{-44000 + 250T}{1 - \frac{3}{N_r}} \end{aligned} \tag{2.61}$$

T is the temperature in °C.

Chapter 3

Interactions of Gad peptides with model membranes: insights from NMR and binding studies

The interactions of AMPs with cell membranes are key aspects of their mechanisms [19, 37, 42, 80]. AMP-membrane interactions can permeabilize the membrane itself and/or disrupt the membrane as a consequence of the AMP's transport across the membrane so it can gain access to intracellular targets [43, 125]. Cell membranes are very complex in nature. However, model membranes can be used to mimic the essential components of cell membranes. The interactions of Gad peptides with model lipid bilayers were studied using solid-state NMR spectroscopy and zeta potential measurements. ^{2}H NMR was employed to investigate the peptide-induced disorder in model lipid membranes. Using zeta potential measurements, the peptide binding to the membrane was quantified in terms of the equilibrium constant, the partition constant, and lipid to peptide molar ratio ($L : P$). Because Gad peptides take on different charges at pH 7.0 and 5.0, the experiments were

carried out at both pHs to gain insight into the charge dependence of the AMP-membrane interactions.

3.1 Materials and methods

3.1.1 Lipids

Eukaryotic cell membranes are mainly composed of zwitterionic lipids (POPC, sphingomyelin, and cholesterol), whereas bacterial membranes also contain POPE and anionic POPG lipids. In order to understand the interactions of Gad peptides with model membranes that mimic bacterial membrane lipid composition, a lipid mixture of POPE/POPG was used. Chain per-deuterated lipid, POPG-d_{31}, along with non-deuterated POPE were purchased from Avanti Polar Lipids (Alabaster, AL). All lipids were used without further purification. The molecular weight and the hydrated bilayer gel to liquid crystal transition temperatures of lipids used in this study are listed in Table 3.1.

Lipid	Molecular weight(g/mole)	Transition temperature (°C)
POPC	760	-2
POPE	718	25
POPG-d_{31}	802	-2

Table 3.1: The molecular weights and the hydrated bilayer gel to liquid crystal transition temperatures of different lipids used in this study. This information was obtained from Avanti Polar Lipids (Alabaster, AL).

3.1.2 ^{2}H NMR

3.1.2.1 Sample preparation

To prepare multilamellar vesicles, 40 mg of POPE/POPG-d_{31} (3:1 molar ratio) dry lipid powder was weighed using a Mettler A260 analytical balance. Lipid powders were dissolved in 4-5 mL chloroform/methanol (2:1) and placed in a round-bottom flask. The organic solvent was removed by rotatory evaporation at 40°C for 20-30 minutes. To make sure that there were no traces of solvent left, the samples were further dried in an evacuated desiccator connected to a pump with liquid nitrogen trap for 6-8 hours. The dry lipid mixture was hydrated with 550 μL of 10 mM potassium acetate buffer at pH 7.0 or 10 mM potassium phosphate buffer at pH 5.0. The pH of each sample was measured with a pH meter (Beckman 340 pH meter) using a micro-probe (Sigma-Aldrich Co.) and adjusted to the desired pH to within $\pm$ 0.1, by adding 0.1 M HCl or 0.1 M NaOH. Finally, samples were transferred to pre-cleaned 400 μL NMR tubes and sealed tightly with teflon tape. To prepare multilamellar vesicles containing Gad peptides, dry powder of the peptide was mixed with the POPE/POPG-d_{31} (3:1) lipid mixture, keeping the $L:P$ ratio at 25:1 (molar ratio). A total of 4.9 mg of Gad-1 and 4.3 mg of Gad-2 dry powder was used in these samples. The dry powder mixture of lipids and peptide was then dissolved in 4-5 mL chloroform/methanol (2:1) and placed in a round-bottom flask. After this, the same steps of solvent removal and hydration were followed as described above for lipid-only samples. All samples were stored in a freezer at -20°C after NMR experiments.

3.1.2.2 Experimental details

All ^{2}H NMR experiments were performed at 61 MHz, corresponding to a magnetic field strength of 9.4 T, on a locally assembled spectrometer. Sample temperatures were controlled to $\pm$ 0.1°C using a PID (Proportional−Integral−Differential) temperature controller (model 325, Lake Shore cryotronics, USA). In order to obtain the powder pattern spectrum, ^{2}H NMR experiments were performed using the quadrupole echo pulse sequence [126] with a $\frac{\pi}{2}$ pulse length of 5.5 μs and pulse separations of 35 μs. A 15 μs delay was applied before the 5 μs acquisition trigger. All spectra were obtained by averaging 4000 transients, with repetition times of 0.9 s. Experiments were performed at two temperatures, 25°C and 37°C. Oriented spectra corresponding to the powder pattern spectra were obtained by dePaking. DePaking is a procedure to transform the multilamellar vesicle sample spectrum to the spectrum that would be expected for an oriented bilayer sample [98]. The McCabe and Wassall [99] approach was used to perform dePaking. The free induction decays used for dePaking were obtained by averaging 60,000 transients. The orientational order parameter values were calculated from these dePaked spectra.

Additional information about the AMP-membrane interactions can be obtained from examination of the quadrupole echo decay rate (T_2^{qe}). The echo decay rate can indicate how the slow motions of lipid bilayers are perturbed by the presence of peptide. To obtain the quadrupole echo decay rate at two temperatures, 25°C and 37°C, ^{2}H NMR experiments were performed using the quadrupole echo pulse sequence with a $\frac{\pi}{2}$ pulse length of 5.5 μs and quadrupole echo pulse separations of 35 μs, 50 μs, 75 μs, 100 μs, 150 μs, 200 μs, 300 μs, and 400 μs. A 15 μs delay was applied before the 5 μs acquisition trigger. For each pulse separation, 800 transients were averaged to obtain the echo amplitude. The repetition time was 0.9 s.

3.1.3 Zeta potential (ζ-potential) measurements

3.1.3.1 Sample preparation

Multilamellar vesicles for zeta potential measurements were prepared at a concentration of 6.8 mM using the protocol described in Section 3.1.2.1. Samples were prepared with total lipid weight of 20 mg using 10 mM sodium acetate buffer at either pH 5.0 or 7.0. The buffer solution was prepared in ultrapure MilliQ water (resistivity 18 MΩ). To make large unilamellar vesicles, samples were subjected to five cycles of freeze-thaw-vortex steps. The samples were frozen in liquid nitrogen for 3-5 minutes and thawed at room temperature. Samples were vortexed after each freeze-thaw step. Unilamellar vesicles of uniform size were prepared by 12 cycles of extrusion using a 200 nm filter (Nuclepore Track-Etched Membranes, Whatman, Toronto ON) under nitrogen gas pressure. Gad peptide stock solutions were prepared at 50 μM concentration using 10 mM sodium acetate buffer at either pH 7.0 or 5.0. The liposome and peptide stock solutions used in this work were 1-5 days old. For each zeta potential measurement, a sample of 2 mL final volume was prepared by mixing appropriate volumes of the liposome, the peptide stock solutions and buffer solution, to obtain the desired final concentrations of lipids and peptide. The liposome concentration was kept constant at 40 μL and the peptide concentration was varied. The pH of each sample was tested with a pH meter using a micro-probe and adjusted to 7.0 $\pm$ 0.1 or 5.0 $\pm$ 0.1 by adding 0.1 M HCl or 0.1 M NaOH. All mixed peptide/lipid samples were prepared and used on the same day.

3.1.3.2 Experimental details

Zeta potential measurements were performed at 25°C in a Malvern Zetasizer Nano ZS apparatus (model ZEN 3600, Malvern Instruments Ltd. U.K.). It was fitted with a 633 nm He−Ne laser. Zetasizer disposable folded capillary cells, DTS 1070 (Malvern Instruments Ltd. U.K.), were used in these experiments. Before each measurement, the cells were washed thoroughly with ethanol and then with ultrapure MilliQ water, and then dried under nitrogen flow. Samples were put in the measuring cells by injecting slowly using a 1 mL BD (Becton, Dickinson and Company) syringe to avoid bubbles that could affect the quality of the measurement. For each sample, 3 measurements (20 runs each), with an initial equilibration time of 5 minutes were performed at a constant voltage of 40 mV. The error bars on the binding isotherms represent the standard deviation in the average three measurements. The entered values of viscosity, refractive index, and dielectric constant were set at 0.8872 cP, 1.330, 78.5 respectively. Malvern DTS software was used to obtain mean zeta potential values.

3.1.4 Synthesis of Gad peptides

Gad peptides, Gad-1 and Gad-2, were chemically synthesized using O-fluorenylmethyloxycarbonyl (Fmoc) solid-phase synthesis on a CS Bio peptide synthesizer (model CS336X, CS Bio Company Inc., Menlo Park, CA). The peptide synthesis started with the attachment of the C-terminal peptide residue to the resin. In order to prevent polymerization of the amino acid, the alpha amino group and all reactive side chains were protected with Fmoc groups. Once the amino acid was attached to the resin, the protecting Fmoc group was removed. Then the next amino acid was coupled to the C-terminal amino acid. This cycle was repeated until the peptide sequence was complete. After this, the peptide was removed from the

resin and purified. The detailed protocol for the synthesis of Gad peptides [26] is described below:

1. All Fmoc amino acids for 0.2 mmole synthesis were weighed out in 5 × excess amounts.

2. 0.43 g rink amide resin (CS Bio Company Inc., Menlo Park, CA) was suspended in N, N-Dimethylformamide (DMF) for at least an hour.

3. Amino acids were loaded in a reverse order i.e. C-terminus first.

4. The resin bottle was attached and nitrogen flow and air compressor were turned on.

5. Reagent bottles 1, 2, 4, and 7 were filled with DMF. Bottle 3 was filled with 20% piperidine in DMF, bottle 5 with 1 M N, N-Diisopropylcarbodiimide (DIC) in DMF, and bottle 6 was filled with 0.4 M 1-hydroxy-benzotriazole (HoBt) in DMF.

6. The dissolution of amino acids was carried out with 0.4 M HoBt dissolved in DMF. The resin washes were performed by DMF and de-blocking of amino acids was achieved with 20% piperidine dissolved in DMF.

7. Once the peptide synthesis was completed, the peptide-containing resin, was transferred to a 10 mL syringe (BD Diagnostics Co.), rinsed with methanol under vacuum and left in the vacuum pump for at least an hour.

8. The cleavage of the peptide from the resin was carried out by using a cleavage cocktail prepared with 9.4 mL trifluoroacetic acid (TFA), 0.1 mL thioanisole, 0.25 mL 1,2- ethanedithiol (EDT), and 0.25 mL distilled water.

9. After adding the cleavage cocktail, the peptide was stirred for at least two hours at room temperature.

10. The resulting solution contained C-terminally amidated peptide. It was transferred into a 50 mL Falcon tube.

11. 40 mL of -20°C diethyl ether was added and the tube was left in -20°C degree freezer overnight for cold precipitation.

12. The white precipitate was centrifuged at 4690 × g at 4°C in Thermo Sorvall RC6+ centrifuge for 10-15 mins. Next, diethyl ether was removed very gently without disturbing the peptide pellet. This was followed by one more overnight diethyl ether precipitation.

13. The peptide was purified by High Pressure Liquid Chromatography (HPLC) as in McDonald et al., 2015 [26]. The molecular weight was confirmed by mass spectrometry (MALDI-TOF MS-Genomics and Proteomics facility, Memorial University). HPLC fractions containing the peptide were pooled and lyophilized.

14. The peptide was desalted by dialysis against 5% acetic acid and then water using 1kDa molecular weight cutoff of dialysis tubing. The resulting peptide solution was lyophilized and stored at 4°C.

3.2 Results

3.2.1 ^{2}H NMR results

NMR was used to assess peptide-induced acyl chain disorder in model lipid bilayers and the effect of peptide on slow motions of lipid bilayers.

As explained in Section 2.1.3.3, the powder pattern of chain per-deuterated lipids is a superposition of Pake doublets each corresponding to a deuteron on the lipid acyl

chain. The prominent edge at the maximum splitting for a spectrum corresponds to the deuterons on carbon atoms close to the lipid head group. The motions of chain segments containing these carbon atom are more constrained and thus more orientationally ordered than those of segments farther from the headgroup. The smallest quadrupole splittings come from the deuterons on the less constrained carbon atoms at the ends of lipid acyl chains. If the interaction of the peptide with lipid bilayers perturbs the lipid acyl chain packing and orientational order, the result will be a change in the range of splittings observed along a deuterated chain. A quantitative analysis of bilayer disruption by the peptide can be made by extracting the orientational order parameter, S_{CD}. The effect of the peptide on slow motions, like bilayer undulation or diffusion over regions of bilayer curvature, can be studied by measuring quadrupole echo decay time, T_2^{qe}. These motions of a lipid bilayer can affect refocussing of the quadrupole echo even if their correlation times are too long to contribute to changes in quadrupole splitting.

3.2.1.1 Peptide-induced disorder in model lipid bilayers

In order to investigate how Gad peptides perturb model lipid bilayers and how this perturbation changes with pH, a series of ^{2}H NMR experiments were performed with multilamellar vesicles containing Gad peptides at pH 7.0 and pH 5.0. All samples were prepared following the protocol described in Section 3.1.2.1. ^{2}H NMR spectra were acquired at two temperatures, 25°C and 37°C, using acquisition parameters listed in Section 3.1.2.2. The resultant ^{2}H spectra are shown in Figures 3.1 (a) and (b). It is evident from Figure 3.1 that the spectra of the lipids themselves did not change with pH. The powder pattern free induction decays obtained from multilamellar vesicles at 37°C were dePaked to obtain the corresponding oriented sample spectrum. The orientational order parameter (S_{CD}) was

calculated from these dePaked spectra using

$$\Delta\nu_Q = \frac{3}{2}\frac{e^2qQ}{\hbar}S_{CD}. \tag{3.1}$$

The dePaked spectra and corresponding order parameter profiles at pH 7.0 and pH 5.0 are shown in Figure 3.2 and Figure 3.3 respectively. It is evident from the order parameter profiles that addition of Gad peptides to POPE/POPG-d_{31}(3:1) lipid bilayers results in the reduction of order parameter values at both pH values. It should be noted that the change in orientational order parameter due to the Gad peptides is small. Comparisons of the order parameter values for each peptide at two pH values are shown in Figure 3.4 (a) and (b). The comparison of order parameter values indicates that for both Gad-1 and Gad-2, peptide-induced disorder in the lipid bilayer was not pH dependent.

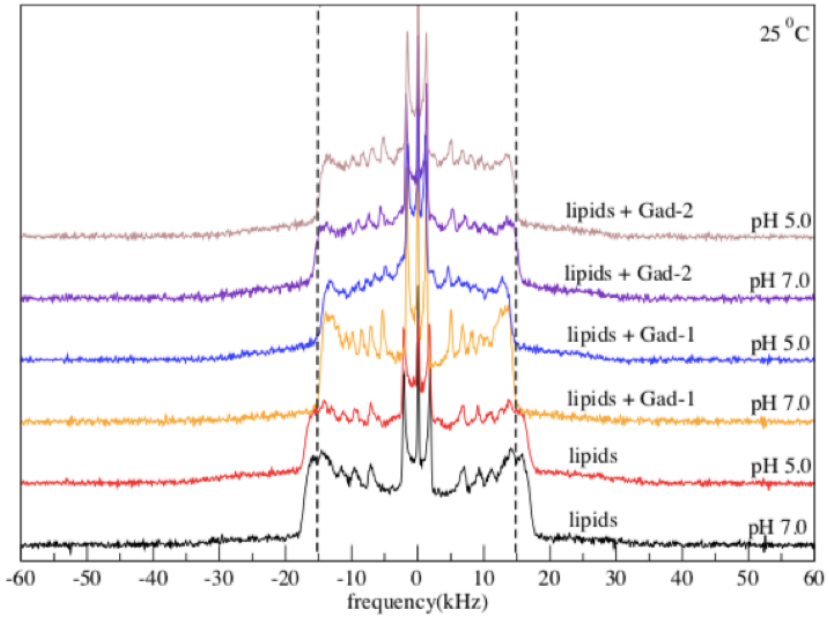

(a)

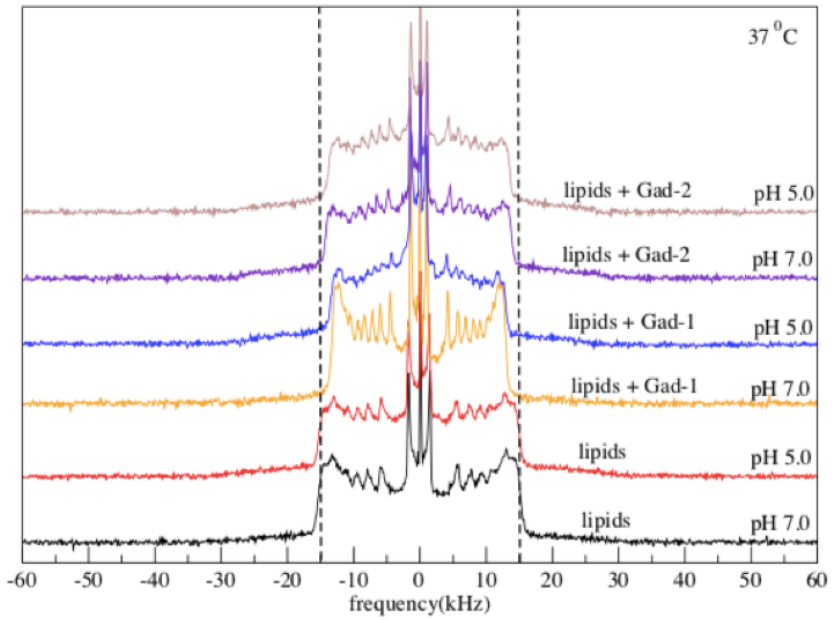

(b)

Figure 3.1: ^{2}H NMR spectra of multilamellar POPE/POPG-d_{31}(3:1) vesicles with and without Gad peptides at two pH values (a) at 25°C (b) 37°C. All spectra were obtained by averaging 4000 transients. Comparison of spectra show a small peptide-induced decrease in splitting. The dashed black lines indicate the maximum quadrupole splitting for deuterons on the most ordered chain segments in the absence of peptide at 37°C. Comparison of maximum splittings for other spectra with the location of the black line provides an indication of the extent to which the presence of the peptide alters the observed quadrupole splitting in each sample.

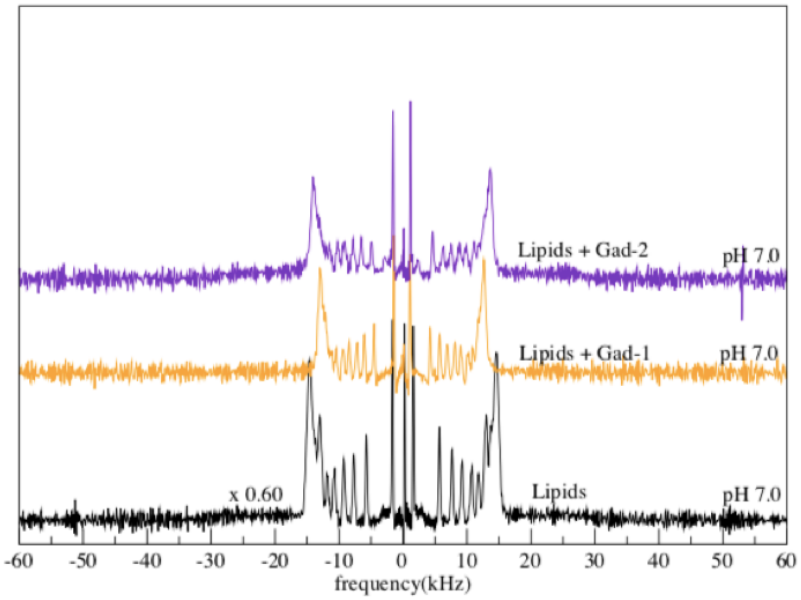

(a)

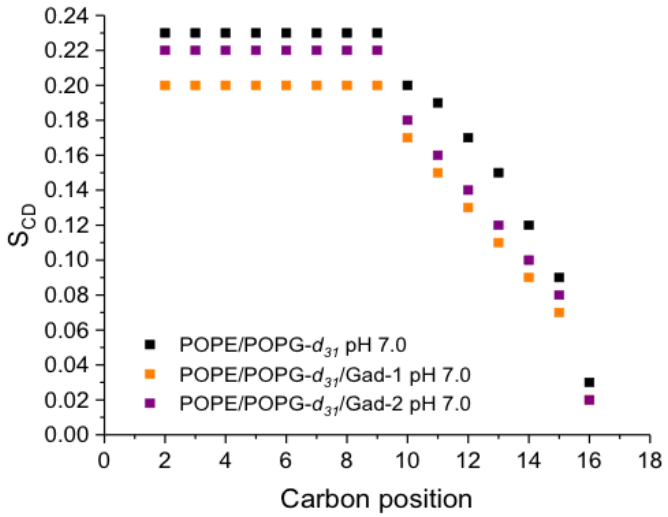

(b)

Figure 3.2: The peptide-induced acyl chain disorder in POPE/POPG-d_{31}(3:1) lipid vesicles was quantitatively analysed by calculating orientational order parameter S_{CD}. For this, the powder pattern spectra of lipids and lipids + Gad peptides were dePaked to obtain the corresponding oriented sample spectra. (a) The oriented spectra corresponding to the powder pattern spectra of POPE/POPG-d_{31}(3:1) lipid vesicles with and without Gad peptides at pH 7.0. (b) Order parameter values of POPE/POPG-d_{31}(3:1) lipid vesicles in the absence and presence of Gad peptides at pH 7.0. The uncertainty in order parameter values was approximately 5%. The addition of either peptide is seen to decrease the order parameter values at this pH value.

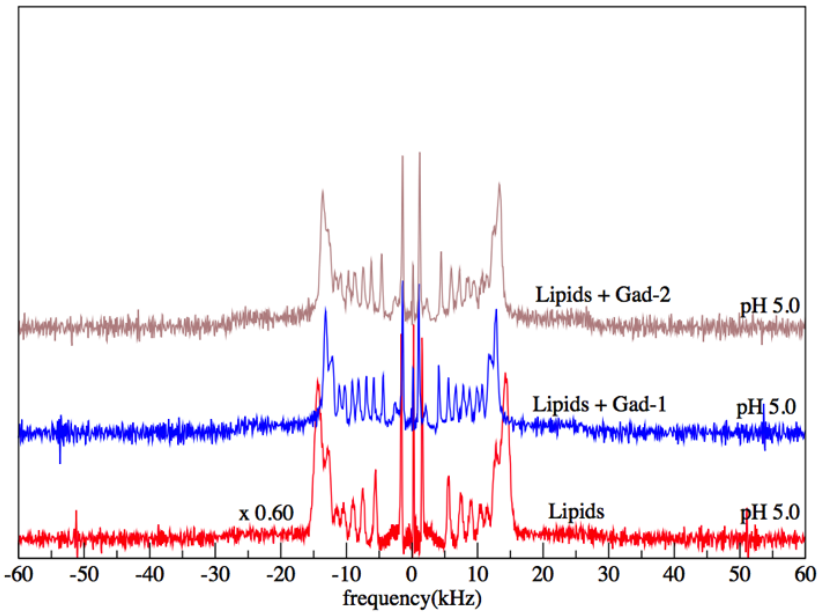

(a)

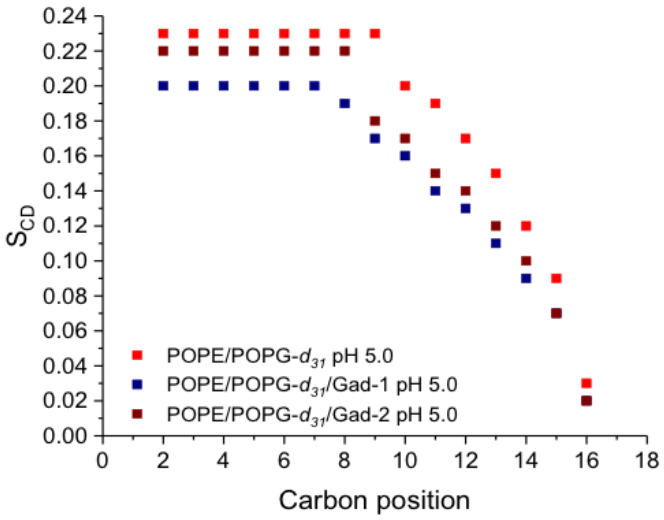

(b)

Figure 3.3: (a) The oriented spectra corresponding to the powder pattern spectra of POPE/POPG-d_{31}(3:1) lipid vesicles with and without Gad peptides at pH 5.0. (b) Order parameter values for POPE/POPG-d_{31}(3:1) lipid vesicles in the absence and presence of Gad peptides at pH 5.0. The uncertainty in order parameter values was approximately 5%. The addition of either peptide is seen to decrease the order parameter values at this pH value.

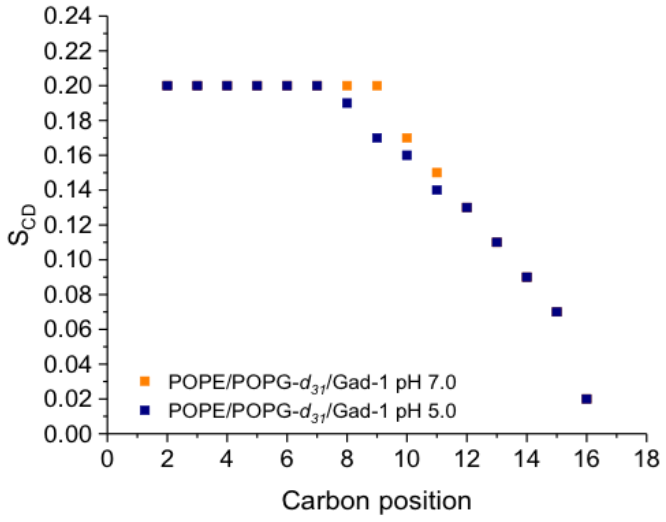

(a)

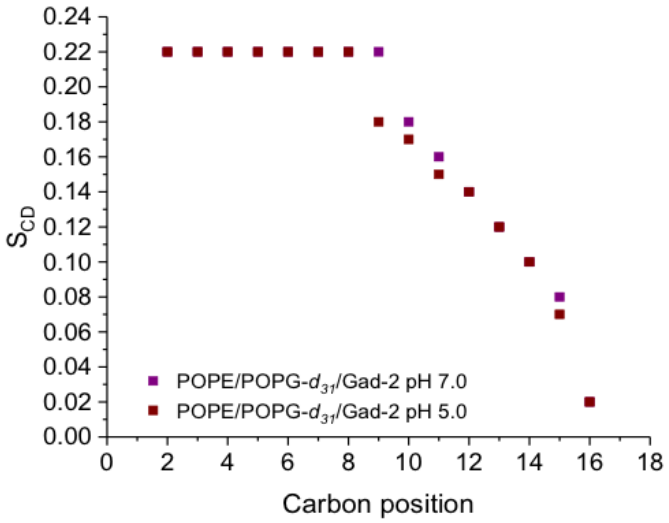

(b)

Figure 3.4: (a) The comparison of order parameter profiles for POPE/POPG-d_{31}(3:1) lipid bilayers interacting with Gad-1 at pH 7.0 and 5.0. (b) The comparison of order parameter profile for POPE/POPG-d_{31}(3:1) lipid bilayers interacting with Gad-2 at pH 7.0 and 5.0. The overlapping of points suggests that peptide-induced disorder in the lipid acyl chains is not sensitive to change in pH for either peptide.

3.2.1.2 Effect of Gad peptides on slow motions of lipid bilayers as determined by quadrupole echo decay time (T_2^{qe})

A series of quadrupole echo decay experiments were carried out to see if Gad peptides can perturb the slow motions of the lipid bilayer and whether any observed perturbations are sensitive to pH. Details of quadrupole echo decay time are described in Section 2.1.3.6.

Quadrupole echo decay time experiments were performed on multilamellar vesicles with and without the addition of Gad peptides at pH 7.0 and pH 5.0. Acquisition parameters listed in the Section 3.1.2.2 were used to perform these experiments. The echo amplitudes were measured for each value of τ. The averaged echo decay times, T_2^{qe}, were obtained by plotting ln $\left(\frac{A(\tau)}{A(0)}\right)$ vs. 2τ and using the initial slope of the echo decay curve. The average echo decay time (T_2^{qe}) results are shown in Figure 3.5 for two temperatures, 25°C and 37°C.

A change in the value of T_2^{qe} with the addition of Gad peptides indicates a perturbation of fast or slow lipid motions by Gad peptides in POPE/POPG-d_{31} (3:1) lipid bilayers. At 25°C and pH 7.0, Gad-1 decrease the echo decay time and Gad-2 has little effect on the echo decay time. At 25°C and pH 5.0, Gad-1 has little effect on the echo decay time and Gad-2 significantly increases the echo decay time. At 37°C and at pH 7.0, Gad-1 decreases the echo decay time slightly and Gad-2 increases the echo decay time. At 37°C and at pH 5.0, Gad-1 has little effect on echo decay time and Gad-2 significantly increases the echo decay time.

A decrease in echo decay time (i.e. the effect of Gad-1 at pH 7.0 at either temperature) could reflect an increase in fast motion correlation time (i.e. slowing down a fast motion) or a decrease in slow motion correlation time (i.e. speeding up a slow motion). The increase in echo decay time (i.e. the effect of Gad-2 at pH 5.0 at either temperature) could reflect a decrease in fast motion correlation time (i.e.

a speeding up of fast motion) or an increase in slow motion correlation time (a slowing down of a slow motion).

For lipid only samples, echo decay time is independent of temperature or only weakly dependent on temperature. The echo decay times for bilayers with a given peptide are not sensitive to pH and thus not sensitive to peptide charge. Gad-1 and Gad-2 seem to have opposite effects on the echo decay times. The interpretation of these observations is discussed in Section 3.3.

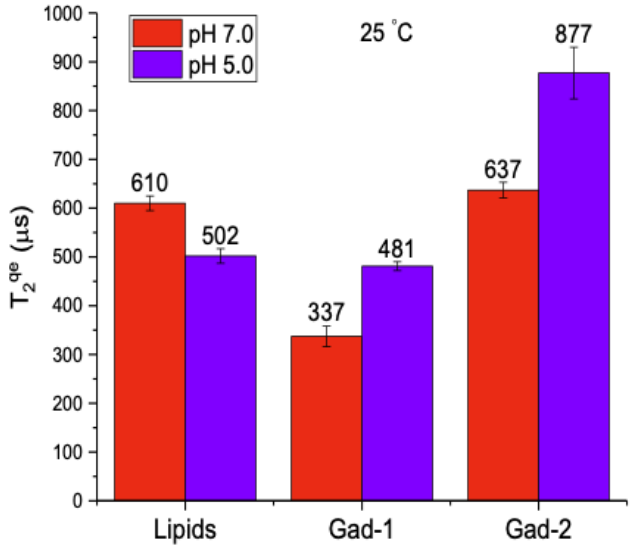

(a)

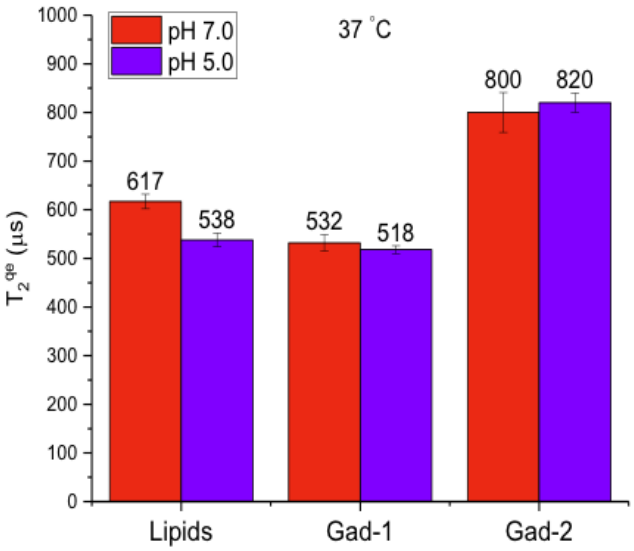

(b)

Figure 3.5: (a) The pH dependence of quadrupole echo decay time (T_2^{qe}) of POPE/POPG-d_{31} (3:1) lipid vesicles with and without the addition of Gad peptides at (a) 25°C (b) 37°C. The error bars represent the uncertainty in the values of T_2^{qe} calculated from the uncertainty in the value of initial slope of echo decay curve.

3.2.2 Zeta potential (ζ-potential) results

The concentration of AMP required to disrupt a bacterial membrane is an important factor. While there needs to be a high enough concentration of AMP for there to be significant interactions with bacterial membranes, the concentration should not be so high that host cells are harmed. This fine balance between maximizing interactions with pathogen membranes and minimizing them with host cell membranes makes it important to understand the binding affinities of peptides to lipid membranes. Gad peptides have higher overall positive charge at pH 5.0 than at pH 7.0. Therefore, a stronger electrostatic interaction between peptide and lipid bilayers was expected at slightly acidic pH than at neutral pH. Also, MIC assay against *E.coli* showed that Gad-2 exhibits greater activity at pH 5.0 than at pH 7.0 [26]. However, ^{2}H NMR results showed that there was no difference in the peptide-induced disorder in POPE/POPG (3:1) lipid bilayers for Gad peptides at pH 7.0 and pH 5.0. A potential hypothesis to explain this discrepancy could be that Gad peptides perturb the lipid acyl chain order in the same way at pH 7.0 and at pH 5.0 but there might be a difference in the binding of the peptides at different pH values. To account for the observed effects of pH on lipid chain order and MIC, it might then be necessary to further hypothesize that MIC correlates with the binding of peptide to the membrane rather than to perturbation of lipid acyl chain order. Two parameters deduced from binding studies, the equilibrium constant (K_{eq}) and the peptide partition constant (K_P), describe the binding process quantitatively [56, 116, 127, 128]. The equilibrium constant and partition constant can be determined by using different methodologies [116] such as UV-Vis absorption spectrophotometry, fluorescence spectroscopy, and zeta potential measurements. In this work, zeta potential measurements were used to quantify peptide binding to model membranes at two pH values. For this purpose, zeta potentials of model lipid membranes were measured with increasing concentrations

of peptide. Binding isotherms were obtained by plotting zeta potential vs. peptide concentration.

3.2.2.1 Binding isotherms

Zeta potentials of POPE/POPG (3:1) lipid vesicles with increasing concentrations of Gad peptides were measured at pH 7.0 and pH 5.0. Large unilamellar vesicles were prepared using the protocol described in the Section 3.1.3.1. The sizes of these vesicles were measured by Dynamic Light Scattering (DLS) using a Malvern Zetasizer Nano ZS apparatus (model ZEN 3600, Malvern Instruments Ltd. U.K.). The observed sizes of these vesicles were 140 ± 10 nm. The pH of each sample was tested with a pH meter using a micro-probe and adjusted to 7.0 ± 0.1 or 5.0 ± 0.1. For all zeta potential measurements, temperature was maintained at 25 ± 0.1 °C. Firstly, the zeta potential was measured for lipid vesicles in the absence of peptide at both pHs. As expected, negative zeta potentials were calculated from electrophoretic mobilities for these liposome samples. This was followed by the measurement of zeta potentials for lipid vesicles in the presence of increasing concentrations of Gad peptides. The appropriate amounts of lipid vesicle stock solution were added to the peptide solution to achieve the desired concentration of peptide. The lipid concentration was kept constant at 40 μM in all measurements. For Gad-1, peptide concentration ranged from 0 μM−20 μM in 1 μM steps (0, 1, 2, 3,....20 μM) while for Gad-2 it was increased from 0 μM−50 μM in 5 μM steps (0, 5, 10.....50 μM). For Gad-2, little change in the zeta potential was observed when peptide concentration was increased in steps of 1 μM. This is presumably due to the fact that Gad-2 has less charge than Gad-1 at both pHs. The values of zeta potential for liposomes with and without the addition of Gad peptides were calculated from their electrophoretic mobility using Henry's equation along with the Smoluchowski approximation [129, 130] using the Malvern DTS software. For a

given population of liposomes, individual zeta potential values form a distribution. The mean zeta potential represents the mean of the zeta potential distribution and is obtained using Malvern instrument software. The error bars were estimated by averaging the deviation from the mean for three measurements. As explained in Section 2.2.2, the Smoluchowski approximation can be used when the particle size is greater than the Debye length ($a >> 1/\kappa$). Using Equation 2.55 [131], Debye lengths were estimated for the solutions in which vesicles were dispersed. These were found to be less than 3 nm in the absence of peptide. Given that addition of peptide is expected to reduce the Debye length, this indicates that the Smoluchowski approximation is valid over the full range of peptide concentrations studied. Binding isotherms were obtained by plotting mean zeta potential vs. total peptide concentration. The binding isotherms for Gad-1 at pH 7.0 and pH 5.0 are shown in Figure 3.6 and the binding isotherms of Gad-2 at pH 7.0 and pH 5.0 are shown in Figure 3.7.

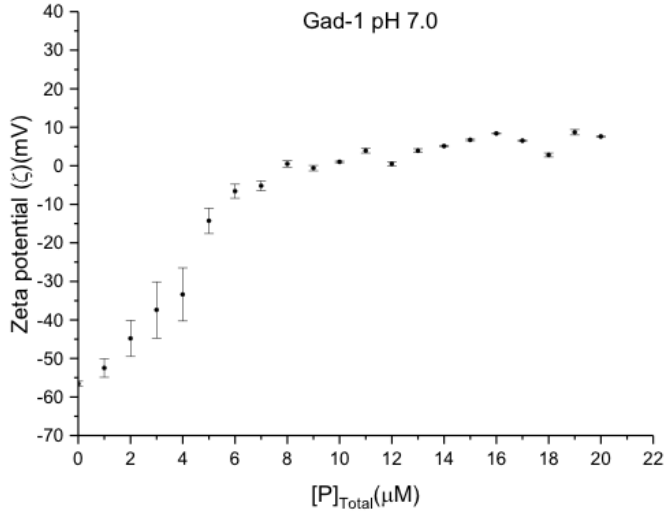

(a)

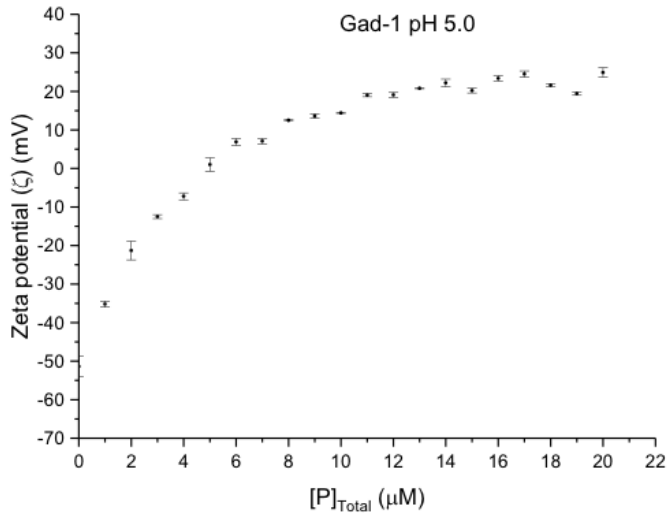

(b)

Figure 3.6: The binding isotherms of Gad-1 at (a) pH 7.0 (b) pH 5.0. Each point represents the average of three independent measurements. The first point in the isotherm represents the zeta potential of liposomes in the absence of peptide. A negative value of zeta potential was calculated in the absence of peptide. As the peptide concentration was increased the zeta potential increased toward a limiting value. When all peptide binding sites are occupied, the limiting value of zeta potential depends on the overall charge of peptide and the $L : P$ ratio. At pH 7.0, Gad-1 has charge of +3 and the limiting value is $\sim$ 5 mV. On the other hand, at pH 5.0 Gad-1 has charge of +8 and the limiting value in this case is $\sim$ 20 mV. The error bars were estimated by averaging the deviation from the mean for three measurements.

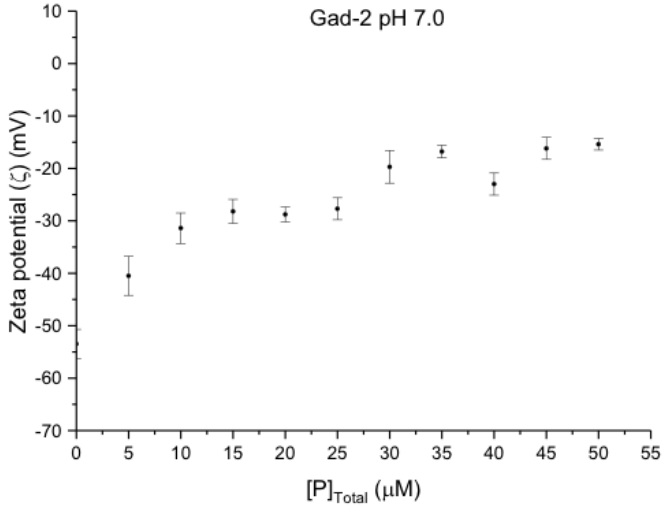

(a)

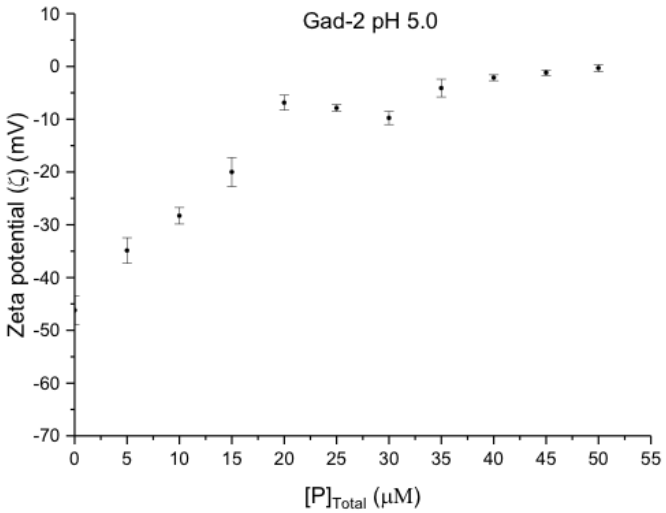

(b)

Figure 3.7: (a) The binding isotherms of Gad-2 at (a) pH 7.0 (b) pH 5.0. Each point represents the average of three independent measurements. The first point in the isotherm represents the zeta potential of liposomes in the absence of peptide. A negative value of zeta potential was calculated in the absence of peptide. As the peptide concentration was increased the zeta potential increased toward a limiting value. When all peptide binding sites were occupied, the limiting value of zeta potential depends on the overall charge of peptide and the $L : P$ ratio. At pH 7.0, Gad-2 has charge of +1 and the limiting value is $\sim$ -20 mV. On the other hand, at pH 5.0 Gad-2 has charge of +5 and the limiting value in this case is $\sim$ 5 mV. The error bars were estimated by averaging the deviation from the mean for three measurements.

A few different adsorption isotherm models can be used to fit the experimental zeta potential data for the purpose of quantifying peptide binding to the membrane. A binding model described by Freire et al. [116] allows the calculation of a partition constant, the molar fraction of peptide bound to the membrane, and the lipid-peptide ratio. Alternatively, a zeta potential model based on the Langmuir isotherm model [132, 133] can be applied to determine the fraction of peptide bound to the membrane, the ratio of available peptide binding sites to total membrane lipids, and an equilibrium constant. Both models allow calculation of the molar fraction of the total peptide in the sample that is bound to the membrane. The lipid-peptide ratios determined from the zeta potential model based on the Langmuir model at high peptide concentration, are the limiting values of the lipid-peptide ratios calculated using the Freire et al. model. A different binding model, described elsewhere [127] relates the binding isotherm to electrostatic interaction and an equilibrium constant.

3.2.2.2 A binding model to calculate the partition constant (K_P)

A model that characterizes peptide binding in terms of a partition constant is described following the treatment of Freire et al. [116]. The main assumption of this model is that when a cationic peptide interacts with a negatively charged membrane, one peptide charge neutralizes one lipid charge. The Freire et al. model treats bound peptide as being dissolved in the lipid environment. This model uses the linear part of the zeta potential binding isotherm to determine the molar fraction of peptide bound to the membrane and partition constant. This model does not use information from the limiting value of the zeta potential at high peptide concentration.

A summary of the model presented by Freire et al. is given below. The interaction of a cationic peptide with a model lipid membrane composed of anionic lipids

results in the reduction of negative surface charge on the membrane. The partition constant, K_P, is defined by Freire et al. as the ratio of the peptide concentration in the lipid to the peptide concentration in the aqueous phase [56, 116, 128] so that

$$K_{\mathrm{P}} = \frac{[P]_{\mathrm{L}}}{[P]_{\mathrm{W}}} \tag{3.2}$$

where $[P]_{\mathrm{L}}$ and $[P]_{\mathrm{W}}$ are the peptide concentrations in the lipid and the water environments respectively. Equation 3.2 can be written as

$$K_{\mathrm{P}} = \frac{\left(\frac{n_{\mathrm{P,L}}}{V_{\mathrm{L}}}\right)}{\left(\frac{n_{\mathrm{P,W}}}{V_{\mathrm{W}}}\right)} \tag{3.3}$$

where $n_{\mathrm{P,L}}$ and $n_{\mathrm{P,W}}$ are the numbers of moles of peptide in lipid and water environments respectively and V_{L} and V_{W} are the volumes of the lipid and water environments, respectively. It should be noted that the volume of the lipid phase is equivalent to the volume of the membrane and it is thus small compared to the volume of the aqueous phase. The total number of moles of peptide is given as

$$n_{\mathrm{P,T}} = n_{\mathrm{P,W}} + n_{\mathrm{P,L}} \tag{3.4}$$

where $n_{\mathrm{P,T}}$ is the total numbers of moles of peptide in water and lipid environments combined.

In terms of the peptide concentration, Equation 3.4 can be written as

$$[P]_{\mathrm{Total}} V_{\mathrm{T}} = [P]_{\mathrm{W}} V_{\mathrm{W}} + [P]_{\mathrm{L}} V_{\mathrm{L}} \tag{3.5}$$

$$[P]_{\mathrm{Total}} = [P]_{\mathrm{W}} \left(\frac{V_{\mathrm{W}}}{V_{\mathrm{T}}}\right) + [P]_{\mathrm{L}} \left(\frac{V_{\mathrm{L}}}{V_{\mathrm{T}}}\right) \tag{3.6}$$

so that

$$[P]_{\mathrm{Total}} \cong [P]_{\mathrm{W}} + [P]_{\mathrm{L}} \left(\frac{V_{\mathrm{L}}}{V_{\mathrm{T}}}\right) \tag{3.7}$$

where $[P]_{\text{Total}}$ is the total peptide concentration over the total volume. It should be noted that the simplification of this expression occurs because the volume of the aqueous phase (V_{W}) is effectively equal to total volume (V_{T}). The volume occupied by the bilayer membrane can be written as

$$V_{\text{L}} = \gamma_{\text{L}}[L]V_{\text{W}} \tag{3.8}$$

where γ_{L} is the molar volume of lipid (i.e the volume occupied by one mole of lipid) and [L] is total lipid concentration.

From Equation 3.3, the partition constant can now be written as

$$K_P = \left(\frac{n_{\text{P,L}}}{n_{\text{P,W}}}\right)\left(\frac{V_{\text{W}}}{V_{\text{L}}}\right). \tag{3.9}$$

Using Equation 3.8, Equation 3.9 becomes

$$K_P = \left(\frac{n_{\text{P,L}}}{n_{\text{P,W}}}\right)\frac{1}{\gamma_{\text{L}}[L]} \tag{3.10}$$

so that

$$n_{\text{P,L}} = n_{\text{P,W}}\gamma_{\text{L}}[L]K_P. \tag{3.11}$$

In the Freire et al. model, the parameter of interest is the molar fraction of peptide that is bound to the membrane,

$$X = \frac{n_{\text{P,L}}}{n_{\text{P,L}} + n_{\text{P,W}}}. \tag{3.12}$$

Using Equation 3.11 and Equation 3.12, X can be written in terms of the partition constant (K_P) as

$$X = \frac{\gamma_{\text{L}}[L]K_P}{1 + \gamma_{\text{L}}[L]K_P}. \tag{3.13}$$

The binding of a peptide to the membrane results in the reduction of membrane

surface charge and this reduction is proportional to the fraction of negatively charged lipids that are neutralized by the peptide charge so that

$$|\frac{\Delta\zeta}{\zeta_0}| = \frac{n_{\mathrm{L^-_{neutralized}}}}{n_{\mathrm{L^-_{total}}}} \tag{3.14}$$

where

$$\Delta\zeta = \zeta - \zeta_0. \tag{3.15}$$

In these equations, ζ_0 is the zeta potential in the absence of peptide, $n_{\mathrm{L^-_{neutralized}}}$ is the number of moles of negatively charged lipid molecules that are neutralized by peptide, and $n_{\mathrm{L^-_{total}}}$ is the total number of moles of charged lipid molecules.
Now assuming that one peptide charge neutralizes one lipid charge, $n_{\mathrm{L^-_{neutralized}}}$ is given as

$$n_{\mathrm{L^-_{neutralized}}} = n_{\mathrm{P,L}} z_{\mathrm{P}} \tag{3.16}$$

where z_{P} is the peptide charge. The values of z_{P} are +3 and +8 for Gad-1 at pH 7.0 and pH 5.0 respectively and +1 and +5 for Gad-2 at pH 7.0 and pH 5.0 respectively. Using Equation 3.12, Equation 3.16 becomes

$$n_{\mathrm{L^-_{neutralized}}} = X n_{\mathrm{P,T}} z_{\mathrm{P}} \tag{3.17}$$

$$= X[P]_{\mathrm{Total}} V_{\mathrm{T}} z_{\mathrm{P}} \tag{3.18}$$

The total number of charged lipid molecules, $n_{\mathrm{L^-_{total}}}$, is given by

$$n_{\mathrm{L^-_{total}}} = [L] V_{\mathrm{T}} f_{\mathrm{L^-}} z_{\mathrm{L^-}} \tag{3.19}$$

where $f_{\mathrm{L^-}}$ is the fraction of lipids that are anionic (0.25 for POPE/POPG (3:1)), $z_{\mathrm{L^-}}$ is the charge of anionic lipids (-1 for POPG), and $[L]$ is the total lipid concentration which is kept constant at 40 μM.

Using Equation 3.18 and Equation 3.19, the relative reduction is zeta potential

for a given overall peptide concentration becomes

$$|\frac{\Delta\zeta}{\zeta_0}| = \frac{X z_{\mathrm{P}}}{f_{\mathrm{L}^-}[L] z_{\mathrm{L}^-}}[P]_{\mathrm{Total}}. \tag{3.20}$$

Equation 3.20 can be arranged to get the normalized zeta potential

$$\frac{\zeta}{\zeta_0} = \frac{X z_{\mathrm{P}}}{f_{\mathrm{L}^-}[L] z_{\mathrm{L}^-}}[P]_{\mathrm{Total}} + 1. \tag{3.21}$$

The slope of $\frac{\zeta}{\zeta_0}$ vs. $[P]_{\mathrm{Total}}$ yields X which allows the calculation of K_P using Equation 3.13. Equation 3.21 indicates a linear dependence between $\frac{\zeta}{\zeta_0}$ and $[P]_{\mathrm{Total}}$. The zeta potential binding isotherms indicates that $\frac{\zeta}{\zeta_0}$ saturates at higher values of $[P]_{\mathrm{Total}}$. Hence Equation 3.21 is not true for higher values of $[P]_{\mathrm{Total}}$. In other words, the Freire et al. model holds only for the linear part of zeta potential binding isotherm.

With the knowledge of X, the local concentration of peptide in the membrane can be determined to be [134]

$$[P]_{\mathrm{L}} = \frac{X[P]_{\mathrm{Total}}}{\gamma_{\mathrm{L}}[L]}. \tag{3.22}$$

The local lipid-to-peptide ratio, $(L:P)_{\mathrm{local}}$, is the number of lipid molecules per peptide molecule within the membrane and can be determined using [134]

$$(L:P)_{\mathrm{local}} = \frac{n_{\mathrm{lipids}}}{n_{\mathrm{P,L}}} \tag{3.23}$$

$$= \frac{n_{\mathrm{lipids}}}{n_{\mathrm{P,T}} X}. \tag{3.24}$$

In terms of peptide and lipid concentration Equation 3.24 becomes

$$(L:P)_{\mathrm{local}} = \frac{[L]V_{\mathrm{T}}}{X[P]_{\mathrm{Total}}V_{\mathrm{T}}} \tag{3.25}$$

$$= \frac{[L]}{X[P]_{\mathrm{Total}}}. \tag{3.26}$$

Using Equation 3.13, Equation 3.26 becomes

$$(L:P)_{\text{local}} = \frac{1 + [L]K_P\gamma_{\text{L}}}{[P]_{\text{Total}}\gamma_{\text{L}}K_P} \tag{3.27}$$

$$= \left(\frac{1}{[P]_{\text{Total}}K_P\gamma_{\text{L}}} + \frac{[L]}{[P]_{\text{Total}}}\right). \tag{3.28}$$

In order to determine the partition constant, a portion of the binding isotherm was selected where the zeta potential appeared to change linearly with increasing total peptide concentration. From the selected linear portion of the graph, the normalized zeta potential was calculated by dividing the zeta potential value for each peptide concentration by the zeta potential value in the absence of peptide. The binding isotherms and corresponding normalized zeta potentials for Gad-1 at pH 7.0 and pH 5.0 are shown in Figure 3.8 and Figure 3.9 respectively. The binding isotherms and corresponding normalized zeta potentials for Gad-2 at pH 7.0 and pH 5.0 are shown in Figure 3.10 and Figure 3.11 respectively. The slopes of normalized zeta potential vs. peptide concentration were used to determine the molar fraction of peptide that is bound to the membrane using Equation 3.21. The partition constant was determined using Equation 3.13. The values of f_{L^-}, z_L, and γ_{L} in Equation 3.21 are 0.25, -1 and 0.763 in liters per mole [56, 135] respectively. The values of X and K_P found in this way for Gad-1 and Gad-2 at pH 7.0 and pH 5.0 are listed in Tables 3.2 and 3.3 respectively. For both Gad-1 and Gad-2, the values of X are smaller at pH 5.0 than at pH 7.0. The values of K_P are on the order of 10^3 for Gad peptides. The larger value of this partition constant reflects the fact that volume of the membrane is very small compared to volume of the aqueous phase so that the amount of peptide bound per unit lipid volume is large. Values of the local peptide concentration ($[P]_{\text{L}}$) and $(L:P)_{\text{local}}$ were calculated using Equation 3.22 and Equation 3.26 [134] and are listed in Table 3.4 and Table 3.5. The $[P]_{\text{L}}$ increased as the total peptide concentration $[P]_{\text{Total}}$ was increased.

Values of $(L:P)_{\text{local}}$ were higher at pH 5.0 than at pH 7.0. The interpretation of these results is discussed in Section 3.3 below.

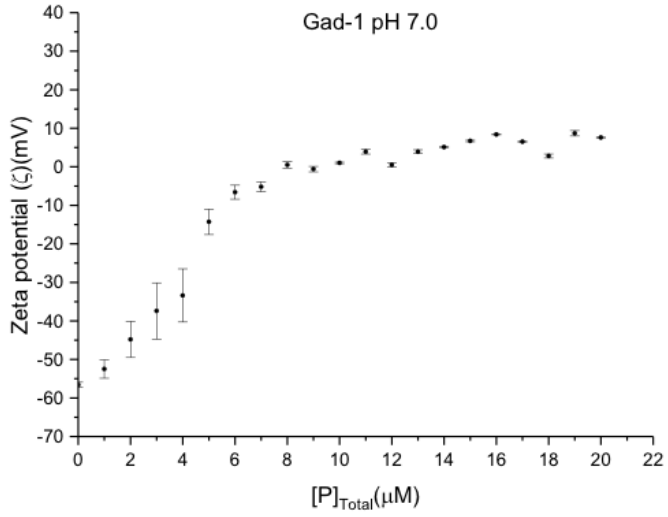

(a)

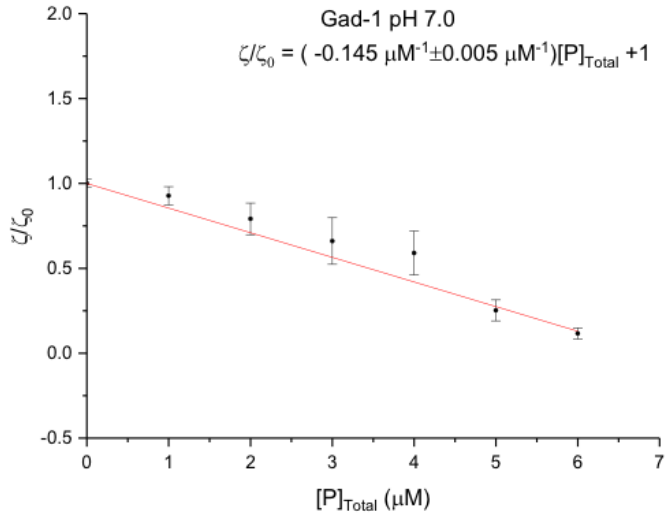

(b)

Figure 3.8: (a) Zeta potential measurements for 40 μM POPE/POPG (3:1) in the presence of Gad-1 at pH 7.0. Addition of peptide to lipid vesicles results in the reduction of zeta potential values. At higher concentration of the peptide, zeta potential approaches a positive limit of $\sim$ 5 mV. The linear portion of this graph, 0 μM - 6 μM peptide concentration, was selected to obtain the normalized zeta potential plotted in panel (b). (b) Normalized zeta potential dependence on the concentration of Gad-1 peptide at pH 7.0. The slope of the linear portion of the binding isotherm was obtained using weighted linear fitting. The size of error bars was taken into account to estimate the uncertainty in the slope. The slope of this graph was used to determine the partition constant.

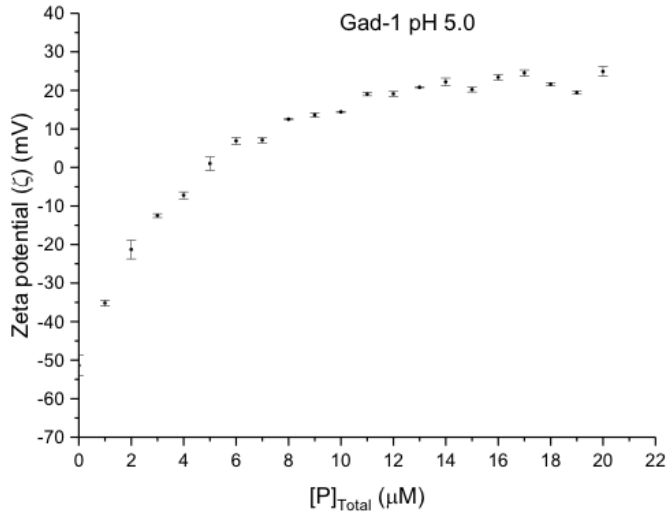

(a)

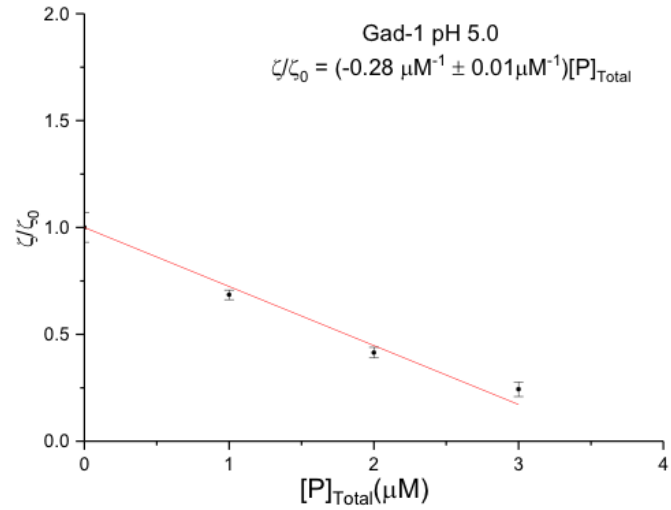

(b)

Figure 3.9: (a) Zeta potential measurements for 40 μM POPE/POPG (3:1) in the presence of Gad-1 at pH 5.0. Addition of peptide to lipid vesicles results in the reduction of zeta potential values. At higher concentrations of the peptide, zeta potential value approaches a limit of $\sim$ 20 mV. The linear portion of this graph, 0 μM - 3 μM peptide concentration, was selected to obtain the normalized zeta potential plotted in panel (b). (b) Normalized zeta potential dependence on the concentration of Gad-1 peptide at pH 5.0. The slope of the linear portion of the binding isotherm was obtained using weighted linear fitting. The size of error bars was taken into account to estimate the uncertainty in the slope. The slope of this graph was used to determine the partition constant.

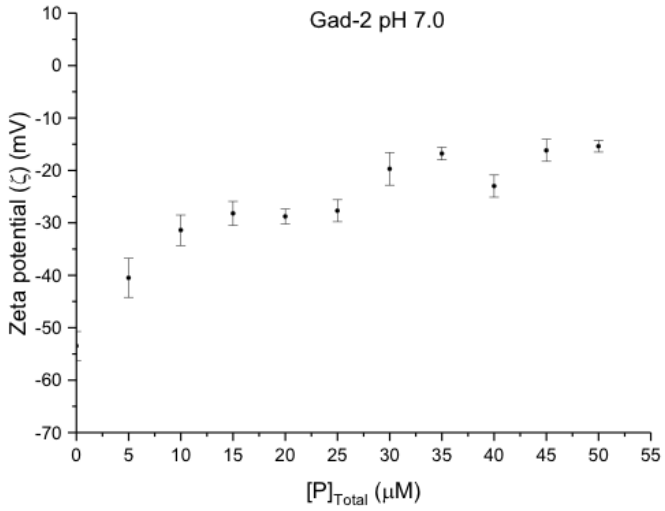

(a)

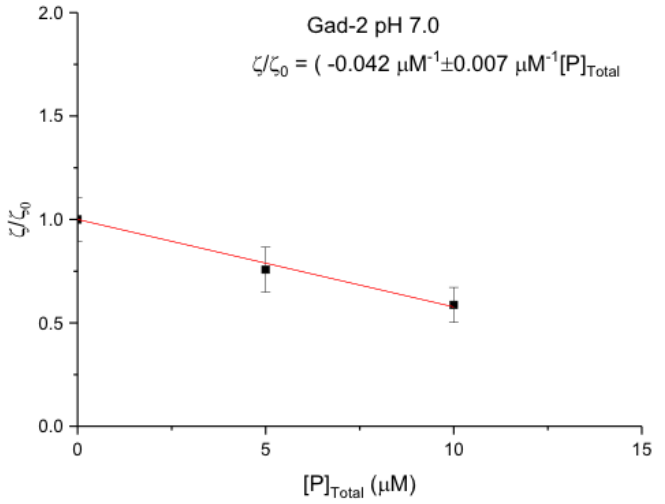

(b)

Figure 3.10: (a) Zeta potential measurements for 40 μM POPE/POPG (3:1) in the presence of Gad-2 at pH 7.0. At higher concentrations of the peptide, the zeta potential approaches a negative limit of $\sim$ -20 mV. The first three points in the graph were selected to obtain the normalized zeta potential plotted in panel (b). (b) Normalized zeta potential dependence on the concentration of Gad-2 peptide at pH 7.0. The slope of the linear portion of the binding isotherm was obtained using weighted linear fitting. The size of error bars was taken into account to estimate the uncertainty in the slope. The slope of this graph was used to determine the partition constant.

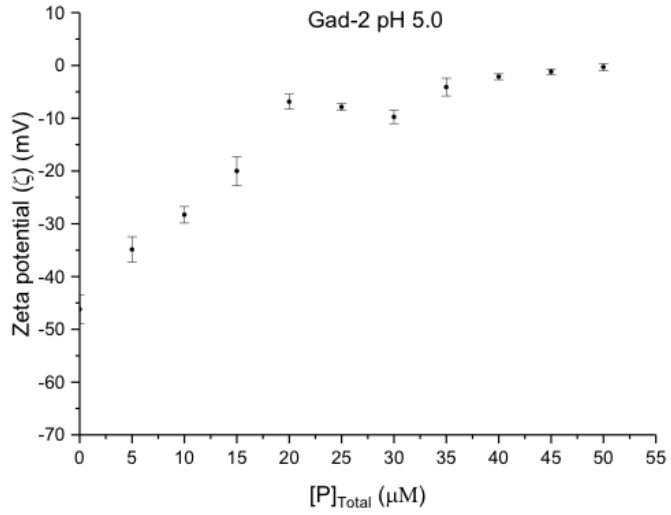

(a)

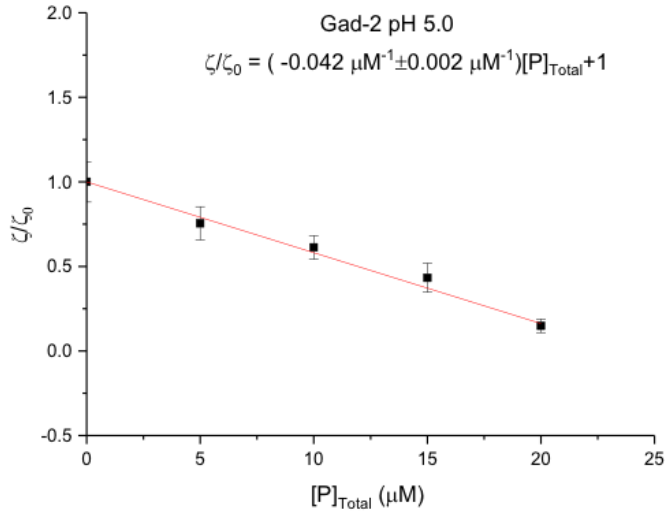

(b)

Figure 3.11: (a) Zeta potential measurements for 40 μM POPE/POPG (3:1) in the presence of Gad-2 at pH 5.0. Addition of peptide to lipid vesicles results in the reduction of zeta potential values. At higher concentrations of the peptide zeta potential value approaches a positive limit of $\sim$ 5 mV. The linear portion of this graph, 0 μM - 20 μM peptide concentration, was used to obtain the normalized zeta potential plotted in panel (b). (b) Normalized zeta potential dependence on the concentration of Gad-1 peptide at pH 7.0. The slope of the linear portion of the binding isotherm was obtained using weighted linear fitting. The size of error bars was taken into account to estimate the uncertainty in the slope. The slope of this graph was used to determine the partition constant.

Gad-1		
pH	Molar fraction of peptide bound to the membrane (X)	Partition constant (K_P)
7.0	0.48±0.02	30,000 ± 2000
5.0	0.35±0.01	17,600± 800

Table 3.2: Calculated molar fractions of peptide bound to the membrane (X) and partition constants (K_P) from zeta potential measurements for Gad-1 at pH 7.0 and pH 5.0. Equation 3.21 and Equation 3.13 were used to calculate X and K_P.

Gad-2		
pH	Molar fraction of peptide bound to the membrane (X)	Partition constant (K_P)
7.0	0.4±0.1	24,000 ± 7000
5.0	0.08±0.01	2,800 ± 400

Table 3.3: Calculated molar fractions of peptide bound to the membrane (X) and partition constants (K_P) from zeta potential measurements for Gad-2 at pH 7.0 and pH 5.0. Equation 3.21 and Equation 3.13 were used to calculate X and K_P.

Gad-1					
$[P]_{\text{Total}}$ (μM)	global $L:P$	pH 7.0		pH 5.0	
		$[P]_{\text{L}}$ (mM)	$(L:P)_{\text{local}}$	$[P]_{\text{L}}$ (mM)	$(L:P)_{\text{local}}$
1	40	16	83	11	114
2	20	31	42	22	57
3	13	47	28	34	38
4	10	63	21	46	28
5	8	79	17	57*	23*
6	6	94	14	68*	19*

Table 3.4: The global $L:P$ is calculated for the total peptide concentration 1 μM - 6 μM. The range of total peptide concentration is selected from the linear portion of Figure 3.8 (a). The local peptide concentration in the membrane and $(L:P)_{\text{local}}$ are also calculated using Equation 3.22 and Equation 3.26 for corresponding total peptide concentration at pH 7.0 and pH 5.0. Note that $(L:P)_{\text{local}}$ represents the lipid to peptide ratio for lipid and peptide complexes.
Note: The values of $[P]_{\text{L}}$ and $(L:P)_{\text{local}}$ with * fell outside of the linear region of zeta potential binding isotherm for Gad-1 at pH 5.0.

Gad-2					
$[P]_{\text{Total}}$ (μM)	global $L:P$	pH 7.0		pH 5.0	
		$[P]_{\text{L}}$ (mM)	$(L:P)_{\text{local}}$	$[P]_{\text{L}}$ (mM)	$(L:P)_{\text{local}}$
5	8	69	19	13	100
10	4	137	10	26	50
15	3	-	-	39	33
20	2	-	-	52	25

Table 3.5: The global $L:P$ is calculated for the total peptide concentration 5 μM- 15 μM. The range of total peptide concentration is selected from the linear portion of Figure 3.11 (a). The local peptide concentration in the membrane and $(L:P)_{\text{local}}$ are also calculated using Equation 3.22 and Equation 3.26 for corresponding total peptide concentration at pH 7.0 and pH 5.0. It should be noted that $(L:P)_{\text{local}}$ represents the lipid to peptide ratio for lipid and peptide complexes.

3.2.2.3 Modeling peptide dependence of the zeta potential using a Langmuir isotherm approach

The Langmuir isotherm model [132, 133] describes the monolayer surface adsorption of an adsorbate onto an absorbent. This model assumes 1:1 stoichiometry between binding sites and adsorbate molecules. The primary parameters extracted using a zeta potential model based on the Langmuir isotherm model are an equilibrium constant (K_{eq}) and the number of lipids per peptide binding site. The equilibrium constant is the ratio of adsorption to desorption rate and reflects the strength of binding.

Both the zeta potential model based on the Langmuir isotherm model and the model described by Freire et al. consider the reduction in membrane surface charge when a cationic peptide interacts with a model membrane composed of anionic lipids. In the Freire et al. model, only the linear portion of a binding isotherm is taken into account. Our zeta potential model based on the Langmuir isotherm is an extension of Freire et al. approach. It takes into account the linear part and the plateau region of a zeta potential binding isotherm where zeta potential approaches a limiting value. Both models allow calculation of the fraction of peptide bound to the membrane and lipid-peptide stoichiometry. The main difference between the two models is that the Freire et al. approach considers the peptide to be dissolved in the lipid bilayer volume while the zeta potential model based on the Langmuir isotherm treats the peptide as being adsorbed on the surface. A model relating the peptide concentration dependence of zeta potential to Langmuir isotherm adsorption is outlined below.

For a model in which the total number of moles of lipids is given by n_{lipids}, the number of available binding sites, $n_{\text{sites available}}$, is assumed to be some fraction, Q,

of n_{lipids} so that

$$n_{\text{sites available}} = Qn_{\text{lipids}}. \tag{3.29}$$

If $n_{\text{P,ad}}$ represents the total number of adsorbed peptide molecules, then the number of vacant binding sites is

$$n_{\text{sites vacant}} = Qn_{\text{lipids}} - n_{\text{P,ad}}. \tag{3.30}$$

Each occupied binding site thus contains $1/Q$ lipids and one peptide. In accordance with the Langmuir isotherm model, the rate of peptide adsorption is given as [132]

$$r_{\text{ad}} = k_{\text{ad}}[P]_{\text{W}}\left(\frac{Qn_{\text{lipids}} - n_{\text{P,ad}}}{A_{\text{lipid}}}\right) \tag{3.31}$$

where k_{ad} is the adsorption rate constant, $[P]_{\text{W}}$ is the peptide concentration in the aqueous environment, A_{lipid} represent the lipid area, and $\left(\frac{Qn_{\text{lipids}} - n_{\text{P,ad}}}{A_{\text{lipid}}}\right)$ is the surface concentration of vacant sites in number per unit area. The rate of desorption depends on the concentration of filled sites [132] and is thus given by

$$r_{\text{d}} = k_{\text{d}}\left(\frac{n_{\text{P,ad}}}{A_{\text{lipid}}}\right). \tag{3.32}$$

where k_{d} is the desorption rate constant. At equilibrium, the rate of adsorption equals the rate of desorption [136]. The ratio of the adsorption and desorption rate constants is thus

$$\frac{k_{\text{ad}}}{k_{\text{d}}} = \frac{1}{[P]_{\text{W}}}\left(\frac{n_{\text{P,ad}}}{Qn_{\text{lipids}} - n_{\text{P,ad}}}\right). \tag{3.33}$$

The ratio of adsorption rate to desorption rate defines the equilibrium constant (K_{eq}) of the binding process so that

$$K_{\mathrm{eq}} = \frac{n_{\mathrm{P,ad}}}{[P]_{\mathrm{W}}\Big(Qn_{\mathrm{lipids}} - n_{\mathrm{P,ad}}\Big)}. \tag{3.34}$$

Using Equation 3.34, the fractional occupancy of the binding sites is given by

$$\frac{n_{\mathrm{P,ad}}}{Qn_{\mathrm{lipids}}} = \frac{K_{\mathrm{eq}}[P]_{\mathrm{W}}}{1 + K_{\mathrm{eq}}[P]_{\mathrm{W}}}. \tag{3.35}$$

If X represents the fraction of peptide that is bound to the membrane then the number of peptides in water ($n_{\mathrm{P,W}}$) is given as

$$n_{\mathrm{P,W}} = (1 - X)n_{\mathrm{P,T}} \tag{3.36}$$

where $n_{\mathrm{P,T}}$ is the total number of moles of peptide in both environments combined. In Equation 3.36, X is the same fraction as that defined in the context of the Freire et al. approach in Equation 3.13. Dividing by total volume (V_{T}) gives

$$[P]_{\mathrm{W}} = (1 - X)[P]_{\mathrm{Total}}. \tag{3.37}$$

The fractional occupancy of binding sites can be related to zeta potential by

$$\frac{\Delta\zeta}{\Delta\zeta_{max}} = 1 - \left(\frac{n_{\text{sites vacant}}}{n_{\text{sites available}}}\right) \tag{3.38}$$

$$= 1 - \left(\frac{Qn_{\mathrm{lipids}} - n_{\mathrm{P,ad}}}{Qn_{\mathrm{lipids}}}\right) \tag{3.39}$$

$$= \frac{n_{\mathrm{P,ad}}}{Qn_{\mathrm{lipids}}} \tag{3.40}$$

where,

$$\triangle\,\zeta = \zeta - \zeta_0 \tag{3.41}$$

and

$$\triangle\,\zeta_{max} = \zeta_{max} - \zeta_0. \tag{3.42}$$

The parameters ζ_0, $\Delta\zeta$, and $\triangle\zeta_{max}$ are schematically shown in Figure 3.12.

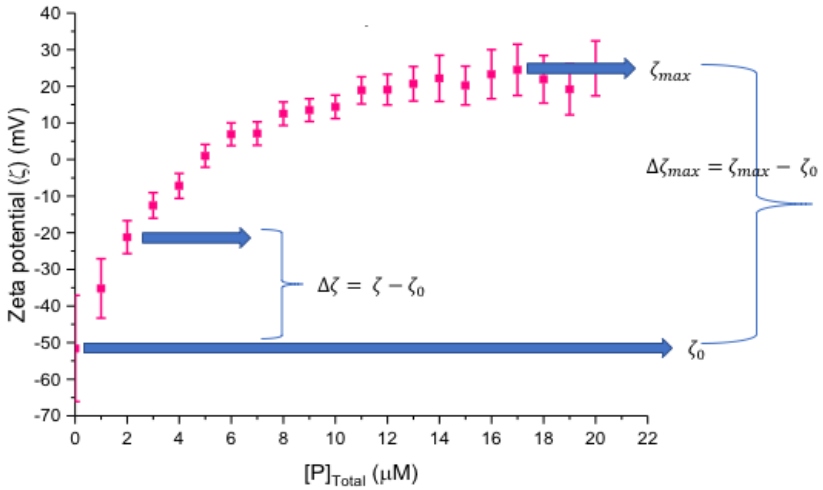

Figure 3.12: Schematic representation of zeta potential parameters ζ_0, $\Delta\zeta$, and $\triangle\zeta_{max}$. ζ_0 is the value of zeta potential in the absence of peptide. ζ represents the value of zeta potential at a given peptide concentration. ζ_{max} is the maximum value zeta potential in the plateau region of bindng isotherm. $\Delta\zeta$ is the difference between given value of zeta potential and ζ_0. $\triangle\zeta_{max}$ is the difference between ζ_{max} (maximum value of zeta potential in the binding isotherm) and ζ_0 (minimum value of zeta potential in the binding isotherm).

It should be noted that ζ_0 is a negative quantity for vesicles containing anionic lipids. From Equation 3.35 and Equation 3.40

$$\frac{\Delta\zeta}{\Delta\zeta_{max}} = \frac{K_{\mathrm{eq}}[P]_{\mathrm{W}}}{1 + K_{\mathrm{eq}}[P]_{\mathrm{W}}}. \tag{3.43}$$

The concentration of peptides in the aqueous phase, $[P]_{\mathrm{W}}$, is unknown but the total concentration of peptides, $[P]_{\mathrm{Total}}$, is a known quantity. Equation 3.37 can be used to write $[P]_{\mathrm{W}}$ in terms of $[P]_{\mathrm{Total}}$ so that the normalized change in zeta potential becomes

$$\frac{\Delta\zeta}{\Delta\zeta_{max}} = \frac{K_{\mathrm{eq}}(1-X)[P]_{\mathrm{Total}}}{1 + K_{\mathrm{eq}}(1-X)[P]_{\mathrm{Total}}} \tag{3.44}$$

where X is the molar fraction of peptide bound to the membrane and it is the same parameter used in Equation 3.13 in the Freire et al. approach. For small $[P]_{\mathrm{Total}}$,

$\frac{\Delta\zeta}{\Delta\zeta_{max}}$ depends linearly on $[P]_{\text{Total}}$ and slope of this linear regime is $K_{\text{eq}}(1-X)$. Both, K_{eq} and X, are unknown parameters and coupled together in the expression for slope.

Now, the total number of peptide molecules in a sample is $[P]_{\text{Total}}V_{\text{T}}$ so the number of adsorbed peptide molecules can be written as

$$n_{\text{P,ad}} = X[P]_{\text{Total}}V_{\text{T}}. \tag{3.45}$$

The total number of lipids can be given as

$$n_{\text{lipids}} = [L]V_{\text{T}}. \tag{3.46}$$

Using Equations 3.45 and 3.46, Equation 3.40 becomes

$$\frac{\Delta\zeta}{\Delta\zeta_{max}} = \frac{X}{Q[L]}[P]_{\text{Total}} \tag{3.47}$$

This gives another expression, $\frac{X}{Q[L]}$, for the slope of the normalized $\Delta\zeta$ vs. $[P]_{\text{Total}}$ curve in the linear regime.

In this expression, Q is the ratio of available peptide binding sites to the total number of lipids and is an unknown parameter. It can be determined using the limiting value of zeta potential. The zeta potential approaches its limiting value when all binding sites are occupied by peptide molecules and it corresponds to the plateau region in the binding isotherm. The ratio of the limiting zeta potential value to the peptide-free value of zeta potential is then

$$\frac{\zeta_{max}}{\zeta_0} = \frac{Qn_{\text{lipids}}z_{\text{P}} + n_{\text{lipids}}f_{\text{L}^-}z_{\text{L}^-}}{n_{\text{lipids}}f_{\text{L}^-}z_{\text{L}^-}} \tag{3.48}$$

so that

$$Q = \frac{\Delta\zeta_{max}}{\zeta_0}\frac{f_{\mathrm{L}^-} z_{\mathrm{L}^-}}{z_{\mathrm{P}}} \tag{3.49}$$

where f_{L^-} is the fraction of lipids that are anionic, z_{L^-} is the charge of an anionic lipid, and z_{P} is the peptide charge. The denominator of Equation 3.48 represents the total anionic lipid charge in the membrane. That charge is proportional to the peptide-free value of zeta potential. The numerator is the sum of total anionic lipid charge and total charge of adsorbed peptides. Using an expression for Q from Equation 3.49, the initial slope of $\frac{\Delta\zeta}{\Delta\zeta_{max}}$ versus $[P]_{\mathrm{Total}}$, from Equation 3.47, becomes

$$\text{slope} = \left(\frac{X z_{\mathrm{P}}}{f_{\mathrm{L}^-} z_{\mathrm{L}^-}[L]}\right)\left(\frac{\zeta_0}{\Delta\zeta_{max}}\right). \tag{3.50}$$

The above expression for slope is similar to the expression for initial slope obtained for the Freire et al. binding model as shown in Equation 3.21. The only difference in the expression of slope from two models is a normalization factor, $\frac{\zeta_0}{\Delta\zeta_{max}}$.

The limiting value of zeta potential can be used to determine Q using Equation 3.49. The slope of the linear regime of $\frac{\Delta\zeta}{\Delta\zeta_{\mathrm{max}}}$ vs. $[P]_{\mathrm{Total}}$ can thus be used to find X. The K_{eq} can be determined using the expression, $K_{\mathrm{eq}}(1-X)$, for slope from Equation 3.44. In the zeta potential model based on the Langmuir isotherm, a binding isotherm is obtained by plotting $\frac{\Delta\zeta}{\Delta\zeta_{\mathrm{max}}}$ vs. $[P]_{\mathrm{Total}}$, while in the Friere et al. model, $\frac{\zeta}{\zeta_0}$ vs. $[P]_{\mathrm{Total}}$ was plotted. The binding isotherms showing the variation of $\frac{\Delta\zeta}{\Delta\zeta_{\mathrm{max}}}$ vs. $[P]_{\mathrm{Total}}$ and corresponding selected linear regimes for Gad-1 at pH 7.0 and pH 5.0 are shown in Figure 3.13 and Figure 3.14 respectively. The binding isotherms showing the variation of $\frac{\Delta\zeta}{\Delta\zeta_{\mathrm{max}}}$ vs. $[P]_{\mathrm{Total}}$ and corresponding selected linear regimes for Gad-2 at pH 7.0 and pH 5.0 are shown in Figure 3.15 and Figure 3.16 respectively. For Gad-1 and Gad-2, the calculated parameters obtained by using the Langmuir isotherm approach are listed in Tables 3.6 and Table 3.7 respectively. For both Gad-1 and Gad-2, values of X are smaller at pH

5.0 than at pH 7.0. The values of $1/Q$ indicate that at pH 7.0, a binding site consists of a smaller number of lipids than at pH 5.0. For Gad-1, K_{eq} is higher than Gad-2 at both pHs. These observations are interpreted in the discussion Section below.

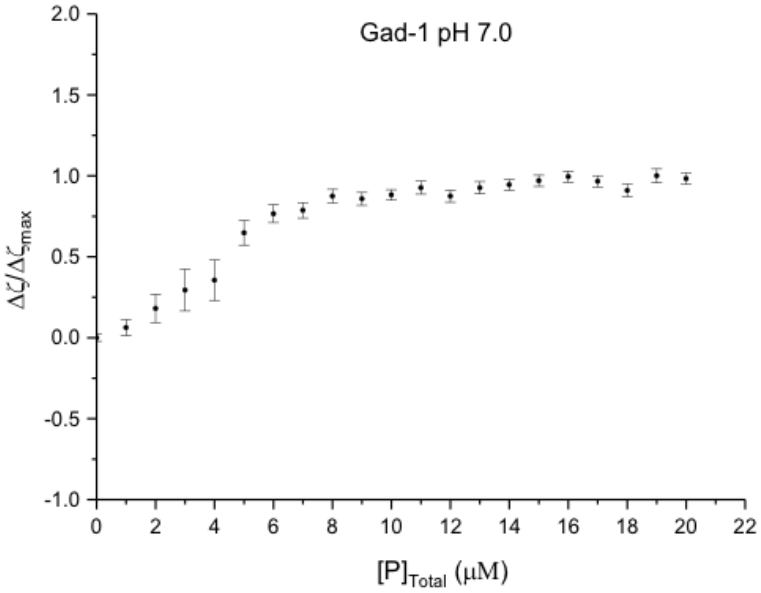

(a)

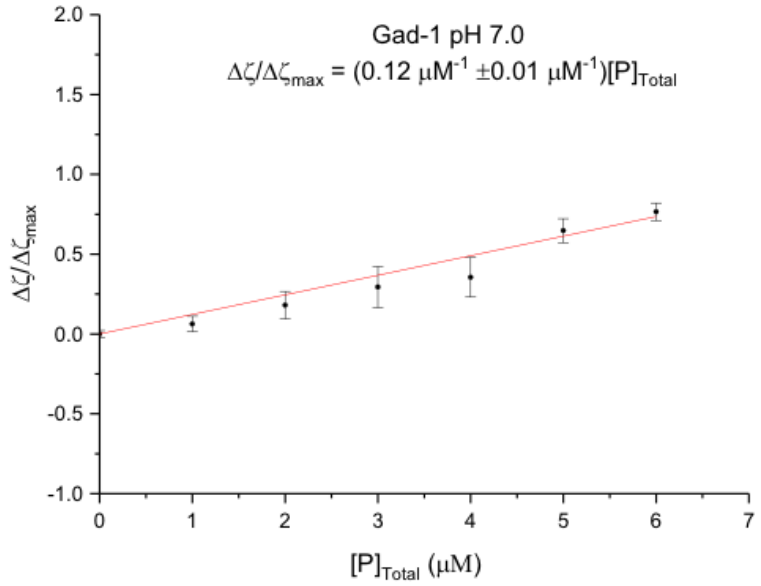

(b)

Figure 3.13: (a) $\dfrac{\Delta\zeta}{\Delta\zeta_{\max}}$ vs. $[P]_{\text{Total}}$ for Gad-1 at pH 7.0. (b) The linear regime (0 μM - 6 μM) was selected and slope of this region was used to find X. The slope of the linear portion of the binding isotherm was obtained using the weighted linear fitting. The size of error bars was taken into account to estimate the uncertainty in the slope. Q was determined from the limiting value of zeta potential using Equation 3.49. The equilibrium constant (K_{eq}) was determined using the expression, $K_{\text{eq}}(1 - X)$, for slope from Equation 3.44.

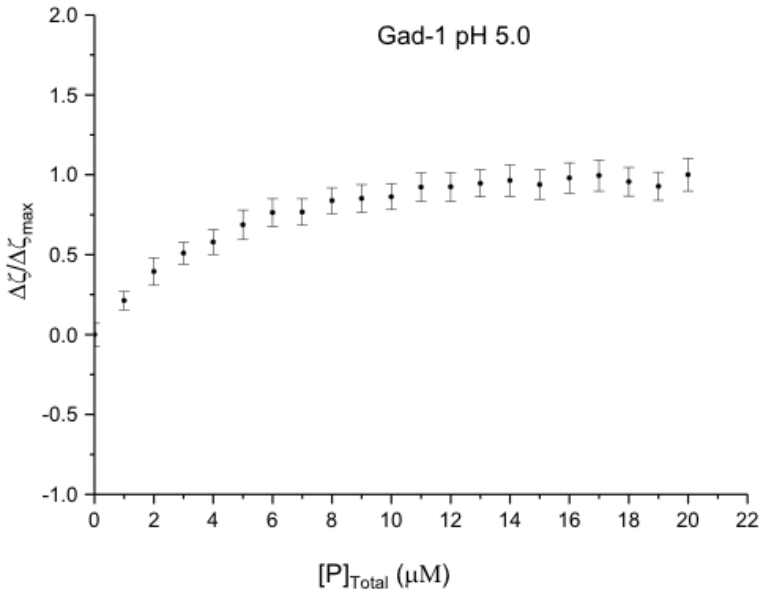

(a)

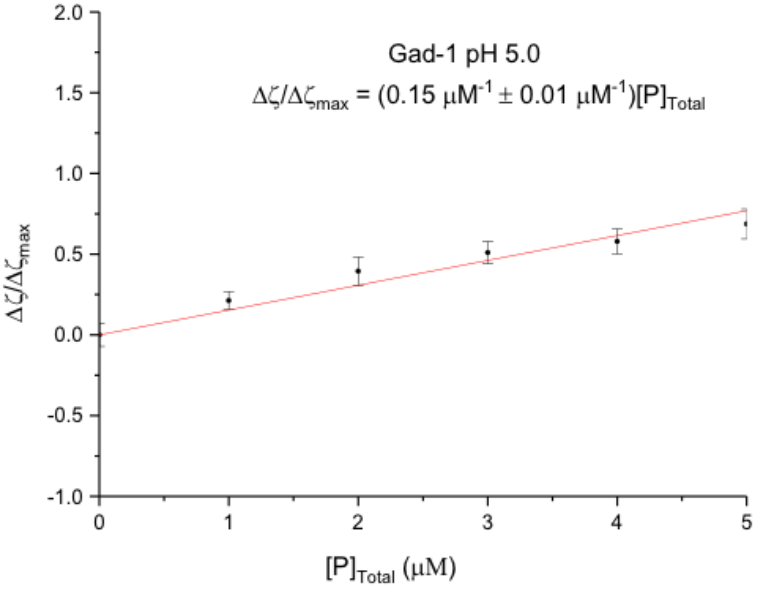

(b)

Figure 3.14: (a) $\frac{\Delta\zeta}{\Delta\zeta_{\max}}$ vs. $[P]_{\text{Total}}$ for Gad-1 at pH 5.0. (b) The linear regime (0 μM - 5 μM) was selected and slope of this region was used to find X. The slope of the linear portion of the binding isotherm was obtained using the weighted linear fitting. The size of error bars was taken into account to estimate the uncertainty in the slope. Q was determined from the limiting value of zeta potential using Equation 3.49. The equilibrium constant (K_{eq}) was determined using the expression, $K_{\text{eq}}(1 - X)$, for slope from Equation 3.44.

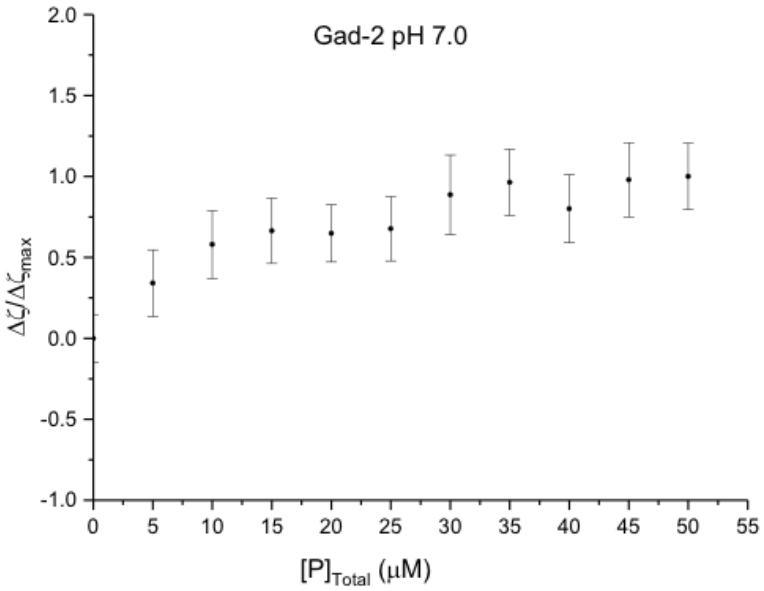

(a)

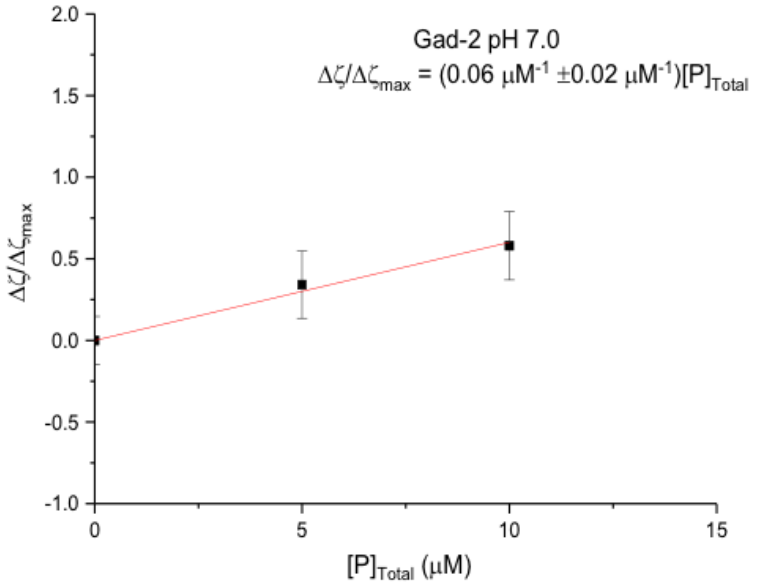

(b)

Figure 3.15: (a) $\dfrac{\Delta\zeta}{\Delta\zeta_{\max}}$ vs. $[P]_{\text{Total}}$ for Gad-2 at pH 7.0. (b) The linear regime (0 μM - 10 μM) was selected and slope of this region was used to find X. The slope of the linear portion of the binding isotherm was obtained using the weighted linear fitting. The size of error bars was taken into account to estimate the uncertainty in the slope. Q was determined from the limiting value of zeta potential using Equation 3.49. The equilibrium constant (K_{eq}) was determined using the expression, $K_{\text{eq}}(1-X)$, for slope from Equation 3.44.

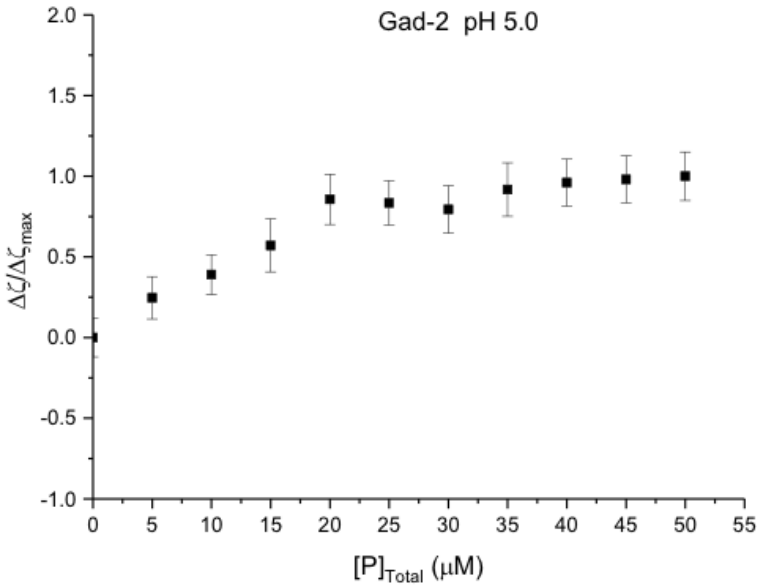

(a)

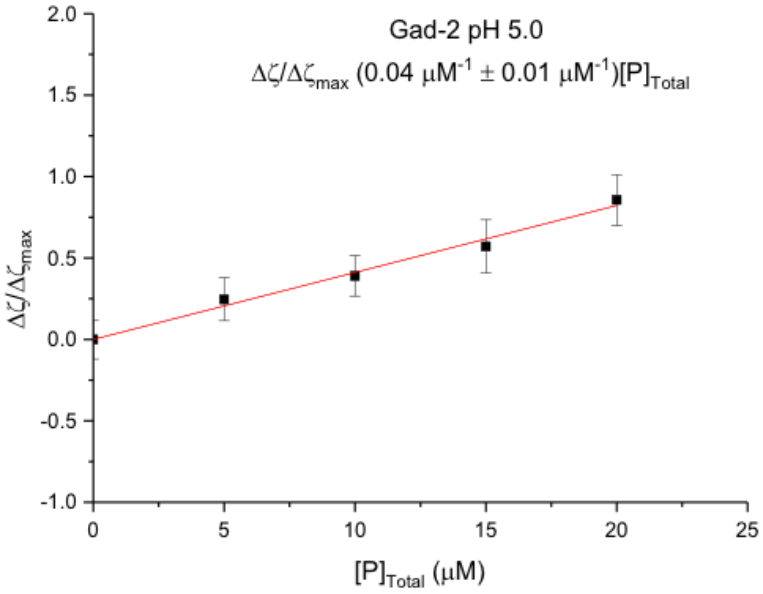

(b)

Figure 3.16: (a) $\dfrac{\Delta\zeta}{\Delta\zeta_{\max}}$ vs. $[P]_{\text{Total}}$ for Gad-2 at pH 5.0. (b) The linear regime (0 μM - 20 μM) was selected and slope of this region was used to find X. The slope of the linear portion of the binding isotherm was obtained using the weighted linear fitting. The size of error bars was taken into account to estimate the uncertainty in the slope. Q was determined from the limiting value of zeta potential using Equation 3.49. The equilibrium constant (K_{eq}) was determined using the expression, $K_{\text{eq}}(1 - X)$, for slope from Equation 3.44.

Gad-1			
pH	Molar fraction of peptide bound to the membrane (X)	$1/Q$ (number of lipids per peptide binding site)	Equilibrium constant, K_{eq} (μM^{-1})
7.0	0.46±0.04	10± 1	0.22±0.03
5.0	0.28±0.03	21 ± 3	0.21± 0.02

Table 3.6: The values of X, $1/Q$, K_{eq} for Gad-1 at pH 7.0 and pH 5.0.

Gad-2			
pH	Molar fraction of peptide bound to the membrane (X)	$1/Q$(number of lipids per peptide binding site)	Equilibrium constant, K_{eq} (μM^{-1})
7.0	0.4±0.2	6± 1	0.11±0.06
5.0	0.08±0.02	20 ± 3	0.04± 0.01

Table 3.7: The values of X, $1/Q$, K_{eq} for Gad-2 at pH 7.0 and pH 5.0.

3.3 Discussion

The addition of Gad peptides to POPE/POPG-d_{31}(3:1) lipid vesicles was found to cause a small decrease in the quadrupole splitting of the NMR spectra as indicated in Figure 3.1. This was observed for both Gad-1 and Gad-2 at pH 7.0 and pH 5.0. The first observation made from order parameter profiles shown in Figures 3.2 and 3.3 was that both peptides reduce the orientational order parameter values, particularly in the plateau region (i.e. carbon number 2 to carbon number 10), at both pH values. The orientational order parameter profile comparison suggests that the two peptides have only small effects on the amplitudes of fast motions that contribute to motional narrowing. A potential explanation for the observed change in order parameter is as follows. The peptide likely pushes the lipid head groups apart which would increase the area per lipid and, in turn, allow the acyl chains more freedom to move as shown in Figure 3.17(b). The resulting increase in averaged motion of the lipid acyl chains would increase the extent to which the quadrupole interaction is averaged and make the splitting smaller. This is consistent with the idea that many AMPs perturb the bilayer integrity of bacterial membranes to achieve their antimicrobial activity. Previous model membrane studies have shown that the addition of AMP causes the reduction in the order parameter values of model lipid vesicles. The histidine-rich synthetic peptide LAH4-L1 at acidic pH values [75] and Alamethicin, Ampullosporin [137] induced a slight reduction in the order parameter values of POPE/POPG-d_{31} lipid vesicles which is comparable to the effect of Gad peptides on the lipid acyl chain order of POPE/POPG-d_{31} lipid vesicles. Other peptides including MSI-78, MSI-594 [138], IL-8α [139], and LL-37 [140] reduced the order parameter values of POPC/POPG-d_{31} lipid vesicles. While comparing the interactions of different AMPs with lipid bilayers in model membranes, it is important to consider the

different experimental conditions. For example, all the peptides listed above have been shown to perturb the lipid bilayer integrity by reducing the order parameter values, but the POPE/POPG lipid mixture is more relevant to Gram-negative bacterial membrane than POPC/POPG lipid bilayers. The comparison of order parameter profiles for each peptide in Figure 3.4 suggests that peptide-induced bilayer perturbation is not strongly pH-dependent for either peptide between pH 7.0 and pH 5.0. This was unexpected because MIC assay experiments of Gad peptides against *E.coli* have shown that Gad-2's antimicrobial activity is more pH-dependent [26].

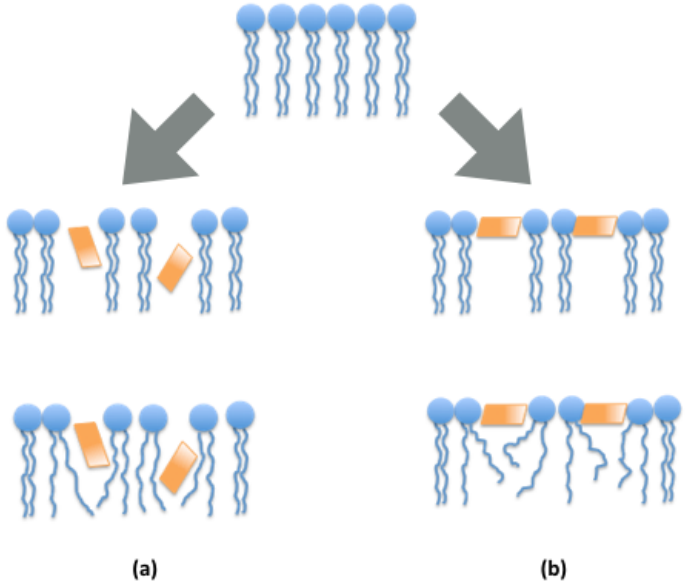

Figure 3.17: Schematic representation of the interaction of the peptide (in orange) with lipid molecules (in blue). (a) If the peptide locates mainly to the acyl chain region, it may impede the motion of the chains and only a small change may be seen in the motion of the lipid chains. (b) If the peptide binds the membrane in the lipid polar head groups region, it may increase the distance between them which makes the acyl chains more flexible to move. This Figure is reprinted with the permission of Dr. Valerie Booth.

Additional information about the membrane-peptide interactions was obtained from the quadrupole echo decay time which reflects the perturbation, by Gad peptides, of slow or fast motions in POPE/POPG-d_{31} (3:1) lipid bilayers. The change in the values of T_2^{qe} with the addition of Gad peptides indicates that both peptides perturb the bilayer motions even though there was not much effect on the spectrum splittings.

For the lipid-only samples, echo decay time is independent or at most, weakly dependent on temperature. This is consistent with previous observations for lipid bilayers in the liquid crystalline phase [141, 142]. Aside from Gad-1 at 25°C, echo decay times for bilayers with a given peptide are not sensitive to pH and thus not sensitive to peptide charge. It was observed that Gad-1 decreases the echo decay time at pH 7.0 while at pH 5.0 it had little effect on the echo decay time. The decrease in the echo decay time might indicate slowing down of a fast motion or speeding up a slow motion. On the other hand, Gad-2 increases the echo decay time at either pH. The increase in the echo decay time might indicate speeding up a fast motion or slowing down of a slow motion with the addition of peptide. Gad-1 and Gad-2 seem to have opposite effects on echo decay times. Since charge does not seem to be much of a factor, this must reflect differences in structural effects on motions. Both Gad-1 and Gad-2 have similar effects on chain order which suggests that they have similar effects on fast (short correlation time) motions. This suggests that difference in the perturbation of echo decay time by Gad-1 and Gad-2 reflects effects on slower (longer length scale) motions like bilayer undulation. If so, the results suggest that Gad-2 tends to increase the slow motion correlations times (i.e. damp the motions a bit). Gad-1 has a smaller effect, mostly in the opposite direction.

To study the binding of Gad peptides in quantitative detail, the molar fractions of peptide bound to model lipid vesicles (X) were determined from the slopes of the linear regimes of zeta potential binding isotherms. The partition constant (K_P) was determined using the Freire et al. approach while the equilibrium constant (K_{eq}) was determined using the zeta potential model based on the Langmuir Isotherm. The partition constant reflects the peptide partitioning between the membrane and water while the equilibrium constant reflects the strength of binding. Higher values of K_P indicate strong partitioning of the peptide towards the lipid membrane, while higher equilibrium constants indicate tighter lipid-peptide binding. Both the Freire et al. and the Langmuir isotherm models allow the characterization of lipid-peptide stoichiometry in terms of number of lipids per bound peptide. The local peptide concentration in the membrane (P_{local}) and the ($L : P$) ratio were estimated using X and K_P. The number of lipids per peptide binding site ($1/Q$) was determined using the limiting zeta potential value.

In the absence of a peptide, a negative zeta potential of $\sim$ -55 mV is calculated from experimentally observed mobilities for POPE/POPG (3:1) lipid vesicles at pH 7.0 and pH 5.0. The addition of peptide results in neutralization of the negative zeta potential of the lipid vesicles. Similar zeta potential trends were reported for peptides pepR and BP100 in model lipid vesicles of POPC/POPG [116]. This reduction in the magnitude of the zeta potential indicates an interaction of the negatively charged membrane with the positive peptide. At lower peptide concentrations, zeta potential varies linearly with peptide concentration. At higher concentrations of Gad peptides, the zeta potential approaches a negative, neutral, or positive limiting value depending on the charge of the peptide and the ($L : P$) ratio when all binding sites are occupied. Figure 3.18 illustrates how increased peptide binding affects the observed zeta potential.

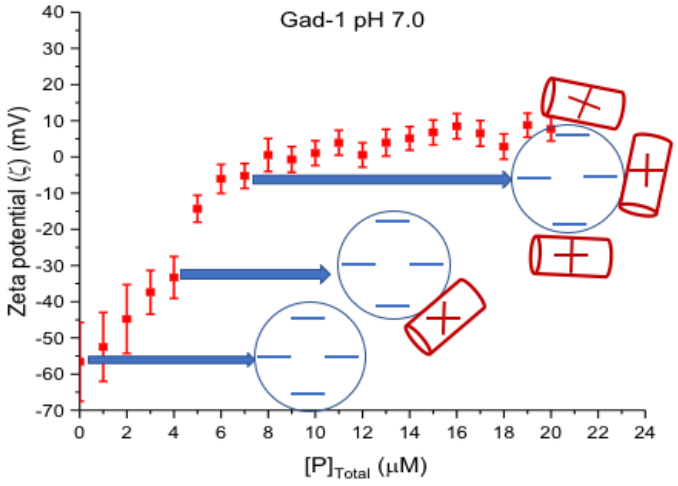

Figure 3.18: The depiction of lipid-peptide interactions corresponding to the different points of the binding isotherm. When no peptide is bound, the zeta potential is negative. The peptide binding to the lipid vesicle results in the reduction in the magnitude of the negative zeta potential value. The plateau region of binding isotherm represents the saturation of lipid vesicles with peptide. At this point, all the binding sites are occupied and zeta potential does not change with further addition of the peptide.

Gad-1 carries a charge of +3 at pH 7.0 and +8 at pH 5.0, whereas Gad-2 has a charge of only +1 at neutral pH and +5 at pH 5.0. At higher concentrations of Gad-1 (10 μM onwards), the zeta potential approaches a positive limit of $\sim$+5 mV at pH 7.0, while at pH 5.0 it reaches a positive limit of +20 mV. The fact that the plateau region is positive, rather than neutral indicates that there are hydrophobic interactions, in addition to electrostatic interactions, at play when the peptide interacts with the membrane. On the other hand, for Gad-2 at pH 7.0, zeta potential values change more slowly with the addition of peptide. At pH 5.0, the addition of Gad-2 results in a positive limit of $\sim$+1 mV in the zeta potential. The point of electroneutrality (where zeta potential is zero) depends on the overall charge of peptide. For Gad-1, zeta potential becomes zero at an overall peptide concentration of 8 μM for pH 7.0. For Gad-1, the higher peptide

charge at pH 5.0 neutralizes the membrane charge at a peptide concentration of 5 μM. For Gad-2 at pH 7.0, zeta potential does not go to zero and at pH 5.0 the electroneutrality point occurs at an overall peptide concentration of 45 μM.

The binding of Gad peptides is characterized in terms of molar fraction of peptide bound to the membrane (X), the partition constant (K_P), the equilibrium constant (K_{eq}), and ($L : P$) ratios. The values of X determined using both models, the Freire et al. approach and the zeta potential model based on the Langmuir isotherm, are listed in Table 3.8. The two binding models gave consistent results for X.

Molar fraction of peptide bound to the membrane (X)				
model	Gad-1		Gad-2	
	pH 7.0	pH 5.0	pH 7.0	pH 5.0
Freire et al. approach	0.48±0.02	0.35±0.01	0.4±0.1	0.08±0.01
zeta potential model based on the Langmuir isotherm	0.46±0.04	0.28±0.03	0.4±0.2	0.08±0.02

Table 3.8: Comparison of values of X for Gad peptides calculated using Freier et al. approach and zeta potential model based on the Langmuir isotherm. Both models give the consistent results for X.

The zeta potential model based on the Langmuir adsorption isotherm provided a way to extract a binding equilibrium constant. The equilibrium constant (K_{eq}) is the ratio of the peptide adsorption to desorption rates and it reflects the strength of binding. The higher the value of the equilibrium constant, the greater the strength of binding. The partition constant (K_P) was determined using the Freire et al. approach. In the Freire et al. approach, only the linear part of the binding isotherm was used to determine binding parameters, while the Langmuir isotherm

approach used the linear part and the limiting value of zeta potential to characterize the peptide binding. The comparison of the values of K_{eq} and K_{P} is shown in Table 3.9.

Partition constant (K_P) and equilibrium constant (K_{eq})				
pH	Gad-1		Gad-2	
	K_P	K_{eq}	K_P	K_{eq}
7.0	30,000 ± 2400	0.22 ± 0.03	24,000 ± 7000	0.11 ± 0.06
5.0	17,600 ± 800	0.21 ± 0.02	2800 ± 400	0.04 ± 0.01

Table 3.9: The partition constant (K_P) and the equilibrium constant (K_P) for Gad-1 and Gad-2 at pH 7.0 and pH 5.0. The values of K_P and K_{eq} convey information about how much peptide is bound to the membrane and how tightly bound is the peptide to the membrane. The greater the value of K_P, the stronger the partitioning of peptide towards the membrane, while higher value of K_{eq} indicate tighter peptide binding to the membrane. The values of K_P and K_{eq} are higher at pH 7.0 than at pH 5.0 for both Gad-1 and Gad-2.

Both binding models allow the characterization of the stoichiometry of lipid-peptide interactions for Gad peptides at two pHs. The $(L : P)_{\mathrm{local}}$ ratios were calculated using the Freire et al. approach. The zeta potential model based on the Langmuir isotherm allows the calculation of number of lipids that correspond to one binding site and this is expected to be the limiting value of $(L : P)_{\mathrm{local}}$ ratio. The results of lipid-to-peptide ratios obtained using both the models are listed in Table 3.10.

The insights from the comparisons of the binding parameters for Gad peptides at the two pH values are discussed below. For both Gad-1 and Gad-2, the fraction of peptide bound to the membrane is smaller at slightly acidic pH than at neutral pH. This is schematically represented in Figure 3.19. This suggests that when a peptide

local lipid-to-peptide ratios				
pH	Gad-1		Gad-2	
	$L:P$	$1/Q$	$L:P$	$1/Q$
7.0	14±1	10±1	10±2	6±1
5.0	19±1	21±3	25±3	20±3

Table 3.10: Local lipid-to-peptide ratios determined using Freire et al. approach and zeta potential model based on the Langmuir isotherm. For Gad-1, $L:P$ corresponds to 6 μM total peptide concentration. For Gad-2, $L:P$ values corresponds to 10 μM and 20μM total peptide concentrations at pH 7.0 and pH 5.0 respectively. These total peptide concentrations are the highest peptide concentrations in the linear region of the zeta potential binding isotherms. $1/Q$ represents the limiting value of lipid-to-peptide ratios and are calculated using zeta potential model based on the Langmuir isotherm. Both models gave consistent results for lipid-to-peptide ratios.

has higher positive charge, a smaller number of peptides can be accommodated on the membrane surface. This may be due to the fact that when a peptide has higher positive charge, less peptide is needed to neutralize the membrane surface charge. In addition, repulsive electrostatic interactions between bound peptides are expected to be stronger at lower pH and this also might limit the peptide binding.

Comparing the values of X (Table 3.8) for Gad-1 and Gad-2 at pH 7.0 and at pH 5.0 shows that the extent to which peptide binding to the membrane depends on overall peptide charge is not the same for Gad-1 and Gad-2. At pH 7.0, Gad-1 has a charge of +3 and Gad-2 has a charge of +1. Regardless of the difference in peptide charge at pH 7.0, the fraction of Gad-2 bound to the membrane is approximately the same as the fraction of Gad-1 bound to the membrane.

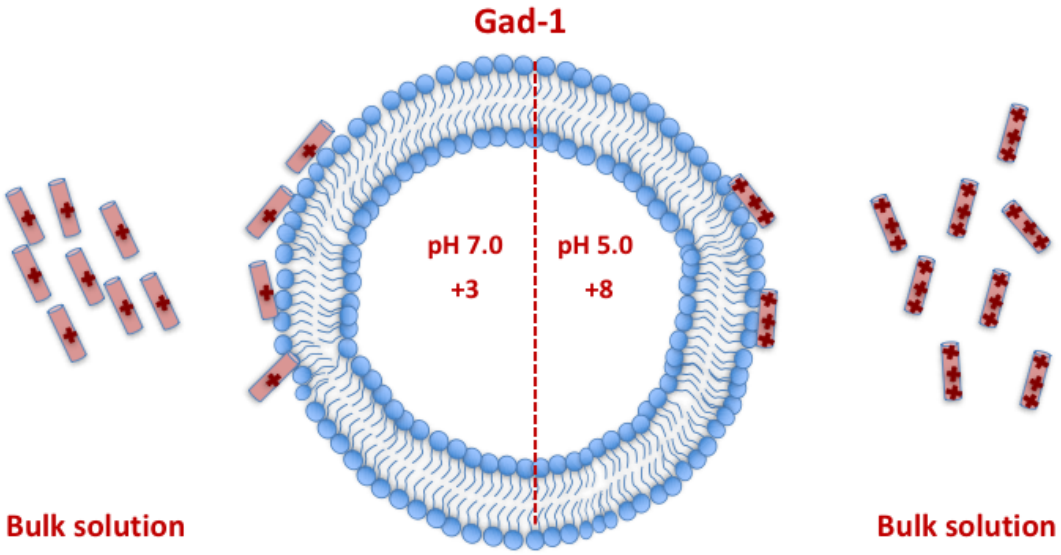

(a)

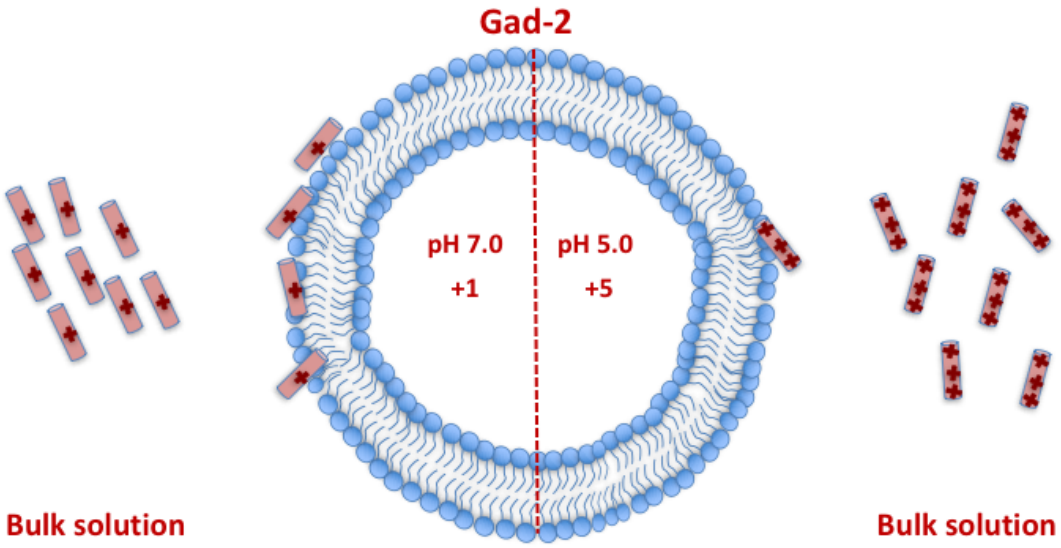

(b)

Figure 3.19: An illustration of lipid-peptide interactions for (a) Gad-1 at pH 7.0 and pH 5.0. (b) Gad-2 at pH 7.0 and pH 5.0. For each peptide, less peptide binds to the membrane at pH 5.0. At pH 7.0 the amount of peptide that binds to the membrane is almost the same for both peptides. At pH 5.0, less Gad-2 binds to the membrane than Gad-1.

A different case is observed at acidic pH. At pH 5.0, Gad-1 carries a charge of +8 and Gad-2 has a charge of +5. Irrespective of its having a smaller charge than Gad-1, much less Gad-2 binds to the membrane.

After investigating the fraction of peptide bound to the membrane, the differences in the strength of binding of Gad-1 and Gad-2 were examined by comparing the values of K_{eq}. Higher values of the equilibrium constant for Gad peptides indicate that at pH 7.0, the binding of Gad-1 is 2-fold stronger than that of Gad-2. At pH 5.0, Gad-2's binding is 5-fold weaker than that of Gad-1. Gad-1's equilibrium constant does not change with pH, while Gad-2's binding is weaker at pH 5.0 than at pH 7.0. Gad-1 has higher values of the equilibrium constant than Gad-2 at both pH values. This suggests that lipid-peptide interactions are stronger for Gad-1 compared to Gad-2. Also, for Gad-2 the equilibrium constant values are more sensitive to changes in pH. The greater sensitivity of Gad-2's binding to pH may reflect a higher sensitivity of its structure to changes in pH.

A potential explanation for the differences in the binding of Gad-1 and Gad-2 is as follows. Structure-function relationship studies of Gad peptides [26] reveal that Gad-1 and Gad-2 are more helical at pH 7.0 than at pH 5.0. The percent helicity of both peptides decreases as pH decreases from 7.0 to 5.0. The smaller degree of Gad peptide helical structure at pH 5.0 compared to pH 7.0 may result in less peptide being bound to the membrane at lower pH. Gad-1 is more helical than Gad-2 at both pHs. Also, Gad-1 has higher overall positive charge than Gad-2 at pH 7.0 and pH 5.0. The combined effect of higher degree of helicity and higher cationic nature of Gad-1 may result in a stronger binding of Gad-1 than Gad-2 at both pHs as indicated by higher values of K_{eq} of Gad-1 compared to Gad-2 at both pH values (Table 3.9). This may indicate that greater helicity of peptide leads to greater amphipathicity that may drive stronger binding of the peptide to the membrane. The helicity of Gad-2 is also more sensitive to changes in pH than that

of Gad-1. Note that Gad-2 has fewer histidines than Gad-1 but that it also has two histidine-pairs while Gad-1 has only one histidine-pair. Previous molecular dynamics simulations with Gad peptides have shown that most helical peptide structures prefer to interact with planar bilayer regions while histidine-histidine pairs prefer to interact with disordered bilayer regions [143]. This may explain the weaker binding of Gad-2 than Gad-1 at both pHs. The greater sensitivity of Gad-2's helicity to pH and the presence of two histidine pairs may result in an amphipathic structure with a charge distribution that amplifies the sensitivity of its binding to changes in pH. Changes in binding with pH might reflect changes in helicity but might also reflect the smaller number of peptides needed to neutralize the bilayer and the stronger electrostatic interactions between peptides.

The partition constant (K_P) provides another way to look at the amount of peptide bound to the membrane. The Gad peptide partition constants extracted from the zeta potential measurements are of the order of 10^3. This means that the peptide concentration in the lipid phase is approximately 10,000 times higher than its concentration in the aqueous phase [56]. The values of the partition constant for Gad peptides are comparable with the values found for other AMPs including Melittin, Omiganan, Indolicidin, Dermaseptin, Cecropin, and Magainin-2-amide [56, 144–146]. The partition constant for the above-listed peptides is in the range of $10^3 - 10^5$ and was determined using titration calorimetry and fluorescence spectroscopy.

The comparison of values of X describes how the fraction of peptide bound to the membrane was affected by the different properties of peptide. When a certain fraction of peptide is bound to the membrane, the number of lipids interacting with one molecule of bound peptide may also depend on the properties of the peptide. This was investigated by comparing the lipid-to-peptide ratios for Gad peptides at different pH values. The limiting values of $(L:P)_{\text{local}}$, as determined

by the Freire et al approach, are consistent with the values of $1/Q$ extracted from the zeta potential model based on the Langmuir isotherm (Table 3.11). $L : P$ ratios were higher at pH 5.0 than at pH 7.0 for both Gad-1 and Gad-2. This suggested that the higher the peptide charge, the larger the number of lipids per bound peptide. The molecular interactions between cationic Gad peptides and anionic membrane lipids can result in the promotion of anionic lipid clustering. Other AMPs including Myxinidin, Aurein 1.2, Arginine rich peptides (PR−9), (RR−9), (PI−9), and LL−37 [147–151] have been shown to be able to cluster anionic lipids.

The local peptide concentration ($[P]_{\mathrm{L}}$) was calculated for a selected range of total peptide concentration ($[P]_{\mathrm{Total}}$). The range of ($[P]_{\mathrm{Total}}$) was selected from the linear portion of the Gad peptide binding isotherms. For Gad-1, this range is 0 μM - 6 μM and for Gad-2 it is 0 μM - 20 μM. It should be noted that $[P]_{\mathrm{Total}}$ is the peptide concentration over the total volume and $[P]_{\mathrm{L}}$ is peptide concentration in the membrane at a given lipid concentration. The local peptide concentrations were lower at pH 5.0 than at pH 7.0 for both Gad-1 and Gad-2. The comparison of the $[P]_{\mathrm{L}}$ and the $(L : P)$ ratios for Gad-1 and Gad-2, indicates that at pH 5.0, Gad-2 has lower $[P]_{\mathrm{L}}$ and higher $(L : P)_{\mathrm{local}}$ values. In other words, less Gad-2 binds to the membrane and there are more lipid molecules per bound Gad-2 peptide at pH 5.0 than for Gad-1 at same pH. This might suggest that the interaction of peptide with lipid membrane does not involve only the overall charge of the peptide but rather the combined effects of parameters like overall positive charge, distribution of charge, $L : P$ ratios, amphipathicity, and hydrophobicity [152–154].

The results of MIC (Minimal Inhibitory Concentration) assays for the effect of Gad peptides on bacterial growth of *E.coli* [26] are shown in Figure 1.6. It is evident from Figure 1.6 that Gad-1 has lower MIC values than Gad-2. Also, Gad-2's anti-*E.coli* activity is sensitive to pH. Binding studies indicate that the

binding of a single peptide is stronger for Gad-1 than for Gad-2. This suggests that for Gad-1 and Gad-2, tighter peptide binding to the membrane corresponds to higher peptide antimicrobial activity. This rule of "stronger the peptide binding more active is the peptide" does hold true for Gad-1 at pH 7.0 and pH 5.0. For Gad-2, on the other hand, there appears to be no simple rule for correlating the peptide binding to the peptide activity. In particular, it is found that despite the reduced accommodation of Gad-2 peptide and weaker peptide binding at pH 5.0 than at pH 7.0, Gad-2 MIC values at pH 5.0 are lower than those seen at pH 7.0. This difference between Gad-1 and Gad-2 might be explained as follows. Gad-1 is more helical than Gad-2 and Gad-2's structure is more sensitive to pH. Also, Gad-2 has two histidines pairs while Gad-1 has only one histidine pair. The greater sensitivity of Gad-2's structure to pH and the presence of two histidine pairs may be related to the pH sensitivity of its antimicrobial activity against *E.coli*. It should be noted that MIC assay experiments were performed with real bacteria. Typical bound P:L ratios needed to inhibit bacterial growth in assays for AMP antimicrobial activity are 100:1. On the other hand, bound P:L ratios needed to cause significant perturbation in model embrane studies is typically 1:200 [35]. This very large difference (about 4 orders of magnitude) may indicate that peptide may bind to other components of the bacterial membrane such as the peptidoglycan layer and the lipopolysaccharide layer of the outer membarne.

For instance, the presence of salt can affect the antimicrobial activity of a peptide. It has been shown in previous studies that antimicrobial activity of peptides such as Magainin, Thanatin, and s-Thanatin decreased with the increasing concentration of salt [155, 156].

At pH 5.0, both Gad-1 and Gad-2 have higher overall positive charge and thus stronger lipid-peptide electrostatic interaction was expected at slightly acidic pH than at pH 7.0. However, the binding studies of Gad-1 and Gad-2 reveal that less

peptide binds to the membrane at pH 5.0 than at pH 7.0. Also, Gad peptides interact with a larger number of lipids at pH 5.0 than at pH 7.0. The MIC assay results showed that Gad-2's anti-*E.coli* activity is sensitive to pH while ^{2}H NMR results showed that peptide-induced disorder in model lipid bilayers was not pH-dependent. If perturbation of the amplitudes of lipid acyl chains motions is not sensitive to small differences in the amount of peptide accommodated on the membrane surface, then the insensitivity of peptide-induced disorder, as observed by the ^{2}H NMR spectrum splittings, might be expected. This suggests that Gad peptides might disrupt membrane stability by inducing anionic lipid clustering and that the peptide may not perturb the lipid integrity in a way that increases the amplitude of lipid acyl chain motion.

Chapter 4

Alignment of Gad peptides in mechanically oriented model lipid bilayers determined by ^{15}N NMR spectroscopy

AMP-membrane interactions are a key component in AMP mechanism. Knowledge of the angle of the helical axis of the peptides with respect to the membrane surface can reveal their structure and function relationships. For ^{15}N-labelled peptides interacting with mechanically oriented bilayers, chemical shifts observed using solid-state ^{15}N NMR spectroscopy are sensitive to peptide orientation with respect to the membrane surface. In this work, solid-state ^{15}N experiments have been used to characterize the alignment of Gad-1 and Gad-2 in mechanically oriented model membranes at different pH values.

4.1 Materials and methods

4.1.1 Lipids

The chain perdeuterated lipids POPC-d_{31} along with non-deuterated lipids POPC and POPG were purchased from Avanti Polar Lipids (Alabaster, AL). These lipids were used without further purification.

4.1.2 Solid support (Mica)

To make mechanically oriented lipid bilayers, Muscovite mica ($KAl_2(Si_3Al)O_{10}(OH,F)_2$) was used as a solid support because it is an anionic surface that helps lipids to orient in one direction. The V-1 grade mica sheets of dimensions 50×25 mm were purchased from SPI supplies (West Chester, PA).

4.1.3 Mechanically Oriented Lipid Bilayers

In order to obtain data on the alignment of the peptide from the ^{15}N experiments, it was important to prepare bilayers with as high a degree of uniform mechanical orientation as possible. The following describes the protocol used for the preparation of mechanically oriented bilayers with and without incorporated peptides.

4.1.3.1 Appropriate lipid mixtures

The first step in the preparation of mechanically oriented lipid bilayers is to select the appropriate lipids. Ideally, it would be best to use the same lipid composition as were employed in the liposome experiments in Chapter 3. POPE tends to

form wedge-like units because the cross-sectional area of the head group is smaller than that of the acyl chains. On the other hand, POPC tends to form cylindrical units with cross-sectional area of the head group equal to that of the acyl chains. Attempts to prepare oriented bilayers with POPE were not successful, persumably because of POPE's small head-group to acyl chain area ratio. On the other hand, oriented lipid bilayers were successfully prepared with POPC and it has commonly been used in previous studies of this type [157–159].

Another important consideration is that the lipid environment chosen should induce a high level of helicity in the Gad peptides. The percentage helicity of both Gad-1 and Gad-2 in POPC lipid environments was found to be less than 50%, as shown in Table 4.1. It is evident from Table 4.1 that Gad peptides have

Lipid	pH	% helicity of Gad-1	% helicity of Gad-2
POPC	5	37%	7%
POPC	6	35%	10%
POPC	7	42%	16%
POPG	5	56%	19%
POPG	6	79%	36 %
POPG	7	100%	100%

Table 4.1: Percent helicity of Gad peptides in POPC and POPG lipid environment at different pH values. This table is adapted from Mark McDonald et al. [26] and used with permission from Elsevier.

higher percent helicities in membranes composed of POPG than in POPC membranes. Furthermore, the membrane of *E.coli* bacteria contains 15% PG and 80% PE lipids [7]. Based on these considerations, it was decided to use POPC/POPG (5:1) as the lipid component for experiments involving ^{15}N-labelled Gad peptides in mechanically oriented bilayers. This lipid mixture has been used in the previous studies of mechanically oriented samples [160, 161].

4.1.3.2 Circular Dichroism (CD)

To assess the helicity of Gad peptides in this lipid mixture, far-ultraviolet circular dichroism (CD) spectra were acquired. Samples were prepared by dissolving POPC/POPG (5:1) in 20 mM potassium phosphate buffer at pH 7.0, and subjecting them to five freeze thaw steps as follows. The samples were frozen in liquid nitrogen for 3-5 mins and thawed at room temperature for 30 mins. The resulting liposome solutions were extruded 12 times through a 200 nm filter (Nuclepore Track-Etched Membranes, Whatman, Toronto ON) under nitrogen gas pressure. Peptide stock solutions were prepared at a concentration of 1 mg/mL by dry weight of peptide in 20 mM potassium phosphate buffer at pH 7.0. Appropriate volumes of the liposome solution and the peptide stock solution were mixed to give a final lipid concentration of 1.4 mM and peptide concentration of 30 μM. CD spectra were collected in milli-degrees using Jasco J-810 spectropolarimeter (Jasco Inc., Easton, MD) in the far ultraviolet range (190-260 nm) with a 0.5 mm quartz cuvette at 25°C. Firstly, a CD spectrum was obtained with a lipid sample at 1.4 mM concentration to get the baseline data and then CD spectra were obtained with liposomes containing Gad peptides. Spectra were normalized by subtracting a baseline and then converting the units to mean-residue ellipticity (MRE). Percent helicity was estimated from the ellipticity value at 222 nm. The conversion to MRE units and the method to calculate the percent helicity are explained in Section 2.3.2. The CD spectra of POPC/POPG (5:1) at 1.4 mM containing Gad peptides at 30 μM are shown in Figure 4.1. The calculated values for helicity obtained from these spectra are 92% and 100% for Gad-1 and Gad-2 respectively. Based on these observations, it was concluded that POPC/POPG (5:1) is an appropriate lipid mixture in which to perform ^{15}N experiments.

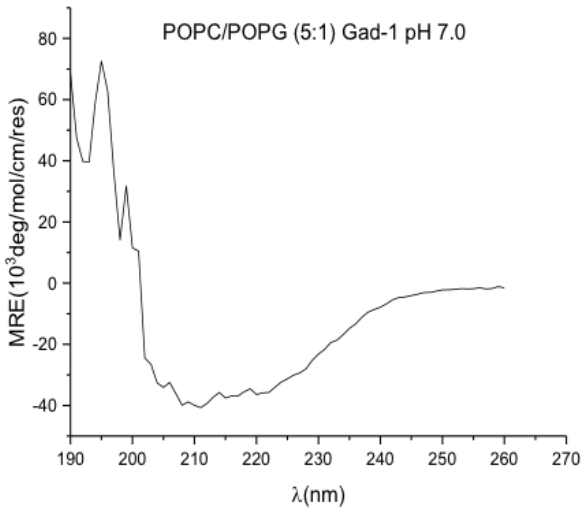

(a)

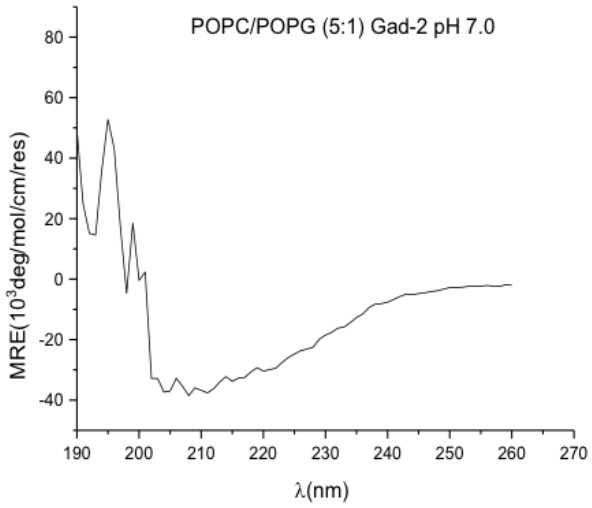

(b)

Figure 4.1: (a) Far-UV CD spectrum of Gad-1 in lipid mixture of POPC/POPG (5:1). (b) CD spectrum of Gad-2 in lipid mixture of POPC/POPG (5:1). These spectra were obtained at 25°C by averaging 20 scans. The observation of two minima at 208 and 222 nm in both spectra suggests that Gad peptides adopt α helical structure in this lipid mixture. See figure 2.14 for comparison of CD spectrum for α helical peptide structure.

4.1.3.3 Protocol for making mechanically oriented lipid bilayers

The detection of ^{15}N signal from a mechanically oriented lipid bilayer sample containing ^{15}N-labelled peptide relies on the degree of orientation of lipid bilayers and amount of peptide. In making the oriented lipid bilayer samples, it was critical to incorporate enough ^{15}N-labelled peptide to see a signal, but not so much that the orientation of the bilayers was disrupted. Mechanically oriented lipid bilayer samples were initially prepared with POPC as the only lipid using the following protocol:

1. Before starting sample preparation of an oriented sample the working space was cleaned to avoid any dust trace deposits on mica plates that can interfere with the lipid orientation.

2. Six mica plates (clean and flat) of dimensions 12×5 mm were cut from a mica sheet using a scalpel. In this step, the mica sheets were peeled apart to produce mica plates as thin as possible. All mica plates were used within two-three hours of preparation.

3. Stock solutions of lipids were prepared using 6 mg of POPC/POPC-d_{31} (7:3) in 60 μL of chloroform/methanol (1:1).

4. This solution was spread (in the middle of each plate) in aliquots of 1 μL on each plate using a micro-pipette. After a cycle of deposition on all mica plates, a time of 3-5 mins was allowed for the lipid solution to dry on the mica plates. Care was taken to avoid spreading lipid to the edge of the mica plates. After completing the first cycle of deposition, the next cyle of 1 μL aliquots was started and this was repeated until all of the solution was deposited on the plates.

5. The sample was left in a fume hood to dry for 1-3 hours.

6. To make sure that no traces of organic solvent were left on the plates, each sample was put in an evacuated desiccator connected to a pump with a liquid nitrogen trap for 6-8 hours.

7. To hydrate the dry lipids on mica plates, 3 μL of deuterium depleted water was deposited on each plate in steps of 1 μL. After depositing 1 μL water on each plate, intervals of 2-3 minutes were allowed for plates to dry before starting a new cycle of water deposition. The challenging part of this step was to deposit water on the dry lipid layer in a way that did not result in the solution spreading to the edges of the mica plate.

8. In order to make sure that lipids formed fully hydrated bilayer assemblies, the sample was put in a sealed hydration chamber with a saturated salt solution of ammonium sulphate dibasic (65 g) in 250 ml of distilled water. 100 mg of sodium azide was added to this salt solution to avoid the growth of bacteria. The hydration chamber was sealed with vacuum grease (Sigma-Aldrich, ON) and the sample was left in the chamber at room temperature for 1-2 days.

9. The hydrated plates were carefully stacked with the addition of one empty plate on top. This stack of plates was then squeezed gently with finger pressure between two flat surfaces to uniformly spread lipids on the plates. Glass microscope slides were used for this purpose. This was the most crucial step in the protocol. To obtain the best results, it was necessary to apply uniform pressure to the stack. If mica plates did not stick to each other after applying pressure, the lipids on the plates were probably not hydrated. In that case sample had to be left in hydration chamber for more time.

10. The stack of sample plates was finally sealed in thin plastic and inserted into a rectangular glass insert. The glass inserts used were 20 mm long with

4.3×6.3 mm ID (inner diameter) and 5.4×7.4 mm OD (outer diameter) and were purchased from New Era Enterprises, Inc. (Newfield, NJ). To maintain the hydration level at higher temperatures, 4 μL of deuterium depleted water was added to the tube and its ends were sealed with wax.

11. The sample was left in a 4°C refrigerator overnight.

12. The sample was left at room temperature for about two hours before performing the NMR experiment.

4.1.4 NMR experimental details

After preparing a mechanically oriented lipid bilayer sample, ^{2}H NMR spectroscopy was used to test the orientation of lipids in the sample. Subsequently, ^{15}N NMR experiment was used to characterize the alignment of Gad peptides in the mechanically oriented lipid bilayers. All experiments were performed at 25°C.

4.1.4.1 ^{2}H NMR

All ^{2}H NMR experiments were performed at 61 MHz in a 9.4 T magnetic field using a locally assembled spectrometer. For mechanically oriented bilayer samples, the sample was inserted into the probe such the bilayer normal was parallel to the external magnetic field. The sample was equilibrated at 25°C for at least 30 minutes before doing the NMR experiment. The ^{2}H NMR spectra were obtained using quadrupole echo pulse sequence with 3.5 μs $\frac{\pi}{2}$ pulses separated by 35 μs. A 15 μs delay was applied before the 5 μs acquisition trigger. All spectra were obtained by averaging 8000 transients with the repetition time of 0.9 s.

4.1.4.2 ^{15}N NMR

Proton decoupled solid-state ^{15}N NMR experiments were performed on a Bruker Advance 14.1 T at 60 MHz in the C-CART facility. All ^{15}N NMR spectra were obtained using the cross polarization (CP) pulse sequence as shown in Figure 4.2. In CP, the polarization is transferred from a high γ nucleus (^{1}H) to a low γ nucleus (^{15}N) and this polarization transfer is mediated by dipolar coupling. Initially, the $\frac{\pi}{2}$ pulse is applied to ^{1}H nuclei. The polarization transfer occurs during contact time and requires that the Hartmann-Hahn condition be satisfied. To satisfy this condition, the Larmor frequencies of the ^{1}H and ^{15}N nuclei in their corresponding RF fields must be set equal by adjusting the power on two channels [87].

Two types of ^{15}N experiments were conducted: first a spectrum was obtained from a dry powder of Gad peptides and then a spectrum was obtained from mechanically oriented lipid bilayers with incorporated ^{15}N-labelled Gad peptides. The acquisition parameters used in these experiments are listed in Table 4.2.

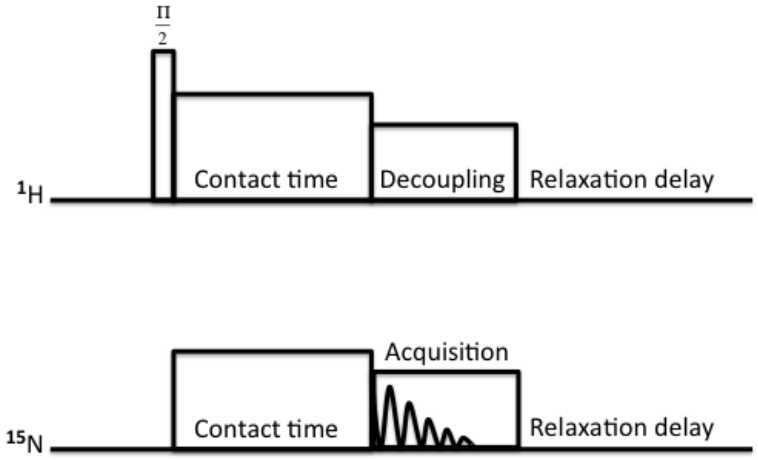

Figure 4.2: The schematic representation of cross polarization (CP) pulse sequence. The $\frac{\pi}{2}$ pulse is applied to ^{1}H channel and polarization is transferred from ^{1}H nucleus to ^{15}N nucleus during contact time. Afterwards, the ^{1}H nuclei are decoupled and FID from ^{15}N nuclei is collected.

Acquisition parameter	Value of the acquisition parameter	
	Dry powder sample	Oriented sample
relaxation delay (s)	5	5
contact time (ms)	1.5	1.5
90°pulse length (μs)	5.5	5.5
90°pulse power level (dB)	0	-1
cross polarization field (kHz)	50	50
decoupling field (kHz)	45	45

Table 4.2: The list of acquisition parameters used in CP ^{15}N NMR experiments.

4.1.5 Synthesis of ^{15}N-labelled Gad peptides

Gad peptides were synthesized by Fmoc solid phase synthesis [26, 162, 163] and were further purified by using High Pressure Liquid Chromatography (HPLC), as explained in Chapter 3. To perform ^{15}N experiments it was necessary to isotopically label peptides with ^{15}N. This was done by using labelled amino acids during peptide synthesis. The cost of ^{15}N-labelled amino acids depends on the amino acid type and it was only practical to label certain types of amino acids, like alanine, valine, and leucine. For Gad-1, it was decided to label valine at position 13 and

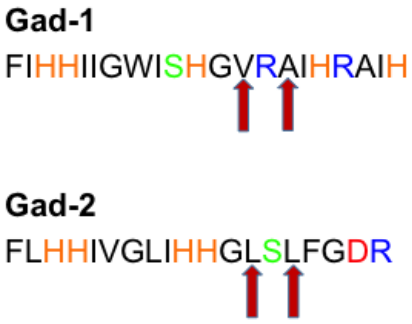

Figure 4.3: Gad peptides selectively labelled with ^{15}N isotopes at two sites indicated by red arrows.

alanine at position 15. For Gad-2, leucine residues at positions 13 and 15 were labelled. The labelled sites are indicated by arrows in Figure 4.3.

The 3D structures determined from solution NMR data show the helical portions of Gad peptides [26]. The ^{15}N-labelled residues for both peptides are expected to be in the same helical segment.

4.1.6 Protein concentration assay

The Bradford assay is a spectroscopic procedure used to measure the concentration of protein. The method is based on the proportional binding of the dye Coomassie Brilliant Blue G-250 to protein. When protein binds to the dye, it results in the dye changing color from red to blue. The blue protein-dye form is detected at 595 nm in the assay using a Genesys 10S UV-Vis spectrophotometer (Thermo Fisher Scientific, ON). The Bradford assay [164] involved following steps.

1. The assay reagent was prepared by dissolving 10 mL of Coomassie dye in 40 mL of distilled water.

2. A stock solution of Gad peptides was prepared in 10 mM sodium acetate buffer.

3. A standard protein solution was prepared by dissolving BSA (Bovine Serum Albumin) protein (Sigma-Aldrich, Co.) at a concentration of 1 mg/mL in 10 mM sodium acetate buffer.

4. A series of peptide standards was prepared by pipetting 1, 2, ... 10 μL volumes of 1 mg/mL BSA standard protein solution into clean test tubes and adding 1 mL of assay reagent to each test tube. Tubes were then vortexed gently to ensure thorough mixing. One blank test tube containing only 1 mL of assay reagent was also prepared.

5. The spectrophotometer was set to 595 nm and zeroed using the blank sample.

6. The absorbances of the standard solutions were then measured at 595 nm and a standard curve was obtained by plotting absorbance vs. volume of standard solutions.

7. Peptide sample dilutions were then prepared by adding 5 μL and 10 μL of Gad peptide solution to 1 mL aliquots of assay reagent. Absorbances of these solutions were measured at 595 nm. If this absorbance did not lie in the range of the standard curve then other sample dilutions were prepared until an absorbance falling within the range of standard curve was obtained.

8. Protein concentration was determined from the standard curve and the dilution factor.

4.2 Results

4.2.1 Mechanically oriented samples of lipids only

As explained above, the preparation of mechanically oriented lipid bilayers was first carried out on samples containing lipids only. ^{2}H NMR spectroscopy was employed to monitor the orientation of the lipid bilayers. A ^{2}H NMR spectrum of mechanically oriented POPC/POPC-d_{31} (7:3) lipid bilayers is shown in Figure 4.4 (a). For POPC bilayers, it was found that good orientation could be obtained by using 1 mg of lipid and 3 μL of water on each plate and allowing a hydration time of at least 24 hours.

For mechanically oriented lipid bilayers with bilayer normals parallel to the external magnetic field, the deuterium NMR spectrum has peaks corresponding to deuterons at different positions on the lipid acyl chains. Any fractions of the sample having randomly oriented bilayer normals are expected to give rise to features

with half of the quadrupole splitting of corresponding features in the spectrum arising from the well-oriented fraction of the sample [86, 158, 162]. With successful sample preparation parameters identified for POPC, the next step was to try this protocol with POPC/POPG (5:1) lipid mixtures. Mechanical orientation of lipid mixtures containing POPG was found to be more challenging but it was possible to make an oriented sample as shown by the ^{2}H NMR spectra in Figure 4.4 (b). It is evident from the spectrum shown in Figure 4.4 (b) that the POPC/POPG (5:1) lipid mixture used to obtain that spectrum had some randomly oriented portions. The red oval on Figure 4.4 (b) indicates spectral features characteristic of bilayers with randomly oriented bilayer normals. Although the orientation of this sample was not perfect, it was felt that the fraction of the sample that was oriented was sufficient to justify proceeding to the stage of incorporating peptide into the oriented samples.

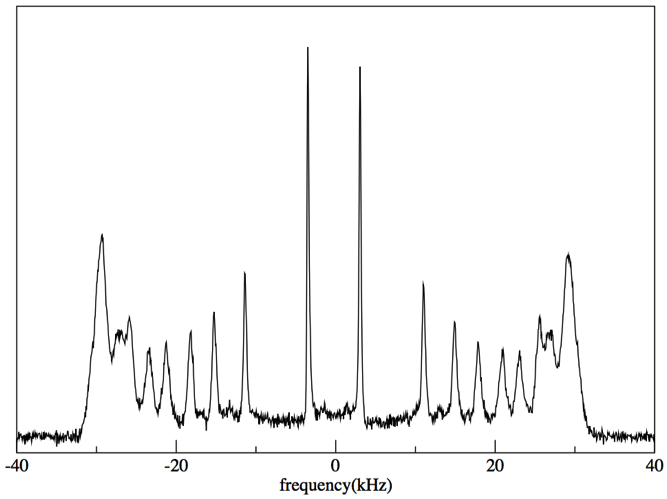

(a)

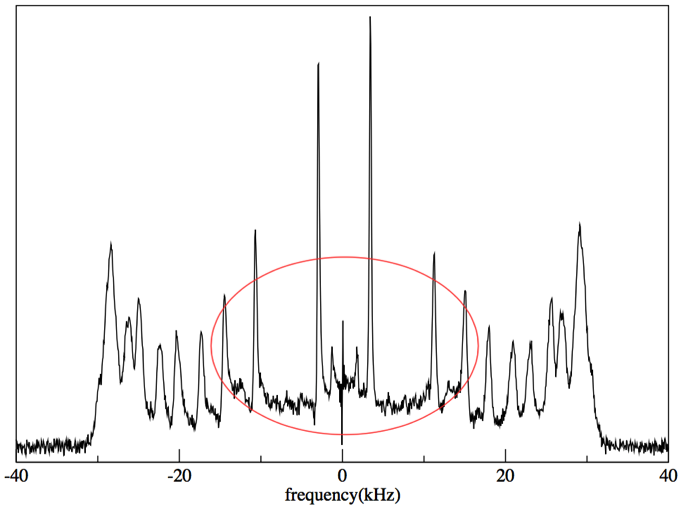

(b)

Figure 4.4: (a) ^{2}H NMR spectrum of mechanically oriented POPC/POPC-d_{31} (7:3) lipid bilayers. (b) ^{2}H NMR spectrum of mechanically oriented POPC-d_{31}/POPG (5:1) lipid bilayers. The addition of POPG resulted in the quadrupole splittings that are characteristic of randomly oriented bilayer fraction, indicated by red oval. For both spectra, a total of 6 mg of lipids were deposited on 6 mica plates. The spectra were obtained at 25°C by averaging 6000 transients.

4.2.2 Mechanically oriented bilayer samples of POPC/POPG (5:1) lipid mixture with incorporated unlabelled Gad peptides

After making acceptably oriented lipid bilayers with POPC/POPG lipid mixtures, the next step was to add peptide to this system. This was first attempted using unlabelled Gad peptides. Keeping the peptide to lipid ratio at 3 mole%, mechanically oriented samples with Gad-1 and Gad-2 were prepared using the protocol described in Section 4.1.3.3. The resulting spectra are shown in Figure 4.5. As for POPC/POPG oriented lipid bilayers in the absence of peptides, these spectra also have some spectral features corresponding to a randomly oriented bilayer fraction. However, the portion of randomly oriented lipid appeared slightly higher with peptide than without, suggesting that the peptide may affect mechanical bilayer orientation. These spectra indicate that approximately 75% of lipid bilayers were oriented. It was decided that this was adequate to perform ^{15}N experiments. Another important consideration in planning for ^{15}N NMR experiments was that, due to the low ^{15}N sensitivity, it was expected that each experiment would need to run for about a week in order to yield an observable signal [162, 165]. For this reason, it was necessary to ensure that samples could remain oriented as well as hydrated for this time period while held at 25°C. In order to check stability, samples were held at room temperature and ^{2}H NMR experiments were repeated over a periods of 12 days for samples containing Gad-1 and 14 days for samples containing Gad-2. The spectra obtained in these experiments are shown in Figure 4.5. The ^{2}H NMR spectra in Figure 4.5 (a) were obtained from the oriented sample of POPC-d_{31}/POPG (5:1) containing Gad-1. The resolution of the spectrum labelled "Day 1" in this series was evidently much poorer that those obtained from

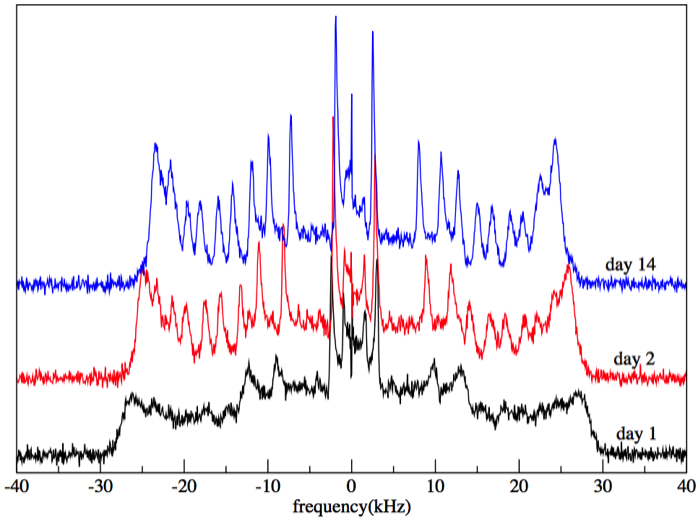

(a)

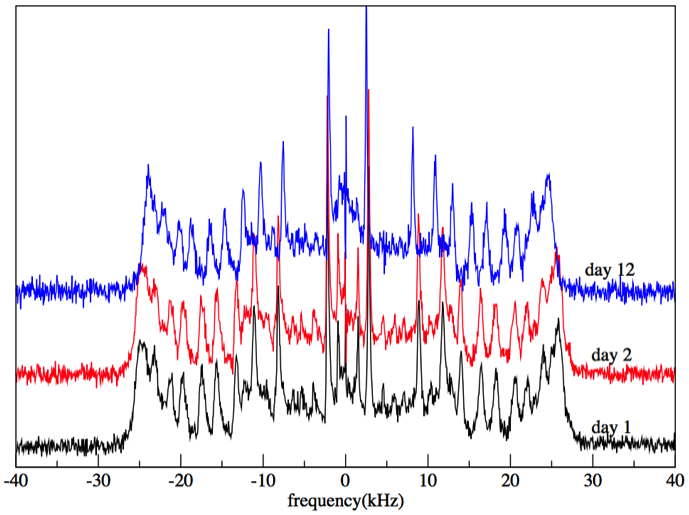

(b)

Figure 4.5: ^{2}H NMR spectra obtained at different intervals after sample preparation (a) mechanically oriented lipid bilayers of POPC-d_{31}/POPG (5:1) with 3 mole% (0.6 mg) of Gad-1 and (b) a mechanically oriented lipid bilayers of POPC-d_{31}/POPG(5:1) with 3 mole% (0.5 mg) of Gad-2. In both cases, 6 mg of POPC-d_{31}/POPG (5:1) lipids were deposited on 6 mica plates. All spectra were obtained at 25°C and by averaging 6000 number of transients.

other oriented bilayer samples. In order to test whether this was due to incomplete hydration of the sample, the sealed NMR tube containing this sample was carefully opened from one end and 3 μL of deuterium-depleted water was added

to the tube. The tube was resealed with wax and left at room temperature for a day after which the better resolved spectrum labelled "Day 2" was obtained. It was concluded that if a spectrum indicated that a sample was not fully hydrated, hydration could be improved by adding more water and allowing it to redistribute through the sample. For oriented POPC-d_{31}/POPG (5:1) lipid bilayers prepared in the presence of Gad-2, the spectrum stayed the same over the period of 12 days as indicated by the well resolved individual deuteron peaks in Figure 4.5 (b). After having gained some experience with the preparation of mechanically oriented bilayer samples containing unlabelled Gad peptides, the next step was to prepare oriented bilayer samples containing ^{15}N-labelled Gad peptides.

4.2.3 Mechanically oriented bilayer samples of POPC/POPG (5:1) lipid mixture with incorporated ^{15}N-labelled Gad peptides

A mechanically oriented lipid bilayer sample of POPC-d_{31}/POPG (5:1) containing 3 mole% (i.e. 0.6 mg) of ^{15}N-labelled Gad-1 was prepared using six mica plates following the protocol explained in Section 4.1.3.3. Before conducting an ^{15}N NMR experiment, bilayer orientation was tested using ^{2}H NMR spectroscopy. The resulting spectra are shown in Figure 4.6.

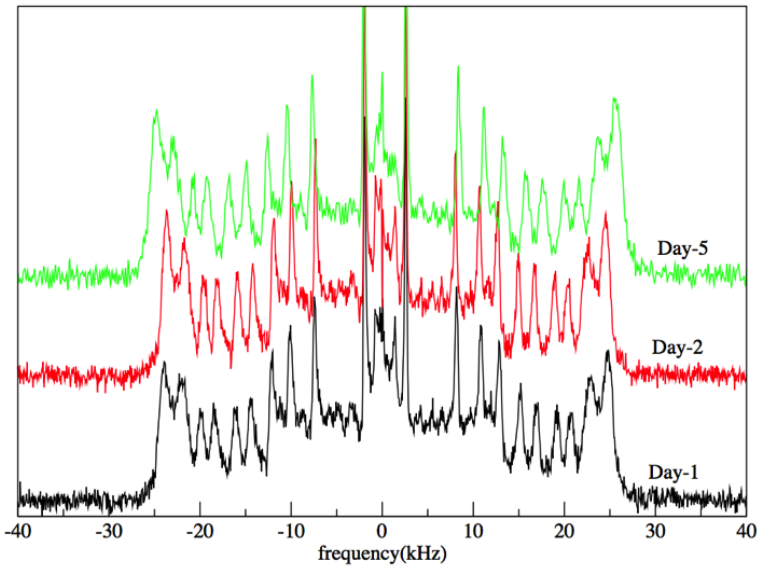

Figure 4.6: ^{2}H NMR spectra from a mechanically oriented sample prepared using 6 mg POPC-d_{31}/POPG (5:1) with the addition of 3 mole%, i.e. 0.6 mg, ^{15}N-labelled Gad-1 peptide. The stability of the sample in terms of hydration and orientation was monitored over a time period of 5 days. The sample was left at room temperature between day 1, day 2, and day 5. All spectra were obtained at 25°C and by averaging 6000 transients.

This series of spectra show that about 75% of lipid bilayers were well oriented and that it remained hydrated for at least five days.

An ^{15}N NMR experiment was then performed on a Bruker Advance 14.1 T at 60 MHz using the acquisition parameters mentioned in Table 4.2. A large number of transients (66,000) were averaged but no ^{15}N signal was observed. The inability to obtain an observable ^{15}N signal from a predominantly oriented and well-hydrated sample suggested that there was not enough peptide in that sample to get an ^{15}N signal. In order to address this problem it was decided to increase the total amount of peptide in the sample. Doing this required increasing the total amount of lipids and hence the number of mica plates. In order to estimate roughly the amount of labelled peptide needed in a sample to get an ^{15}N signal, a ^{15}N NMR experiment was run to obtain a powder pattern spectrum using a dry powder of just labelled peptide. It was thought that if a spectrum could be obtained in a powder sample

where signal was spread over the range of chemical shifts corresponding to all orientations then it should be possible to obtain signal from an oriented sample in which the signal was concentrated at a particular chemical shift. Based on that reasoning, it was expected that if a powder pattern spectrum could be obtained with x mg of labelled peptide by averaging a number y of transients then $\frac{x}{2}$ mg of labelled peptide should be enough to obtain the ^{15}N signal by averaging $4y$ transients since signal-to-noise ratio in an NMR experiment is proportional to the square root of the number of summed transients,

$$\frac{S}{N} \propto \sqrt{no\ of\ averaged\ transients.} \tag{4.1}$$

An experiment was run with 6 mg of dry ^{15}N-labelled Gad-1 peptide powder. A powder pattern was obtained by averaging 12,000 number of transients using the acquisition parameters mentioned in Table 4.2. The resulting powder pattern spectrum of Gad-1 is shown in Figure 4.7. Based on this result, it was estimated

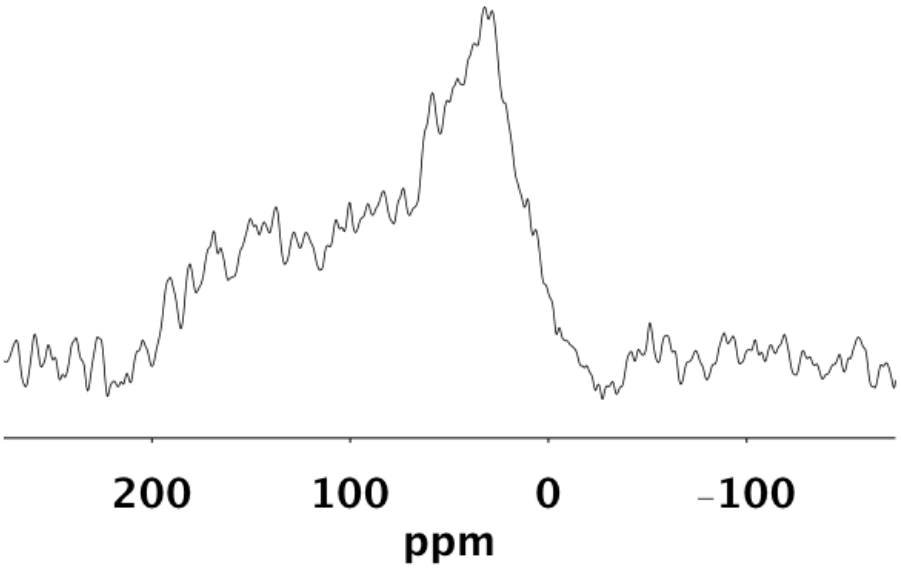

Figure 4.7: ^{15}N powder pattern spectrum obtained from 6 mg of Gad-1 dry powder at 25°C by averaging 12,000 transients.

that approximately 3 mg of labelled peptide would be sufficient to yield an observable ^{15}N signal in a reasonable amount of time. In order to maintain the lipid:peptide ratio while applying the same protocol but using 3 mg of peptide, it was concluded that approximately 24 mica plates would be required.

4.2.4 Mechanically oriented lipid bilayers prepared using 24 mica plates

In order to test the feasibility of preparing samples with 24 mica plates, samples with this number of plates were first prepared using lipids only. The basic protocol was the same as mentioned in Section 4.1.3.3 but the total amount of lipids as well as the number of mica plates, were increased. A total of 40 mg of POPC-d_{31}/POPG (5:1) was dissolved in 560 μL of chloroform/methanol (1:1). After dissolving the lipids in organic solvent, the final volume was reduced to approximately 200 μL by drying under N_2 flow. This solution was deposited on 24 mica plates in steps of 1 μL on each plate until all of the solution was deposited. After this step, the protocol followed was the same as is mentioned in Section 4.1.3.3. The challenging task in this sample preparation was to stack the 24 mica plates. Two ways of stacking mica plates were tried. The first way was to stack all plates together as explained in the preceding protocol. The corresponding spectrum is shown in Figure 4.8. This approach was found to be problematic because after stacking, all of the plates needed to be squeezed together. Having 24 plates all together made it very hard to apply uniform pressure on all plates especially the middle plates. This likely caused a non-uniform distribution of lipids which gave rise to spectral features corresponding to a randomly oriented sample fraction.

An alternative approach involved making four stacks where each stack contained 6 plates wrapped separately. Spectra corresponding to each of these 6-plate stacks

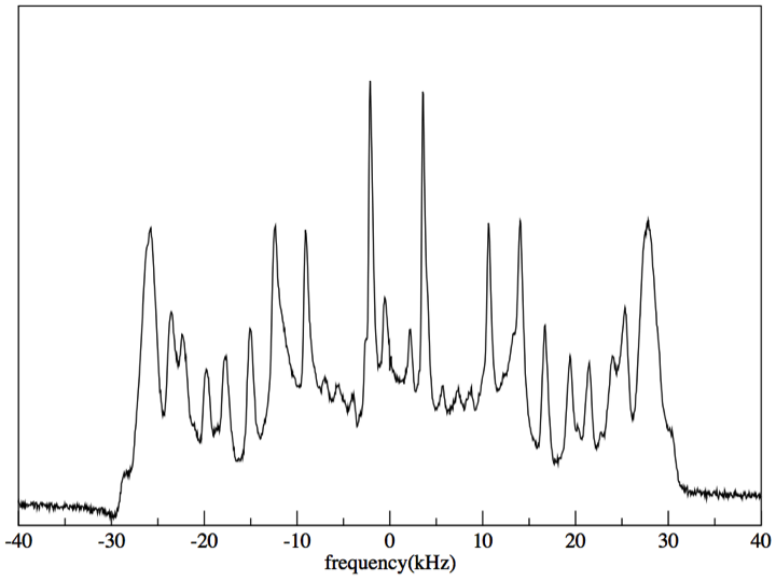

Figure 4.8: ^{2}H NMR spectrum of oriented bilayers prepared using 40 mg of POPC-d_{31}/POPG (5:1) lipids deposited on 24 mica plates. In this case all mica plates were stacked altogether. The spectrum was obtained at 25°C and by averaging 6000 number of transients.

are shown in Figure 4.9 (a). The spectrum of stack 1 is narrower than the spectra of other three stacks. This is likely due to the distribution of water on the mica plates being better in the case of stack 1. These stacks were then very carefully inserted into a rectangular NMR tube in a such way that all stacks were aligned exactly with each other. The resulting spectrum is shown in Figure 4.9 (b).

The degree to which the sample was oriented was almost the same for both plate stacking methods but it was easier to make a small number of separate stacks instead of stacking all plates together. Having demonstrated the feasibility of orienting lipid-only bilayers using 24 mica plates, the next step was to incorporate peptide into the system.

A mechanically oriented sample containing 3.8 mg of unlabelled Gad-1 peptide and 40 mg of POPC-d_{31}/POPG (5:1) was prepared following the procedure described above. Lipid orientation in the four stacks was tested for each stack individually

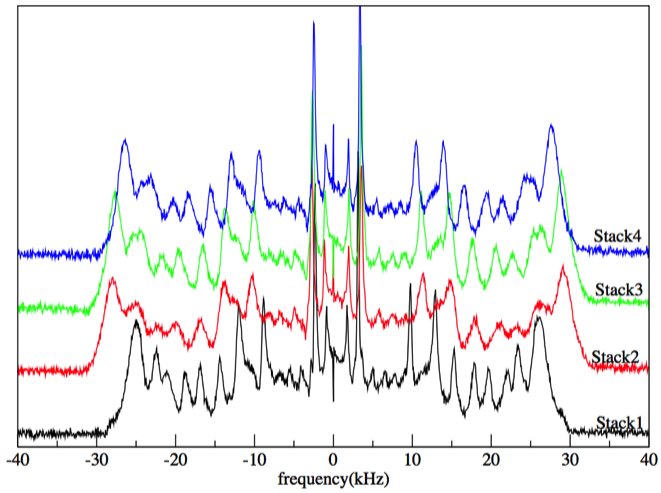

(a)

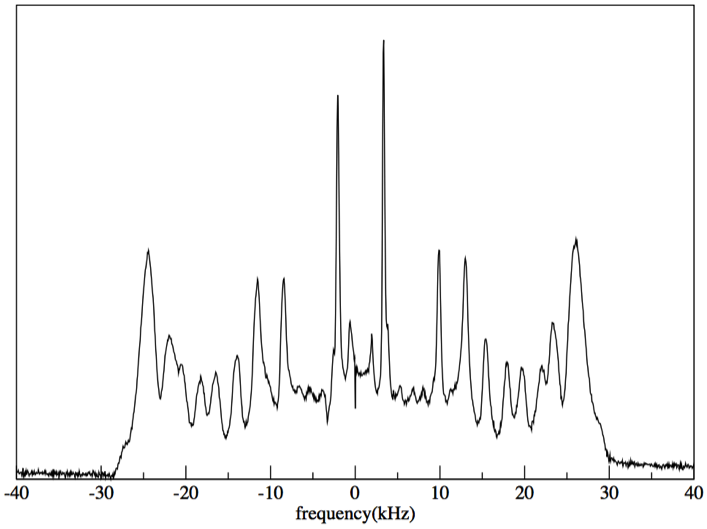

(b)

Figure 4.9: ^{2}H NMR spectra of 40 mg POPC-d_{31}/POPG (5:1) lipid mixture prepared using 24 mica plates. The mica plates were divided into four groups, each having six plates. (a) Spectra obtained from each six-plate stack independently (b) Spectra obtained after sealing the 4 six-plate stacks together in a rectangular NMR tube. All spectra were obtained at 25°C and by averaging 6000 number of transients.

and after sealing the four stacks together. The resulting ^{2}H NMR spectra are shown in Figure 4.10. In terms of hydration and orientation, the sample was stable over the period of nine days and more than half of the lipid bilayer fraction

was oriented.

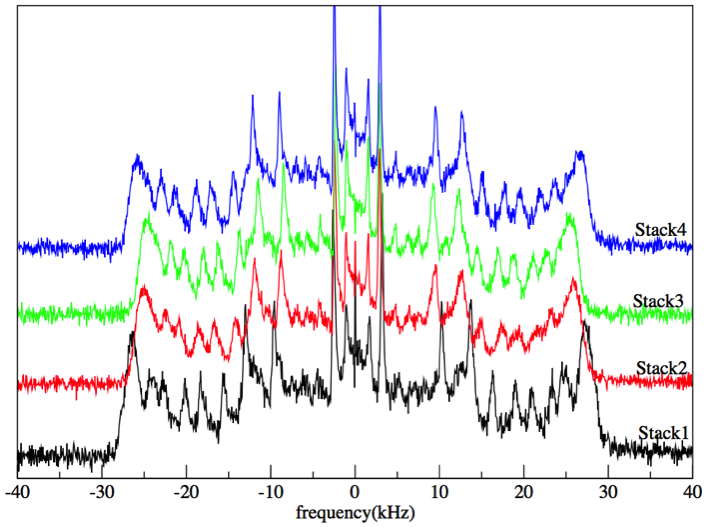

(a)

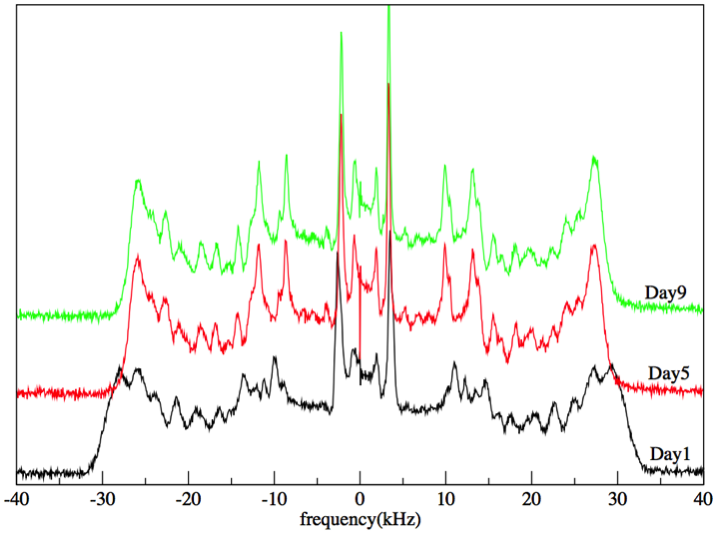

(b)

Figure 4.10: ^{2}H NMR spectra of 40 mg POPC-d_{31}/POPG (5:1) containing 3.8 mg of Gad-1 peptide. (a) Spectra obtained from each six-plate stack independently (b) Spectrum obtained after sealing the 4 six-plate stacks together in a rectangular NMR tube. Spectra were also collected five and nine days after preparation in order to monitor the stability of orientation and changes in hydration due to redistribution of water within the stacked bilayers. All spectra were obtained at 25°C and by averaging 6000 number of transients.

4.2.5 Adjusting the pH of mechanically oriented lipid bilayers

Up to this point, efforts were focused on preparing well oriented and hydrated mechanically oriented lipid bilayers with enough peptide to get an observable ^{15}N NMR signal. The main goal of the next part of the project was to study the alignment of Gad peptides in oriented bilayers at low and high pH values. It was thus necessary to ensure that it was possible to prepare mechanically oriented bilayers at a specific pH. The following protocol [86] describes the preparation of mechanically oriented lipid bilayers in the presence of Gad peptides with inclusion of an extra step to test and adjust the sample pH.

1. 40 mg of lipids POPC-d_{31}/POPG (5:1) and 3 mole% of Gad peptides were dissolved in 1500 μL of 10 mM sodium acetate buffer at the desired pH.
2. The sample pH was monitored using a pH meter and adjusted to the desired pH to within $\pm$ 0.1 by adding 0.1 M HCl or 0.1 NaOH.
3. The sample was then freeze-dried overnight.
4. The dried sample was then suspended in chloroform/methanol (1:1) to make a final volume of 180 μL.

Subsequent steps in preparation of the pH-controlled samples were done as described in Section 4.1.3.3. Figure 4.11 shows the ^{2}H NMR spectrum obtained from a mixture of POPC-d_{31}/POPG (5:1) at pH 7.0 following preparation using this protocol. The lipid bilayers were oriented up to same extent as the previous oriented lipid bilayers prepared without the control of pH.

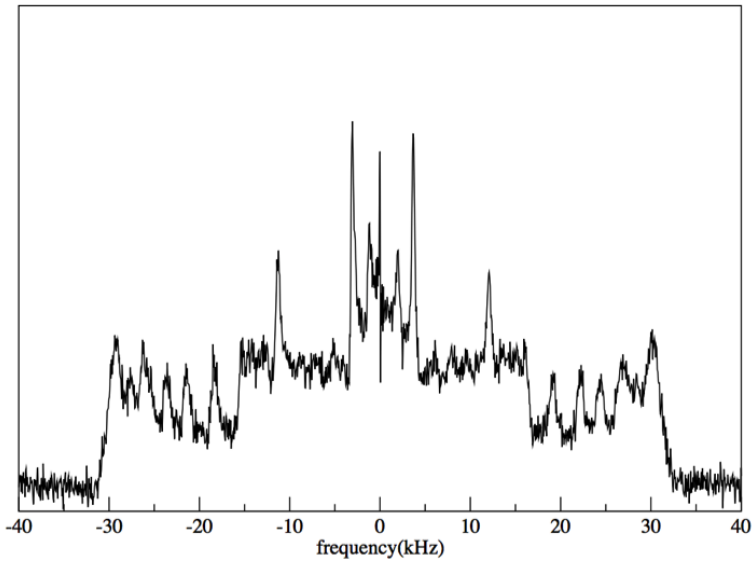

Figure 4.11: ^{2}H NMR spectrum of oriented POPC-d_{31}/POPG (5:1) bilayers at pH 7.0 prepared using the protocol described in Section 4.3.5. A total of 40 mg of lipids POPC-d_{31}/POPG (5:1) were deposited on 24 mica plates. The spectrum was obtained at 25°C by averaging 6000 transients.

4.2.6 Alignment of Gad-1 in mechanically oriented lipid bilayers of POPC-d31/POPG (5:1) at pH 7.0

To study the alignment of Gad-1 in oriented lipid bilayers at pH 7.0, a mechanically oriented sample at pH 7.0 was prepared using the protocol described in Section 4.2.5. In this sample, 3 mole% (3.8 mg) of ^{15}N-labelled Gad-1 peptide was mixed with 40 mg of POPC-d_{31}/POPG (5:1).

In order to test bilayer orientation in this sample, a series of ^{2}H NMR experiments were performed on each 6-plate stack individually and on the sample obtained by sealing the four 6-plate stacks together in a rectangular NMR tube. The corresponding spectra are shown in Figure 4.12. These spectra indicate that more than half of the fraction of POPC-d_{31}/POPG (5:1) lipid bilayers containing Gad-1 was oriented.

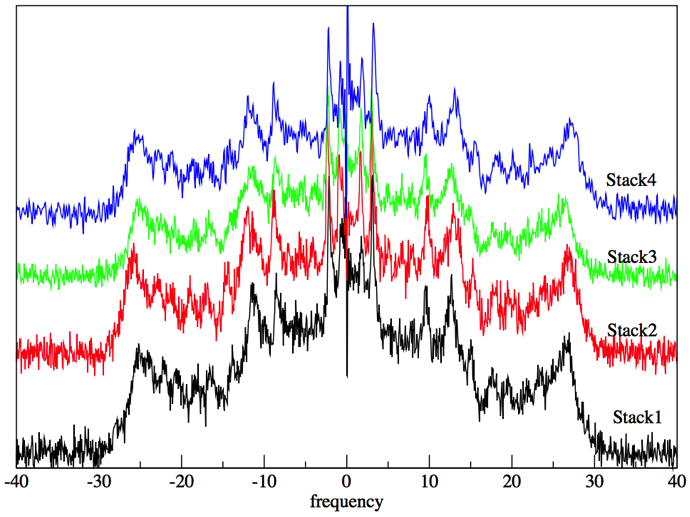

(a)

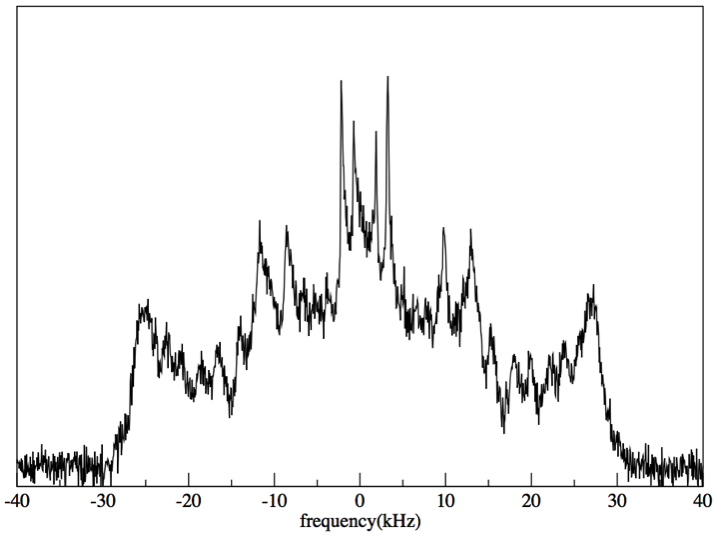

(b)

Figure 4.12: ^{2}H NMR spectrum of POPC-d_{31}/POPG(5:1) at pH 7.0 containing ^{15}N-labelled Gad-1 peptide. (a) Spectra obtained from each six-plate stack independently (b) Spectrum obtained after sealing the 4 six-plate stacks together in a rectangular NMR tube. A total of 40 mg of POPC-d_{31}/POPG (5:1) mixed with 3.8 mg of Gad-1 were deposited on 24 mica plates. All spectra were obtained at 25°C by averaging 6000 transients.

With sample orientation characterized by ^{2}H NMR, the next step was to carry out a proton-decoupled ^{15}N NMR experiment using a Bruker Advance 14.1 T at 60 MHz. This experiment was conducted using the acquisition parameters listed in the Table 4.1. The number of transients averaged was 46,000. The resulting ^{15}N spectrum is shown in Figure 4.13 (a). The orientation and hydration of lipid bilayers was tested after the ^{15}N experiment. The resulting ^{2}H NMR spectrum is shown in Figure 4.13 (b). The comparison of ^{2}H NMR spectra before and after the ^{15}N experiment indicate that sample was less hydrated after the ^{15}N experiment. This dehydrating could occur due to radio frequency induced heating of the sample in the NMR probe.

In order to test how peptide alignment changes in less hydrated lipid bilayers, the ^{15}N experiment was repeated with the same sample 20 days later than the first experiment. The spectrum obtained in the second ^{15}N experiment is shown in Figure 4.14 (a). The ^{15}N chemical shift obtained from the peptide in this sample changed significantly between the time of the initial spectrum and the one obtained 20 days later. However, the chemical shift of <100 ppm in both cases indicates the alignment of peptide was parallel to the membrane surface for both experiments. The orientation and hydration of lipid bilayers was tested after the second ^{15}N experiment. The resulting ^{2}H NMR spectrum is shown in Figure 4.14 (b). The two ^{15}N spectra are compared in Figure 4.15.

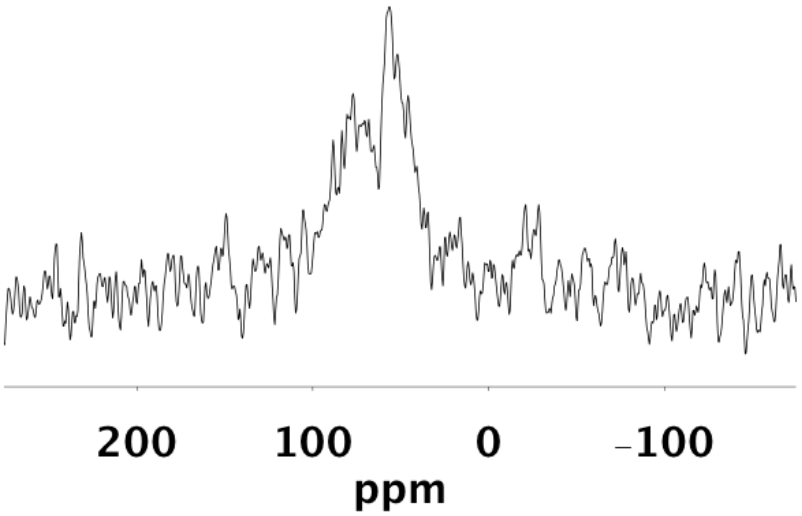

(a)

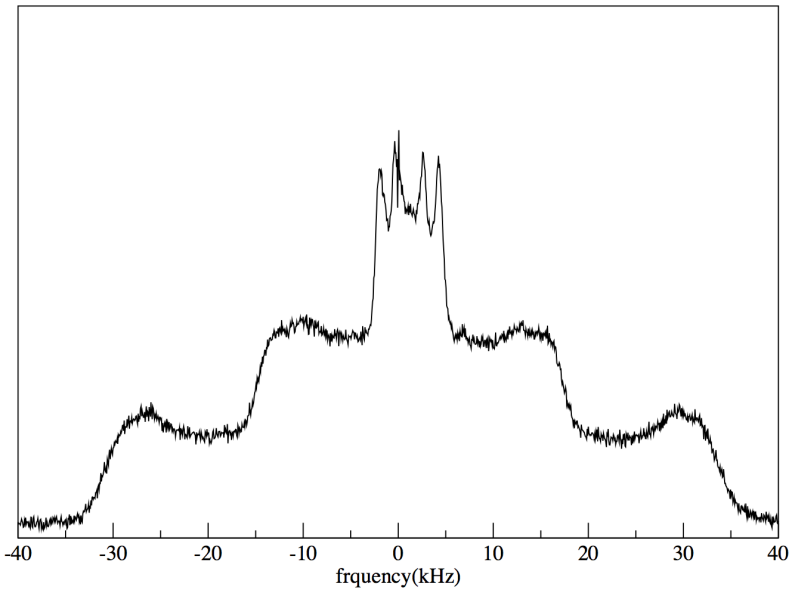

(b)

Figure 4.13: (a) Proton-decoupled ^{15}N solid-state NMR spectrum of Gad-1 reconstituted into mechanically oriented lipid bilayers of POPC-d_{31}/POPG (5:1) at pH 7.0. This sample was prepared by mixing 40 mg of POPC-d_{31}/POPG (5:1) lipids with 3.8 mg ^{15}N-labelled Gad-1. The spectrum was obtained at 25°C and by averaging 46,000 number of transients. (b) ^{2}H NMR spectrum obtained with the same sample after ^{15}N experiment. This spectrum was obtained at 25°C and by averaging 6000 transients.

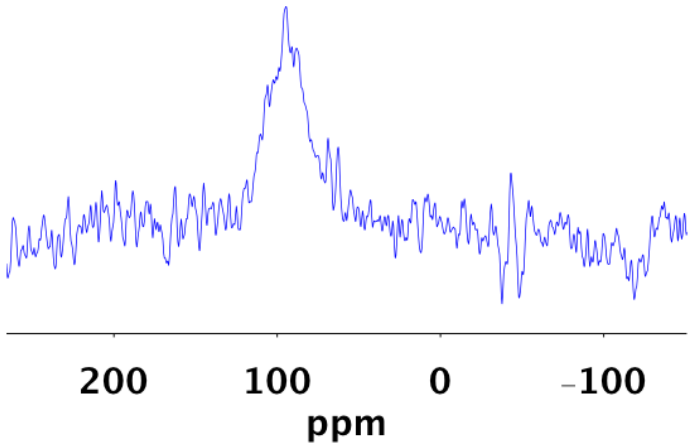

(a)

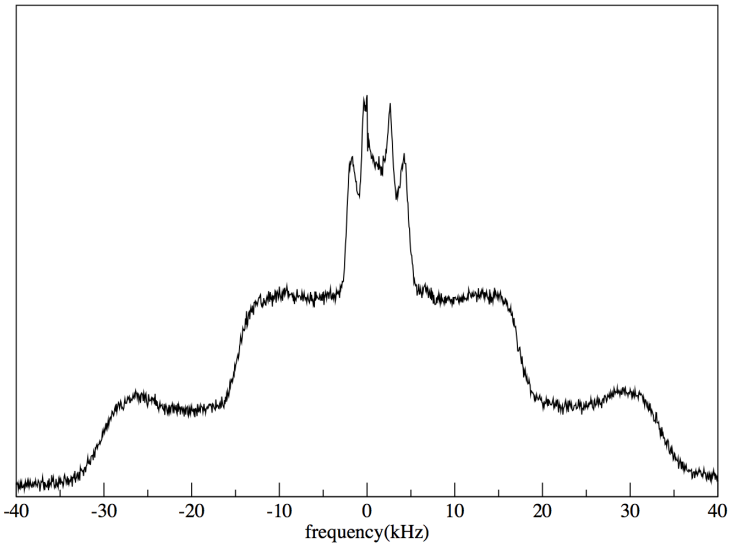

(b)

Figure 4.14: Proton-decoupled ^{15}N solid-state NMR spectrum of Gad-1 reconstituted into mechanically oriented lipid bilayers of POPC-d_{31}/POPG (5:1) at pH 7.0. This experiment was conducted 20 days later than the first ^{15}N experiment. The spectrum was obtained at 25°C and by averaging 46,000 number of transients. (b) ^{2}H NMR spectrum obtained with the same sample after ^{15}N experiment. This spectrum was obtained at 25°C and by averaging 6000 transients.

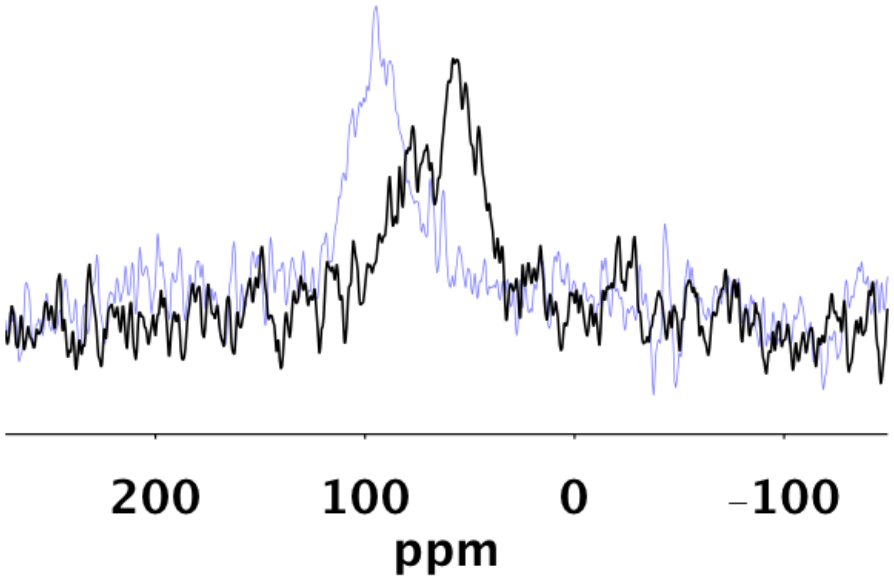

Figure 4.15: The comparison of two ^{15}N spectra of Gad-1 reconstituted into mechanically oriented lipid bilayers of POPC-d_{31}/POPG (5:1) at pH 7.0. The spectrum shown in blue was obtained 20 days later than the first spectrum shown in red.

4.2.7 Alignment of Gad-2 in mechanically oriented lipid bilayers of POPC-d31/POPG (5:1) at pH 7.0

After obtaining the ^{15}N spectrum for Gad-1 at pH 7.0, the next step was to attempt the same experiment with Gad-2 in oriented lipid bilayers at pH 7.0.

Before preparing an oriented sample, an ^{15}N experiment was run on 3.2 mg of Gad-2 dry powder to obtain the powder pattern. The resulting spectrum is shown in Figure 4.16. This spectrum was obtained using the acquisition parameters listed in Table 4.1. The number of transients averaged was 100,000. Judging from the powder pattern spectrum with 3.2 mg of Gad-2 dry powder I expected to need at least 50,000 transients to get a useable ^{15}N spectrum from an oriented sample, with the same amount of peptide. After obtaining the powder pattern spectrum with

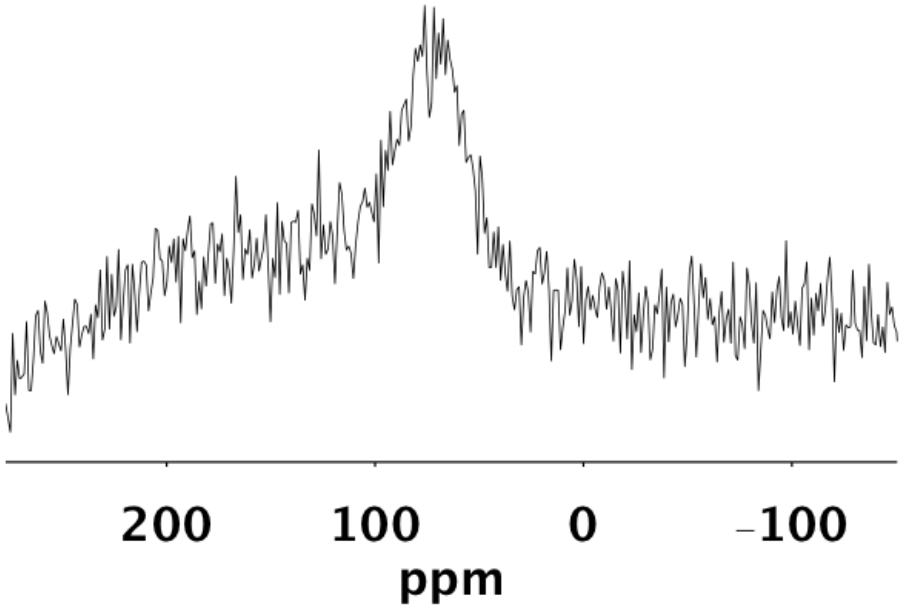

Figure 4.16: ^{15}N powder pattern spectrum of Gad-2 acquired with 3.2 mg of ^{15}N-labelled Gad-2 dry powder. The spectrum is obtained at 25°C by averaging 100,000 transients.

labelled Gad-2 dry powder, a mechanically oriented sample of POPC-d_{31}/POPG (5:1) with 3 mole% (3.2 mg) ^{15}N-labelled Gad-2 peptide was prepared by following the protocol described in Section 4.2.5. A series of ^{2}H NMR experiments were then conducted to test the orientation of the lipid bilayers. The resulting ^{2}H NMR spectra are shown in Figure 4.17. These spectra indicate that a large enough fraction of POPC-d_{31}/POPG (5:1) lipid bilayers containing Gad-2 was oriented and that it was acceptable to proceed with ^{15}N experiments. A proton-decoupled ^{15}N NMR experiment was then performed on a Bruker Advance 14.1 T at 60 MHz using the acquisition parameters listed in the Table 4.1. The number of transients averaged were 78,000 and very little ^{15}N signal was observed. The resulting ^{15}N spectrum is shown in Figure 4.18.

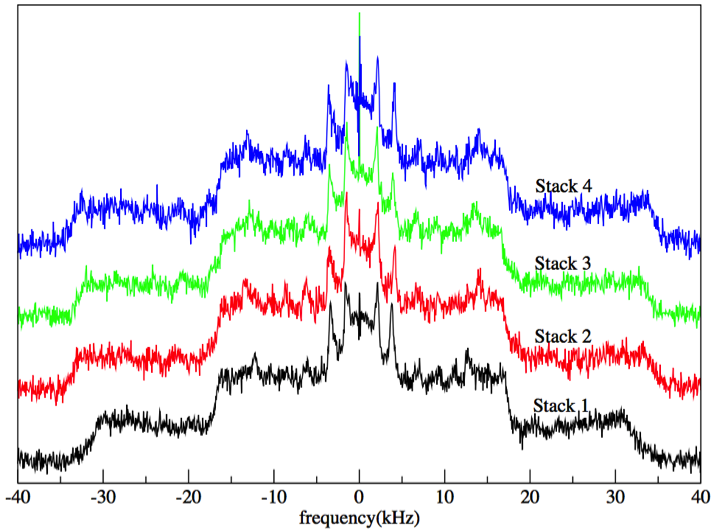

(a)

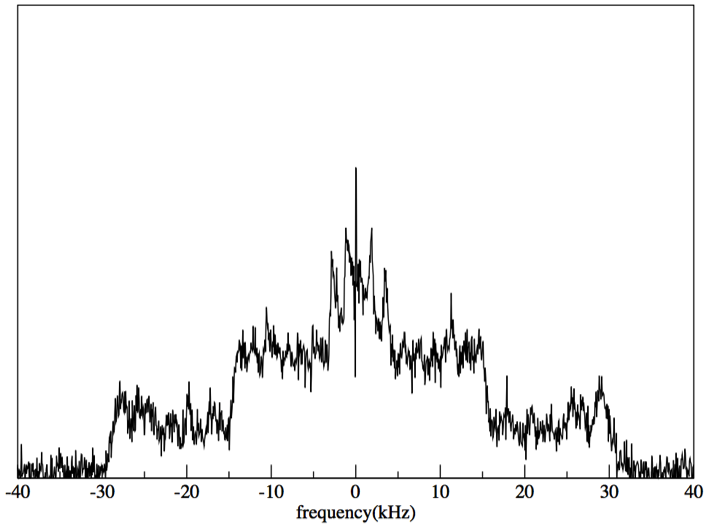

(b)

Figure 4.17: ^{2}H NMR spectra of mechanically oriented POPC-d_{31}/POPG (5:1) lipid bilayers at pH 7.0 containing ^{15}N-labelled Gad-2 peptide. (a) Spectra obtained from six-plate stack independently (b) Spectrum obtained after sealing 4 six-plate stacks together in a rectangular NMR tube. Total 40 mg of POPC-d_{31}/POPG (5:1) mixed with 3.2 mg of Gad-2 were deposited on 24 mica plates. All spectra were obtained at 25°C by averaging 6000 transients.

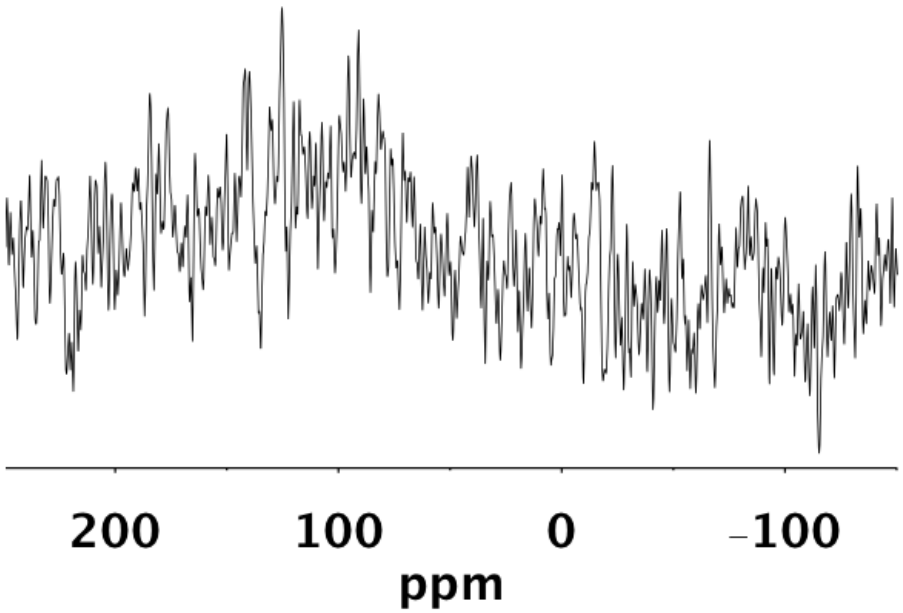

Figure 4.18: Proton-decoupled ^{15}N solid-state NMR spectrum of Gad-2 reconstituted into mechanically oriented lipid bilayers of POPC-d_{31}/POPG (5:1) at pH 7.0. This sample was prepared by mixing 40 mg of POPC-d_{31}/POPG (5:1) lipids with 3.2 mg of ^{15}N-labelled Gad-2. The spectra were obtained at 25°C and by averaging 78,000 transients.

4.3 Discussion

Gad peptides selectively labelled with ^{15}N at two sites were incorporated into mechanically oriented lipid bilayers of POPC-d_{31}/POPG (5:1). The alignment of Gad peptides was investigated by proton-decoupled ^{15}N NMR spectroscopy.

For Gad-1 at pH 7.0, two ^{15}N experiments were conducted on the same sample and the resulting spectra are shown in Figure 4.15. The ^{15}N spectrum obtained from the first experiment consists of two peaks; one centered at $\sim$ 55 ppm and the second at $\sim$ 80 ppm. ^{15}N spectra of helical peptides and different angles with respect to the bilayer have been simulated [166]. Smaller ^{15}N chemical shifts correspond to more in-plane orientations while larger ^{15}N chemical shifts indicate

more transmembrane orientations. A simplified "rule of thumb" is ^{15}N chemical shifts >200 ppm corresponds to the transmembrane orientation of peptide with respect to the membrane surface while ^{15}N chemical shifts <100 ppm correspond to in-plane alignment of peptide [108–110]. The ^{15}N spectrum of Gad-1 at pH 7.0 indicates chemical shifts of <100 ppm corresponding to in-plane alignment of Gad-1 in oriented bilayers. A second ^{15}N experiment was conducted on this sample 20 days after the first one. The resulting ^{15}N spectrum is shown in 4.14 (a). It is evident from second experiment that, after 20 days, the ^{15}N spectrum has evolved into a single, narrower chemical shift peak centered at $\sim$ 95 ppm. This might mean the peptide orientation has become more uniform with time. However, the change in shift from $\sim$ 80 to $\sim$ 95 ppm suggests that the peptide has become more tilted within the membrane [166]. Mechanically oriented lipid bilayers are known to be less hydrated than liposomes sample [86] and old oriented lipid bilayer samples tend to dehydrate more as indicated by the ^{2}H NMR spectra of before and after the second ^{15}N NMR experiment. This drying of lipid bilayers may cause the observed change in the alignment of peptide. The observation that the overall chemical shift was still <100 ppm indicates that the peptide alignment remained relatively parallel to the membrane surface. It is interesting that the peptide appears to have become slightly more tilted as the membrane became dehydrated.

For Gad-2 at pH 7.0, the observed ^{15}N spectrum is shown in Figure 4.18. There is a small bulge at $\sim$ 100 ppm but the signal-to-noise ratio is very poor. There are two factors that might have contributed to the poor signal-to-noise ratio in this sample:

(i) orientation and hydration of the lipid bilayers

(ii) amount of peptide in the sample

It is evident from Figure 4.17 that the oriented lipid bilayers prepared in the

presence of Gad-2 were at least partially oriented. Comparison of the spectra in Figures 4.17 and 4.12 suggest that the bilayers in the ^{15}N-labelled Gad-2 sample were not substantially less oriented than those in the ^{15}N-labelled Gad-1 sample. Therefore, it was expected that an ^{15}N signal from Gad-2 should be observable in approximately the same amount of Gad-1. The signal-to-noise ratio of ^{15}N spectrum obtained from oriented lipid bilayer sample containing 3 mole% Gad-2 is very poor compared to ^{15}N signal observed from oriented lipid bilayer sample prepared with 3 mole% of Gad-1. Based on these considerations, attention then focused on the second potential explanation i.e that the amount of peptide actually present in the prepared sample might have resulted in the poor signal-to-noise ratio in case of Gad-2.

The dry weight of a chemically synthesized peptide is known to contain a substantial amount of non-peptide contaminants, mainly salt from the HPLC purification. It is not possible to get rid of all the contaminants even by using desalting methods such as dialysis or gel filtration. It is possible there is a larger fraction of salt in Gad-2 than for other peptides and thus less peptide in my sample than indicated by the dry weight.

The Bradford assay was used to estimate the actual peptide concentration present in the dry powder and oriented bilayer samples for which ^{15}N NMR spectra were obtained. Apparent peptide concentrations were obtained and are listed in Table 4.3. These concentrations were then used to estimate the actual masses of Gad peptides present in each of the dry powder and oriented bilayer samples. In Table 4.4, the masses determined from the Bradford assay are compared with the masses of dry peptide used in the preparation of each sample. It is noted that the Bradford assay gives only an estimate of the actual peptide mass present in the dry powder. This estimate is poorer for small peptides than for large proteins. Since Gad-1

and Gad-2 are similar in size it is thus illustrative to compare the Bradford assays for the two peptides.

Peptide	Total dry powder peptide concentration	Apparent peptide concentration based on Bradford assay result
Gad-1	1 mg/ml	0.35 mg/ml
Gad-2	1 mg/ml	0.2 mg/ml

Table 4.3: The apparent concentrations of Gad peptides determined using Bradford assay.

Peptide	Dry powder sample		Oriented lipid bilayer sample	
	Peptide dry powder mass	Apparent peptide mass	Peptide dry powder mass	Apparent peptide mass
Gad-1	6 mg	2.1 mg	3.8 mg	1.3 mg
Gad-2	3.2 mg	0.6 mg	3.2 mg	0.6 mg

Table 4.4: The mass of Gad peptides in powder and oriented lipid bilayer samples calculated using Bradford assay result.

It can be seen that for Gad-1, it is likely that the 3.8 mg of dry, nominally peptide powder used to prepare the oriented bilayer sample actually contained 1.3 mg of peptide. For Gad-2, however, the amount of peptide found in the sample by Bradford assay was only a fifth of the nominal mass added in the preparation. This presumably reflects the presence of additional non-peptide material in the dry Gad-2 powder. The overall effect is that the amount of Gad-2 peptide in the oriented bilayer sample appears to have been slightly less than half of the amount of Gad-1 in the corresponding sample. This may account for the significant difference in signal obtained from the two samples.

In order to enhance the signal-to-noise ratio, one option would be to increase the amount of labelled Gad-2 peptide in the sample. The Bradford assay result indicates that in order to have 1.3 mg of Gad-2 peptide in an oriented bilayer

sample it would be necessary to use 6.5 mg of peptide dry powder to prepare the sample. Increasing the amount of peptide in an oriented bilayer sample by the factor of two would require to double the amount of lipids as well as number of mica plates. It is extremely difficult to prepare an oriented lipid bilayer sample using 48 mica plates.

Another option would be to run NMR experiment for longer time. In order to enhance the signal-to-noise ratio by the factor of two, it would be necessary to collect four times as many transients. In NMR the signal-to-noise ratio varies as

$$\frac{S}{N} \propto \sqrt{no\ of\ averaged\ transients.} \tag{4.2}$$

The ^{15}N spectrum of Gad-2 peptide shown in Figure 4.16 is obtained by averaging 78,000 number of transients. In order to enhance the signal-to-noise ratio by the factor of two it would be necessary to average 200,000 number of transients. It is impractical to run the experiment for this long a time. Therefore, it was decided that ^{15}N experiments on Gad-2 would not be pursued further. In summary, the best oriented sample preparation strategy is to make uniform and thin mica plates and then doing good practice to deposit lipid solution on small mica plates before making final samples. The crucial step in the sample preparation was to stack the mica plates together. It should be made sure to apply uniform pressure to stack the mica plates together. Any mistake in this step can result in the randomly oriented part of lipids. The main finding from this chapter was that Gad-1 is nearly in-plane with the membrane in well hydrated lipid bilayers, but becomes slightly more tilted as the bilayer dehydrates. Combined with the observations from Chapter 3, this suggests that Gad-1 aligns parallel to the membrane surface and promotes the clustering of anionic lipids.

Chapter 5

Investigating the role of cardiolipin in the AMP-membrane interactions

5.1 Introduction

AMPs show specificity for bacterial membranes over host membranes. This specificity is thought to come from, at least in part, differences in the anionic lipid content of bacterial membrane and host cell membrane [16, 26, 35, 41, 167]. Bacterial membranes have a high proportion of anionic lipids such as POPG and cardiolipin, while host membranes are mainly composed of zwitterionic lipids such as POPC and sphingomyelin. Because of the electrostatic interactions between the cationic peptide and anionic lipids in the bacterial membrane, the binding of AMPs with the bacterial membrane can be stronger than AMP binding to host membranes [35]. Model membranes composed of anionic lipids which mimic the bacterial membrane can be used to understand important features of AMP-membrane interactions. In Chapter 3, interactions of Gad peptides with model

lipid membranes composed of POPE and POPG lipids were studied. In addition to POPG, bacterial membranes also have cardiolipin (CL) as an anionic lipid component. For the purpose of understanding the role of CL in AMP-membrane interactions, model membranes composed of POPE, POPG and CL were used. The work reported in this chapter examined how the presence of cardiolipin affects the AMP-membrane interactions and how these interactions were affected by the change in peptide charge. The AMP-membrane interactions of Gad-1 with model membranes containing CL were characterized using ^{2}H NMR spectroscopy and zeta potential measurements. Gad-1 is a histidine-rich peptide and takes on a different charge at pH 7.0 and at pH 5.0. To examine how AMP-membrane interactions are affected by peptide overall charge, all experiments were performed at pH 7.0 and pH 5.0.

5.2 Cardiolipin in bacterial membranes

Cardiolipin is an anionic glycerophospholipid. Unlike many other phospholipids, cardiolipin has a single headgroup glycerol molecule shared by two phosphatidyl moieties. This chemical structure results in a relatively small head group and large hydrophobic region formed by four acyl chains (Figure 5.1). It can carry two negative charges [168–171]. The small size of the polar head group brings the hydrocarbon chains closer, which in turn elevates the transition temperature of CL relative to other phospholipids [172]. The transition temperature of tetramyristoylcardiolipin is 47°C. A recent study with synthetic CL provided evidence that the CL headgroup behaves as a strong dibasic acid with first pK_{a1} at 2.15 and second pK_{a2} one unit larger [171]. The smaller size of its polar head group enhances the tendency of CL to form inverted non-lamellar phases [173].

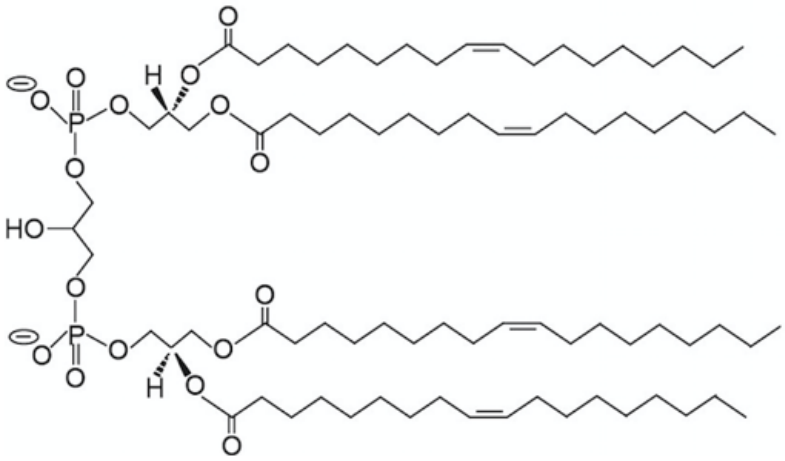

Figure 5.1: Chemical structure of cardiolipin (CL). This Figure is taken from Alder et al. [171] and reused with permission from Elsevier.

Furthermore, because the CL headgroup is shared by two phosphatidate moieties, the cardiolipin headgroup is less flexible compared to other phospholipid headgroups [174]. The restricted mobility and conformational inflexibility of the headgroup also makes it less likely to have interactions with other headgroup moieties. Hence CL−containing membranes are more exposed to interactions with water, ions, peptides, and proteins [172]. The cardiolipin structure contributes to membrane structural stability. Cardiolipin is found in the membranes of many Gram-positive and Gram-negative bacteria (Table 5.1).

Bacterial species	CL(% of total lipids by weight)	PG(% of total lipids by weight)	PE(% of total lipids by weight)
Gram-negative bacteria			
Escherichia coli	5	15	80
Escherichia cloacae	3	21	74
Yersinia kristensenii	20	20	60
Proteus mirabilis	5	10	80
Klebsiella pneumoniae	6	5	82
Pseudomonas aeruginosa	11	21	60
Gram-positive bacteria			
S*taphylococcus aureus*	42	58	0
Streptococcus pneumonia	50	50	0
Bacillus cereus	17	43	40
Bacillus polymyxa	8	3	60

Table 5.1: The lipid composition of various Gram-positive and Gram-negative bacteria. Table is adapted from Wang et. al [7] and reused with permission from Elsevier.

5.3 Materials and Methods

Due to the very small yield of Gad-2 in chemical synthesis, it was decided to use only Gad-1 peptide in studies of interactions with model membranes containing cardiolipin.

5.3.1 Lipids

Chain per-deuterated lipid, POPG-d_{31} along with the non-deuterated lipids POPE and cardiolipin were purchased from Avanti Polar Lipids (Alabaster, AL). All lipids were used without further purification.

5.3.2 Gad-1 peptide

A part of the Gad-1 used in these experiments was purchased from Genscript (GenScript Inc. NJ, USA) and the rest of the peptide was chemically synthesized in our laboratory using O-fluorenylmethyl-oxycarbonyl (Fmoc) solid-phase synthesis as described in Section 3.1.4. The peptide from both the sources, was desalted using dialysis against 5% acetic acid and then water using dialysis tubing with a 1kDa molecular weight cutoff. The resulting peptide solution was lyophilized and stored at 4°C.

5.3.3 ^{2}H NMR

5.3.3.1 Sample preparation

Multilamellar vesicles were prepared with POPE/ POPG-d_{31}/CL molar ratios of 79/16/5, 75/15/10, and 83/6/11 using the protocol described in Section 3.1.2.1. A sample with 79/16/5 molar ratio was prepared at 5% CL concentration of total lipids and effective zwitterionic to negative lipid ratio was kept 3:1. After that CL concentration was increased to 10% of total lipid concentration and a sample was prepared at molar ratio of 75/15/10. In this sample the effective zwitterionic to negative lipid ratio was not 3:1 but POPE/POPG ratio was kept the same as the previous sample prepared at molar ratio 79/16/5. After that, a sample was prepared at molar ratio of 83/6/11. In this sample the CL concentration was 10% of total lipid concentration and effective zwitterionic to negative lipid ratio was 3:1.

5.3.3.2 Experimental detail

All ^{2}H NMR experiments were performed as detailed in Chapter 3 at temperatures of 25°C, 37°C, and 50°C. For each sample, the temperature was raised sequentially to 25°C, 37°C, and 50°C, then lowered to 37°C and finally to 25°C.

5.3.4 Zeta potential measurements

5.3.4.1 Sample preparation and Experimental detail

For zeta potential measurements, multilamellar vesicles were prepared using POPE/POPG-d_{31}/CL (79/16/5 molar ratio) at concentration of 6.8 mM. The protocol described

in Section 3.1.3.1 was used to prepare samples for zeta potential measurements. All zeta potential measurements were performed following the procedure explained in Section 3.1.3.2.

5.4 Results

The work reported in this chapter examines how the presence of cardiolipin (CL) affects the interaction of Gad-1 with POPE/POPG membranes. To this end, ^{2}H NMR and zeta potential experiments were performed using model membranes composed of a POPE/POPG/CL lipid mixture. Firstly, the effects of CL on the membrane dynamics of POPE/POPG lipid bilayers were investigated by using ^{2}H NMR. After this, ^{2}H NMR was used to study the effects of Gad-1 on lipid acyl chain order and bilayer motions in POPE/POPG/CL lipid bilayers. In addition, peptide binding to POPE/POPG/CL lipid bilayers was characterized by measuring binding parameters, the partition constant, the equilibrium constant, and molar fraction of peptide bound to the membrane, using zeta potential measurements. In order to examine how AMP-membrane interactions were affected by the presence of CL, ^{2}H NMR and zeta potential results of POPE/POPG lipid bilayers were compared with the results of POPE/POPG/CL lipid bilayers in the presence of Gad-1. For this purpose, the effective zwitterionic to negative lipid ratio was kept the same (3:1 molar ratio) in both lipid-only samples. The effective zwitterionic to anionic lipid ratio was calculated by dividing the total number of zwitterionic lipids by total number of anionic lipids. For CL−containing samples, CL is taken as equivalent to two anionic phospholipids.

5.4.1 ^{2}H NMR

5.4.1.1 ^{2}H NMR spectra of POPE/POPG-d_{31}/CL lipid bilayers at pH 7.0 and pH 5.0

In order to investigate the mixing of cardiolipin with POPE and POPG in lipid bilayers, model membranes were prepared using POPE/POPG-d_{31}/CL (79/16/5 molar ratio) following the protocol described in Section 3.1.2.1. A series of ^{2}H NMR spectra were acquired at selected temperatures using the acquisition parameters listed in Section 3.1.2.2. Experiments were carried out at different temperatures beginning at 25°C. After this, temperature was raised from 37°C to 50°C (above the transition temperature of CL, 47°C). Then the sample was cooled back to 25°C. The sample was allowed to equilibrate for at least 30 minutes at each temperature after which a spectrum was acquired at that temperature. The resulting spectra are shown in Figure 5.2. Vertical dotted black lines are included to facilitate comparison of quadrupole splittings. It can be seen that the splittings of the prominent spectral edges decrease as the sample is initially warmed from 25°C to 50°C. This reflects the fact that, at higher temperature, the model lipid bilayer is more fluid and the amplitudes of lipid acyl chain motion are larger compared to the amplitudes of acyl chain motion at 25°C.

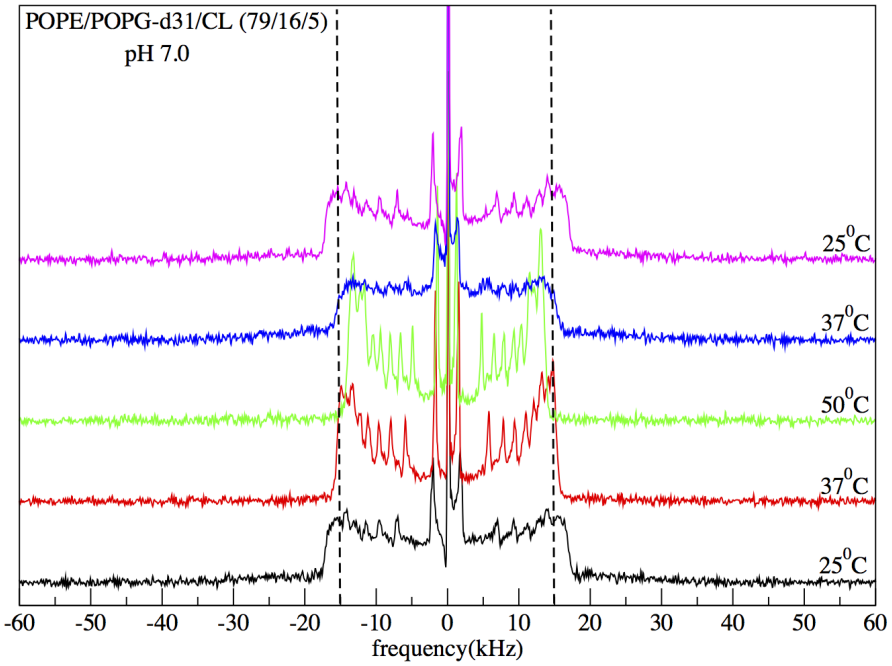

Figure 5.2: A series of ^{2}H NMR spectra of model membranes composed of POPE/POPG-d_{31}/CL (79/16/5 molar ratio) at pH 7.0. The spectra are shown from bottom to top, in the order of acquisition. For each spectrum, 10000 transients were averaged and a minimum time of 30 minutes was given to equilibrate the sample at each temperature. The dotted black lines mark the prominent spectral edges observed at 37°C. The prominent edges correspond to the most ordered chain segments of lipid acyl chains. For the shown spectra, the rotatory evaporation step during the sample preparation was done at 40°C.

An important point to note from the set of spectra shown in Figure 5.2 is that the line width of the quadrupole doublet features did not change reversibly with temperature. In particular, the spectra obtained while first warming through 37°C and at 50°C had sharper peaks than the 37°C spectrum subsequently observed on cooling. This might indicate that warming above the CL bilayer transition temperature was necessary to obtain complete mixing of lipid components that were not fully mixed after the initial sample hydration. It should be noted that during

this sample preparation, the organic solvent was removed by rotatory evaporation at 40°C, which was below the transition temperature of CL. To test the possibility that the spectra of Figure 5.2 were affected by changes in lipid mixing, a new sample was prepared at the same composition but using rotatory evaporation at 50°C. The resulting spectra at selected temperatures are shown in Figure 5.3.

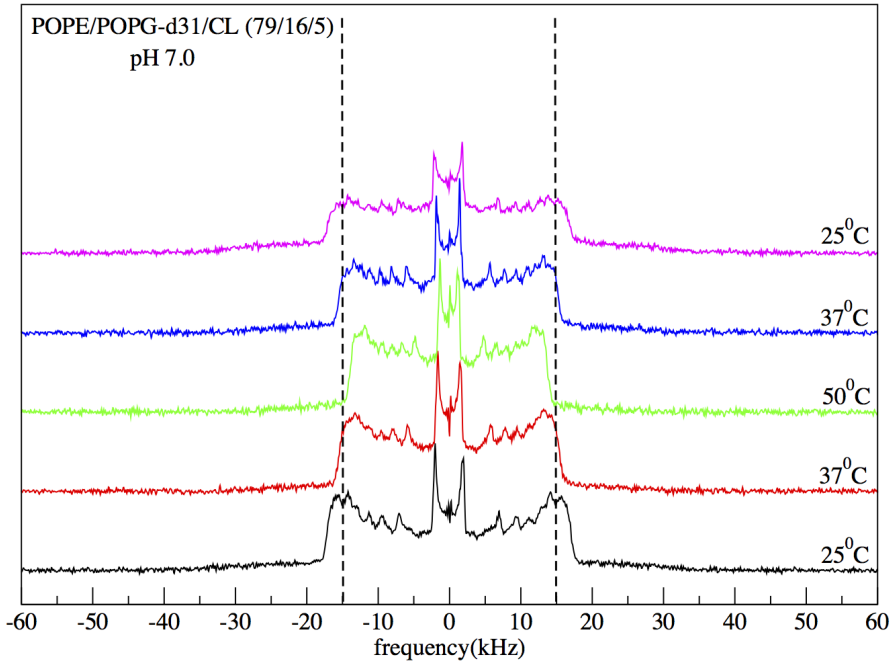

Figure 5.3: A series of ^{2}H NMR spectra of model membrane composed of lipids POPE/POPG-d_{31}/CL (79/16/5 molar ratio) at pH 7.0. The spectra are shown from bottom to top, in the order of acquisition. For each spectrum, 8000 transients were averaged and a minimum time of 30 minutes was given to equilibrate the sample at each temperature. The dotted black lines indicate the prominent spectral edge observed at 37°C. For the shown spectra, the rotatory evaporation step during the sample preparation was done at 50°C.

It can be seen from Figure 5.3 that the spectra obtained at 37°C were less sensitive to whether or not the sample had already been cycled to a higher temperature.

This suggests that mixing of lipids at a temperature above the transition temperature of all lipid components facilitated a more homogenous initial sample mixing. The rotatory evaporation was done at 50°C for the rest of the experiments.

In order to learn how the addition of CL affected the lipid acyl chain order of POPE/POPG-d_{31}, the ^{2}H NMR spectrum of POPE/POPG-d_{31}/CL (79/16/5 molar ratio) was compared with the spectrum of POPE/POPG-d_{31} (3:1 molar ratio). It should be noted that in both spectra, the effective zwitterionic to negative lipid ratio was 3:1. The compared spectra are shown in Figure 5.4.

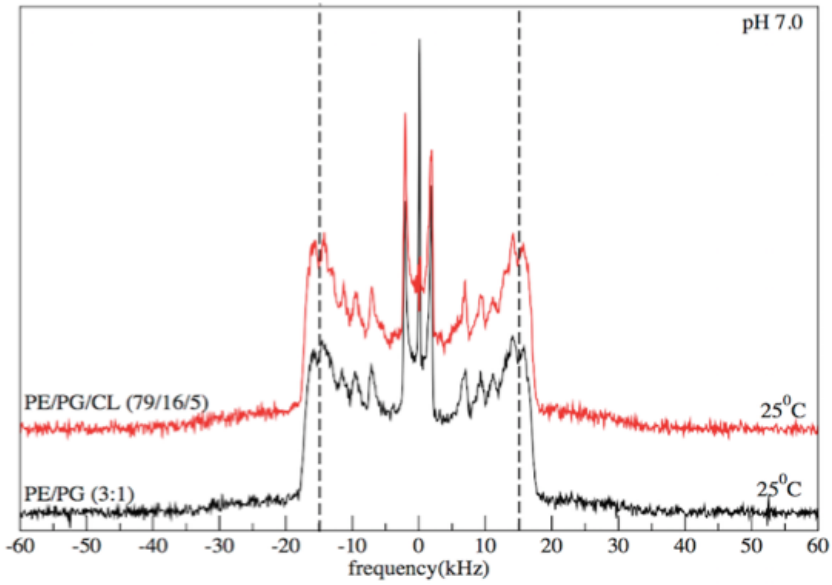

Figure 5.4: The ^{2}H NMR spectra of POPE/POPG-d_{31} (3:1 molar ratio) and POPE/POPG-d_{31}/CL (79/16/5 molar ratio) at pH 7.0. The dotted black lines facilitate comparison of the spectral splittings observed at 25°C. The zwitterionic to negative charge ratio in the samples was 3:1. It should be noted that CL carries a charge of -2 while, POPG has a charge of -1.

Comparison of the spectra in Figure 5.4 indicates that addition of CL to POPE/POPG at this molar fraction did not change ^{2}H NMR spectrum doublet splittings. In other words, the presence of CL did not affect the amplitudes of lipid acyl chain motions in POPE/POPG/CL (79/16/5 molar ratio) lipid bilayers. In this sample,

CL was only 5% of the total lipid composition and it is possible that this amount of CL in the sample was too small to make any substantial changes in the ^{2}H NMR spectrum splittings. In the next step, a sample was prepared with double the amount of CL while keeping the POPE/POPG lipid ratio the same so that the POPE/POPG/CL proportions were 75:15:10 (by mole). An effective zwitterionic to anionic lipid ratio was calculated by dividing total number of zwitterionic lipids (75) by total number of anionic lipids(15+20). CL is taken as equivalent to two anionic lipids. This results in an effective zwitterionic to anionic lipid ratio of about 2:1 rather than 3:1. The resulting spectra are shown in Figure 5.5.

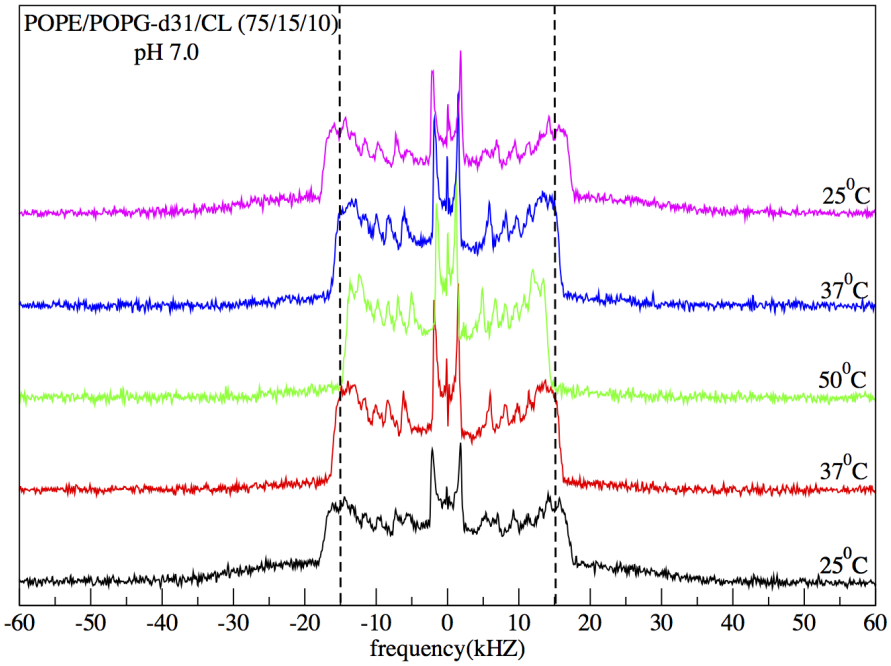

Figure 5.5: A series of ^{2}H NMR spectra of model membranes composed of lipids POPE/POPG-d_{31}/CL (75/15/10) at pH 7.0. The spectra are shown, from bottom to top in the order of acquisition. For each spectrum, 6000 transients were averaged and a minimum time of 30 minutes was given to equilibrate the sample at each temperature. The dotted black lines indicate the prominent spectral edges observed at 37°C. In this sample the POPE : POPG ratio (5:1) was kept the same as the sample shown in Figure 5.3, but the CL fraction was doubled from 5% to 10% of total lipid composition.

Comparison of the spectra shown in Figure 5.3 and Figure 5.5 suggests that increasing the amount of CL from 5% to 10% of total lipid composition did not change the ^{2}H NMR spectrum splittings.

Next, a sample was prepared with a 10% CL fraction of total lipid composition and with an effective zwitterionic to negative lipid ratio of 3:1. In the calculation of this ratio, CL is again treated as being equivalent to two anionic lipids. The

resulting spectra of POPE/POPG-d_{31}/CL (83/6/11 molar ratio) are shown in Figure 5.6. Comparison of the spectra shown in Figures 5.3, 5.5, and 5.6, indicates that changing the CL concentration from 5% to 10% of total lipid composition and changing the POPE:POPG ratio still did not change the ^{2}H NMR spectrum doublet splittings.

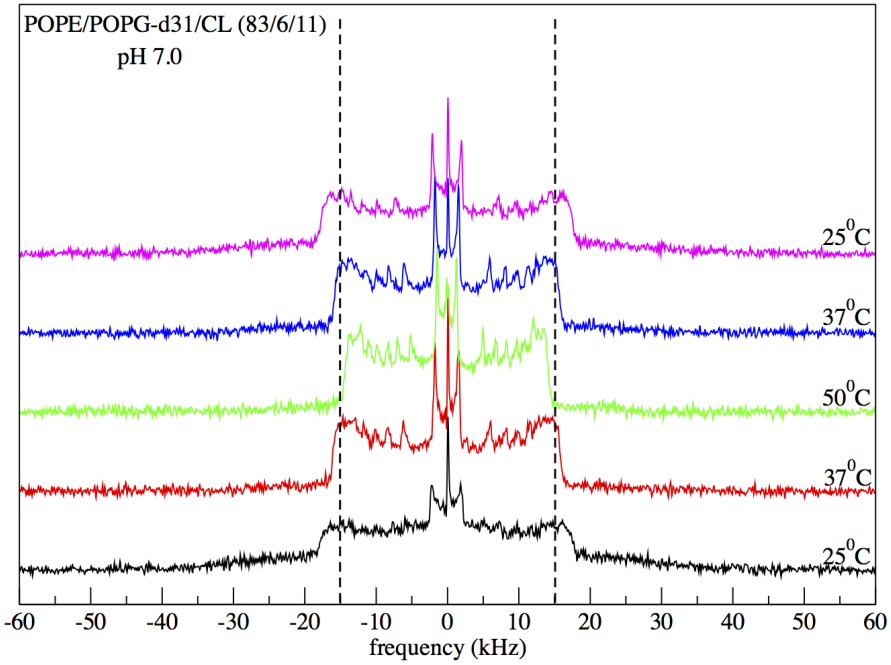

Figure 5.6: A series of ^{2}H NMR spectra of model membranes composed of lipids POPE/POPG-d_{31}/CL (83/6/11 molar ratio) at pH 7.0. The spectra are shown, from bottom to top, in the order of acquisition. For each spectrum 6000 transients were averaged and a minimum time of 30 minutes was given to equilibrate the sample at each temperature. The dotted black lines show the prominent edges observed at 37°C. In this sample the POPE:POPG ratio is 15:1 and the zwitterionic to negative charge ratio was 3:1.

The spectra shown in Figures 5.1 to 5.6 suggest that CL did not change the ^{2}H NMR doublet splittings of POPE/POPG. In other words, the addition of CL to POPE/POPG up to the molar CL fraction studies, did not affect the amplitudes of lipid acyl chain motions that contribute to motional narrowing.

The next step was to examine the changes in the spectrum of POPE/POPG-d_{31}/CL resulting from a change in pH from 7.0 to 5.0. For this purpose, ^{2}H NMR spectra of POPE/POPG-d_{31}/CL (79/16/5 molar ratio) at pH 5.0 were first obtained at selected temperatures. The resulting spectra are shown in Figure 5.7.

To see if the spectra of POPE/POPG-d_{31}/CL change with pH, ^{2}H NMR spectra of POPE/POPG-d_{31}/CL were compared at pH 7.0 and pH 5.0 (Figure 5.8). It can be seen that changing pH from 7.0 to 5.0 did not change the ^{2}H NMR spectra of POPE/POPG-d_{31}/CL (79/16/5 molar ratio).

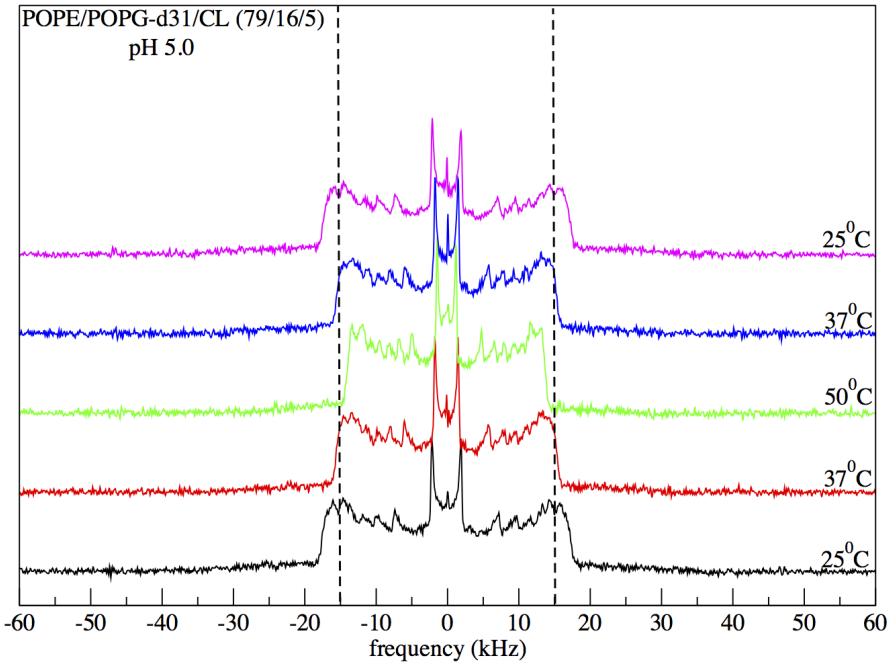

Figure 5.7: A series of ^{2}H NMR spectra of model membranes composed of lipids POPE/POPG-d_{31}/CL (79/16/5 molar ratio) at pH 5.0. The spectra are shown, from bottom to top, in the order of acquisition. For each spectrum 6000 transients were averaged and a minimum time of 30 minutes was given to equilibrate the sample at each temperature. The dotted black lines indicate the prominent edges observed at 37°C.

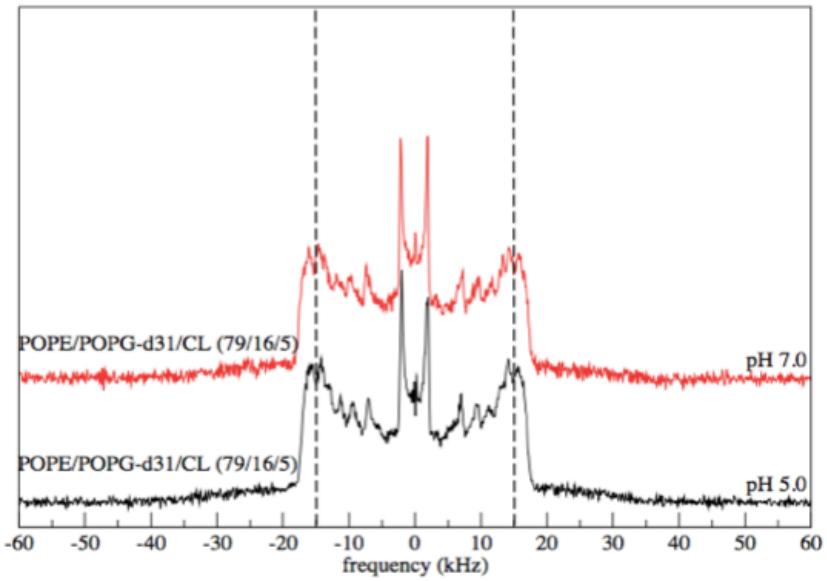

Figure 5.8: Comparison of ^{2}H NMR spectra of POPE/POPG-d_{31}/CL (79/16/5 molar ratio) at pH 7.0 and pH 5.0. Both spectra were obtained at 25°C.

5.4.1.2 Effect of CL on the slow motions of POPE/POPG-d_{31} lipid bilayers at pH 7.0 and pH 5.0

Slow motions whose correlation times are greater than the characteristic NMR time (10^{-5}s) do not contribute to motional narrowing. Along with faster motions, such slow motions can perturb the refocusing of the quadrupole echo and change the quadrupole echo decay time [175]. How fast or slow motions of POPE/POPG lipid bilayers were perturbed by the addition of CL was examined by measuring the quadrupole echo decay time. The quadrupole echo decay experiments were performed using the acquisition parameters listed in Section 3.1.2.2. The quadrupole echo experiments with POPE/POPG-d_{31}/CL at pH 5.0 and pH 7.0 show that CL reduces the echo decay times at both pHs (Figure 5.9 and Figure 5.10). The reduction in echo decay time resulting from the addition of CL to POPE/POPG bilayers indicates either the slowing down of a fast lipid motion or the speeding up of a slow bilayer motion. Since CL does not have any effect on the amplitudes of fast lipid acyl chain motions, it seems likely that CL perturbs the slower diffusive or collective motions of POPE/POPG lipid bilayers. The interpretation of these results is discussed in the Section 5.5.

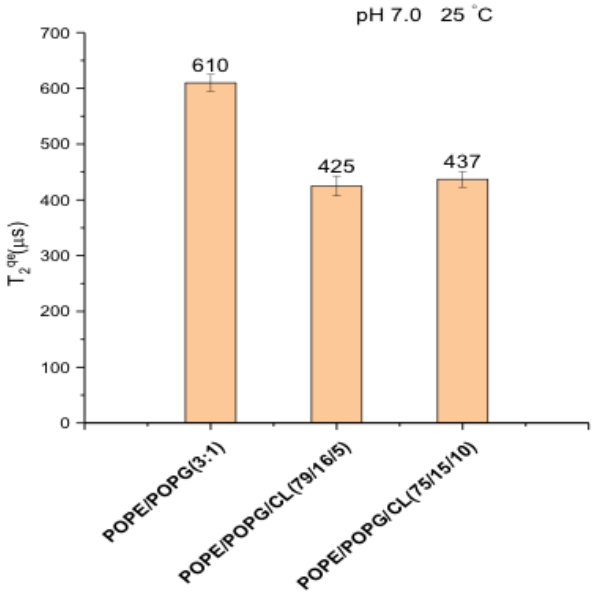

(a)

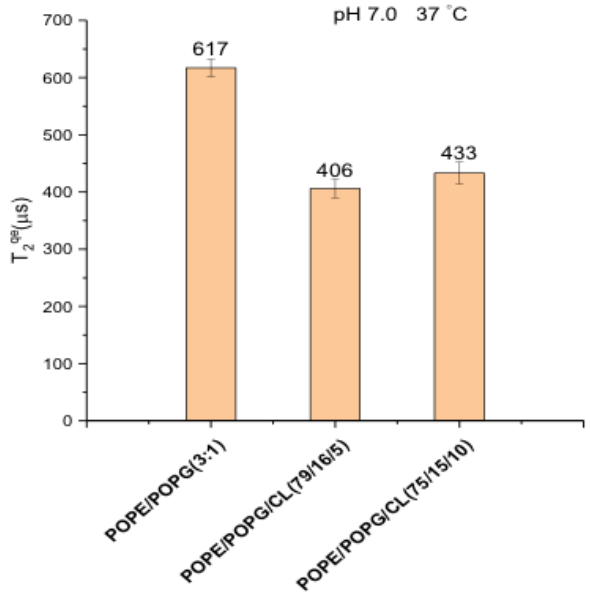

(b)

Figure 5.9: The quadrupole echo decay time of POPE/POPG-d_{31}/CL lipid mixture at pH 7.0 (a) at 25°C (b) 37°C. The addition of CL to POPE/POPG-d_{31} lipid mixture decreased the echo decay time.

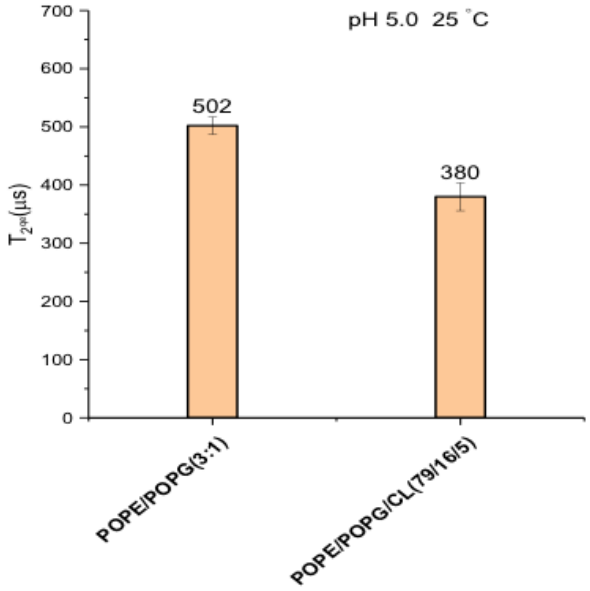

(a)

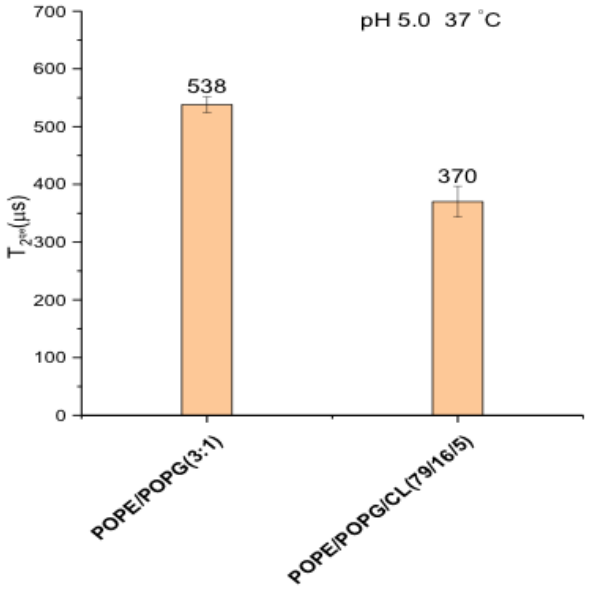

(b)

Figure 5.10: The quadrupole echo decay time of POPE/POPG-d_{31} and POPE/POPG-d_{31}/CL lipid mixture at pH 5.0 (a) at 25°C (b) 37°C. The addition of CL to POPE/POPG-d_{31} lipid mixture decreased the echo decay time.

5.4.1.3 ^{2}H NMR spectra of POPE/POPG-d_{31}/CL lipid bilayers in the presence of Gad-1 at pH 7.0 and pH 5.0

After having obtained spectra from POPE/POPG/CL model membranes, the next question asked was how the presence of CL in a model bacterial membrane might affect the response of the lipid bilayer to a peptide like Gad-1. To address this, ^{2}H NMR spectra of POPE/POPG-d_{31}/CL (79/16/5 molar ratio) with added Gad-1 were obtained at various temperatures for pH 7.0. The lipid-to-peptide ratio was kept at 25:1(molar ratio). The resulting spectra are shown in Figure 5.11. It is apparent that the presence of Gad-1 reduced the resolution of quadrupole doublets in the spectra of POPE/POPG/CL+Gad-1. This may reflect a peptide-induced decrease in quadrupole echo decay time.

Figure 5.12 compares spectra of the lipids with and without CL and Gad-1. It can be seen from the spectra compared in Figure 5.12 that the addition of Gad-1 to both POPE/POPG-d_{31} and POPE/POPG-d_{31}/CL lipid bilayers slightly reduces all of the quadrupole doublet splittings which indicates a reduction in chain orientational order. In addition to a change in splittings, there was a qualitative change in the spectrum with the addition of Gad-1 and CL together. In particular, the addition of Gad-1 to POPE/POPG-d_{31}/CL lipid bilayers resulted in a significant broadening of the individual doublets of the spectrum. The interpretation of this observation is discussed in Section 5.5.

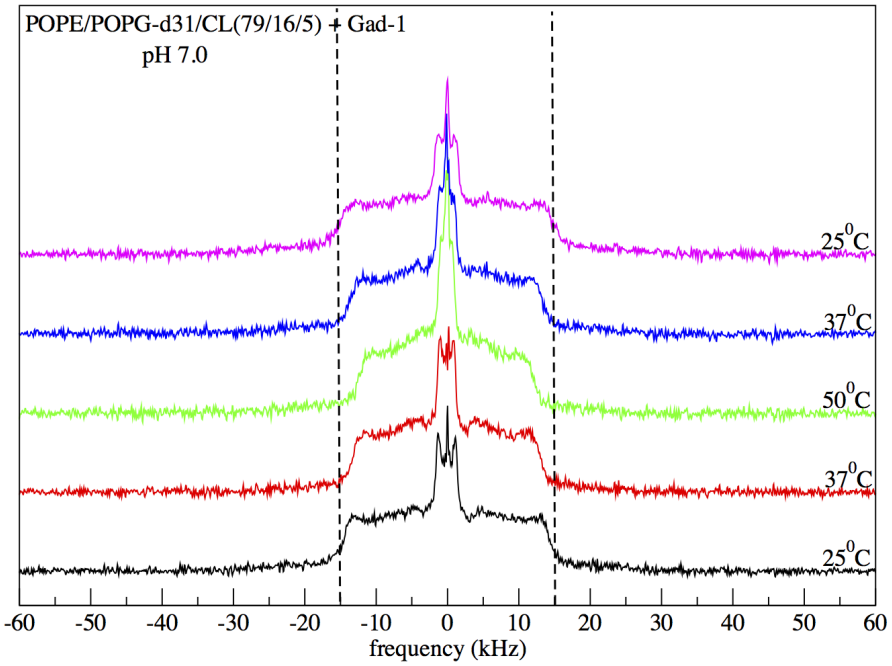

Figure 5.11: A series of ^{2}H NMR spectra of POPE/POPG-d_{31}/CL (79/16/5 molar ratio) + Gad-1 at pH 7.0. The zwitterionic to negative lipid ratio was 3:1(molar ratio) and the lipid-to-peptide ratio was 25:1(molar ratio). The spectra are shown, from bottom to top, in the order of acquisition. For each spectrum 6000 transients were averaged and a minimum of 30 minutes was given for the sample to equilibrate at each temperature. The dotted black lines represent the prominent spectral edges observed at 25°C .

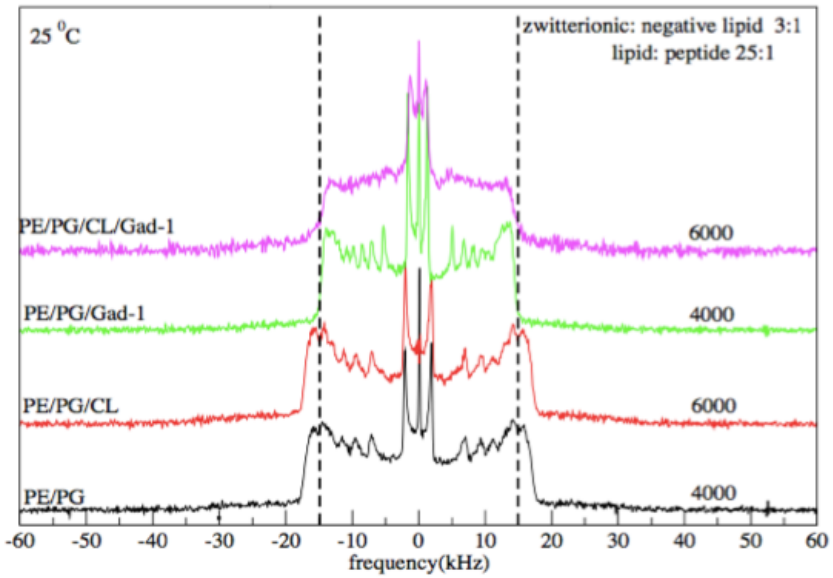

Figure 5.12: ^{2}H NMR spectra of POPE/POPG-d_{31} acquired at 25°C with addition of CL and/or Gad-1 at pH 7.0. The number of transients averaged for each spectrum are indicated on the spectrum. The black dotted lines are intended to facilitate comparison of the prominent edges in different spectra. The zwitterionic to negative lipid ratio was 3:1(molar ratio) and lipid:peptide ratio was 25:1 (molar ratio) in these spectra.

In order to examine whether changing the peptide overall charge has any effect on the AMP-membrane interactions in POPE/POPG-d_{31}/CL lipid bilayers, spectra were also obtained from samples in which peptide charge was altered by changing pH from 7.0 to 5.0 (Figure 5.13).

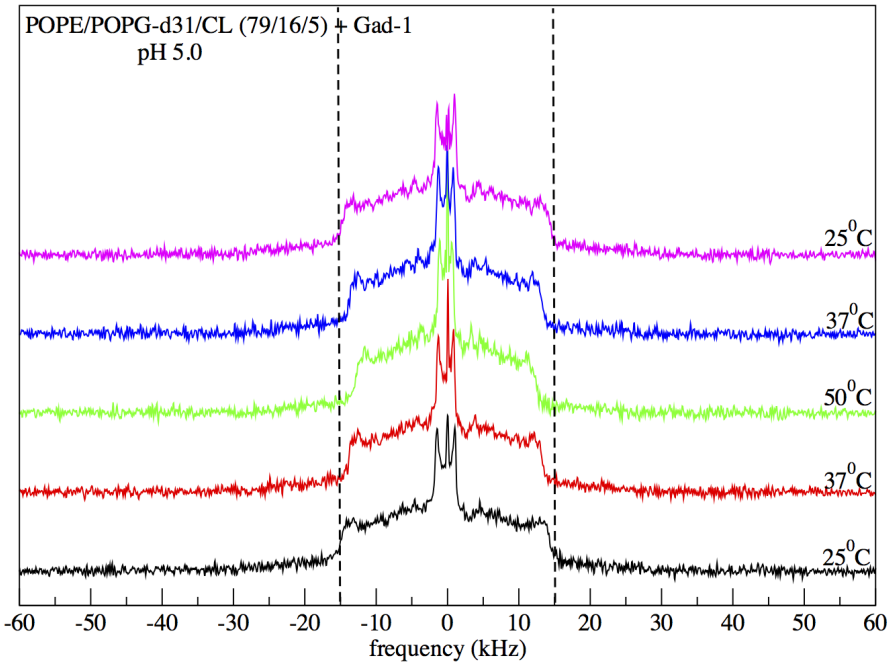

Figure 5.13: A series of ^{2}H NMR spectra of model membrane composed of lipids POPE/POPG-d_{31}/CL(79/16/5) + Gad-1 at pH 5.0. For each spectrum 6000 transients were averaged and a minimum of 30 minutes was given for the sample to equilibrate at each temperature. The dotted black lines are intended to facilitate comparison of the prominent edges in different spectra. The lipid:peptide ratio was 25:1(molar ratio).

To show how peptide charge affects the perturbation of a POPE/POPG bilayer by Gad-1 in the presence of CL, Figure 5.14 compares a spectrum of POPE/POPG-d31/CL (79/16/5) obtained at 25°C and pH 5.0 with a 25°C spectrum of POPE/POPG-d31/CL (79/16/5) from Figure 5.7 and 25°C spectra of POPE/POPG-d31 (3:1) with and without Gad-1, from Figure 3.1. These comparisons indicate that similarly to the results at pH 7.0, the addition of Gad-1 to POPE/POPG-d_{31} and POPE/POPG-d_{31}/CL lipid bilayers at pH 5.0 slightly reduces lipid chain quadrupole splittings, which indicates a reduction in chain orientational order.

Also, addition of the peptide also broadened spectral doublets for lipid bilayers containing CL.

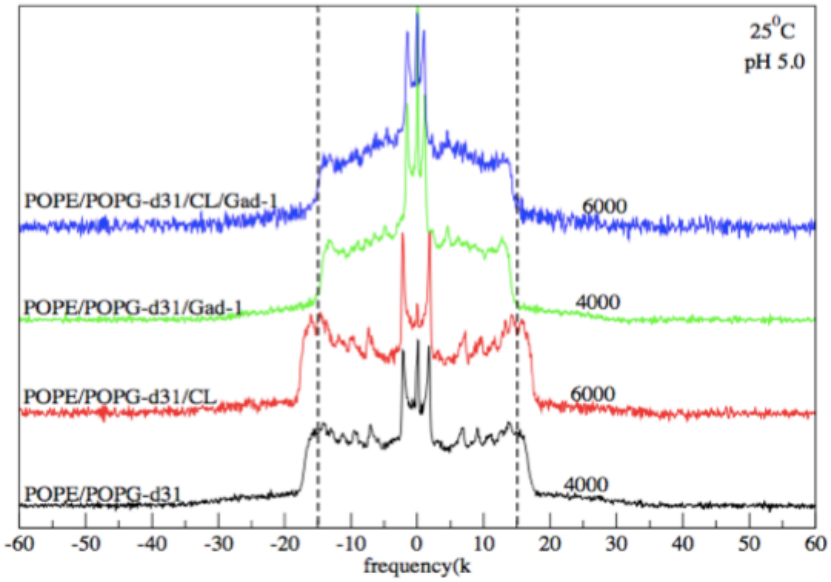

Figure 5.14: ^{2}H NMR spectra of POPE/POPG-d_{31} acquired at 25°C with addition of CL and/or Gad-1 at pH 5.0. The number of transients averaged for each spectrum are indicated on the spectrum. The black dashed lines facilitate comparison of prominent spectral edges. The zwitterionic to negative lipid ratio was 3:1(molar ratio) and the lipid:peptide ratio was 25:1 (molar ratio).

To show how pH affects the perturbation of POPE/POPG/CL bilayers by Gad-1, spectra for POPE/POPG-d_{31}/CL(79/16/5) with and without Gad-1 at pH 5.0 and pH 7.0 are compared in Figure 5.15. These comparisons indicate that perturbation of POPE/POPG-d_{31}/CL lipid bilayers by Gad-1 is not pH-sensitive.

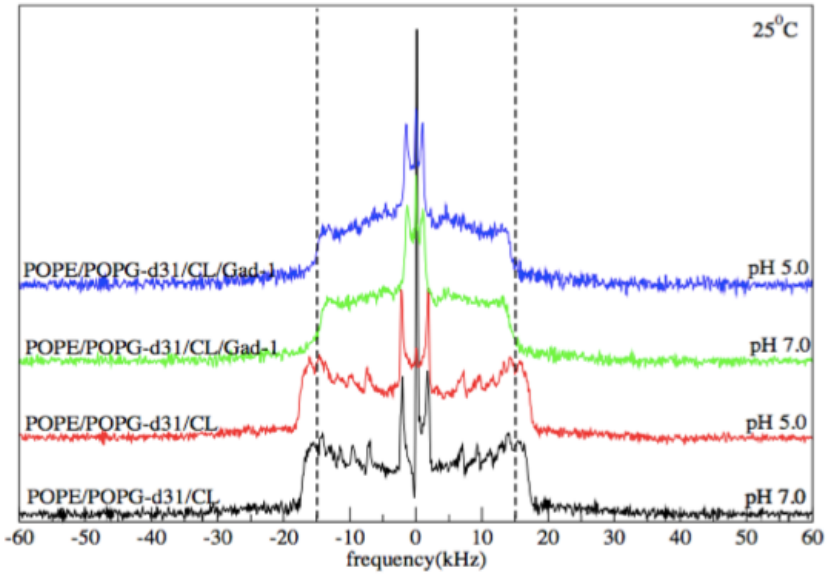

Figure 5.15: Comparison of the ^{2}H NMR spectra of POPE/POPG-d_{31}/CL with and without the addition of Gad-1 at pH 7.0 and pH 5.0. The dotted black lines are intended to facilitate comparison of prominent spectral edges.

5.4.1.4 Effects of Gad-1 on the slow motions of POPE/POPG-d_{31}/CL lipid bilayers at pH 7.0 and pH 5.0

How fast or slow motions of POPE/POPG/CL lipid bilayers were perturbed by the addition of Gad-1 was examined by measuring the quadrupole echo decay time. In order to examine how the presence of CL affects the perturbation of fast or slow motions of POPE/POPG bilayers by Gad-1, the quadrupole echo decay times of POPE/POPG/CL bilayers with and without Gad-1, were compared with the echo decay times of POPE/POPG bilayers with and without the addition of Gad-1. These comparisons at two temperatures, 25°C and 37°C, are shown in Figure 5.16 and Figure 5.17 for pH 7.0 and pH 5.0 respectively. Interestingly, the addition of Gad-1 to POPE/POPG/CL had opposite effects at pH 7.0 and pH 5.0. At pH 7.0, Gad-1 decreased the echo decay time of POPE/POPG-d_{31}/CL while at pH 5.0 the echo decay time of POPE/POPG-d_{31}/CL bilayers increased with the addition of Gad-1. Interpretation of these observations will be discussed in Section 5.5.

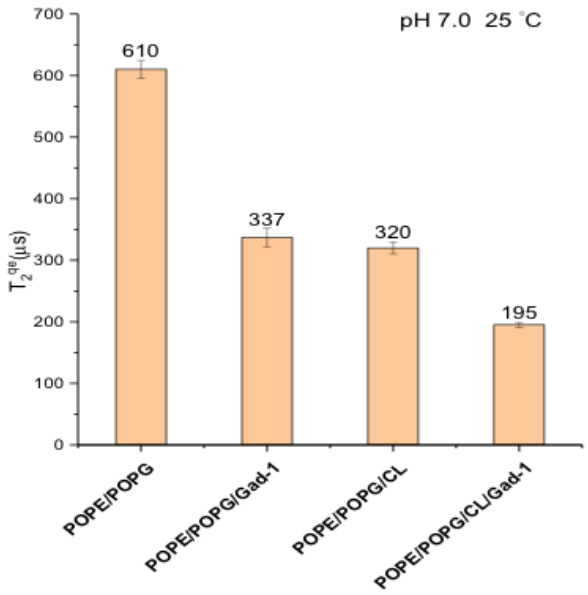

(a)

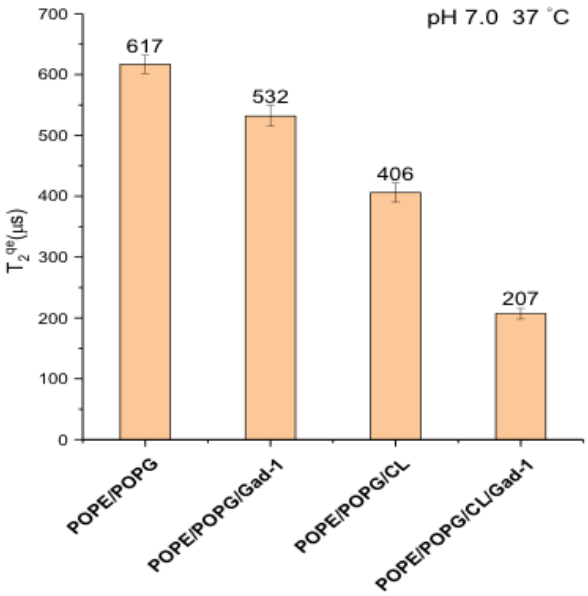

(b)

Figure 5.16: The quadrupole echo decay time of POPE/POPG-d_{31} and POPE/POPG-d_{31}/CL lipid mixture with and without the addition of Gad-1 at pH 7.0 (a) at 25°C (b) 37°C. The addition of CL to POPE/POPG-d_{31} lipid mixture decreased the echo decay time and addition of Gad-1 to POPE/POPG-d_{31}/CL further decreased the echo decay time.

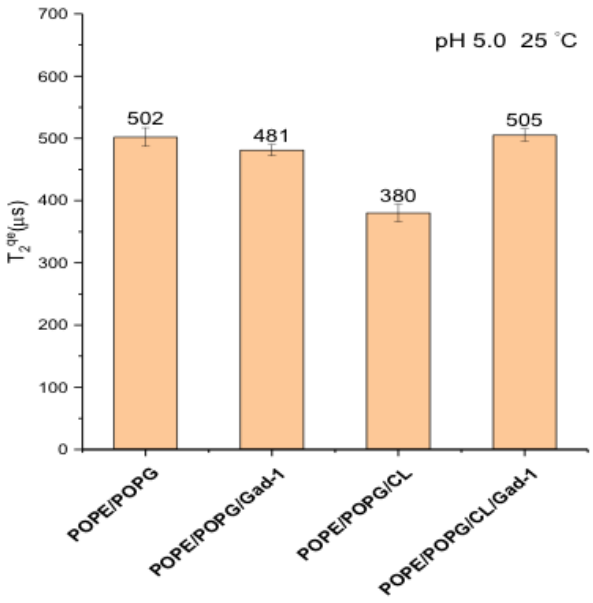

(a)

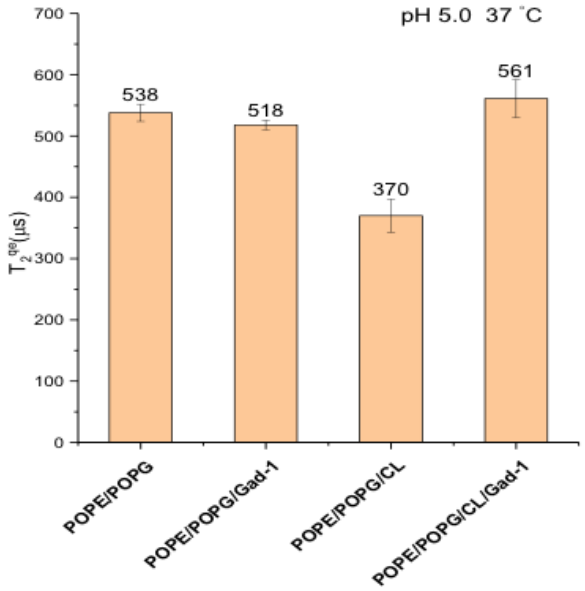

(b)

Figure 5.17: The quadrupole echo decay time of POPE/POPG-d_{31} and POPE/POPG-d_{31}/CL lipid mixture with and without the addition of Gad-1 at pH 5.0 (a) at 25°C (b) 37°C. The addition of CL to POPE/POPG-d_{31} lipid mixture decreased the echo decay time and addition of Gad-1 to POPE/POPG-d_{31}/CL increased the echo decay time.

5.4.2 Zeta potential

To examine the binding of Gad-1 to model membranes, zeta potentials of POPE/POPG/CL (79/16/5 molar ratio) vesicles were measured with and without the addition of Gad-1. To study the peptide binding quantitatively, several binding parameters were obtained. A binding model described by Freire et al. allows the calculation of the partition constant (K_{P}), molar fraction of the peptide bound to the membrane (X), local concentration of peptide in the membrane ($[P]_{\mathrm{L}}$), and stoichiometry of lipid- peptide complexes. A slightly different zeta potential model based on the Langmuir isotherm was used to determine the equilibrium constant (K_{eq}), the molar fraction of the peptide bound to the membrane (X), and number of lipids per bound peptide. These models are described in detail in Sections 3.2.2.2 and 3.2.2.3 in Chapter 3. The zeta potential binding isotherms were obtained by plotting zeta potential vs. total peptide concentration. To compare the binding of Gad-1 to POPE/POPG/CL lipid bilayers with the binding of the peptide to POPE/POPG lipid bilayers, the zwitterionic to negative charge ratio was kept same at 3:1(molar ratio). Because Gad-1 takes different charge at pH 7.0 and pH 5.0. All experiments were performed at pH 7.0 and pH 5.0 to study how peptide overall charge could affect the peptide binding.

5.4.2.1 Binding isotherm

Zeta potentials of POPE/POPG/CL (79/16/5 molar ratio) lipid vesicles with increasing concentrations of Gad-1 were measured at pH 7.0 and pH 5.0 as described in the Section 3.1.3.1 and Section 3.1.3.2. The sizes of these vesicles were measured by Dynamic Light Scattering (DLS) using a Malvern Zetasizer Nano ZS apparatus (model ZEN 3600, Malvern Instruments Ltd. U.K.). The observed sizes of these vesicles were 145± 10 nm. The zeta potential binding isotherms for

POPE/POPG/CL + Gad-1 at pH 7.0 and pH 5.0 are shown in the Figure 5.18 (a) and (b) respectively.

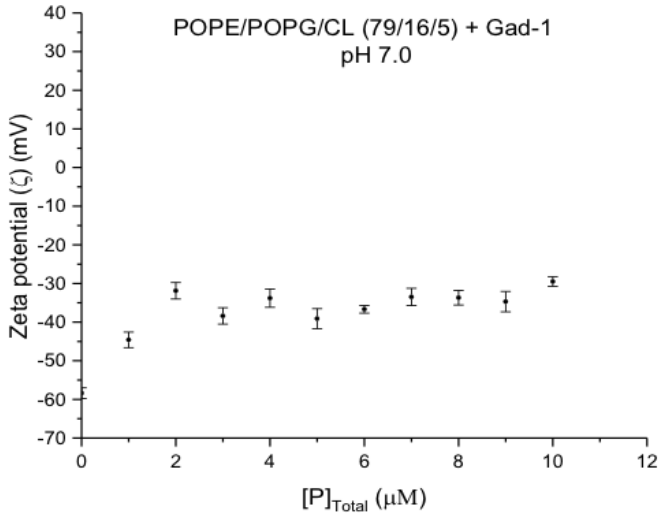

(a)

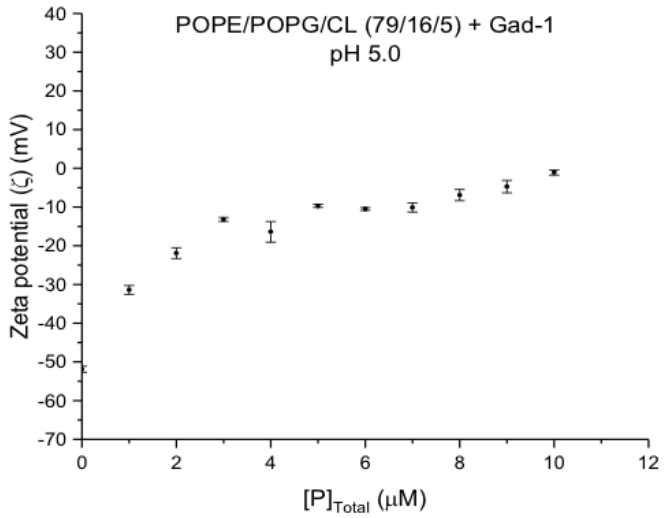

(b)

Figure 5.18: (a) The binding isotherms of Gad-1 at (a) pH 7.0 (b) pH 5.0. Each point represents the average of three independent measurements. The first point in the isotherm represents the zeta potential of liposomes in the absence of peptide. A negative value of zeta potential was observed in the absence of peptide. As the peptide concentration was increased the zeta potential increased toward a limiting value. When all peptide binding sites were occupied, the limiting value of zeta potential depends on the overall charge of peptide and the $L : P$ ratio. At pH 7.0, Gad-1 has charge of +3 and the limiting value is $\sim$ -35 mV. On the other hand, at pH 5.0 Gad-1 has charge of +8 and the limiting value in this case is $\sim$ -10 mV. The error bars were estimated by averaging the deviation from the mean for three measurements.

5.4.2.2 Characterizing the binding of Gad-1 to POPE/POPG/CL lipid bilayers using Freire et al. binding model

The binding isotherms and corresponding normalized zeta potentials for Gad-1 at pH 7.0 and pH 5.0 are shown in Figure 5.19 and Figure 5.20 respectively. As in Section 3.2.2.2, the slope of linear regime of the normalized zeta potential vs. peptide concentration plot was used to determine the molar fraction (X) of Gad-1 that is bound to the membrane using

$$\frac{\zeta}{\zeta_0} = \frac{X z_{\mathrm{P}}}{f_{\mathrm{L}^-}[L] z_{\mathrm{L}^-}}[P]_{\mathrm{Total}} + 1. \tag{5.1}$$

The partition constant (K_{P}) was determined using

$$X = \frac{\gamma_{\mathrm{L}}[L]K_{\mathrm{P}}}{1 + \gamma_{\mathrm{L}}[L]K_{\mathrm{P}}} \tag{5.2}$$

where z_{P} is the peptide charge, $[L]$ is the total lipid concentration, f_{L^-} is the fraction of lipid accounted for by anionic species, z_{L} is the charge of the anionic lipids, and γ_{L} is the lipid molar volume. The value of molar volume of lipids is 0.763 in liters per mole [56]. The values of X and K_{P} for Gad-1 at pH 7.0 and pH 5.0 are listed in Table 5.2. The values of X were smaller at pH 5.0 than at pH 7.0. The value of K_{P} at pH 7.0 is ten times higher than the value at pH 5.0. This suggests that a smaller amount of peptide is accommodated on the membrane at pH 5.0 compared to at pH 7.0.

The values of the local peptide concentration ($[P]_{\mathrm{L}}$) and $(L:P)_{\mathrm{local}}$ were calculated using

$$[P]_{\mathrm{L}} = \frac{X[P]_{\mathrm{Total}}}{\gamma_{\mathrm{L}}[L]}. \tag{5.3}$$

$$(L:P)_{\text{local}} = \frac{1 + [L]K_{\text{P}}\gamma_{\text{L}}}{[P]_{\text{Total}}\gamma_{\text{L}}K_P} \tag{5.4}$$

$$= \left(\frac{1}{[P]_{\text{Total}}K_P\gamma_{\text{L}}} + \frac{[L]}{[P]_{\text{Total}}}\right). \tag{5.5}$$

The values of $[P]_{\text{L}}$ and $(L:P)_{\text{local}}$ for Gad-1 at pH 7.0 and pH 5.0 are listed in Table 5.3. The $[P]_{\text{L}}$ increases as the total peptide concentration $[P]_{\text{Total}}$ increases. The $(L:P)_{\text{local}}$ values were higher at pH 5.0 than at pH 7.0. This indicates that one peptide molecule interacts with a larger number of lipids at pH 5.0 than at pH 7.0. The interpretation of these results is discussed in Section 5.5.

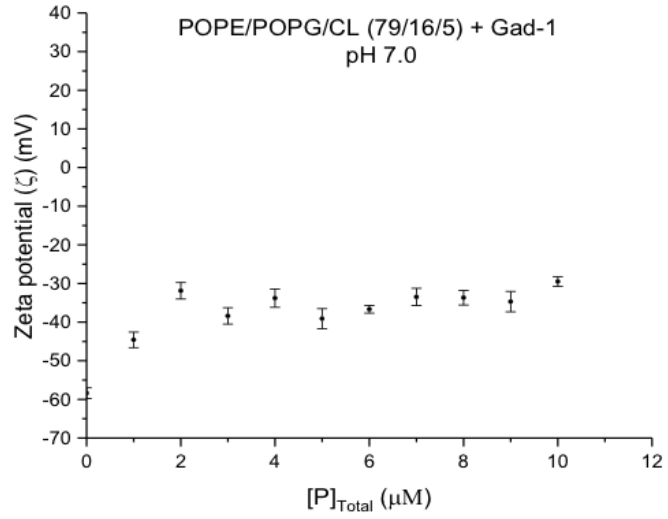

(a)

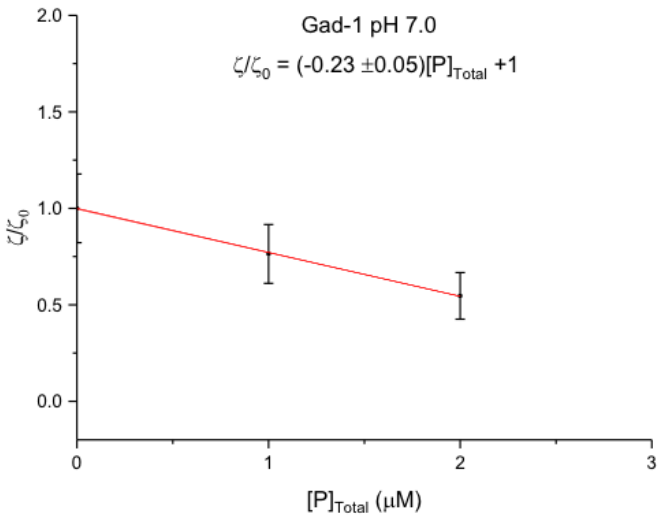

(b)

Figure 5.19: (a) Zeta potential measurements for 40 μM POPE/POPG/CL (79/16/5) in the presence of Gad-1 at pH 7.0. Addition of peptide to lipid vesicles results in the reduction of zeta potential values. The linear portion of this graph, 0 μM - 2 μM peptide concentration, was selected to obtain the normalized zeta potential plotted in panel (b). (b) Normalized zeta potential dependence on the concentration of Gad-1 peptide at pH 7.0. The slope of the linear portion of the binding isotherm was obtained using the weighted linear fitting. The size of error bars was taken into account to estimate the uncertainty in the slope. The slope of this graph was used to determine the molar fraction of peptide bound to the membrane (X) and partition constant (K_{P}).

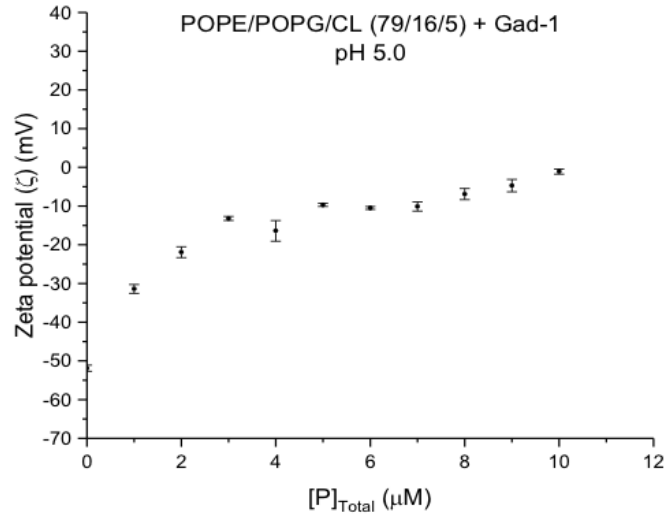

(a)

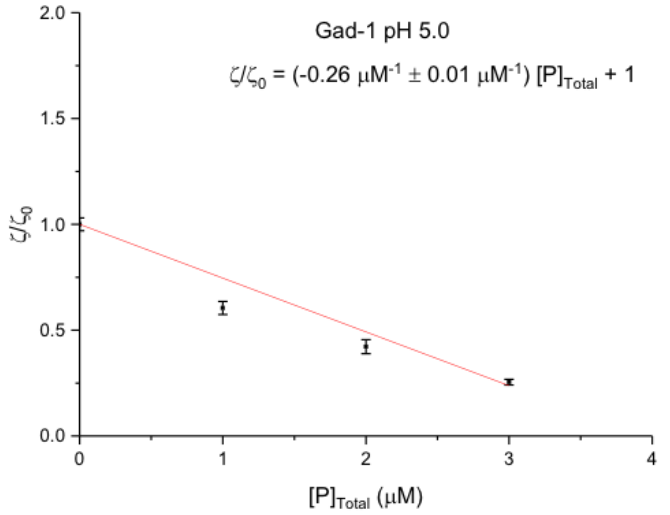

(b)

Figure 5.20: (a) Zeta potential measurements for 40 μM POPE/POPG/CL (79/16/5 molar ratio) in the presence of Gad-1 at pH 5.0. Addition of peptide to lipid vesicles results in the reduction of zeta potential values. The linear portion of this graph, 0 μM - 6 μM peptide concentration, was selected to obtain the normalized zeta potential plotted in panel (b). (b) Normalized zeta potential dependence on the concentration of Gad-1 peptide at pH 7.0. The slope of the linear portion of the binding isotherm was obtained using the weighted linear fitting. The size of error bars was taken into account to estimate the uncertainty in the slope. The slope of this graph was used to determine the molar fraction of peptide bound to the membrane (X) and partition constant (K_{P}).

Gad-1		
pH	Molar fraction of peptide bound to the membrane (X)	Partition constant (K_P)
7.0	0.8±0.2	100,000 ± 90000
5.0	0.32±0.01	15,400± 700

Table 5.2: Calculated molar fractions of peptide bound to the membrane (X) and partition constants (K_{P}) from zeta potential measurements for Gad-1 at pH 7.0 and pH 5.0.

Gad-1					
$[P]_{\mathrm{Total}}$ (μM)	global $L:P$	pH 7.0		pH 5.0	
		$[P]_{\mathrm{local}}$ (mM)	$(L:P)_{\mathrm{local}}$	$[P]_{\mathrm{local}}$ (mM)	$(L:P)_{\mathrm{local}}$
1	40	26	50	10	125
2	20	52	25	21	63
3	13	78	17	31	42

Table 5.3: The global L:P is calculated for the total peptide concentration 1 μM - 3 μM. The range of total peptide concentration is selected from the linear portion of the zeta potential binding isotherms of Gad-1. The local peptide concentration ($[P]_{\mathrm{local}}$) in the membrane and local $L:P$ are also calculated for corresponding total peptide concentration at pH 7.0 and pH 5.0. Note that $(L:P)_{\mathrm{local}}$ represents the lipid to peptide ratio for lipid and peptide complexes.

5.4.2.3 Modeling peptide dependence of the zeta potential using the Langmuir isotherm approach

The zeta potential model based on the Langmuir isotherm also considers the reduction in membrane surface charge when a cationic peptide interacts with a model membrane composed of anionic lipids. It takes into account both the linear part and plateau region of a zeta potential binding isotherm where zeta potential approaches a limiting value. The main difference between the two models is that the Freire et al. approach considers the peptide to be dissolved in the lipid bilayer volume while the zeta potential model based on the Langmuir isotherm treats the peptide as being adsorbed on the surface. The summary of the zeta potential model based on the Langmuir isotherm was given in Chapter 3. This model was used to determine the equilibrium constant (K_{eq}), molar fraction of peptide bound to the membrane (X), and number of lipids constituting the peptide binding sites ($1/Q$). To determine these parameters, the binding isotherms showing the variation of $\dfrac{\Delta\zeta}{\zeta_{\mathrm{max}}}$ vs $[P]_{\mathrm{Total}}$ were obtained.

The slope of the linear regime of $\dfrac{\Delta\zeta}{\zeta_{\mathrm{max}}}$ vs $[P]_{\mathrm{Total}}$ was used to determine X using

$$\mathrm{slope} = \left(\frac{X z_{\mathrm{P}}}{f_{\mathrm{L}^-} z_{\mathrm{L}^-}[L]}\right)\left(\frac{\zeta_0}{\Delta\zeta_{\mathrm{max}}}\right). \tag{5.6}$$

where f_{L^-} is the fraction of lipids that are anionic, z_{L^-} is the charge of an anionic lipid, z_{P} is the peptide charge, and $[L]$ is the total lipid concentration.

The equilibrium constant K_{eq} was determined using

$$\frac{\Delta\zeta}{\Delta\zeta_{\mathrm{max}}} = \frac{K_{\mathrm{eq}}(1-X)[P]_{\mathrm{Total}}}{1 + K_{\mathrm{eq}}(1-X)[P]_{\mathrm{Total}}}. \tag{5.7}$$

In the linear region of the binding isotherm, the expression for the slope, $K_{\mathrm{eq}}(1-X)$, allows the calculation of K_{eq}. The limiting value of the zeta potential was used to determine Q, the ratio of available peptide binding sites to total lipids, using

$$Q = \frac{\Delta\zeta_{\max}}{\zeta_0}\frac{f_{\mathrm{L}^-}z_{\mathrm{L}^-}}{z_{\mathrm{P}}}. \tag{5.8}$$

The binding isotherms showing the variation of $\frac{\Delta\zeta_{\max}}{\zeta_0}$ vs $[P]_{\mathrm{Total}}$ and corresponding linear regime for Gad-1 at pH 7.0 and pH 5.0 are shown in Figure 5.21 and Figure 5.22 respectively. The error bars in the binding isotherm at pH 7.0 are larger than the error bars in the binding isotherm at pH 5.0. This is due to the difference in the value of maximum zeta potential value obtained at pH 7.0 and pH 5.0. At pH 5.0 the value of maximum zeta potential is positive while at pH 7.0 it is a negative quantity. This resulted in the difference in the relative uncertainties $\frac{\Delta\zeta_{\max}}{\zeta_0}$.

The calculated values of X, K_{eq}, and $1/Q$ for Gad-1 at pH 7.0 and pH 5.0 are shown in Table 5.4. The values of X and K_{eq} are smaller at pH 5.0 than at pH 7.0. This suggests that when a peptide has more positive charge, less peptide is accommodated on the membrane surface and less peptide is needed to neutralize the membrane charge. Also, electrostatic repulsions between individual peptide molecules might limit the peptide binding to the membrane. The peptide binding to the membrane is stronger at pH 7.0 compared to pH 5.0 as indicated by the higher values of K_{eq} at pH 7.0. The number of lipids per bound peptide are higher at pH 5.0 than at pH 7.0. The interpretation of these results is given in Section 5.5.

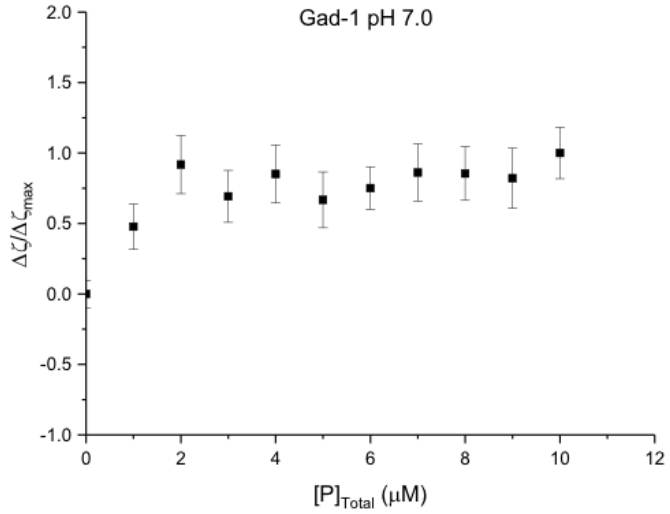

(a)

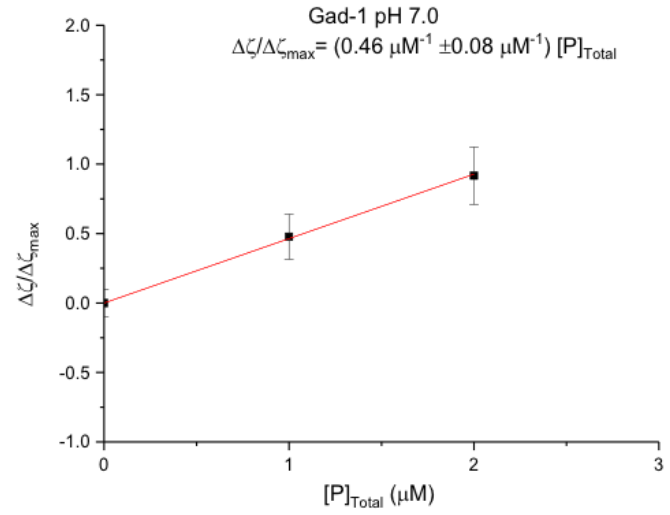

(b)

Figure 5.21: (a) $\frac{\Delta\zeta}{\Delta\zeta_{\max}}$ vs. $[P]_{\text{Total}}$ for Gad-1 at pH 7.0. (b) The linear regime (0 μM - 2 μM) was selected and slope of this region was used to find X using Equation 5.6. The slope of the linear portion of the binding isotherm was obtained using the weighted linear fitting. The size of error bars was taken into account to estimate the uncertainty in the slope. Q was determined from the limiting value of zeta potential using Equation 5.8. The equilibrium constant (K_{eq}) was determined using the expression, $K_{\text{eq}}(1 - X)$, for slope from Equation 5.7.

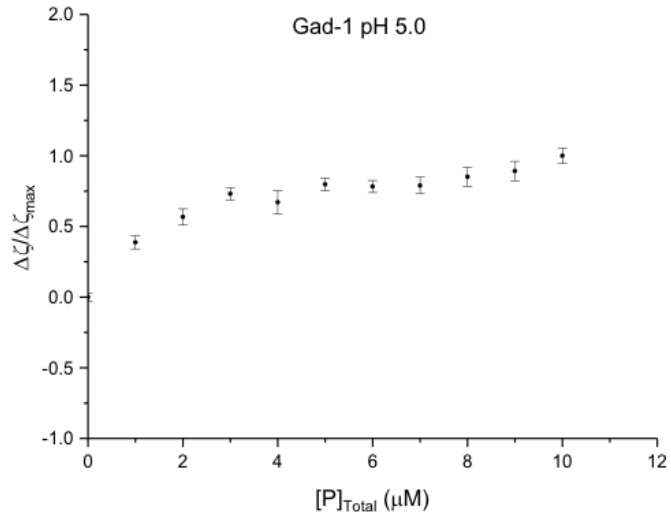

(a)

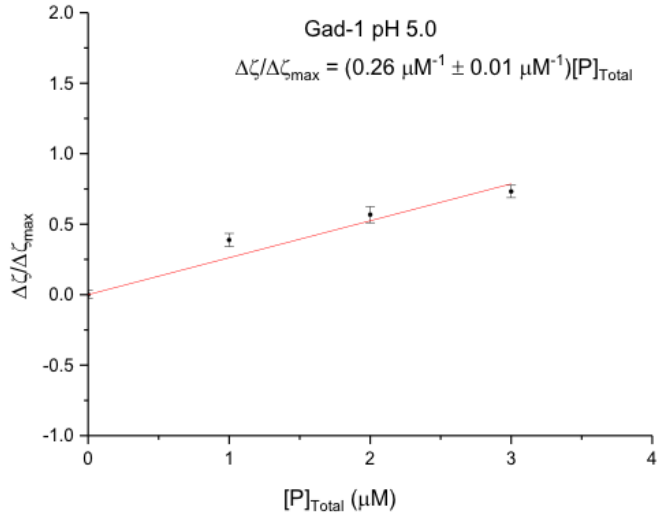

(b)

Figure 5.22: (a) $\frac{\Delta\zeta}{\Delta\zeta_{\max}}$ vs. $[P]_{\text{Total}}$ for Gad-1at pH 7.0. (b) The linear regime (0 μM - 3 μM) was selected and slope of this region was used to find X using Equation 5.6. The slope of the linear portion of the binding isotherm was obtained using the weighted linear fitting. The size of error bars was taken into account to estimate the uncertainty in the slope. Q was determined from the limiting value of zeta potential using Equation 5.8. The equilibrium constant (K_{eq}) was determined using the expression, $K_{\text{eq}}(1 - X)$, for slope from Equation 5.7.

Gad-1			
pH	Molar fraction of peptide bound to the membrane (X)	$1/Q$ (number of lipids per peptide binding site)	Equilibrium constant,K_{eq} (μM^{-1})
7.0	0.8±0.1	24± 3	2±1
5.0	0.31±0.01	33 ± 2	0.38± 0.04

Table 5.4: The values of X, $1/Q$, K_{eq} for Gad-1 at pH 7.0 and pH 5.0.

5.5 Discussion

In order to understand the role of cardiolipin (CL) in AMP-membrane interactions, a series of ^{2}H NMR and zeta potential experiments were performed with model membranes composed of POPE/POPG/CL in the presence of Gad-1. To investigate how these membrane-peptide interactions were affected by the change in overall peptide charge, all experiments were performed at two pH values, 7.0 and 5.0.

The first step was to characterize how incorporation of CL modified the properties of POPE/POPG lipid bilayers. To examine how the addition of CL affects the fast motions of POPE/POPG-d_{31} lipid bilayers that contribute to the motional narrowing, the ^{2}H NMR spectrum of POPE/POPG-d_{31}/CL was obtained and compared to the ^{2}H NMR spectrum of POPE/POPG-d_{31} (Figure 5.4). This comparison suggests that addition of CL to POPE/POPG-d_{31} lipid bilayers did not change quadrupole splittings of the spectral doublets. In other words, CL did not affect the amplitude of lipid acyl chain motions that can result in motional narrowing.

In order to investigate the effect of pH on the lipid−only spectrum of POPE/POPG-d_{31}/CL, the ^{2}H NMR spectrum of POPE/POPG-d_{31}/CL at pH 7.0 was compared

with the spectrum of bilayers with the same composition obtained at pH 5.0 (Figure 5.8). This comparison indicates that changing the pH from 7.0 to 5.0 did not have any effect on the spectral shape and spectrum maximum splitting of ^{2}H NMR spectrum of POPE/POPG-d_{31}/CL.

The comparison described immediately above indicates that the presence of CL did not perturb the fast motions of POPE/POPG-d_{31} lipid bilayers that contribute to motional narrowing. In order to investigate if CL perturbs motions of POPE/POPG-d_{31} lipid bilayers with correlation times longer than the characteristic ^{2}H NMR timescale ($10^{-5}s$), the quadrupole echo decay time was determined in the presence of CL. Figure 5.9 and Figure 5.10 show the quadrupole echo decay times of POPE/POPG-d_{31} lipid bilayers with and without the addition of CL at pH 7.0 and at pH 5.0. The addition of CL reduced the quadrupole echo decay time of POPE/POPG-d_{31} lipid bilayers at pH 7.0 and at pH 5.0. As the addition of CL to POPE/POPG-d_{31} did not seem to affect the fast motion of lipid bilayers that contribute to the motional narrowing, the changes in the quadrupole echo decay time with the addition of CL to POPE/POPG-d_{31} lipid bilayers suggests that CL perturbs the slower motions of POPE/POPG-d_{31} lipid bilayers, such as bilayer undulations. The contribution to echo decay rate for slow motions is inversely proportional to correlation time. The decrease in echo decay times (increase in echo decay rate) with the addition of CL indicates the reduction in correlation times for the slower motions.

To investigate whether higher CL concentrations might affect the fast motions of POPE/POPG-d_{31} lipid bilayers that contribute to the motional narrowing, ^{2}H NMR spectra of POPE/POPG-d_{31}/CL were also obtained when the amount of CL was doubled from 5% to 10% of the total lipid concentration. Comparison of ^{2}H NMR spectra for POPE/POPG-d_{31}/CL at two concentrations of CL (Figure 5.3 and Figure 5.5) indicates that increasing CL concentration did not affect the fast

lipid chain motions that can change the quadrupole splitting. Figure 5.9, shows the values of echo decay times for two concentrations of CL at both pH values and both temperatures studied. The echo decay times of the observed spectra did not change with an increase in CL concentration. Taken together, these results showed adding a small amount of CL (5% of total lipid composition) changed the echo decay times but doubling the amount (10% of total lipid composition) added did not increase the effect. This implies that the presence of CL does perturb the motions that determine echo decay time but that the effect saturates at a relatively small CL concentration so that adding more CL did not enhance the effect.

After investigating the effects of CL on the bilayer motions of POPE/POPG, the interactions of Gad-1 with POPE/POPG-d_{31}/CL lipid bilayers were examined. To investigate how the presence of CL affects the response of POPE/POPG bilayers to Gad-1, the ^{2}H NMR spectra of POPE/POPG-d_{31}/CL and POPE/POPG-d_{31} at pH 7.0 were compared in the presence and absence of Gad-1 (Figure 5.12). The addition of Gad-1 to both POPE/POPG-d_{31} and POPE/POPG-d_{31}/CL lipid bilayers reduced all of the POPG-d_{31} acyl chain quadrupole doublet splittings. This means the peptide slightly increased the amplitude of lipid acyl chain motion. The extent of this perturbation is same in both POPE/POPG-d_{31} and POPE/POPG-d_{31}/CL bilayers. In addition to this, however, Gad-1 also broadened the quadrupole peaks in the case of POPE/POPG-d_{31}/CL. This might indicate that Gad-1 perturbs slow motions of lipid bilayers that affect the refocusing of the quadrupole echo signal. This can be investigated by determining the quadrupole echo decay time as discussed later in this Section.

The next step was to investigate if peptide-induced disorder in POPE/POPG-d_{31}/CL bilayers by Gad-1 was sensitive to pH. For this, the ^{2}H NMR spectrum of POPE/POPG-d_{31}/CL was obtained with the addition of Gad-1 at pH 5.0 and

compared to the spectrum obtained at pH 7.0 (Figure 5.15). This comparison indicates that the perturbation of POPE/POPG-d_{31}/CL lipid bilayers by Gad-1 was not pH- sensitive and thus not sensitive to the charge of Gad-1.

Additional information about the peptide-induced perturbation of POPE/POPG-d_{31}/CL lipid bilayers was obtained from the quadrupole echo decay time. The changes in the echo decay time of POPE/POPG-d_{31}/CL with the addition of Gad-1 indicates the perturbation of slower bilayer motions with correlation times greater than the characteristic ^{2}H NMR time scale ($10^{-5}s$). A reduction in spectrum splittings at the same time as the individual doublets are broadened suggests that both fast and slow motions were affected by the presence of CL.

Figure 5.16 and Figure 5.17 shows the quadrupole echo decay times for POPE/POPG-d_{31} and POPE/POPG-d_{31}/CL lipid bilayers, with and without the addition of Gad-1, at pH 7.0 and pH 5.0, at two temperatures, 25°C and 37°C. For lipid only samples (POPE/POPG-d_{31} and POPE/POPG-d_{31}/CL) the quadrupole echo decay time was only weakly dependent on temperature. The addition of CL to POPE/POPG-d_{31} lipid bilayers the reduced quadrupole echo decay time. This reduction in the echo decay time was not pH-sensitive. In the presence of Gad-1, the quadrupole echo decay time of POPE/POPG-d_{31}/CL lipid bilayers was independent of temperature. Notably, Gad-1 seemed to have opposite effects on the echo decay time of POPE/POPG-d_{31}/CL lipid bilayers at pH 7.0 and pH 5.0. The addition of Gad-1 to POPE/POPG-d_{31}/CL lipid bilayers decreased the echo decay time at pH 7.0 while it increased the echo decay time at pH 5.0. Gad-1 had similar effects on chain orientational order which suggests that the effects of Gad-1 on fast (short correlation time) motion is similar for both pH values. Any pH-dependence in the perturbation of quadrupole echo decay by Gad-1 reflects effects on slower (longer length scale) motions like bilayer undulation. Another interesting observation is that adding Gad-1 and CL together to POPE/POPG-d_{31}

lipid bilayers reduced the quadrupole echo decay time. This might indicate that CL perturbs the slow motions of lipid bilayer in a similar way as Gad-1 perturbs the slow bilayer motions.

After observing the effects of Gad-1 on the fast and slow motions of POPE/POPG-d_{31}/CL lipid bilayers, the binding of Gad-1 to POPE/POPG/CL lipid bilayers was studied quantitatively using zeta potential measurements. In the absence of peptide, a negative zeta potential of ∼-55 mV is observed for POPE/POPG/CL (79/16/5 molar ratio) lipid vesicles at pH 7.0 and pH 5.0. The addition of peptide results in progressive neutralization of the negative zeta potential of the lipid vesicles. This reduction in the magnitude of the zeta potential indicates an interaction of the negatively charged membrane with the positive peptide. At higher concentrations of Gad-1 peptide, the zeta potentials of POPE/POPG/CL vesicles approach negative limiting values depending on the charge of the peptide and the $(L : P)$ ratio when all binding sites are occupied. The sign of the limiting zeta potential, at high peptide concentration, is an interesting difference between the vesicles with and without CL incorporated.

Comparison of the zeta potential binding isotherms of POPE/POPG/CL (79/16/5 molar ratio) and POPE/POPG (3:1 molar ratio) provides a way to compare the binding of Gad-1 to two lipid vesicles qualitatively. At pH 7.0, the zeta potential reached a positive limit of ∼+5 mV for POPE/POPG lipid vesicles while it approached a negative limit of ∼-25 mV for POPE/POPG/CL vesicles. At pH 5.0, the zeta potential reached the positive limit of ∼+20 mV for POPE/POPG lipid vesicles while it approached a negative limit of ∼-5 mV for POPE/POPG/CL vesicles. It should be noted that for both lipid vesicles the effective zwitterionic to negative lipid ratio was 3:1. Comparisons of the zeta potential binding isotherms indicate that in the presence of CL, Gad-1 did not fully neutralize the membrane

charge. This suggests that it is the presence of CL, not just the membrane charge, that affects the binding of Gad-1 to POPE/POPG lipid bilayers.

The comparison of values of X for POPE/POPG and POPE/POPG/CL lipid bilayers gives an idea how the presence of CL could affect the total amount of peptide that can be accommodated on the membrane surface. For Gad-1, the fraction of peptide bound to the membrane at pH 7.0 is greater than the fraction of peptide bound to the membrane at pH 5.0 for both lipid mixtures. This suggests that the higher the peptide charge, the smaller the amount of peptide accommodated on the membrane. This may be due to the fact that when a peptide has more positive charge, less peptide is needed to neutralize the membrane charge and electrostatic repulsive interactions between peptide molecules limit the peptide binding to the membrane. The values of X for POPE/POPG and POPE/POPG/CL lipid bilayers are compared in Table 5.5. This comparison indicates that the fraction of Gad-1 bound to POPE/POPG/CL lipid bilayers is approximately two times greater than the fraction of Gad-1 bound to POPE/POPG lipid bilayers at pH 7.0. At pH 5.0, the fraction of Gad-1 bound to both types of lipid bilayers is approximately same. It is interesting to observe that even though the zwitterionic to negative lipid ratio is same in both type of lipid bilayers, the presence of CL allows more peptide to be accommodated on the lipid bilayer at pH 7.0. It has been reported in the previous peptide binding studies that CL increases binding of the peptide to lipid bilayers [176, 177]. AMPs have also been shown to induce the clustering of anionic lipids [147, 148, 150, 151, 178]. The clustering of anioinic lipids creates a region that is rich in negative charge and a cationic peptide might be attracted to this negative-charge-rich lipid domain due to strong electrostatic interactions. Clustering of CL would form a CL-rich domain that has more negative charge compared to PG-rich domain. In addition to this, CL has a relatively smaller head group compared to its acyl chain region. Hence CL provides more

room for peptide to accommodate in the head group area. This might explain that the increased accommodation of peptide on the membrane surface in the presence of CL.

Molar fraction of peptide bound to the membrane (X)		
lipid bilayers	Gad-1	
	pH 7.0	pH 5.0
POPE/POPG-d_{31}	0.48±0.02	0.35±0.01
POPE/POPG-d_{31} /CL	0.8±0.1	0.31±0.02

Table 5.5: Comparison of values of X for Gad-1 peptide for POPE/POPG-d_{31} and POPE/POPG-d_{31}/CL bilayers at pH 7.0 and pH 5.0.

After investigating the fraction of peptide bound to the membrane, the next step was to examine how tightly the peptide is bound to the membrane and how the presence of CL affects this binding strength? The binding strength of Gad-1 to POPE/POPG/CL lipid bilayers was characterized in terms of the equilibrium constant (K_{eq}). The Gad-1 the equilibrium constants for POPE/POPG-d_{31} and POPE/POPG-d_{31}/CL bilayers at pH 7.0 and pH 5.0 are listed in Table 5.6. The higher value of K_{eq} at pH 7.0 than at pH 5.0 suggests that the binding of Gad-1 to POPE/POPG/CL is tighter at pH 7.0 than at pH 5.0. In addition to this, the binding strength of Gad-1 to POPE/POPG/CL lipid bilayers is pH-sensitive. When compared to the binding strength of Gad-1 to POPE/POPG lipid bilayers, it was observed that the presence of CL makes the binding of Gad-1 stronger. This may be due to clustering of CL in the presence of Gad-1. As explained above, the domain formation may result in the accommodation of more peptide on the membrane and stronger binding of the peptide. However, the binding of Gad-1 to POPE/POPG/CL lipid bilayers was weaker at pH 5.0 than at pH 7.0.

This may be due to the fact that Gad-1 is less helical at pH 5.0 compared to pH 7.0. It has been observed in molecular dynamics simulations with Gad peptides that more helical peptide structures tend to interact more strongly with planar regions while peptide structure with smaller helical contents tend to interact with disordered bilayer regions [143]. This may result in the weaker binding of Gad-1 to the membrane at pH 5.0 than at pH 7.0.

(K_{eq})		
lipid bilayers	Gad-1	
	pH 7.0	pH 5.0
POPE/POPG-d_{31}	0.22±0.03	0.21±0.02
POPE/POPG-d_{31} /CL	2±1	0.38±0.04

Table 5.6: Comparison of values of K_{eq} for Gad-1 peptide for POPE/POPG-d_{31} and POPE/POPG-d_{31}/CL bilayers at pH 7.0 and pH 5.0.

The comparison of X shows how the fraction of peptide bound to the membrane was affected by the different properties of peptide and the membrane. When a certain fraction of peptide is bound to the membrane, the number of lipids interacting with one molecule of bound peptide may also depend on properties of the peptide and the membrane. This was investigated by comparing the lipid-to-peptide ratios for Gad-1 peptide bound to two lipid bilayers, POPE/POPG and POPE/POPG/CL, at different pH values (Table 5.7). $L : P$ ratios were higher at pH 5.0 than at pH 7.0 for both type of lipid bilayers. This suggests that the higher the peptide charge, the larger the number of lipids per bound peptide. AMPs are cationic and can interact more strongly with anionic lipids than with zwitterionic lipids. A consequence of added Gad peptides recruiting anionic lipids could result in domains or patches that are rich in anionic lipids surrounding the peptide. Other AMPs including Myxinidin, Aurein 1.2, Arginine rich peptides

(PR−9), (RR−9), (PI−9), and LL−37 [147, 148, 150, 151, 178] have been shown to be able to cluster anionic lipids. For POPE/POPG/CL the $L : P$ ratios were higher than the $L : P$ ratios for Gad-1 bound to POPE/POPG at both pH 7.0 and pH 5.0. This suggests that, in the presence of CL, Gad-1 interacts with a larger numbers of lipids. It has been reported in previous studies that CL can translocate from the inner bilayer leaflet to the outer leaflet (CL flip-flop) in the presence of polycationic substances [176, 179]. Considering these observations, Gad-1 might be able to induce CL flip-flop and hence a higher number of interactions between the peptide and lipid molecules.

$1/Q$		
lipid bilayers	Gad-1	
	pH 7.0	pH 5.0
POPE/POPG-d_{31}	10±1	21±3
POPE/POPG-d_{31}/CL	24±3	33±2

Table 5.7: Comparison of values of $1/Q$ for Gad-1 peptide for POPE/POPG-d_{31} and POPE/POPG-d_{31}/CL bilayers at pH 7.0 and pH 5.0.

CL is, relatively, a small component of the bacterial membrane lipid composition, but it appears to play an important role in AMP-membrane interactions. The presence of CL allows the membrane to accommodate more Gad-1. In addition to this, the peptide binds more strongly with the lipid bilayers containing CL and it interacts with larger numbers of lipids in CL-containing model membranes. Considering these observations, binding of Gad-1 to the membrane might cause the clustering of anionic lipids (POPG and CL). This redistribution of lipids would concentrate the negative charge in anionic lipid-rich domains to which more

cationic peptide would be attracted. In addition to promoting the peptide concentration on the anionic membrane surface, domain formation could create phase boundaries that could lead to the membrane destabilization [180].

Chapter 6

Discussion

The cell membrane is the primary target of AMPs [1, 2]. To fully understand the mechanism of membrane destabilization by AMPs, it is important to elucidate how membrane properties are affected by the binding of AMPs [3, 26, 35, 181–185].

Gad peptides are histidine-rich peptides, which makes the peptide overall charge pH-dependent. This pH-dependence provides a way to understand the role of peptide charge in AMP-membrane interactions. Also, Gad-1 and Gad-2 are paralogous genes (coded by related genes), and hence have a potential to demonstrate how specificity is tuned in natural peptide sequences [26]. In addition to antibacterial activities, some AMPs have anticancer properties. The pH level of the extracellular space surrounding solid tumors is significantly lower than the pH of normal cells. Therefore, many attempts have been made to develop new pH-dependent anti-cancer therapies which can be active in the lower pH space of solid tumors [1, 186, 187]. The pH-dependent activity of histidine-rich Gad peptides provides a way to understand their potential to treat tumors.

The major focus of this study was to understand how Gad peptides interact with model lipid membranes, with particular attention to the question of how these

interactions depend on the peptide overall charge and composition of model membranes. In addition to variation of AMP-membrane interaction with pH, we are also interested in studying the differences in AMP-membrane interactions for Gad-1 and Gad-2. Physical methods, including NMR spectroscopy, zeta potential measurements, and circular dichroism spectroscopy were used to study the AMP-membrane interactions with Gad peptides. ^{2}H NMR experiments were performed to investigate how Gad peptides perturb the lipid bilayer integrity. Circular dichroism spectroscopy was used to examine the secondary structure of Gad peptides in model lipid membranes. To gain insights into the binding of Gad peptides to model lipid membranes, zeta potential measurements were performed. To examine the positioning of Gad peptides in the lipid bilayers ^{15}N NMR experiments were carried out. All experiments were performed with model lipid membranes that mimic the bacterial membrane lipid composition. Firstly, ^{2}H NMR and zeta potential experiments were performed with a lipid mixture of POPE/POPG. Secondly, experiments were performed with a lipid mixture of POPE/POPG/CL to gain insights into the role of CL in AMP-membrane interactions. ^{15}N NMR experiments were performed with mechanically oriented lipid bilayers using a lipid mixture of POPC/POPG.

When a peptide interacts with the model lipid membrane, the peptide may perturb the packing of hydrophobic acyl chains. Perturbation of model bilayers by Gad peptides was studied using ^{2}H NMR. It was found that adsorption of Gad peptides to POPE/POPG-d_{31} bilayers slightly reduced the lipid acyl chain order. Many helical cationic peptides such as MSI-78 [188], LL-37, Magainin [189], alamethicin [190], ampullosporin [137], have been shown to induce disorder in bilayer lipid acyl chains. Gad peptides perturb the membrane to a similar degree to the other mentioned peptides. The decrease in lipid acyl chain order has been related to the membrane thinning induced by the presence of peptide [189, 191, 192]. This

membrane destabilization by AMPs can result in impairment of many membrane-associated functions [45, 57]. Next, pH-dependence of peptide-induced disorder was examined and it was found that the reduction in order parameter by Gad peptides was not pH-dependent. The histidine-rich synthetic peptide LAH4-L1 also induced a slight reduction in the order parameter values of POPE/POPG-d_{31} lipid vesicles. However, in the case of L4H4-1, the reduction in order parameter was weakly dependent on pH [75]. This may suggest that different AMPs disrupt the membrane by different means. It is still unclear whether there is one fundamental mechanism or there are different multiple mechanisms for AMP action[193].

Knowledge of AMP peptide orientation in the membrane can contribute to understanding of the mechanism of membrane destabilization by AMPs. The alignment of Gad-1 in oriented model lipid bilayers was examined using ^{15}N NMR, (Chapter 4). The ^{15}N NMR observation showed that Gad-1 aligned parallel to the membrane surface. Other alpha-helical peptides such as Magainin [85], Piscidin-1, Piscidin-3 [194], Cecropin A [195] have also been shown to adopt in-plane alignment with respect to the membrane. While ^{15}N NMR was found to be useful for samples containing Gad-1, it was found that obtaining ^{15}N NMR spectra with Gad-2 peptide was not feasible. The dry weight of a chemically synthesized peptide is known to contain a substantial amount of non-peptide contaminants, mainly salt form the HPLC purification. However, Gad-2 peptide dry powder contained larger fraction of salt than for Gad-1(discussed in Section 4.3). The amount of salt present in the dry peptide powder reduced the amount of peptide actually present in the sample and the obtained ^{15}N NMR spectrum had poor signal-to-noise ratio.

Binding studies of Gad peptides with model lipid membranes showed that there is a difference in the binding of Gad-1 and Gad-2 to the membrane even though peptide-induced disorder was similar for the two peptides in the same model lipid

membrane composed of POPE and POPG lipids. Also, unlike the case for peptide-induced acyl chain disorder, the binding of Gad peptides to the membrane was also found to have a pH-dependence. The results showed that for both Gad-1 and Gad-2, smaller amounts of peptide bind to the membrane at slightly acidic pH compared to neutral pH. Also, the peptide interacts with a larger number of lipid molecules at acidic pH than at neutral pH. Added cationic Gad peptides can interact more strongly with anionic lipids than with zwitterionic lipids due to electrostatic forces. The molecular interactions between cationic Gad peptides and anionic lipids can result in the reorganization of membrane lipids and promotion of anionic lipid clustering. Taken together, ^{2}H NMR and zeta potential results suggest that Gad peptides might disrupt membrane integrity by clustering the anionic lipids rather than by inducing a disorder in the hydrophobic core of the lipid membrane. The lipid clustering model has been proposed for other AMPs as well [45, 57, 149, 180]. The differences in the binding of Gad-1 and Gad-2 to the model lipid membrane may be attributed to the differences in the distribution of charge, to differences in helical contents of their secondary structure upon binding to the membrane, and to differences in the presence of histidine pairs in their sequences.

To understand the role of CL in AMP-membrane interactions, ^{2}H NMR and zeta potential experiments were performed with model membranes containing CL in the presence of Gad-1 (Chapter 5). The main finding was that the presence of CL allows the membrane to accommodate more Gad-1. It was also found that the presence of CL allows the peptide to bind more strongly with the membrane and to interact with a larger number of lipids. The stronger interactions between cationic peptides and anionic lipids (POPG and CL) can result in a reorganization of membrane lipids, increasing the concentration of anionic lipids and cationic peptide within a membrane domain. In other words, the interactions of Gad

peptides with model membranes containing CL may result in the promotion of anionic lipid clustering. More experiments could be performed by using increasing amounts of CL. Table 5.1 indicates that different bacterial species have different amounts of CL in the membrane. The results of experiments at different CL concentrations could contribute to understanding of how different amounts of CL affects the AMP-membrane interactions.

The AMP-membrane interaction studies of Gad peptides described here suggest that Gad peptides might be able to cause the clustering of anionic lipids in the membrane. It has been reported in the literature that several peptides can target the membrane lipids and can alter the bulk physical properties of the membrane [196]. Peptide-induced clustering of anionic lipids is also likely to perturb existing domains in the membrane and might destabilize the membrane by introducing boundary defects [197–201].

The AMP-membrane interaction is a key factor in the antimicrobial action, both when the membrane is the primary target or when the membrane is permeabilized in the course of peptides gaining access to the intracellular components. The work in this thesis contributes to our understanding of how a specific type of AMP, the Gad peptides, interact with membranes at different pH values. The study of AMP-membrane interactions will help to identify criteria to recognize the important features of natural AMP sequences involved in the antimicrobial action and thus assist in the design of AMP-based antibiotics to combat drug resistance problem.

6.0.1 Directions for future work

The work reported in this thesis investigates the interactions of histidine-rich Gad peptides at different pH values. The AMP-membrane interactions for other histidine-rich peptides have been studied but those studies have focused on incorporating histidine residue in designed peptide sequences. On the other hand, Gad peptides are natural histidine-rich peptides, and hence provide a way to alter the AMP charge and understand its role in AMP-membrane interactions. Another important point about this work is that AMP-membrane interactions are investigated quantitatively in terms of different binding parameters using zeta potential measurements. Much of the vast literature on interactions of AMPs with model membranes is devoted to using lipids POPE, POPC, POPG for the model membranes. This thesis reports the interactions of Gad peptides with model membranes containing cardiolipin (CL), which is an important lipid-component of bacterial membranes.

The main observation of this study was that Gad peptides might be able to cause the clustering of anionic lipids in the membrane. In order to further investigate this point, differential scanning calorimetry (DSC) experiments could be performed to study phase/domain formation by Gad peptides in the model lipid membrane. It is possible that histidine pairs in Gad peptide sequences might play a role in AMP-membrane interactions. To understand the role of histidine pairs, future ^{2}H NMR and zeta potential experiments could be performed by using a scrambled peptide sequence in which histidine is not present in pairs. The model membranes used in this study mimic the membrane of *E. coli* which is a gram negative bacteria. It would be interesting to investigate how Gad peptides interact with model membranes mimicing the composition of gram positive bacteria. In terms of looking

at the bigger picture of AMP study, future binding study experiments could be planned with real bacterial membranes.

Appendices

Appendix A

Density operator formulation of spin $\frac{1}{2}$ and spin 1 system

A.1 Density operator

The total magnetization is the sum of innumerable small contributions from individual spins. One way to acquire this summation is to treat all spins individually and then add the results to get net magnetization. Another alternative is to use the concept of density operator, which describes the quantum state of an entire sample, without referring to individual spins. The density operater formulation treats the sample as an ensemble average where ensemble is a collection of independent identical systems.

For spin $\frac{1}{2}$ system, a single spin state can be represented as the superposition of states α and β [87]

$$|\Psi\rangle = C_\alpha |\alpha\rangle + C_\beta |\beta\rangle \tag{A.1}$$

where C_α and C_β represent the probability of α and β states respectively. In the matrix form spin state can be written as

$$|\Psi\rangle = \begin{bmatrix} C_\alpha \\ C_\beta \end{bmatrix} \qquad \langle\Psi| = \begin{bmatrix} C_\alpha & C_\beta \end{bmatrix}. \tag{A.2}$$

The expectation value of any operator $\hat{Q}$ can be expressed in terms of Ψ [87]

$$\begin{aligned} \langle\hat{Q}\rangle &= \langle\Psi|\,\hat{Q}\,|\Psi\rangle \\ &= Tr[\langle\Psi|\,|\Psi\rangle]\hat{Q} \end{aligned} \tag{A.3}$$

where

$$\langle\Psi|\,|\Psi\rangle = \begin{bmatrix} C_\alpha C_\alpha^* & C_\alpha C_\beta^* \\ C_\beta C_\alpha^* & C_\beta C_\beta^* \end{bmatrix}. \tag{A.4}$$

Consider a system of two independent spins with spin states Ψ_1 and Ψ_2, respectively. In this case, the observed value of Q is given as

$$Q_{Observable} = \langle\Psi_1|\,\hat{Q}\,|\Psi_1\rangle + \langle\Psi_2|\,\hat{Q}\,|\Psi_2\rangle \tag{A.5}$$

$$= Tr[\langle\Psi_1|\,|\Psi_1\rangle + \langle\Psi_2|\,|\Psi_2\rangle]\hat{Q}. \tag{A.6}$$

The above formulation can be extended to a system containing N number of spins

$$Q_{Observable} = \langle\Psi_1|\,\hat{Q}\,|\Psi_1\rangle + \langle\Psi_2|\,\hat{Q}\,|\Psi_2\rangle + ... + \langle\Psi_N|\,\hat{Q}\,|\Psi_N\rangle \tag{A.7}$$

$$= Tr[\langle\Psi_1|\,|\Psi_1\rangle + \langle\Psi_2|\,|\Psi_2\rangle + ... + \langle\Psi_N|\,|\Psi_N\rangle]\hat{Q} \tag{A.8}$$

$$= NTr[\hat{\rho}\hat{Q}]. \tag{A.9}$$

The expectation value of operator Q is

$$< \hat{Q} >= Tr[\hat{\rho}\hat{Q}] \tag{A.10}$$

where

$$\hat{\rho} = \frac{1}{N}[\langle\Psi_1|\,|\Psi_1\rangle + \langle\Psi_2|\,|\Psi_2\rangle + ... + \langle\Psi_N|\,|\Psi_N\rangle] \tag{A.11}$$

is called the density operator.

It is important to note that the $< \hat{Q} >$ is not an expectation value for a single spin, but rather, it is the average over the entire ensemble. Therefore, the result of any macroscopic observable can be calculated by using two operators. One is the density matrix operator representing the spin state of the entire system without referring to individual spins, and second is the observable itself [87, 90].

Furthermore, the density operator for a spin $\frac{1}{2}$ system is a $2 * 2$ matrix

$$\hat{\rho} = \begin{bmatrix} C_\alpha C_\alpha^* & C_\alpha C_\beta^* \\ C_\beta C_\alpha^* & C_\beta C_\beta^* \end{bmatrix}. \tag{A.12}$$

The diagonal elements of the density matrix are called the populations, and the off diagonal elements are called the coherences. The difference between the populations give the net magnetization in z axis, while coherences represent the magnetization in the xy plane [90, 91]. This density matrix concept can be used to understand the effect of RF pulses on equilibrium magnetization.

A.2 Density operator formulation of spin $\frac{1}{2}$ system for $(\frac{\pi}{2})_x$ pulse

In order to understand how an oscillating magnetic field produced by a RF pulse perturbs the equilibrium magnetization away from the z axis, it is helpful to explain the behavior of a spin system in terms of the density operator[87, 89, 90, 93]. The density operator represents the quantum mechanical state of an entire spin system without referring to the individual spins (Section A.1). The density

operator treats the spin system as an ensemble and can be written in the matrix form. For a spin $\frac{1}{2}$ system, the density operator is a 2×2 matrix. The diagonal elements represent the populations of α and β states and the difference between the diagonal elements gives the net magnetization in the direction of field i.e. the longitudinal component of magnetization. This represents the thermal equilibrium state of a spin system. The off-diagonal elements of a density matrix are called coherences. They oscillate harmonically in time. The vanishing of the off-diagonal elements represent the equilibrium state of spin system. On the other hand, if off-diagonal elements do not vanish it results in time varying observable signal in the direction perpendicular to the static magnetic field [88]. The equation of motion for the density operator ρ is given as [87, 89, 93]

$$\frac{d\rho}{dt} = -i[H, \rho] \tag{A.13}$$

where H is the Hamiltonian of the spin system and ρ is the density operator. The density operator can be written in terms of the unit operator, 1_{op}, and a set of three other independent operators $\bar{P}$ [87, 93]

$$\rho(t) = \sum_{P} C_P(t)\bar{P} \tag{A.14}$$

where

$$Tr[\bar{P}, \bar{P'}] = \delta_{PP'}. \tag{A.15}$$

In Equation A.14, the C_P represent the coefficients of different spin states. Using Equation A.14, the Equation of motion of the density operator becomes

$$\frac{d(\sum_P C_P(t)\bar{P})}{dt} = -i[H, \sum_{P} C_P(t)\bar{P}]. \tag{A.16}$$

For spin $\frac{1}{2}$ system, there are three independent terms in the density operator. So the Cartesian components of angular momentum can be used as independent operators

$$I_x = 1/2 \begin{bmatrix} 0 & 1 \\ 1 & 0 \end{bmatrix}, \qquad I_y = 1/2 \begin{bmatrix} 0 & -i \\ i & 0 \end{bmatrix}, \qquad I_z = 1/2 \begin{bmatrix} 1 & 0 \\ 0 & -1 \end{bmatrix}.$$

(i) Zeeman Hamiltonian:

Before and after the RF pulse, the spin system evolves under the Zeeman Hamiltonian, H_z [87, 93]

$$H_z = -\omega_0 I_z. \tag{A.17}$$

Using this Hamiltonian, the Equation A.13 becomes

$$\frac{d[C_x I_x + C_y I_y + C_z I_z]}{dt} = -i[-\omega_0 I_z, C_x I_x + C_y I_y + C_z I_z] \tag{A.18}$$

$$I_x \frac{dC_x}{dt} + I_y \frac{dC_y}{dt} + I_z \frac{dC_z}{dt} = i\omega_0 \{[I_z, C_x I_x], [I_z, C_y I_y], [I_z, C_z I_z]\} \tag{A.19}$$

$$= i\omega_0 \{iC_x I_y - iC_y I_x\}. \tag{A.20}$$

The commutation relation $[I_i, I_j] = i\varepsilon_{ijk} I_k$ is used in the above equation. By comparing the coefficients on both sides we have

$$\frac{dC_x}{dt} = -i\omega_0 C_y \tag{A.21}$$

$$\frac{dC_y}{dt} = i\omega_0 C_x \tag{A.22}$$

$$\frac{dC_z}{dt} = 0. \tag{A.23}$$

The solution to the above equations can be written as

$$\begin{aligned} C_x(t) &= C_x(0)cos\omega_0 t - C_y(0)sin\omega_0 t \\ C_y(t) &= C_y(0)cos\omega_0 t + C_x(0)sin\omega_0 t \\ C_z(t) &= constant. \end{aligned} \tag{A.24}$$

Initially, there is no magnetization in the xy plane. Therefore, $C_x(0) = C_y(0) = 0$ and Equation A.24 becomes

$$\begin{aligned} C_x(t) &= 0 \\ C_y(t) &= 0 \\ C_z(t) &= constant. \end{aligned} \tag{A.25}$$

If the initial conditions are set right i.e. $C_x(0) = C_y(0) = 0$, then the evolution of spin system under the Zeeman Hamiltonian corresponds to the net magnetization in the z axis.

(ii) $\frac{\pi}{2}$ pulse along x axis:

When a $\frac{\pi}{2}$ pulse is applied along the x axis, the system evolves under the following Zeeman Hamiltonian [87, 93]

$$H_x = -\omega_1 I_x. \tag{A.26}$$

The equation of motion for the density operator becomes

$$\begin{aligned} \frac{d[C_x I_x + C_y I_y + C_z I_z]}{dt} &= -i[\omega_1 I_x, C_x I_x + C_y I_y + C_z I_z] \\ &= -i\{[I_x, C_x I_x] + [I_x, C_y I_y] + [I_x, C_z I_z]\} \\ &= -i\omega_1\{iC_y I_z - iC_z I_y\}. \end{aligned} \tag{A.27}$$

Again, by comparing the coefficients on both sides we have

$$\frac{dC_z}{dt} = \omega_1 C_y. \tag{A.28}$$

$$\frac{dC_y}{dt} = -\omega_1 C_z. \tag{A.29}$$

The solutions of the above equations are given as

$$C_z(t) = C_z(0)cos\omega_1 t + C_y(0)sin\omega_1 t \tag{A.30}$$

$$C_y(t) = C_y(0)cos\omega_1 t - C_z(0)sin\omega_1 t. \tag{A.31}$$

For the special case

$C_z(0) = M_0, \quad C_y(0) = 0, \quad and \quad \omega_1 t = \frac{\pi}{2}$, the above solutions becomes:

$$C_z(t) = 0 \tag{A.32}$$

$$C_y(t) = -M_0 \tag{A.33}$$

Hence, it can be seen that a $\frac{\pi}{2}$ pulse applied along the x axis flips the magnetization from the z to the$-y$ axis. This is depicted in Figure A.1. After the $\frac{\pi}{2}$ pulse, Equations A.24 describe precession of the magnetization about the z axis. The density operator formulation can be used to understand the evolution of magnetization for any pulse sequence.

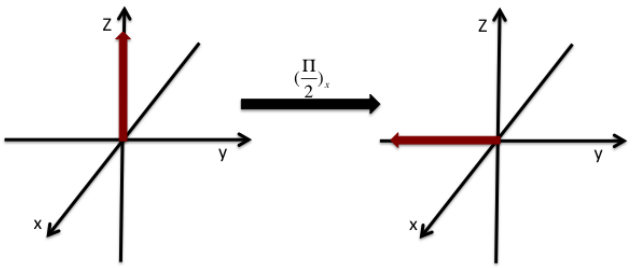

Figure A.1: When the external magnetic field is applied along the z axis, the equilibrium magnetization is formed in the direction of field. At this point, if $(\frac{\pi}{2})_x$ pulse is applied, it flips the magnetization from the z to the -y axis.

A.3 Density operator treatment of spin 1 system

The following treatment is based on the description presented by Bloom [93]. The density operator formulation can be used to understand the refocusing of magnetization with quadrupole pulse sequence. Using Equation A.13 we have

$$\frac{d(\sum_q C_q(t)\bar{q})}{dt} = -i[H, \sum_q C_q(t)\bar{q}] \tag{A.34}$$

Following 8 operators are used to express the density matrix of spin 1 system [93].

$$\bar{1} = \frac{1}{\sqrt{2}} I_x \ , \qquad \bar{2} = \frac{1}{\sqrt{2}} I_y \ , \qquad \bar{3} = \frac{1}{\sqrt{2}} I_z$$
$$\bar{4} = \frac{1}{\sqrt{6}}(3I_z^2 - 2)$$
$$\bar{5} = \frac{1}{\sqrt{2}}(I_x I_z + I_z I_x), \qquad \bar{6} = \frac{1}{\sqrt{2}}(I_y I_z + I_z I_y)$$
$$\bar{7} = \frac{1}{\sqrt{2}}(I_x^2 - I_y^2), \qquad \bar{8} = \frac{1}{\sqrt{2}}(I_x I_y + I_y I_x)$$

Taking the trace with $\bar{P}$ on both sides of Equation A.34, we have

$$\begin{aligned} \frac{dC_P}{dt} &= -iTr\{\bar{P}[H, \sum_q C_q(t)\bar{q}]\} \\ &= iTr\{\bar{P}[\sum_q C_q(t)\bar{q}, H\} \\ &= i\sum_q C_q\{Tr\bar{P}[\bar{q}, H]\} \end{aligned} \tag{A.35}$$

When magnetic filed is applied in the z direction it results in the equilibrium magnetization in the direction of field. Therefore,

$$\begin{aligned} C_3 &= M_0 \\ C_1 &= C_2 = 0 \end{aligned} \tag{A.36}$$

A.3.1 $\frac{\pi}{2}$ pulse along x axis

In this case, the spin system evolves under the Hamiltonian $H_1 = -\sqrt{2}\omega_1\bar{1}$ [93]. The rate change of magnetization along z axis is given as

$$\frac{dC_3}{dt} = -\sqrt{2}\omega_1 i \sum_q C_q Tr\{\bar{3}[\bar{q}, \bar{1}]\}. \tag{A.37}$$

The following commutator relation can be obtained by using the definition of operators

$$[\bar{2}, \bar{1}] = \frac{-i}{\sqrt{2}}\bar{3}. \tag{A.38}$$

Therefore, Equation A.37 becomes

$$\frac{dC_3}{dt} = -\omega_1 C_2 \tag{A.39}$$

Following the same treatment, the rate change of C_2 can be determined

$$\frac{dC_2}{dt} = \sqrt{2}\omega_1 i \sum_q C_q Tr\{\bar{2}[\bar{q}, \bar{1}]\} \tag{A.40}$$

$$\frac{dC_2}{dt} = -\omega_1 C_3 \tag{A.41}$$

The solution of differential Equations A.39 and A.41 are given as

$$C_3(t) = C_3(0)cos(\omega_1 t) - C_2(0)sin(\omega_1 t) \tag{A.42}$$

$$C_2(t) = C_3(0)sin(\omega_1 t) - C_2(0)cos(\omega_1 t) \tag{A.43}$$

For special case:

$C_3(0) = M_0$, $C_2(0) = 0$, and $\omega_1 t = \frac{\pi}{2}$

$$C_2(\frac{\pi}{2\omega_1}) = M_0 \tag{A.44}$$

$$C_3(\frac{\pi}{2\omega_1}) = 0 \tag{A.45}$$

Hence, the $\frac{\pi}{2}$ pulse applied along x axis results in the magnetization along y axis.

A.3.2 For time τ the spin system evolves under the Quadrupole Hamiltonian

After the first $\frac{\pi}{2}$ pulse, the magnetization precesses in the xy plane under the influence of the Quadrupole Hamiltonian

$$H_Q = \sqrt{\frac{2}{3}}\omega_Q \bar{4}. \tag{A.46}$$

The rate change of the magnetization along y axis is given as

$$\frac{dC_2}{dt} = i\sqrt{\frac{2}{3}}\omega_Q \sum_q C_q Tr\{\bar{2}[\bar{q}, \bar{4}]\}. \tag{A.47}$$

Using the commutator relation

$$[\bar{5}, \bar{4}] = -i\sqrt{\frac{3}{2}}\bar{2} \tag{A.48}$$

Equation A.47 becomes

$$\frac{dC_2}{dt} = \omega_Q C_5. \tag{A.49}$$

Now, the rate change of C_5 is given as

$$\frac{dC_5}{dt} = i\sqrt{\frac{2}{3}}\omega_Q \sum_q C_q Tr\{\bar{5}[\bar{q}, \bar{4}]\}. \tag{A.50}$$

$$\frac{dC_5}{dt} = -\omega_Q C_2 \tag{A.51}$$

The solutions of Equations A.49 and A.51 are

$$C_2 = C_2(0)cos(\omega_Q t) + C_5(0)sin(\omega_Q t) \tag{A.52}$$

$$C_5 = C_2(0)sin(\omega_Q t) - C_5(0)cos(\omega_Q t) \tag{A.53}$$

.

For special case:

$C_2(0) = M_0$, $t = \tau$, and $C_5(0) = 0$ above solutions becomes

$$C_2(\tau) = M_0 cos(\omega_Q \tau) \tag{A.54}$$

$$C_5(\tau) = M_0 sin(\omega_Q \tau). \tag{A.55}$$

A.3.3 $\frac{\pi}{2}$ pulse along y axis

During the second $\frac{\pi}{2}$ pulse is applied, the spin system precesses under the effect of Hamiltonian

$$H_2 = -\sqrt{2}\omega_1 \bar{2} \tag{A.56}$$

In this case $C_2 = M_0 cos(\omega_Q \tau)$ is invariant and rate change of C_5 is

$$\frac{dC_5}{dt} = -i\sqrt{2}\omega_1 \sum_q C_q Tr\{\bar{5}[q, \bar{2}]\}. \tag{A.57}$$

Using the commutator relations $[\bar{4},\bar{2}] = -i\sqrt{\frac{3}{2}}\bar{5}$ and $[\bar{7},\bar{2}] = \frac{i}{\sqrt{2}}\bar{5}$, Equation A.57 becomes

$$\begin{aligned}\frac{dC_5}{dt} &= -\sqrt{3}\omega_1 C_4 + \omega_1 C_7 \\ &= -\omega_1\{\sqrt{3}C_4 - C_7\}.\end{aligned} \tag{A.58}$$

Moreover, the rate change of C_4 and C_7 can be obtained as

$$\begin{aligned}\frac{dC_4}{dt} &= -i\sqrt{2}\omega_1 \sum_q C_q Tr\{\bar{4}[\bar{q},\bar{2}]\} \\ &= \sqrt{3}\omega_1 C_5\end{aligned} \tag{A.59}$$

$$\begin{aligned}\frac{dC_7}{dt} &= -i\sqrt{2}\omega_1 \sum_q C_q Tr\{\bar{7}[\bar{q}.\bar{2}]\} \\ \frac{dC_7}{dt} &= \omega_1 C_5.\end{aligned} \tag{A.60}$$

The Equations A.58 and A.60 can be combined as

$$\sqrt{3}\frac{dC_4}{dt} + \frac{dC_7}{dt} = 4\omega_{1C_5}. \tag{A.61}$$

In this case the equations of motion are

$$\frac{dC_5}{dt} = -\omega_1(\sqrt{3}C_4 + C_7) \tag{A.62}$$

$$\frac{d(\sqrt{3}C_4 + C_7)}{dt} = 4\omega_1 C_5. \tag{A.63}$$

The solutions to above equations are

$$C_5 = C_5(0)cos(2\omega_1 t) - \{\sqrt{3}C_4(0) + C_7(0)\}cos(2\omega_1 t) \tag{A.64}$$

$$\sqrt{3}C_4 + C_7 = C_5(0)sin(2\omega_1 t) + \{\sqrt{3}C_4(0) + C_7(0)\}cos(2\omega_1 t). \tag{A.65}$$

For special case:

$\sqrt{3}C_4(0) + C_7(0) = 0$ ans $C_5(0) = M_0 sin(\omega_Q \tau)$

$$C_5 = -M_0 sin(\omega_Q \tau) \tag{A.66}$$

$$\sqrt{3}C_4 + C_7 = 0 \tag{A.67}$$

Now, if the system is further allowed to evolve under H_Q for τ, Equation A.52 and A.53 can be used to write expression for C_2 and C_5

$$C_2 = M_0 cos^2(\omega_Q \tau) + M_0 sin^2(\omega_Q \tau) = M_0 \tag{A.68}$$

$$C_5 = M_0 cos(\omega_Q \tau) sin(\omega_Q \tau) - sin(\omega_Q \tau) cos(\omega_Q \tau) = 0 \tag{A.69}$$

Therefore, an echo is formed at the end of 2τ and refocuses the magnetization along y axis.

Appendix B

NMR spectrometer and the temperature controller

B.1 NMR spectrometer

The basic operational principle of a NMR spectrometer involves the irradiation of a sample with a RF pulse generated by the transmitter section. This RF pulse goes to the probe section and induces an oscillating magnetic field in the coil. If the duration of the pulse is carefully chosen, this leaves the magnetization in the xy plane where it precesses at the Larmor frequency. The FID signal produced by the precessing magnetization in the coil is directed towards the receiver section where it is amplified and processed to get a NMR spectrum. The main components of a NMR spectrometer are explained below.

B.1.1 The magnet

The magnet is a heart of the NMR spectrometer. It produces a homogeneous and static magnetic field that is used to generate the bulk magnetization in a sample.

The magnet consists of a superconducting wire solenoid immersed in liquid helium contained in a vessel that is surrounded by liquid nitrogen to minimize the helium loss. The whole assembly is enclosed in a vacuum chamber to further reduce heat flow. The probe containing the NMR sample is placed in the vertical tube passing through the middle of the magnet.

B.1.2 The transmitter and the probe section

The main function of the transmitter section is to generate a RF pulse of desired frequency, amplitude, and pulse length. The RF pulse from the transmitter is delivered to the probe where sample is irradiated with the RF pulse to manipulate the net magnetization of the sample.

The probe section consists of a coil and two capacitors known as matching and tuning capacitors. The coil locates the sample in the homogeneous magnetic field. When RF pulse is applied, it generates an oscillating current in the coil, which in turn produces an oscillating magnetic field. This magnetic field exerts an external torque on the net magnetization vector and moves it away form the z axis. The precessing magnetization left after the $\frac{\pi}{2}$ pulse produces an oscillating current in the coil that is amplified and stored as time domain FID signal.

B.1.2.1 Matching and tuning

In order to have maximum energy transfer from RF pulse to a sample, it is important to match the impedance of the transmitter section with the impedance of probe circuit. Once impedance is matched, the RF pulse can be transferred to the probe without any reflection. For impedance matching a variable capacitor known as matching capacitor is used. Although, impedance matching ensures the maximum transfer of RF pulse energy to sample but it is also necessary to tune

the probe to enhance the amplitude of both the oscillating magnetic field produce by RF pulse in the coil and the oscillating current produced by the precessing magnetization in the same coil. This is achieved by using another variable capacitor known as the tuning capacitor. Basically, the tuning capacitor and the coil (inductor) makes a tank circuit whose resonance frequency depends upon the values of capacitance (C) and inductance (L) through

$$\omega_0 = \frac{1}{\sqrt{(LC)}}. \tag{B.1}$$

The RF pulse generates oscillations in the coil. If the frequency of the RF pulse matches with the resonance frequency of the tank circuit, the amplitude of these oscillations is enhanced. This results in the large oscillating magnetic field produce by the RF pulse in the coil. The amplitude of the oscillating current produced by the precessing magnetization in the coil is also amplified if the LC circuit is tuned [103].

B.1.2.2 Quarter wavelength transmission line

It is important to note that in a NMR experiment, same coil is used to excite the sample and to detect the FID signal. Therefore, it is necessary to separate the transmitter and the receiver sections. In other words, the RF pulse must be directed towards the probe and blocked from travelling towards the receiver section where it can damage the pre-amplifier. On the other hand, the FID signal should go to the receiver section and must not travel back to the transmitter. To achieve this, two set of crossed diodes and $\frac{\lambda}{4}$ transmission line is used as shown in Figure B.1. An individual set of the crossed diodes act like a switch that are open for small voltage signal (FID signal) and closed for high voltage signals (RF pulse). An individual set of the crossed diodes act like a switch that are open for

small voltage signal (FID signal) and closed for high voltage signals (RF pulse).To protect the pre-amplifier from the RF pulse during transmission, a set of crossed diodes is placed just before the preamplifier and connected to ground. Both diode switches are closed for high voltage RF signal. As soon as voltage developed at point B is more than the forward bias voltage of the diodes, it will be shorted to ground. Furthermore, if the distance between points A and B is exactly the quarter of the wavelength then for a reflected wave, an anti-node and node is formed at point A and B respectively. Thus, with this transmission set-up RF pulse is directed towards the probe. On the other hand, the voltage of FID signal is much too small to turn on the diodes. Therefore, the FID signal proceeds to the pre-amplifier [103].

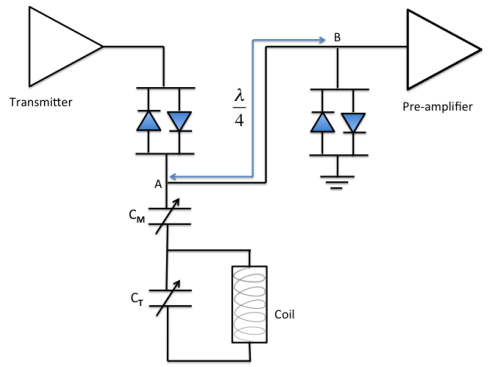

(a)

(b)

Figure B.1: (a) The schematic representation of the probe section of the NMR spectrometer with two crossed diode switches and $\frac{\lambda}{4}$ transmission line. (b) A picture of the NMR probe used in this work. The white rectangular piece at the top of probe is the coil used to hold the sample.

B.1.3 Receiver section

The receiver section of a NMR spectrometer consists of a pre-amplifier and digitizer. The FID signal is amplified by the pre-amplifier. The next step is the digitization of FID signal followed by the Fourier transformation to obtain the NMR spectrum in the frequency domain.

B.2 Temperature controller

To do NMR experiments at desired temperatures, a temperature controller is connected to the probe. The temperature controller used in this work is a PID controller, model 325 (Lake Shore cryotronics, USA) where PID stands for Proportional (P), Derivative (D) and Integral (I). It is a control loop feedback system and the output of controller is sensed. The desired temperature is called a set point. Based on the difference between set point and measured value, an error is calculated. This error determines the correction provided by three controllers P, I, and D [202].

(i) Proportional term: The proportional term must have value greater than zero in order for the control loop to work. The proportional response is given by an error multiplied with a constant known as proportional gain

$$P = K_p e(t). \tag{B.2}$$

The higher value of a K_p results in the large change in the output for a given change in error while a smaller value of it generates a slight change in the temperature fluctuations from the desired set point.

(ii) Integral term: The integral term takes into account both the magnitude and duration of an error. It is the accumulation of the instantaneous errors over time given as

$$I = K_I \int_0^t e(t)dt \tag{B.3}$$

where K_I is called the integral gain. Combined with the proportional term, the integral term moves the measured value towards the set point quickly. It is noted that the integral term responds to the past errors therefore, it can result in the overshooting of the present value of measured variable.

(iii) The derivative term: The derivative term consists of the rate change of error multiplied by a constant called derivative gain

$$D = K_D \frac{de(t)}{dt}. \tag{B.4}$$

It slows down the rate change of output and damps the overshooting.

The response of P, I, and D for a given set point is shown in Figure B.2.

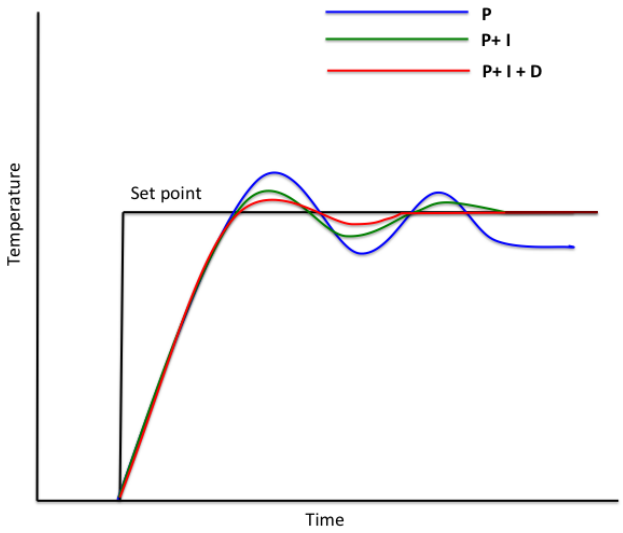

Figure B.2: The output of a PID temperature controller is shown in the above figure. A horizontal line represent the set point. The orange line shows the response of P,I,and D terms together.

Bibliography

[1] J. Lee and D. G. Lee, "Antimicrobial peptides (AMPs) with dual mechanisms: membrane disruption and apoptosis," *Journal of Microbiology and Biotechnology*, vol. 25, no. 6, pp. 759–764, 2014.

[2] T. H. Lee, K. N. Hall, and M. I. Aguilar, "Antimicrobial peptide structure and mechanism of action: a focus on the role of membrane structure," *Current Topics in Medicinal Chemistry*, vol. 16, no. 1, pp. 25–39, 2015.

[3] L. T. Nguyen, E. F. Haney, and H. J. Vogel, "The expanding scope of antimicrobial peptide structures and their modes of action," *Trends in Biotechnology*, vol. 29, no. 9, pp. 464–472, 2011.

[4] B. S. Brown, *Biological membrane*. Biochemical Society, 1911.

[5] L. Buehler, *Cell membranes*. New York, NY: Garland Science, 2015.

[6] E. F. Haney, S. Nathoo, H. J. Vogel, and E. J. Prenner, "Induction of non-lamellar lipid phases by antimicrobial peptides: a potential link to mode of action," *Chemistry and Physics of Lipids*, vol. 163, no. 1, pp. 82–93, 2010.

[7] G. Wang, B. Mishra, R. F. Epand, and R. M. Epand, "High-quality 3D structures shine light on antibacterial, anti-biofilm and antiviral activities of human cathelicidin LL-37 and its fragments," *Biochimica et Biophysica Acta - Biomembranes*, vol. 1838, no. 9, pp. 2160–2172, 2014.

[8] Y. H. M. Chan and S. G. Boxer, "Model membrane systems and their applications," *Current Opinion in Chemical Biologyiology*, vol. 11, no. 6, pp. 581–7, 2007.

[9] M. Eeman and M. Deleu, "From biological membranes to biomimetic model membranes," *Biotechnology, Agronomy, Society and Environment*, vol. 14, no. 4, pp. 719–736, 2010.

[10] T. Nakatsuji and R. L. Gallo, "Antimicrobial peptides: old molecules with new ideas," *The Journal of Investigative Dermatology*, vol. 132, pp. 887–95, 2012.

[11] R. E. W. Hancock and G. Diamond, "The role of cationic antimicrobial peptides in innate host defences," *Trends in Microbiology*, vol. 8, no. 9, pp. 402–410, 2000.

[12] Y. Li, Q. Xiang, Q. Zhang, Y. Huang, Z. Su, A. A. Bahar, D. Ren, J. Wiesner, and A. Vilcinskas, "Antimicrobial peptides: the ancient arm of the human immune system," *Peptides*, vol. 6, no. 12, pp. 207–215, 2013.

[13] R. E. Hancock, "Cationic peptides: effectors in innate immunity and novel antimicrobials," *The Lancet Infectious Diseases*, vol. 1, no. 3, pp. 156–164, 2001.

[14] D. M. Easton, A. Nijnik, M. L. Mayer, and R. E. W. Hancock, "Potential of immunomodulatory host defense peptides as novel anti-infectives," *Trends in Biotechnology*, vol. 27, no. 10, pp. 582–590, 2009.

[15] Y. Lai and R. L. Gallo, "AMPed up immunity: how antimicrobial peptides have multiple roles in immune defense," *Trends in Immunology*, vol. 30, no. 3, pp. 131–141, 2009.

[16] L. T. Nguyen, E. F. Haney, and H. J. Vogel, "The expanding scope of antimicrobial peptide structures and their modes of action," *Trends in Biotechnology*, vol. 29, no. 9, pp. 464–72, 2011.

[17] R. E. W. Hancock and H. G. Sahl, "Antimicrobial and host-defense peptides as new anti-infective therapeutic strategies," *Nature Biotechnology*, vol. 24, no. 12, pp. 1551–7, 2006.

[18] M. Zasloff, "Antimicrobial peptides of multicellular organisms," *Nature*, vol. 415, pp. 389–395, 2002.

[19] F. Guilhelmelli, N. Vilela, P. Albuquerque, L. D. S. Derengowski, I. Silva-Pereira, and C. M. Kyaw, "Antibiotic development challenges: the various mechanisms of action of antimicrobial peptides and of bacterial resistance," *Frontiers in Microbiology*, vol. 4, pp. 1–12, 2013.

[20] K. A. Brogden, "Antimicrobial peptides: pore formers or metabolic inhibitors in bacteria?," *Nature Reviews Microbiology*, vol. 3, pp. 238–251, 2005.

[21] L. Steinstraesser, U. Kraneburg, F. Jacobsen, and A. B. Sammy, "Host defense peptides and their antimicrobial-immunomodulatory duality," *Immunobiology*, vol. 216, no. 3, pp. 322–333, 2011.

[22] Z. Wang and G. Wang, "APD : the antimicrobial peptide database," *Nucleic Acids Research*, vol. 32, pp. 590–592, 2004.

[23] S. H. Marshall, "Antimicrobial peptides: a natural alternative to chemical antibiotics and a potential for applied biotechnology," *Electronic Journal of Biotechnology*, vol. 6, no. 2, pp. 271–284, 2003.

[24] W. Aoki and M. Ueda, "Characterization of antimicrobial peptides toward the development of novel antibiotics," *Pharmaceuticals*, vol. 6, pp. 1055–1081, 2013.

[25] M. J. Browne, C. Y. Feng, V. Booth, and M. L. Rise, "Characterization and expression studies of Gaduscidin-1 and Gaduscidin-2; paralogous antimicrobial peptide-like transcripts from Atlantic cod (Gadus morhua)," *Developmental and Comparative Immunology*, vol. 35, no. 3, pp. 399–408, 2011.

[26] M. Mcdonald, M. Mannion, D. Pike, K. Lewis, A. Flynn, A. M. Brannan, M. J. Browne, D. Jackman, L. Madera, M. R. Power, D. W. Hoskin, M. L. Rise, and V. Booth, "Structure - function relationships in histidine-rich antimicrobial peptides from Atlantic cod," *BBA - Biomembranes*, vol. 1848, no. 7, pp. 1451–1461, 2015.

[27] Canadian Antimicrobial Resistance Alliance., "Comprehensive overview of antibiotic resistance in Canada," tech. rep., 2006.

[28] S. B. Levy and B. Marshall, "Antibacterial resistance worldwide: causes, challenges and responses," *Nature Medicine*, vol. 10, pp. S122–S129, 2004.

[29] S. B. Levy, "The challenge of antibiotic resistance," *Scientific American*, vol. 278, no. 3, pp. 46–53, 1998.

[30] Centres for Disease Control and Prevention (US), "Antibiotic resistance threats in the United States, 2013," tech. rep., 2013.

[31] G. Dantas and M. O. A. Sommer, "How to fight back against antibiotic resistance," *American Scientist*, vol. 102, no. 1, pp. 42–51, 2014.

[32] E. Klein, D. L. Smith, and R. Laxminarayan, "Hospitalizations and deaths caused by methicillin-resistant *Staphylococcus aureus*, United States, 1999-2005," *Emerging Infectious Diseases*, vol. 13, no. 12, pp. 1840–1846, 2007.

[33] C. A. Arias and B. E. Murray, "Antibiotic-resistant bugs in the 21st century-a clinical super-challenge," *New England Journal of Medicine*, vol. 360, no. 5, pp. 439–443, 2009.

[34] A. Peschel and H. G. Sahl, "The co-evolution of host cationic antimicrobial peptides and microbial resistance," *Nature Reviews Microbiology*, vol. 4, no. 7, pp. 529–36, 2006.

[35] W. C. Wimley, "Describing the mechanism of antimicrobial peptide action with the interfacial activity model," *ACS Chemical Biology*, vol. 5, no. 10, pp. 905–917, 2010.

[36] A. K. Marr, W. J. Gooderham, and R. E. Hancock, "Antibacterial peptides for therapeutic use: obstacles and realistic outlook," *Current Opinion in Pharmacology*, vol. 6, no. 5, pp. 468–472, 2006.

[37] A. A. Bahar and D. Ren, "Antimicrobial peptides," *Pharmaceuticals*, vol. 6, no. 12, pp. 1543–1575, 2013.

[38] M. Yasir, M. Willcox, D. Dutta, M. Yasir, M. D. P. Willcox, and D. Dutta, "Action of antimicrobial peptides against bacterial biofilms," *Materials*, vol. 11, no. 12, p. 2468, 2018.

[39] S. Park, Y. Park, and K. Hahm, "The role of antimicrobial peptides in preventing multidrug-resistant bacterial infections and biofilm formation," *International Journal of Molecular Sciences*, vol. 12, pp. 5971–5992, 2011.

[40] K. Fosgerau and T. Hoffmann, "Peptide therapeutics: current status and future directions," *Drug Discovery Today*, vol. 20, no. 1, pp. 122–128, 2015.

[41] W. W. C. Wimley and K. Hristova, "Antimicrobial peptides: successes, challenges and unanswered questions," *The Journal of Membrane Biologyology*, vol. 239, no. 1-2, pp. 27–34, 2011.

[42] N. W. Schmidt and G. C. Wong, "Antimicrobial peptides and induced membrane curvature: geometry, coordination chemistry, and molecular engineering," *Current Opinion in Solid State & Materials Science*, vol. 17, no. 4, pp. 151–163, 2013.

[43] Y. Li, Q. Xiang, Q. Zhang, Y. Huang, and Z. Su, "Overview on the recent study of antimicrobial peptides: origins, functions, relative mechanisms and application," *Peptides*, vol. 37, no. 2, pp. 207–215, 2012.

[44] Y. Shai, "Active antimicrobial peptides," *Biopolymers - Peptide Science Section*, vol. 66, pp. 236–248, 2002.

[45] L. T. Nguyen, E. F. Haney, and H. J. Vogel, "The expanding scope of antimicrobial peptide structures and their modes of action," *Trends in Biotechnology*, vol. 29, no. 9, pp. 464–472, 2011.

[46] M. C. Wolfgang, C. M. Dozois, M. Mahlapuu, J. Hakansson, L. Ringstad, and C. Bjorn, "Antimicrobial peptides: an emerging category of therapeutic agents," *Frontiers in Cellular and Infection microbiology*, vol. 6, 2016.

[47] A. Spaar, C. Münster, and T. Salditt, "Conformation of peptides in lipid membranes, studied by x-ray grazing incidence scattering," *Biophysical Journal*, vol. 87, no. 1, pp. 396–407, 2004.

[48] L. Yang, T. A. Harroun, T. M. Weiss, L. Ding, and H. W. Huang, "Barrel-stave model or toroidal model? A case study on melittin pores," *Biophysical Journal*, vol. 81, no. 3, pp. 1475–1485, 2001.

[49] O. Toke, "Antimicrobial peptides: new candidates in the fight against bacterial infections," *Biopolymers - Peptide Science Section*, vol. 80, no. 6, pp. 717–735, 2005.

[50] L. Yang, T. A. Harroun, T. M. Weiss, L. Ding, and H. W. Huang, "Barrel-stave model or toroidal model ? A case study on Melittin pores," *Biophysical Journal*, vol. 81, no. 3, pp. 1475–1485, 2001.

[51] H. Leontiadou, A. E. Mark, and S. J. Marrink, "Antimicrobial peptides in action," *Journal of the American Chemical Society*, vol. 128, pp. 12156–12161, 2006.

[52] D. Sengupta, H. Leontiadou, A. E. Mark, and S. J. Marrink, "Toroidal pores formed by antimicrobial peptides show significant disorder," *Biochimica et Biophysica Acta (BBA)*, vol. 1778, no. 10, pp. 2308–17, 2008.

[53] M. Jarva, F. T. Lay, T. K. Phan, C. Humble, I. K. H. Poon, M. R. Bleackley, M. A. Anderson, M. D. Hulett, and M. Kvansakul, "X-ray structure

of a carpet-like antimicrobial defensin - phospholipid membrane disruption complex," *Nature Communications*, vol. 9, no. 1, p. 1962, 2018.

[54] R. Chen and A. E. Mark, "The effect of membrane curvature on the conformation of antimicrobial peptides : implications for binding and the mechanism of action," *European Biophysics Journal*, vol. 2, pp. 545–553, 2011.

[55] D. I. Fernandez, A. P. Le, T. C. Whitwell, M. A. Sani, and F. Separovic, "The antimicrobial peptide aurein 1 . 2 disrupts model membranes via the carpet mechanism," *Physical Chemistry Chemical Physics*, vol. 14, pp. 15739–15751, 2012.

[56] M. N. Melo, R. Ferre, and M. A. R. B. Castanho, "Antimicrobial peptides : linking partition, activity, and high membrane-bound concentrations," *Nature Reviews Microbiology*, vol. 7, pp. 245–250, 2009.

[57] R. M. Epand and R. F. Epand, "Bacterial membrane lipids in the action of antimicrobial agents," *Journal of Peptide Science*, vol. 17, no. 5, pp. 298–305, 2011.

[58] W. N. Konings, A. Bisschop, M. Veenhuis, and C. A. Vermeulen, "Small cationic antimicrobial peptides delocalize peripheral membrane proteins," *Journal of Bacteriology*, vol. 116, no. 3, pp. 1456–1465, 1973.

[59] P. Nicolas, "Multifunctional host defense peptides: intracellular-targeting antimicrobial peptides.," *The FEBS Journal*, vol. 276, no. 22, pp. 6483–96, 2009.

[60] K. A. Brogden, "Antimicrobial peptides: Pore formers or metabolic inhibitors in bacteria?," *Nature Reviews Microbiology*, vol. 3, no. 3, pp. 238–250, 2005.

[61] F. G. Avci, B. S. Akbulut, and E. Ozkirimli, "Membrane active peptides and their biophysical characterization," *Biomolecules*, vol. 8, no. 77, pp. 1–43, 2018.

[62] D. L. Worcester, "Antimicrobial peptide pores in membranes detected by neutron in-plane scattering," *Biochemistry*, vol. 34, pp. 15614–15618, 1995.

[63] F. Y. Chen, M. T. Lee, and H. W. Huang, "Evidence for membrane thinning effect as the mechanism for peptide-induced pore formation," *Biophysical Journal*, vol. 84, pp. 3751–3758, 2003.

[64] M. Hassan, M. Bromberek, I. Saika-voivod, and V. Booth, "Molecular dynamics simulations of histidine-containing cod antimicrobial peptide paralogs in self-assembled bilayers," *BBA - Biomembranes*, vol. 1838, no. 11, pp. 2778–2787, 2014.

[65] B. Bechinger, "Rationalizing the membrane interactions of cationic amphipathic antimicrobial peptides by their molecular shape," *Current Opinion in Colloid and Interface Science*, vol. 14, no. 5, pp. 349–355, 2009.

[66] B. Bechinger, "Insights into the mechanisms of action of host defence peptides from biophysical and structural investigations," *Journal of Peptide Science*, vol. 17, no. 5, pp. 306–14, 2011.

[67] B. Bechinger and K. Lohner, "Detergent-like actions of linear amphipathic cationic antimicrobial peptides," *Biochimica et Biophysica Acta - Biomembranes*, vol. 1758, no. 9, pp. 1529–1539, 2006.

[68] M. Mihajlovic and T. Lazaridis, "Charge distribution and imperfect amphipathicity affect pore formation by antimicrobial peptides," *Biochimica et Biophysica Acta (BBA)*, vol. 1818, no. 5, pp. 1274–83, 2012.

[69] D. Gaspar, A. Veiga, and M. A. R. B. Castanho, "From antimicrobial to anticancer peptides. A review," *Frontiers in Microbiology*, vol. 4, pp. 1–16, 2013.

[70] A. S. Benna, Y. Shai, F. Jacobsen, and L. Steinstraesser, "Oncolytic Activities of host defense peptides," *International Journal of Molecular Sciences*, vol. 12, no. 11, pp. 8027–8051, 2011.

[71] R. E. W. Hancock, A. T. Y. Yeung, S. L. Gellatly, and R. E. W. Hancock, "Multifunctional cationic host defence peptides and their clinical applications," *Cellular and Molecular Life Sciences*, vol. 68, no. 13, pp. 2161–2176, 2011.

[72] I. Tannock and D. Rotin, "Acid pH in tumors and its potential for therapeutic exploitation," *Cancer research*, vol. 49, no. 16, pp. 4373–4384, 1989.

[73] L. Kacprzyk, V. Rydengard, M. Morgelin, M. Davoudi, M. Pasupuleti, M. Malmsten, and A. Schmidtchen, "Antimicrobial activity of histidine-rich peptides is dependent on acidic conditions," *Biochimica et Biophysica Acta (BBA)*, vol. 1768, no. 11, pp. 2667–80, 2007.

[74] J. S. Mader and D. W. Hoskin, "Expert opinion on investigational drugs cationic antimicrobial peptides as novel cytotoxic agents for cancer treatment cationic antimicrobial peptides as novel cytotoxic agents for cancer," *Expert Opinion on Investigational Drugs*, vol. 15, no. 8, pp. 933–946, 2006.

[75] A. J. Mason, C. Gasnier, A. Kichler, G. Prevost, D. Aunis, M. H. Boutigue, and B. Bechinger, "Enhanced membrane disruption and antibiotic action against pathogenic bacteria by designed histidine-rich peptides at acidic pH," *Antimicrobial Agents and Chemotherapy*, vol. 50, no. 10, pp. 3305–3311, 2006.

[76] A. Makovitzki, A. Fink, and Y. Shai, "Suppression of human solid tumor growth in mice by intratumor and systemic inoculation of histidine-rich and pH-dependent host defense-like lytic peptides," *Cancer Research*, vol. 69, no. 8, pp. 3458–3463, 2009.

[77] Z. Tu, A. Young, C. Murphy, and J. F. Liang, "The pH sensitivity of histidine-containing lytic peptides," *Journal of Peptide Science*, vol. 15, no. 11, pp. 790–795, 2009.

[78] D. I. Fernandez, J. D. Gehman, and F. Separovic, "Membrane interactions of antimicrobial peptides from Australian frogs," *Biochimica et Biophysica Acta (BBA)*, vol. 1788, no. 8, pp. 1630–8, 2009.

[79] M. Bastos, G. Bai, P. Gomes, D. Andreu, E. Goormaghtigh, and M. Prieto, "Energetics and partition of two cecropin-melittin hybrid peptides to model membranes of different composition," *Biophysical Journal*, vol. 94, no. 6, pp. 2128–2141, 2008.

[80] N. Papo and Y. Shai, "Can we predict biological activity of antimicrobial peptides from their interactions with model phospholipid membranes?," *Peptides*, vol. 24, no. 11, pp. 1693–703, 2003.

[81] C. Kim, J. Spano, E. K. Park, and S. Wi, "Evidence of pores and thinned lipid bilayers induced in oriented lipid membranes interacting with the antimicrobial peptides, magainin-2 and aurein-3.3," *Biochimica et Biophysica Acta (BBA)*, vol. 1788, no. 7, pp. 1482–96, 2009.

[82] H. Sato and J. B. Feix, "Peptide-membrane interactions and mechanisms of membrane destruction by amphipathic alpha-helical antimicrobial peptides," *Biochimica et Biophysica Acta (BBA)*, vol. 1758, no. 9, pp. 1245–56, 2006.

[83] E. S. Salnikov, A. J. Mason, and B. Bechinger, "Membrane order perturbation in the presence of antimicrobial peptides by ^{2}H solid-state NMR spectroscopy," *Biochimie*, vol. 91, no. 6, pp. 734–743, 2009.

[84] E. S. Salnikov, H. Friedrich, X. Li, P. Bertani, S. Reissmann, C. Hertweck, J. D. J. O'Neil, J. Raap, and B. Bechinger, "Structure and alignment of the membrane-associated peptaibols ampullosporin A and alamethicin by oriented ^{15}N and ^{31}P solid-state NMR spectroscopy," *Biophysical Journal*, vol. 96, no. 1, pp. 86–100, 2009.

[85] E. S. Salnikov and B. Bechinger, "Lipid-controlled peptide topology and interactions in bilayers : structural insights into the synergistic enhancement

of the antimicrobial activities of PGLa and magainin 2," *Biophysical Journal*, vol. 100, no. 6, pp. 1473–1480, 2011.

[86] J. Misiewicz, S. Afonin, and A. S. Ulrich, "Control and role of pH in peptide-lipid interactions in oriented membrane samples," *Biochimica et Biophysica Acta (BBA)*, vol. 1848, pp. 833–841, 2015.

[87] M. J. Duer, *Solid state NMR spectroscopy: principles and applications*. John Wiley & Sons, 2008.

[88] C. P. Slichter, *Principles of magnetic resonance*. Springer Science and Business Media, 2013.

[89] A. Abragam, *The principles of nuclear magnetism*. Oxford university press, 1961.

[90] M. H. Levitt, *Spin dynamics: basics of nuclear magnetic resonance*. John Wiley & Sons, 2001.

[91] P. T. Callaghan, *Principles of nuclear magnetic resonance microscopy*. Oxford University Press on Demand, 1993.

[92] J. Keeler, *Understanding NMR spectroscopy*. John Wiley & Sons, 2011.

[93] M. Bloom, "NMR studies of membranes and whole cells," *Zeitschrift für Physikalische Chemie*, vol. 153, pp. 67—-67, 1987.

[94] M.H. Cohen and F. Reif, "Quadrupole effects in nuclear magnetic resonance studies of solids," *Solid State Physics*, vol. 5, pp. 321–438, 1957.

[95] J. Seelig, "Deuterium magnetic resonance: theory and application to lipid membranes," *Quarterly Reviews of Biophysicsiophysics*, vol. 10, no. 03, pp. 353–418, 1977.

[96] J. H. Davis, "The description of membrane lipid conformation, order and dynamics by ^{2}H NMR," *Biochimica et Biophysica Acta (BBA)*, vol. 737, pp. 117–171, 1983.

[97] M. Mehring, *High resolution NMR spectroscopy in solids*. Springer Science and Business Media, 2012.

[98] M. Bloom, J. H. Davis, and A. L. Mackay, "Direct determination of the oriented sample NMR spectrum from the powder spectrum for systems with local axial symmetry," *Chemical Physics Letters*, vol. 80, no. 1, pp. 198–202, 1981.

[99] M. A. McCabe and S. R. Wassall, "Fast-fourier-transform dePaking," *Journal of Magnetic Resonance, Series B*, vol. 106, no. 1, pp. 80–82, 1995.

[100] E. Sternin, *Depaking of NMR Spectra*. PhD thesis, The University of British Columbia, 1980.

[101] M. Lafleur, B. Fine, E. Sternin, P. R. Cullis, and M. Bloomt, "Smoothed orientational order profile of lipid bilayers by ^{2}H-nuclear magnetic resonance," *Biophysical Journal*, vol. 56, no. 5, pp. 1037–1041, 1989.

[102] J. Davis, K. Jeffrey, M. Bloom, M. Valic, and T. Higgs, "Quadrupolar echo deuteron magnetic resonance spectroscopy in ordered hydrocarbon chains," *Chemical Physics Letters*, vol. 42, pp. 390 – 394, 1976.

[103] E. Fukushima and S. B. Roeder, *Experimental pulse NMR: a nuts and bolts approach*. Addison-Wesley Reading, MA, 1981.

[104] M. R. Morrow, J. Stewart, S. Taneva, A. Dico, and K. M. W. Keough, "Perturbation of DPPC bilayers by high concentrations of pulmonary surfactant protein SP-B," *European Biophysics Journal*, vol. 33, pp. 285–290, 2004.

[105] A. S. Dico, J. Hancock, M. R. Morrow, J. Stewart, S. Harris, and K. M. W. Keough, "Pulmonary surfactant protein SP-B interacts similarly with dipalmitoylphosphatidylglycerol and dipalmitoylphosphatidylcholine in phosphatidylcholine/phosphatidylglycerol mixtures pulmonary surfactant protein SP-B interacts similarly with dipalmitoylphos," *Biochemistry*, vol. 2960, no. 96, pp. 4172–4177, 1997.

[106] H. Singh, J. Emberley, and M. R. Morrow, "Pressure induces interdigitation differently in DPPC and DPPG," *European Biophysics Journal*, vol. 37, no. 6, pp. 783–792, 2008.

[107] K. P. Pauls, A. L. Mackay, M. Bloom, A. K. Tanjea, and R. S. Hodges, "Dynamic properties of the backbone of an integral membrane polypeptide measured by ^{2}H-NMR," *European Biophysics Journal*, vol. 12, pp. 1–11, 1985.

[108] B. Bechinger and C. Sizun, "Alignment and structural analysis of membrane polypeptides by ^{15}N and ^{31}P solid-state NMR spectroscopy," *Concepts in Magnetic Resonance Part A: Bridging Education and Research*, vol. 18, no. 2, pp. 130–145, 2003.

[109] B. Bechinger, C. Aisenbrey, and P. Bertani, "The alignment, structure and dynamics of membrane-associated polypeptides by solid-state NMR spectroscopy," *Biochimica et Biophysica Acta - Biomembranes*, vol. 1666, no. 1-2, pp. 190–204, 2004.

[110] E. Y. Chekmenev, B. S. Vollmar, and M. Cotten, "Can antimicrobial peptides scavenge around a cell in less than a second?," *BBA - Biomembranes*, vol. 1798, no. 2, pp. 228–234, 2010.

[111] R. J. Hunter, *Foundations of colloid science*. Oxford university press, 2001.

[112] R. Aveyard and D. A. Haydon, *An introduction to the principles of surface chemistry*. CUP Archive, 1973.

[113] R. J. Hunter, *Zeta potential in colloid science: principles and applications*. Academic Press, 1981.

[114] D. C. Grahame, "Electrical double layer and the theory of electrocapillarity," *Chemical Reviews*, vol. 41, no. 3, pp. 441–501, 1947.

[115] Malvern, *Zetasizer nano user manual*, vol. 1. 2007.

[116] J. M. Freire, M. M. Domingues, J. Matos, M. N. Melo, A. S. Veiga, N. C. Santos, and M. A. R. B. Castanho, "Using zeta-potential measurements to quantify peptide partition to lipid membranes," *European Biophysics Journal*, vol. 40, no. 4, pp. 481–487, 2011.

[117] M. Kaszuba, J. Corbett, F. M. Watson, and A. Jones, "High-concentration zeta potential measurements using light-scattering techniques," *Philosophical Transactions of the Royal Society*, vol. 368, pp. 4439–51, 2010.

[118] S. C. Particle, "Electrophoretic mobility of a spherical colloidal particle," *Journal of chemical society*, vol. 74, pp. 1607–1626, 1978.

[119] W. W. Tscharnuter, "Mobility measurements by phase analysis," *Applied Optics*, vol. 40, no. 24, pp. 3995–4003, 2001.

[120] F. McNeil-Watson, W. Tscharnuter, and J. Miller, "A new instrument for the measurement of very small electrophoretic mobilities using phase analysis light scattering (PALS)," *Colloids and Surfaces A: Physicochemical and Engineering Aspects*, vol. 140, no. 1-3, pp. 53–57, 1998.

[121] R. W. Woody, "Circular dichroism," *Methods in Enzymology*, vol. 246, pp. 34–71, 1995.

[122] B. Norden, *Circular dichroism and linear dichroism*. Oxford University Press, USA, 1997.

[123] J. T. Yang, C. S. C. Wu, and H. M. Martinez, "Calculation of protein conformation from circular dichroism," *Methods in Enzymology*, vol. 130, no. 1956, pp. 208–269, 1986.

[124] C. A. Rohl and R. L. Baldwin, "Comparison of NH exchange and circular dichroism as techniques for measuring the parameters of the helix-coil transition in peptides," *Biochemistry*, vol. 36, no. 28, pp. 8435–8442, 1997.

[125] J. M. Henderson, A. J. Waring, F. Separovic, and K. Y. C. Lee, "Antimicrobial peptides share a common interaction driven by membrane line tension reduction," *Biophysical Journal*, vol. 111, no. 10, pp. 2176–2189, 2016.

[126] J. Davis, K. Jeffrey, M. Bloom, M. Valic, and T. Higgs, "Quadrupolar echo deuteron magnetic resonance spectroscopy in ordered hydrocarbon chain," *Chemical Physics Letters*, vol. 42, no. 2, pp. 390–394, 1976.

[127] G. Klocek, T. Schulthess, Y. Shai, and J. Seelig, "Thermodynamics of melittin binding to lipid bilayers. Aggregation and pore formation," *Amercial Chemical Society*, pp. 2586–2596, 2009.

[128] N. C. Santos, M. Prieto, and M. A. R. B. Castanho, "Quantifying molecular partition into model systems of biomembranes: An emphasis on optical spectroscopic methods," *Biochimica et Biophysica Acta - Biomembranes*, vol. 1612, no. 2, pp. 123–135, 2003.

[129] M. M. Domingues, M. A. R. B. Castanho, and N. C. Santos, "What can light scattering spectroscopy do for membrane-active peptide studies?," *Journal of Peptide Science*, vol. 14, pp. 394–400, 2008.

[130] A. V. Delgado, G. F. Caballero, R. J. Hunter, L. K. Koopal, and J. Lyklema, "Measurement and interpretation of electrokinetic phenomena," *Pure and Applied Chemistry*, vol. 77, no. 10, pp. 1753–1805, 2005.

[131] C. H. Chu, I. Sarangadharan, A. Regmi, Y. W. Chen, C. P. Hsu, W. Chang, G. Lee, J. I. Chyi, C. C. Chen, S. C. Shiesh, G. B. Lee, and Y. L. Wang, "Beyond the Debye length in high ionic strength solution: direct protein detection with field-effect transistors (FETs) in human serum," *Scientific Reports*, vol. 7, no. 1, pp. 5256–5257, 2017.

[132] T. K. Popov, F. Microscope, K. Miyano, A. Mori, H. Amemiya, and G. Fuchs, "The Langmuir isotherm adsorption equation : the monolayer approach," *IOP*, vol. 107, 2016.

[133] Y. S. Ho and A. E. Ofomaja, "Biosorption thermodynamics of cadmium on coconut copra meal as biosorbent," *Biochemical Engineering Journal*, vol. 30, no. 2, pp. 117–123, 2006.

[134] M. N. Melo, R. Ferre, L. Feliu, E. Bardají, M. Planas, and M. A. R. B. Castanho, "Prediction of antibacterial activity from physicochemical properties of antimicrobial peptides," *PLoS ONE*, vol. 6, no. 12, pp. 1–6, 2011.

[135] M. Planas, R. Ferre, M. N. Melo, A. D. Correia, L. Feliu, and M. Castanho, "Synergistic effects of the membrane actions of cecropin-melittin antimicrobial hybrid peptide BP100," *Biophysical Chemistry*, vol. 96, pp. 1815–1827, 2009.

[136] I. Langmuir, "The adsorption of gases on plane surfaces of glass, mica and platinum," *Journal of the American Chemical society*, vol. 40, no. 9, pp. 1361–1403, 1918.

[137] E. S. Salnikov, A. J. Mason, and B. Bechinger, "Membrane order perturbation in the presence of antimicrobial peptides by ^{2}H solid-state NMR spectroscopy," *Biochimie*, vol. 91, no. 6, pp. 734–743, 2009.

[138] A. Ramamoorthy, S. Thennarasu, D. K. Lee, A. Tan, and L. Maloy, "Solid-State NMR investigation of the membrane-disrupting mechanism of antimicrobial peptides MSI-78 and MSI-594 derived from magainin 2 and melittin," *Biophysical Journal*, vol. 91, no. 1, pp. 206–216, 2006.

[139] S. Bourbigot, L. Fardy, A. J. Waring, and M. R. Yeaman, "Structure of chemokine-derived antimicrobial peptide IL-8α and interaction with detergent micelles and oriented lipid bilayers," *Biochemistry*, vol. 48, no. 44, pp. 10509–10521, 2010.

[140] K. A. H. Wildman, G. V. Martinez, M. F. Brown, and A. Ramamoorthy, "Perturbation of the hydrophobic core of lipid bilayers by the human peptide LL-37," *Biochemistry*, vol. 43, pp. 8459–8469, 2004.

[141] R. B. Schulz, V. Booth, and M. R. Morrow, "Perturbation of DPPC/POPG bilayers by the N-terminal helix of lung surfactant protein SP-B: A ^{2}H NMR study," *European Biophysics Journal*, vol. 38, no. 5, pp. 613–624, 2009.

[142] A. Flynn, M. Ducey, A. Yethiraj, and M. R. Morrow, "Dynamic properties of bicellar lipid mixtures observed by rheometry and quadrupole echo decay," *Langmuir*, vol. 28, no. 5, pp. 2782–2790, 2012.

[143] M. H. Khatami, M. Bromberek, I. Saika-Voivod, and V. Booth, "Molecular dynamics simulations of histidine-containing cod antimicrobial peptide paralogs in self-assembled bilayers," *Biochimica et Biophysica Acta - Biomembranes*, vol. 1838, no. 11, pp. 2778–2787, 2014.

[144] Y. Pouny, D. Rapaport, A. Mor, P. Nicolas, and Y. Shai, "Interaction of antimicrobial dermaseptin and its fluorescently labeled analogues with phospholipid membranes," *Biochemistry*, vol. 31, no. 49, pp. 12416–12423, 1991.

[145] M. Dathe, H. Nikolenko, J. Meyer, M. Beyermann, and M. Bienert, "Optimization of the antimicrobial activity of magainin peptides by modification of charge," *FEBS letters*, vol. 501, no. 2-3, pp. 146–150, 2001.

[146] G. Beschiaschvili and J. Seelig, "Melittin binding to mixed phosphatidylglycerol/phosphatidylcholine membranes," *Biochemistry*, vol. 29, no. 1, pp. 52–58, 1990.

[147] A. Arouri, M. Dathe, and A. Blume, "Peptide induced demixing in PG/PE lipid mixtures: A mechanism for the specificity of antimicrobial peptides towards bacterial membranes?," *Biochimica et Biophysica Acta - Biomembranes*, vol. 1788, no. 3, pp. 650–659, 2009.

[148] G. Wang, R. F. Epand, B. Mishra, T. Lushnikova, V. C. Thomas, K. W. Bayles, and R. M. Epand, "Decoding the functional roles of cationic side chains of the major antimicrobial region of human cathelicidin LL-37," *Antimicrobial Agents and Chemotherapy*, vol. 56, no. 2, pp. 845–856, 2012.

[149] R. F. Epand, W. L. Maloy, A. Ramamoorthy, and R. M. Epand, "Probing the charge cluster mechanism in amphipathic helical cationic antimicrobial peptides," *Biochemistry*, vol. 49, pp. 4076–4084, 2010.

[150] D. I. Fernandez, A. P. Le Brun, T. C. Whitwell, M. A. Sani, M. James, and F. Separovic, "The antimicrobial peptide aurein 1.2 disrupts model membranes via the carpet mechanism," *Physical Chemistry Chemical Physics*, vol. 14, no. 45, p. 15739, 2012.

[151] R. F. Epand, G. Wang, B. Berno, and R. M. Epand, "Lipid segregation explains selective toxicity of a series of fragments derived from the human cathelicidin LL-37," *Antimicrobial Agents and Chemotherapy*, vol. 53, no. 9, pp. 3705–3714, 2009.

[152] I. A. Edwards, A. G. Elliott, A. M. Kavanagh, J. Zuegg, M. A. T. Blaskovich, and M. A. Cooper, "Contribution of amphipathicity and hydrophobicity to the antimicrobial activity and cytotoxicity of beta- hairpin peptides," *ACS Infectious Diseases*, vol. 2, no. 6, pp. 442–450, 2016.

[153] A. Hollmann, M. Martínez, M. E. Noguera, M. T. Augusto, A. Disalvo, N. C. Santos, L. Semorile, and P. C. Maffía, "Role of amphipathicity and hydrophobicity in the balance between hemolysis and peptide - membrane interactions of three related antimicrobial peptides," *Colloids and Surfaces B: Biointerfaces*, vol. 141, pp. 528–536, 2016.

[154] M. C. Manzini, K. R. Perez, K. A. Riske, J. C. Bozelli, T. L. Santos, M. A. Da Silva, G. K. V. Saraiva, M. J. Politi, A. P. Valente, F. C. L. Almeida, H. Chaimovich, M. A. Rodrigues, M. P. Bemquerer, S. Schreier, and I. M. Cuccovia, "Peptide:Lipid ratio and membrane surface charge determine the mechanism of action of the antimicrobial peptide BP100. conformational and functional studies," *Biochimica et Biophysica Acta - Biomembranes*, vol. 1838, no. 7, pp. 1985–1999, 2014.

[155] S. K. Kandasamy and R. G. Larson, "Effect of salt on the interactions of antimicrobial peptides with zwitterionic lipid bilayers," *Biochimica et Biophysica Acta - Biomembranes*, vol. 1758, no. 9, pp. 1274–1284, 2006.

[156] G. Wu, J. Ding, H. Li, L. Li, R. Zhao, Z. Shen, X. Fan, and T. Xi, "Effects of cations and pH on antimicrobial activity of thanatin and s-thanatin against *Escherichia coli* ATCC25922 and B. subtilis ATCC 21332," *Current Microbiology*, vol. 57, no. 6, pp. 552–557, 2008.

[157] J. K. Rainey and B. D. Sykes, "Optimizing oriented planar-supported lipid samples for solid-state protein NMR," *Biophysical Journal*, vol. 89, no. 4, pp. 2792–2805, 2005.

[158] E. Salnikov, C. Aisenbrey, V. Vidovic, and B. Bechinger, "Solid-state NMR approaches to measure topological equilibria and dynamics of membrane polypeptides," *Biochimica et Biophysica Acta (BBA)*, vol. 1798, no. 2, pp. 258–65, 2010.

[159] B. Bechinger, D. A. Skladnev, A. Ogrel, X. Li, E. V. Rogozhkina, T. V. Ovchinnikova, J. D. J. O. Neil, and J. Raap, "^{15}N and ^{31}P solid-state NMR investigations on the orientation of zervamicin II and alamethicin in phosphatidylcholine membranes," *Biochemistry*, vol. 40, pp. 9428–9437, 2001.

[160] A. Ramamoorthy, S. Thennarasu, D. K. Lee, A. Tan, and L. Maloy, "Solid-state NMR investigation of the membrane-disrupting mechanism of antimicrobial peptides MSI-78 and MSI-594 derived from magainin 2 and melittin," *Biophysical Journal*, vol. 91, no. 1, pp. 206–216, 2006.

[161] D. Palleboina, "Solid-state NMR studies of lung surfactant protein-B fragments in model and natural lung surfactant lipid bilayers," Master's thesis, Memorial University of Newfoundland, 2012.

[162] T. C. Yang, M. Mcdonald, M. R. Morrow, and V. Booth, "The effect of a c-terminal peptide of surfactant protein B (SP-B) on oriented lipid bilayers,

characterized by solid-state ^{2}H and ^{31}P NMR," *Biophysical Journal*, vol. 96, no. 9, pp. 3762–3771, 2009.

[163] V. Booth, A. J. Waring, F. J. Walther, and K. M. W. Keough, "NMR structures of the c-terminal segment of surfactant protein B in detergent," *Biochemistry*, vol. 43, pp. 15187–15194, 2004.

[164] N. J. Kruger, *The Bradford method for protein quantitation*. Springer, 2002.

[165] S. Bourbigot, L. Fardy, A. J. Waring, M. R. Yeaman, and V. Booth, "Structure of chemokine-derived antimicrobial Peptide interleukin-8α and interaction with detergent micelles and oriented lipid bilayers," *Biochemistry*, vol. 48, pp. 10509–21, nov 2009.

[166] B. Bechinger, C. Aisenbrey, and P. Bertani, "The alignment, structure and dynamics of membrane-associated polypeptides by solid-state NMR spectroscopy," *Biochimica et Biophysica Acta (BBA)*, vol. 1666, pp. 190–204, 2004.

[167] G. Wang, B. Mishra, K. Lau, T. Lushnikova, R. Golla, and X. Wang, "Antimicrobial peptides in 2014," *Pharmaceuticals*, vol. 8, pp. 123–150, 2015.

[168] J. D. Unsay, K. Cosentino, and Y. Subburaj, "Cardiolipin effects on membrane structure and dynamics," *Amercial Chemical Society*, vol. 29, 2013.

[169] E. Mileykovskaya and W. Dowhan, "Cardiolipin membrane domains in prokaryotes and eukaryotes," *Biochimica et Biophysica Acta - Biomembranes*, vol. 1788, no. 10, pp. 2084–2091, 2009.

[170] H. Deng and R. Callender, "A new look at cardiolipin," *Biochimica et Biophysica Acta (BBA)*, vol. 1788, pp. 1997–2002, 2009.

[171] M. Sathappa and N. N. Alder, "The ionization properties of cardiolipin and its variants in model bilayers," *BBA - Biomembranes*, vol. 1858, no. 6, pp. 1362–1372, 2016.

[172] R. N. A. H. Lewis and R. N. McElhaney, "The physicochemical properties of cardiolipin bilayers and cardiolipin-containing lipid membranes," *Biochimica et Biophysica Acta - Biomembranes*, vol. 1788, no. 10, pp. 2069–2079, 2009.

[173] R. N. Lewis and R. N. McElhaney, "The physicochemical properties of cardiolipin bilayers and cardiolipin-containing lipid membranes," *Biochimica et Biophysica Acta - Biomembranes*, vol. 1788, no. 10, pp. 2069–2079, 2009.

[174] P. Allegrini, G. Pluschke, and J. Seelig, "Cardiolipin conformation and dynamics in bilayer membranes as seen by deuterium magnetic resonance," *Biochemistry*, vol. 23, no. 26, pp. 6452—-6458, 1984.

[175] M. Bloom and E. Sternin, "Transverse nuclear spin relaxation in phospholipid bilayer membranes," *Biochemistry*, vol. 26, no. 1986, pp. 2101–2105, 1987.

[176] K. Scheinpflug, O. Krylova, H. Nikolenko, C. Thurm, and M. Dathe, "Evidence for a novel mechanism of antimicrobial action of a cyclic R-,W-rich hexapeptide," *PLoS ONE*, vol. 10, no. 4, pp. 1–16, 2015.

[177] T. H. Zhang, J. K. Muraih, N. Tishbi, J. Herskowitz, R. L. Victor, J. Silverman, S. Uwumarenogie, S. D. Taylor, M. Palmer, and E. Mintzer, "Cardiolipin prevents membrane translocation and permeabilization by daptomycin," *Journal of Biological Chemistry*, vol. 289, no. 17, pp. 11584–11591, 2014.

[178] R. M. Epand, R. F. Epand, C. J. Arnusch, P. B. Sternberg, G. Wang, and Y. Shai, "Lipid clustering by three homologous arginine-rich antimicrobial peptides is insensitive to amino acid arrangement and induced secondary structure," *Biochimica et Biophysica Acta - Biomembranes*, vol. 1798, no. 6, pp. 1272–1280, 2010.

[179] A. A. Yaroslavov, E. A. Kiseliova, O. Y. Udalykh, and V. A. Kabanov, "Integrity of mixed liposomes contacting a polycation depends on the negatively charged lipid content," *Langmuir*, vol. 14, no. 18, pp. 5160–5163, 1998.

[180] L. Lombardi, M. I. Stellato, R. Oliva, A. Falanga, M. Galdiero, L. Petraccone, G. D'Errico, A. D. Santis, S. Galdiero, and P. D. Vecchio, "Antimicrobial peptides at work: interaction of myxinidin and its mutant WMR with lipid bilayers mimicking the *P. aeruginosa* and *E. coli* membranes," *Scientific Reports*, vol. 7, pp. 1–15, 2017.

[181] M. A. Sani and F. Separovic, "How membrane-active peptides get into lipid membranes," *Accounts of Chemical Research*, vol. 49, no. 6, pp. 1130–1138, 2016.

[182] O. G. Travkova, H. Moehwald, and G. Brezesinski, "The interaction of antimicrobial peptides with membranes," *Advances in Colloid and Interface Science*, vol. 247, pp. 521–532, 2017.

[183] H. K. Kang, C. Kim, C. H. Seo, and Y. Park, "The therapeutic applications of antimicrobial peptides (AMPs): a patent review," *Journal of Microbiology*, vol. 55, no. 1, pp. 1–12, 2017.

[184] N. Papo and Y. Shai, "Can we predict biological activity of antimicrobial peptides from their interactions with model phospholipid membranes?," *Peptides*, vol. 24, no. 11, pp. 1693–1703, 2003.

[185] S. B. T. Amos, L. S. Vermeer, P. M. Ferguson, J. Kozlowska, M. Davy, T. T. Bui, A. F. Drake, C. D. Lorenz, and A. J. Mason, "Antimicrobial peptide potency is facilitated by greater conformational flexibility when binding to gram-negative bacterial inner membranes," *Scientific Reports*, vol. 6, pp. 1–13, 2016.

[186] A. S. Benna, Y. Shai, F. Jacobsen, and L. Steinstraesser, "Oncolytic activities of host defense peptides," *International Journal of Molecular Sciences*, vol. 12, no. 11, pp. 8027–8051, 2011.

[187] D. W. Hoskin and A. Ramamoorthy, "Studies on anticancer activities of antimicrobial peptides," *Biochimica et Biophysica Acta - Biomembranes*, vol. 1778, no. 2, pp. 357–375, 2008.

[188] S. K. Kandasamy and R. G. Larson, "Binding and insertion of α-helical anti-microbial peptides in POPC bilayers studied by molecular dynamics simulations," *Chemistry and Physics of Lipids*, vol. 132, no. 1, pp. 113–132, 2004.

[189] A. Mecke, D. K. Lee, A. Ramamoorthy, B. G. Orr, and M. M. Banaszak Holl, "Membrane thinning due to antimicrobial peptide binding: an atomic force microscopy study of MSI-78 in lipid bilayers," *Biophysical Journal*, vol. 89, no. 6, pp. 4043–4050, 2005.

[190] K. He, S. J. Ludtke, W. T. Heller, and H. W. Huang, "Mechanism of alamethicin insertion into lipid bilayers," *Biophysical Journal*, vol. 71, no. 5, pp. 2669–2679, 1996.

[191] A. Zemel, A. Ben-Shaul, and S. May, "Membrane perturbation induced by interfacially adsorbed peptides," *Biophysical Journal*, vol. 86, no. 6, pp. 3607–3619, 2004.

[192] S. L. Grage, S. Afonin, S. Kara, G. Buth, and A. S. Ulrich, "Membrane thinning and thickening induced by membrane-active amphipathic peptides," *Frontiers in Cell and Developmental Biology*, vol. 4, 2016.

[193] W. C. Wimley and K. Hristova, "Antimicrobial peptides: successes, challenges and unanswered questions," *Journal of Membrane Biology*, vol. 239, no. 1-2, pp. 27–34, 2011.

[194] E. Y. Chekmenev, B. S. Vollmar, K. T. Forseth, M. N. Manion, S. M. Jones, T. J. Wagner, R. M. Endicott, B. P. Kyriss, L. M. Homem, M. Pate, J. He, J. Raines, P. L. Gor, W. W. Brey, D. J. Mitchell, A. J. Auman, M. J. Ellard, J. Blazyk, and M. Cotten, "Investigating molecular recognition and biological function at interfaces using piscidins, antimicrobial peptides from fish," *Biochimica et Biophysica Acta (BBA)*, vol. 1758, pp. 1359–1372, 2006.

[195] K. K. Awaguchi, K. S. Uita, Y. S. Uzuki, K. U. Memoto, Y. N. Akazawa, and T. A. Sakura, "Orientation of the antimicrobial peptide, cecropin A magainin 2 hybrid, in a lipid bilayer studied by ^{15}N solid-state NMR," *Polymer Journal*, vol. 37, no. 3, pp. 229–233, 2005.

[196] R. M. Epand, C. Walker, R. F. Epand, and N. A. Magarvey, "Molecular mechanisms of membrane targeting antibiotics," *Biochimica et Biophysica Acta - Biomembranes*, vol. 1858, no. 5, pp. 980–987, 2016.

[197] R. M. Epand and R. F. Epand, "Domains in bacterial membranes and the action of antimicrobial agents," *Molecular BioSystems*, vol. 5, no. 6, pp. 580–587, 2009.

[198] S. G. Clerc and T. E. Thompson, "Permeability of dimyristoyl phosphatidylcholine/dipalmitoyl phosphatidylcholine bilayer membranes with coexisting gel and liquid-crystalline phases," *Biophysical Journal*, vol. 68, no. 6, pp. 2333–2341, 1995.

[199] J. F. Francois, S. Castano, B. Desbat, B. Odaert, M. Roux, M. H. Metz-Boutigue, and E. J. Dufourc, "Aggregation of cateslytin
beta-sheets on negatively charged lipids promotes rigid membrane domains. A new mode of action for antimicrobial peptides?," *Biochemistry*, vol. 47, no. 24, pp. 6394–6402, 2008.

[200] H. Komatsu and S. Okada, "Increased permeability of phase-separated liposomal membranes with mixtures of ethanol-induced interdigitated and non-interdigitated structures," *BBA - Biomembranes*, vol. 1237, no. 2, pp. 169–175, 1995.

[201] S. Finger, A. Kerth, M. Dathe, and A. Blume, "The efficacy of trivalent cyclic hexapeptides to induce lipid clustering in PG/PE membranes correlates with their antimicrobial activity," *Biochimica et Biophysica Acta - Biomembranes*, vol. 1848, no. 11, pp. 2998–3006, 2015.

[202] M. Araki, "PID Control," *Control Systems, Robotics, and Automation*, vol. II, 1989.